TESTING

OF

PRINCESS RIVER BRIDGE

by

Rodney William McGee
Bachelor of Engineering with Honours
Graduate Diploma of Business in Professional Management
Associate Diploma in Emergency Management
Bachelor of Social Science (Emergency Management)

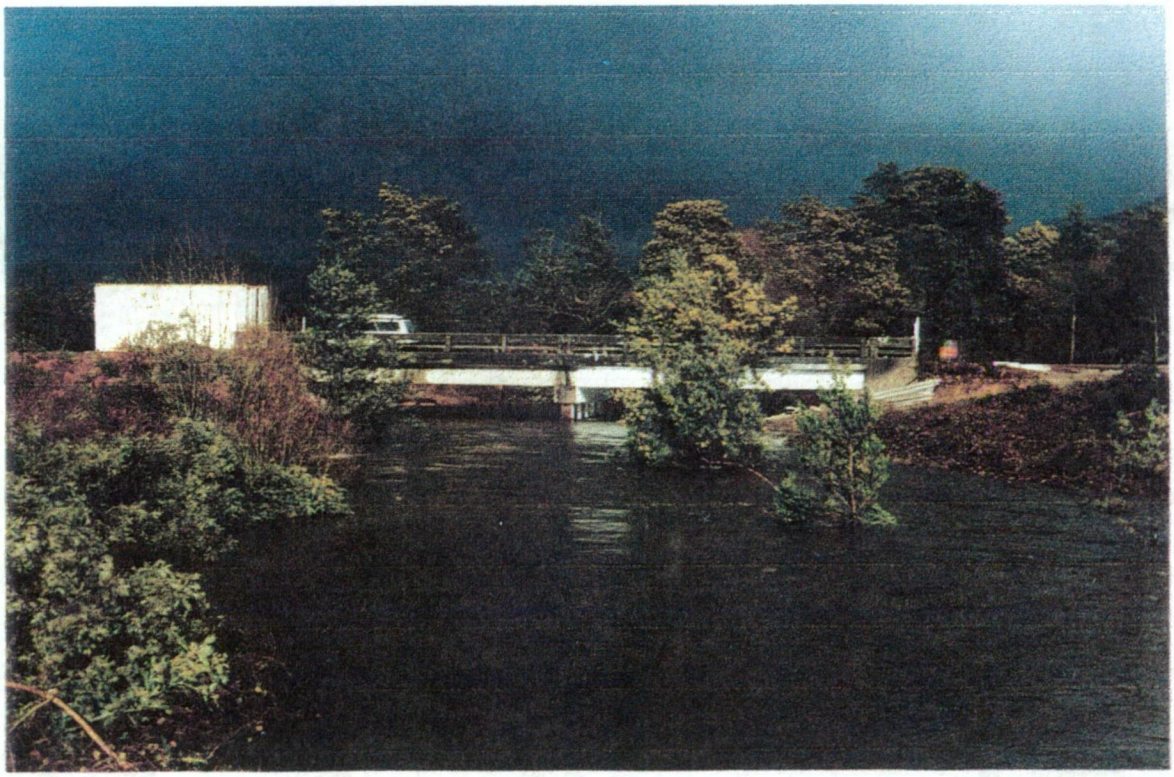

Submitted in fulfilment of the
requirements
for the degree of
Master of Engineering

University of Tasmania, November 1997

STATEMENTS

Declaration

This Thesis contains no material which has been accepted for a degree or diploma by the University of Tasmania or any other institution, and to the best of my knowledge and belief no material previously published or written by another person except where due acknowledgment is made in the text of the Thesis.

Authority of access

This Thesis may be made available for loan and limited copying in accordance with the Copyright Act 1968.

Acknowledgments

Assistance given by others in the test program is detailed in section 20 of the report.

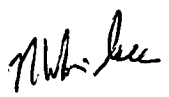

(Rodney William M'Gee)
9 November 1997

AUTHOR

The author is Manager Asset Strategies with the Department of Transport, Tasmania.

He graduated from the University of Tasmania with the degree of Bachelor of Engineering with Honours in 1977 and commenced work with the then Public Works Department in road and bridge construction. This was followed by a period of more than 11 years designing a range of bridges and other civil engineering structures.

In February 1990, the author was appointed to the position of Asset Management Engineer Bridges with responsibility for more than 1200 bridges, major culverts, marine structures and other civil engineering structures managed by the Department. The position also included responsibility for emergency management. He is also convenor of the AUSTROADS concrete durability project.

He has authored or co-authored sixteen technical papers in subject areas including bridge management, bridge design, concrete durability, diagnostic and assessment procedures for bridges, lead paint management, conservation of historic bridges, alkali aggregate reactivity, differential temperature in bridges and critical incident stress management.

Roles in the Princess River Bridge testing included:

- identification of the possibility of testing the bridge
- concept development
- project management
- preliminary design in conjunction with others acknowledged in the report
- site testing
- analysis and reporting.

CONTENTS

ABSTRACT

Princess River Bridge was a two span reinforced concrete T-beam bridge located on the Lyell Highway on Tasmania's west coast. It was inundated in 1991 by the King River Hydro Electric Power Development.

A program of testing was undertaken prior to inundation to assist with the understanding of bridge performance and the overall management of the State's bridge asset. The range of testing included dimensional, cracking and cover surveys, concrete and steel testing, dynamic response, load distribution, deck punching shear behaviour and ultimate capacity.

While bridge dimensions were generally within tolerance, 48% of measurements of cover to reinforcement were outside the range permitted in the current Australian Standard. The variability of cover is however consistent with that reported for bridges in the Sydney area and for other Tasmanian bridges.

Little flexural cracking was evident in the beams prior to testing. There was however a significant amount of random cracking in the deck soffit, which is likely to have been attributable to the permeability of the timber formwork and consequent implications for curing.

Concrete testing showed high strength due to relatively high cement contents. Concrete quality and the high relative humidities at the site would have contributed to the minimal carbonation. Steel tensile strength of 300 MPa was higher than the anticipated 230 to 250 MPa.

Measurements of dynamic response were able to discern the removal of sections of railing, but required substantial damage to beam reinforcement before observable changes in response occurred.

There was reasonable correlation between calculated and measured load distributions, although strains were underestimated.

Loading of the deck showed substantial capacity in punching shear. The load at which the bridge yielded was reasonably well predicted, and the bridge failed in a ductile manner.

1. INTRODUCTION

1.1 Introduction

The Princess River Bridge was located on Tasmania's west coast on the Lyell Highway, about 20 kilometres south of Queenstown. It was one of about sixty reinforced concrete T-beam bridges managed by the then Department of Roads and Transport.

The King River hydro-electric power development resulted in the flooding of the section of highway containing the bridge, providing an opportunity for a range of full-scale testing of a bridge in generally good condition.

1.2 Objectives

A program of testing was developed with the following objectives:

- To assist with rating of the State's bridges
- To assist with the calibration of bridge assessment software
- To confirm the validity of bridge design methods
- To assist with the assessment of durability of existing structures.
- To improve the Department's understanding of bridge behaviour.

1.3 Testing Program

The range of site testing was as follows:

- dimensional, cracking and cover surveys
- concrete and steel testing
- dynamic response
- load distribution
- punching shear behaviour of deck
- ultimate load capacity.

In addition, two beams which had been rejected during construction and left at the site were subsequently tested in flexure and shear.

1.4 Test Program

On-site testing was undertaken between 29 July and 22 August 1991. Ground anchors were installed and steelwork fabricated some time prior to the site testing. Field testing commenced prior to the closure of the section of highway which included the Princess River Bridge. The opening of the new section of highway and Bradshaw Bridge occurred on 7 August 1991.

Severe weather conditions were encountered during the test program, with closures of the Lyell Highway due to snow on at least 8, 9, 13 and 16 August, reducing the scope of the testing that could be conducted because of the inability of personnel to travel to the west coast.

The beams were tested at the Department of Construction's Lutana quarry on 2 and 3 June 1992.

1.5 Other Organisations

During preparation for the testing, a Vicroads research project on the use of dynamic measurements to assess bridge load capacity and the existence of defects affecting structural integrity was identified. The project was being undertaken by ETRS Consultants and University of Melbourne's Department of Civil and Agricultural Engineering, with University of Wollongong in a review role. All four organisations were involved in the field testing.

2. NOTATION

The following symbols are used in this report:

A_s	Area of reinforcing steel
A_{sc}	Area of compressive reinforcing steel
A_{st}	Area of tensile reinforcing steel
A_{ts}	Cross-sectional area of flexural tensile reinforcement
A_v	Total area of web reinforcement within a distance s
b	Width of reinforced concrete member
	Longer side of rectangular element
b_{eff}	Effective width of T-beam flange
C	Compressive force
C_Y	Catchment runoff coefficient for return period Y
c	Shorter side of rectangular element
c′	Factor for calculation of crack width
D	Bridge constant for evaluation of load distribution
	Distance from the point at which crack width is being considered to the extreme compressive fibre of the concrete
d	Depth of reinforced concrete member
d_n	Depth to neutral axis
E	Young's modulus of material
e	Strain
F_b	Allowable bending stress
F'_c	Concrete characteristic compressive strength
F_v	Allowable shear stress
f_c	Compressive stress
f_s	Steel stress
G	Shear modulus of material
g	Load distribution factor
I	Moment of inertia of section
J	Torsional moment of inertia
j	Ratio of lever arm of resisting couple to depth d for a flexural concrete member
k	depth from extreme compressive fibre to neutral axis of flexural concrete member
L	Effective span of a flexural member
l	Length of anchorage for ground anchor
M	Bending moment
M′	Effective moment capacity of concrete member
N	Specified cover to reinforcement
n	Modular ratio
P	Point load applied to member
p	Proportion of reinforcing steel
q	Percentage of reinforcement at midspan
Q_Y	Stream discharge for return period Y
R	Support reaction
r	Radius of gyration of section in the direction of eccentricity or bending
S	Centre to centre spacing of girders
	Factor of safety for ground anchor
s	Spacing interval of web reinforcement
s_o	Cross sectional area of steel reinforcing bar
T	Tensile force
	Capacity of prestressing anchorage
w	Mass per unit length of member or uniform load
V	Shear force
V'_s	External shear on section after deducting shear carried by concrete
Y	Annual frequency for hydrological analysis

y_c	Height to centroid of section
Z	Section modulus
	Factor for calculation of crack width
δ	Deflection
ε	Strain
ϕ	Capacity reduction factor
γ	Material density
μ	Poisson's ratio
ν	Shear stress
ρ	Material density
	Reinforcement ratio
σ	Bending stress
ω	Material density

3. BRIDGE AND SITE

3.1 Description of the Bridge

Princess River Bridge was a reinforced concrete structure with two 10.5m spans and a width of 6.7m between kerbs. The superstructure comprised 6 precast beams of upright rectangular section in each span, with an insitu concrete deck to form a T-beam structure.

The pier and both abutments comprised driven square reinforced concrete piles with insitu crossheads.

Bearings were lead sheets.

The bridge was built in 1959 and 1960 under contract by Hillier and Regan. It is understood that piles and beams were precast in Launceston by the Port of Launceston Authority and that aggregates for the insitu concrete were transported from Launceston.

Design was undertaken by the then Department of Public Works, with the design loading being H20-S16-44-P60.

The bridge superstructure cross-section is shown in Figure 3.1.

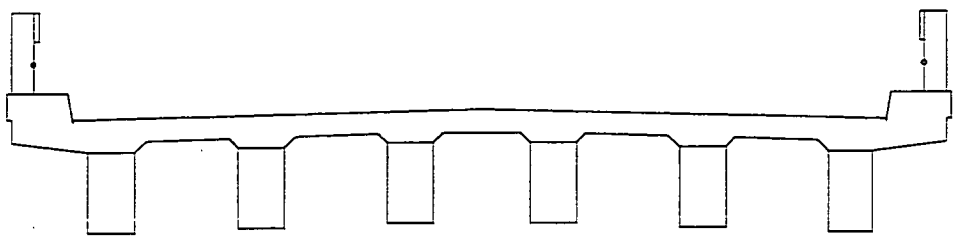

Figure 3.1 - Bridge Cross-section

Condition prior to testing was generally good, with the exception of the reinforced concrete fence and railings where spalling had resulted from corrosion of the reinforcing steel due to low reinforcement cover.

3.2 Geology

The Mines Department geological map (1:250 000) of Queenstown (1974) shows the area of the bridge site to be underlain by alluvium, sand, gravel and talus, with a Lower Devonian-Silurian siltstone-shale sequence to the north west. No rock outcrops were observed at the bridge site.

A limited geotechnical survey was undertaken to assist with the design of the system for loading the structure.

The seismic survey showed a low velocity material (290 to 400m/s) to 1m to 2.5m deep, followed by a material having an average seismic velocity of 1130 to 1420m/s to a depth varying between 6m and 12m, and thence a layer with an average seismic velocity of 4000 to 8000m/s.

Weather, with consequent effects on groundwater and stream levels, during the installation of the ground anchors precluded the taking of cores of foundation material, but drilling conditions confirmed the stratigraphy indicated by the seismic survey.

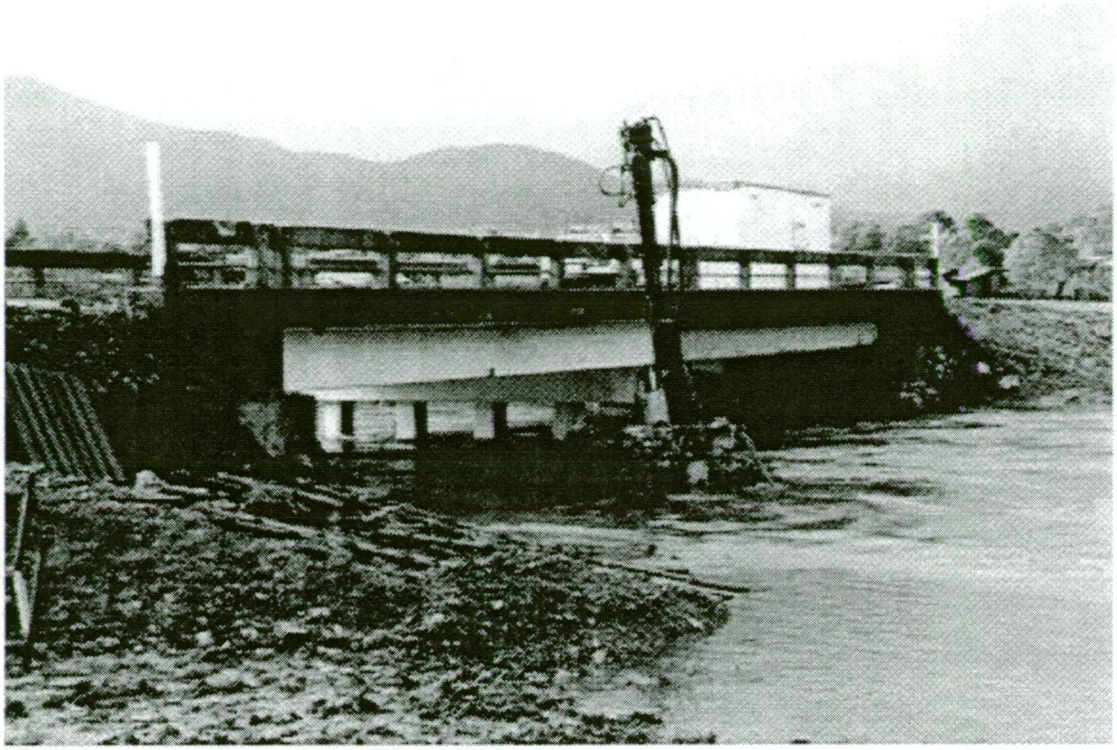

Figure 3.2 - Drilling Rig used for Anchor Installation

3.3 Bridge Records

Department of Transport files include initial contract and tender information but minimal construction records. It is likely that site concrete was site batched and few if any concrete test cylinders taken. No records of compression tests have been identified.

The Port of Launceston Authority had no records for the precast elements.

Records relating to the design and construction of the bridge are thus essentially confined to drawings 1805/P-1, P-2, P-3 and P-4, which are held as Department of Transport microfilms B3/485-488. Piles would have been built to standard drawings 1001 and 1002. Drawings are attached as figures 3.3 to 3.8.

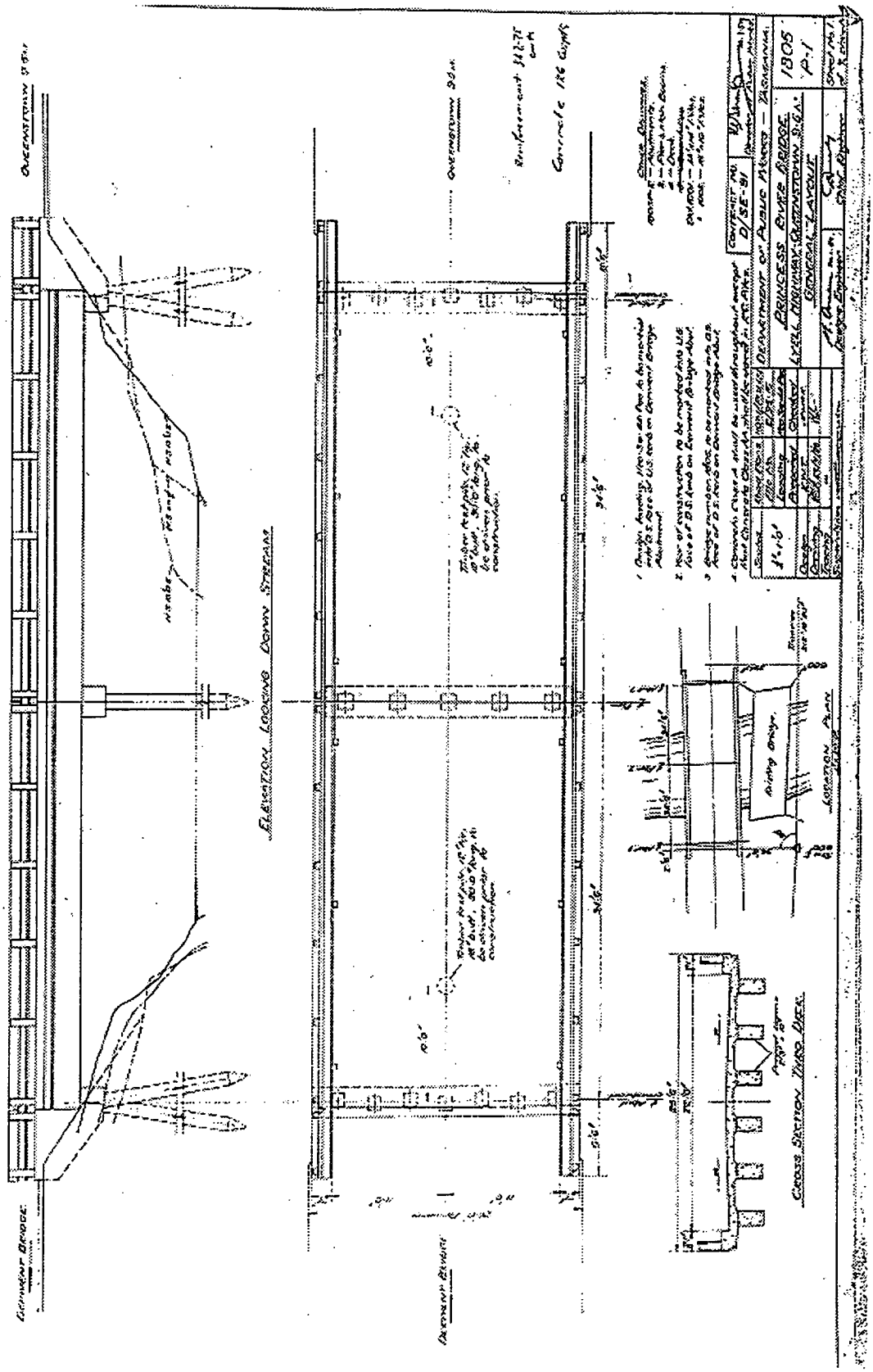

Figure 3.3 - General Layout

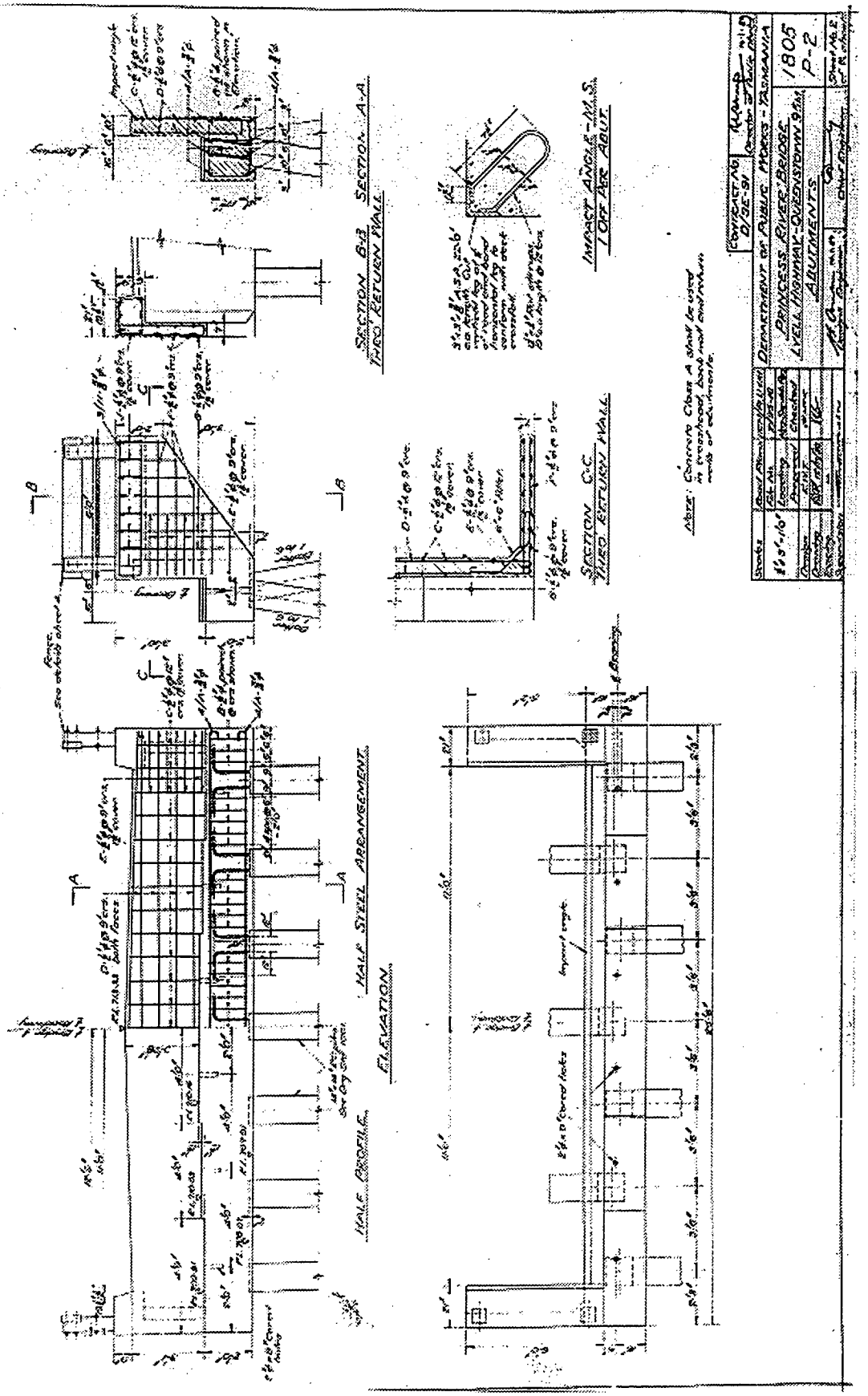

Figure 3.4 - Abutments

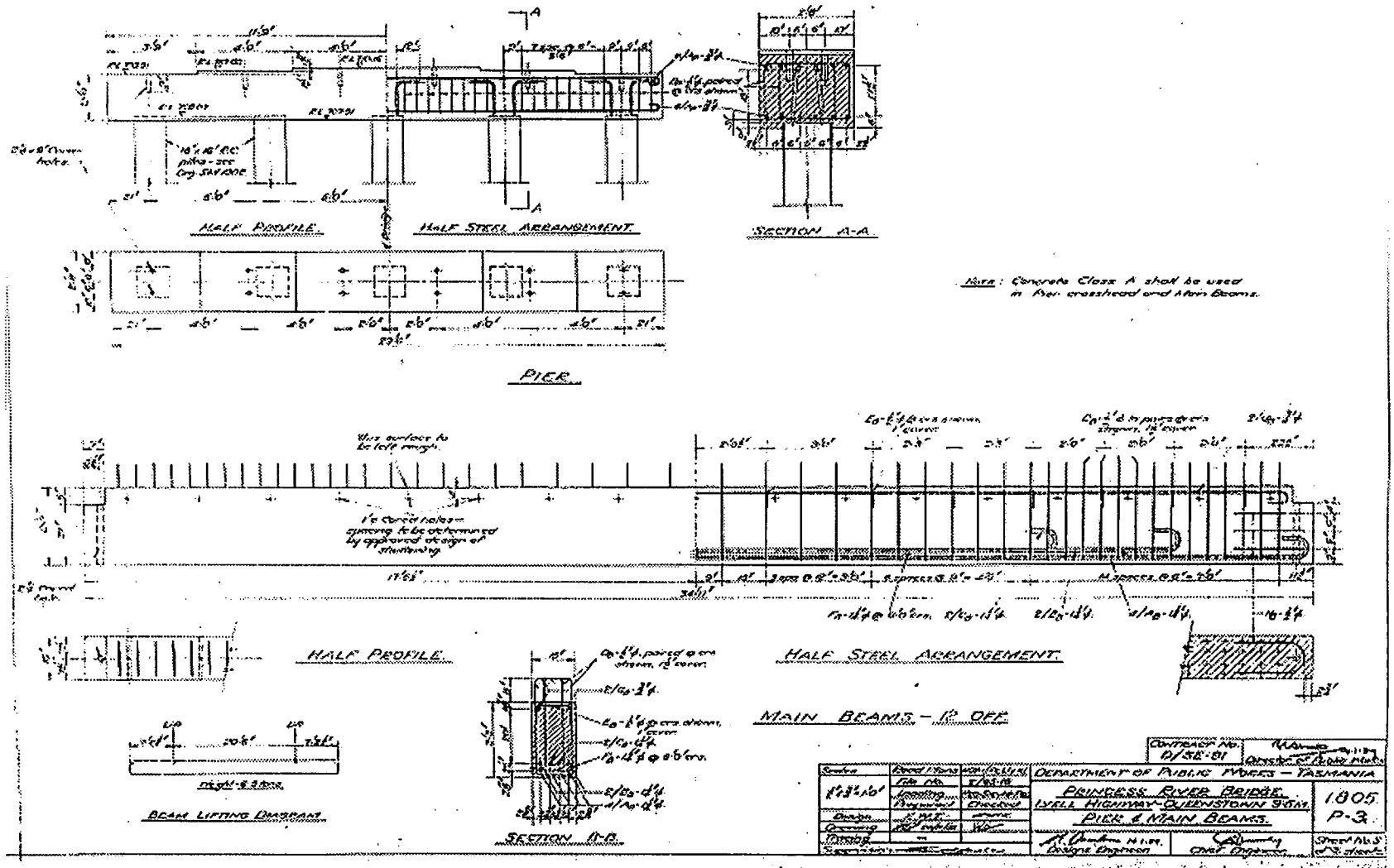

Figure 3.5 - Pier and Main Beams

Figure 3.6 - Deck

Figure 3.7 - 14" Square Pile

Figure 3.8 - 16" Square Pile

4. OBJECTIVES OF TEST PROGRAM

4.1 Background

The Department of Transport and its predecessors, the Department of Transport and Works, Department of Roads and Transport, the Department of Main Roads and the Public Works Department, is and have been the Tasmanian State Government Department responsible for the management of the State's roads, bridges and a number of marine facilities. It formerly had management responsibility, but not ownership, of bridges on council roads but that responsibility now rests with councils themselves, with Departmental involvement limited to generalised advice on bridge issues.

A section of the former Lyell Highway linking Hobart and Queenstown was flooded as part of the King River Power Development. The section of road contained two bridges:

- the King River Bridge, which had steel beams and timber deck supported on timber substructures
- the reinforced concrete Princess River Bridge.

The possibility of undertaking full scale testing of the Princess River Bridge was identified during a routine inspection of the bridge, and a test program developed.

There were five primary objectives of the testing program, which are described in more detail below. The objectives were:

- Rating of existing structures
- Calibration of bridge assessment software
- Confirmation of the validity of bridge design methods
- Assessment of durability and reliability of existing structures
- Improving the Department's understanding of bridge behaviour.

4.2 Rating of existing structures

There are about 60 reinforced concrete T-beam bridges on the classified road network with a replacement cost of the order of $30m. Years of completion range from 1926 to 1965, meaning that all were designed to loadings less than the current Austroads T44 design vehicle of 44t gross and current legal loading of 42.5t for a triaxle semi-trailer. Previous design loadings were H20-S16-44/MS18 with a 33t vehicle and the crusher train loading, which comprised a steam traction engine towing a mobile crushing plant.

A number of the bridges were assessed for structural adequacy as part of the introduction of RORVL A and C vehicle limits (41t and 42.5t gross legal mass for a triaxle semitrailer) into the State. The simplified methods used indicated stresses above those normally permissible in design codes, indicating a need for strengthening or replacement to maintain acceptable levels of risk for the travelling public.

Further, about three-quarters of the State's bridge stock is designed for the H20-S16-44 loading or less. The average age of the stock is over 30 years, with deterioration exacerbating any deficiencies in load capacity.

The testing program was intended to assist with the rating of existing structures for acceptable routine and permit loadings by increasing confidence in analytical methods.

4.3 Calibration of bridge assessment software

At the time of testing, a generalised computer program for the assessment of existing bridges was being developed as Cambridge University as part of a research contract for the Transport and Road Research Laboratory.

Ultimate load test results were used to assist with the calibration of the program.

4.4 Confirmation of the validity of bridge design methods

Few opportunities are available for the verification of the validity of the various methods and computer software used for the design of bridges. The testing provided the opportunity to validate the various methods used by the Department.

4.5 Assessment of durability of existing structures

Management of concrete bridges needs to consider rates of carbonation or chloride penetration or other deterioration processes such as sulphate attack or alkali aggregate reactivity, the quality of the concrete itself and the accuracy of construction. The test program was developed to provide data on a range of aspects of concrete durability for bridges in the Tasmanian west coast environment.

4.6 Improving the Department's understanding of bridge behaviour

Allied to the other objectives, the testing program was intended to provide an opportunity for design, construction and maintenance staff to observe all aspects of a bridge's behaviour.

4.7 Scope of Testing

To achieve the above objectives, the test program involved the following aspects:

- Literature survey
- Collation of data on local climate and hydrology
- Dimensional and cover surveys
- Measurements of pre-existing cracking
- Evaluation of concrete and steel performance
- Testing of individual beams
- Assessment of load distribution behaviour
- Measurement of dynamic response
- Assessment of punching shear capacity
- Determination of ultimate load capacity.

5. LITERATURE REVIEW

5.1 Introduction

An extensive literature review was undertaken as part of the Princess River Bridge test program and its reporting. Some of the relevant literature is described below.

5.2 Literature Review

5.2.1 Site Investigation of the Quality of Reinforcement Placement on Buildings and Bridges (Marrosszeky and Chew, 1989)

The paper reports the results of part of a research program undertaken at the Building Research Centre in New South Wales to investigate factors causing corrosion-induced durability faults in buildings.

The program studied the distribution and density of reinforcement corrosion induced faults on 95 buildings in the Sydney area from the coastline to 27km inland. A number of bridges were also studied.

The studies showed that the individual values and distribution of reinforcement covers varied greatly between projects. It was suggested that the actual cover that is achieved on site is influenced by such a complex combination of causes that no single factor could be identified as being more significant that any other. It was found that standards of reinforcement placement were higher for bridges than for buildings.

Results are shown diagrammatically in Figure 3.1, where N is the specified cover to reinforcement.

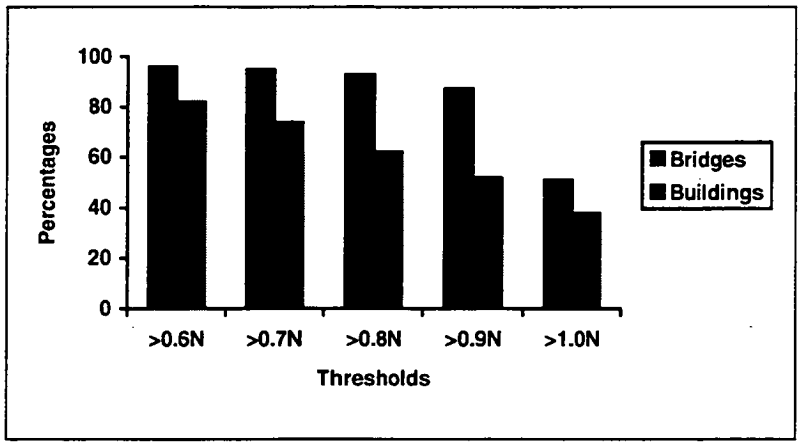

Figure 3.1 - Standards of Reinforcement Placement

5.2.2 Dimensional Variations in Reinforced-Concrete Members (Udoeyo and Ugbem, 1995)

The authors examined geometric variations in reinforced concrete members on three large project sites in Nigeria. All total of 3,380 measurements were taken, and analysed statistically. The study showed that increased levels of inspection reduced the variation in member sizes, and that normal distributions could be used for probability models of dimensional imperfections.

5.2.3 Effect of Core Diameter on Concrete Core Strengths (Bartlett and M*Gregor, 1994)

Small diameter cores are often used to assess concrete strength because they are easier to drill, handle and store than larger cores. Possible conflicts with reinforcing steel are minimised and a smaller hole is left for subsequent repair. It is often feasible to obtain a large number of small diameter cores from a structure. Small diameter cores may be the only

option where there are specific requirements, such as a length to diameter ratio of two with a thin section.

There has however been criticism that small diameter cores are unreliable. The paper reviews data from studies by others concerning the effect of specimen diameter on the magnitude and precision of the compressive strength of concrete cores.

Effects to be considered include size effects, core surface effects such as microcracking from drilling and cutting of aggregate particles, and inhomogeneity in concrete strength within a section.

The following conclusions were drawn:

1. The effect of damage to the surface layer in reducing the strength of small cores counteracts and overwhelms bias due to testing procedures or that might be explained by the weakest link theory.
2. The predicted average strength of a 2 inch diameter core is 94% of the predicted average strength of a 4 inch diameter core and 92% of the predicted average strength of a 6 inch diameter core.
3. Ratios of the average strength of 2 inch and 4 inch diameter cores have considerable scatter.
4. The core length-to-diameter ratio effect is greater for 2 inch diameter cores than it is for 4 inch diameter cores. If a correction factor of 0.88 is used to reduce the strength of a 4 inch diameter core with l/d = 1 to the equivalent strength of a core with l/d = 2, then a correction factor of about 0.80 should be used for 2 inch diameter cores.
5. The variability of measured strengths of small diameter cores is particularly sensitive to being inflated by the variability of insitu strength across the section being cored.
6. For cores with large diameters, the coefficient of variation of the core strength depends mostly on the variability of the undamaged interior region. For smaller diameter cores, the coefficient of variation depends mostly on the variance of the thickness of the damaged region.

5.2.4 A New Look at Shrinkage Cracking (Base and Murray, 1982)

Shrinkage cracks are induced in structures by shrinkage and thermal strains in the concrete. For the purposes of their paper, Base and Murray define shrinkage cracks as those that penetrate completely through the member. Detrimental consequences can include leakage, tiling damage in floors, and aesthetics. The paper discusses the difference between shrinkage and flexural cracking, and presents design formulae, graphs and procedures for limiting shrinkage cracking in structures.

5.2.5 Causes, Evaluation and Repair of Cracks in Concrete Structures (ACI Committee 224)

Cracks in concrete have many causes. They may affect appearance only, or they may indicate structural distress or a lack of durability. Their significance depends on the type of structure as well as the nature of the cracking. Successful repair depends on knowing the causes of the cracking and selecting the appropriate repair method. The report discusses causes and control of cracking in both plastic and hardened concrete, evaluation of cracking and methods of crack repair.

5.2.6 Lateral Distribution Factors for Highway Bridges (Bakht and Moses, 1988)

The American Association of State Highway and Transportation Officials (AASHTO) specifications for highway bridge design provide simplistic distribution factors, which lead to fairly conservative designs. The simplicity of the AASHTO method is predicated on three basic assumptions:

1. the transverse pattern of distribution of a load effect is independent of the longitudinal position of the loads and the reference sections
2. the transverse patterns of distributions of various load effects are similar, and

3. the bridge conforms to a basic form and it does not possess any complicating factors such as edge stiffening, skew, etc.

The paper discusses the limitations of the AASHTO method and presents the method incorporated in the Ontario Highway Bridge Design Code, which uses two characterising parameters, an additional dimensionless parameter and a series of charts. Different factors are used for bending and for shear. Different loading conditions are used for fatigue design.

The method was validated by comparing its results to those obtained by the rigorous finite element analysis of several actual bridges.

5.2.7 Wheel Load Distribution on Simply Supported Skew I-Beam Composite Bridges (Bishara, Liu and El-Ali, 1993)

The paper presents distribution factor expressions for wheel load distributions to the interior and exterior girders of multibeam composite steel girder bridges derived from finite element analyses of 36 bridges of varying spans, widths and skews and with differing cross-bracing configurations. The validity of the results was confirmed by testing of a 137′ span four lane bridge.

The following conclusions were drawn:

- distribution factors for both interior and exterior girders were significantly lower than those determined from AASHTO methods
- bending moments in interior girders in skew bridges were significantly lower than those in right bridges, with reductions of around 5% for a skew angle of 30° to 28% for a skew angle of 60°. The reductions are less in exterior girders in smaller skew, with a slight increase at the higher skew angles.
- the distribution factor for interior girders was practically insensitive to span length for the 75′, 100′ and 125′ span lengths used.
- for the same size of cross-frames, a reduced spacing improves load distribution.

5.2.8 Distribution of Wheel Loads on Highway Bridges (National Co-operative Highway Research Program, 1992)

The document is a digest of the findings from the final report of National Co-operative Highway Research Program Project 12-26, which was conducted in the mid-1980's in order to develop comprehensive specification provisions for the distribution of wheel loads in highway bridges. The project encompassed beam-and-slab, box girder, slab, multibox beam and spread box beam bridges and three levels of analysis, from detailed modelling of bridge decks, through graphical methods and simplified computer programs, to simple formulae.

At the time of the study, the American Association of State Highway and Transportation Officials bridge design specifications allowed for simplified analysis of bridge superstructures using the concept of a wheel load distribution factor for bending moments in the interior girders of most types of bridges. The distribution factor is given by:

$$g = S/D$$

where g = a factor used to multiply the total longitudinal response due to a single longitudinal line of wheel loads in order to determine the maximum response of a single girder; S = the centre-to-centre girder spacing; and D = a constant that varies with bridge type and geometry.

The distribution factors had been developed for non-skewed, simply supported bridges, but there were no other guidelines for the common situation where those conditions did not apply.

The study found that finite element analysis of bridge decks provided accurate results, provided that extreme care was taken in preparation of the model and that the computer program was capable of accurately modelling the responses being investigated. Where the program reports stresses and strains, care must be taken in calculating the associated moment and shear values. Grillage analysis presents a good alternative to other simplified bridge deck analysis methods, and will generally produce more accurate results. The digest presented simplified formulae for load distribution which, although more complex than the current specifications, provided more accurate results from a relatively simple calculation.

5.2.9 Distribution of Wheel Loads on Highway Bridges (Zokaie, Imbsen and Osterkamp, 1991)

The paper presents the findings of research on the distribution of wheel loads on highway bridges undertaken as part of the National Highway Co-operative Research Program. Bridge types investigated were beam and slab, box girder, slab, multi box-beam and spread box-beam bridges. Three levels of analysis were considered:

- detailed modelling of the bridge superstructure
- graphical methods, nomographs, influence surfaces and simplified computer programs used to apply such methods
- simple formulae to predict lateral load distribution.

Simplified procedures incorporated in AASHTO specifications in use for some 55 years were developed for non-skewed simply supported bridges. Contemporary practice however involves a large number of bridges to be built with skewed supports, on curved alignments and/or continuous over interior supports. The accuracy of the simplified formulae was assessed to range from highly unconservative (more than 40%) to highly conservative (more than 50%). The formulae developed as part of the research program gave results within 5% of the highest level (most-accurate) analysis. Grillage analysis was found to be a good alternative to the simplified graphical or computer methods. Recommendations of computer programs for the highest level analysis are made.

5.2.10 Nonlinear Finite Element Analysis of Deteriorated RC Slab Bridge (Shahrooz, Ho, Aktan, de Borst, Blaauwendrad, van der Veen, Iding and Miller, 1994)

The paper focuses on the presentation of predictive analyses, using nonlinear finite element analysis software, of the responses of a decommissioned bridge with experimental results.

The bridge was a 38 year old three-span reinforced concrete skewed slab bridge which had been decommissioned because of its deteriorated state. Causes of deterioration are not described, but may have been attributable to the use of deicing salts on the roadway. Standard tests on concrete cores indicated an average compressive strength of 52 MPa, tensile strength of 4.5 MPa and modulus of elasticity of 34,000 MPa. Reinforcing bar had yield and ultimate stresses of 345 MPa and 680 MPa respectively with a modulus of elasticity of 199,800 MPa and strain hardening modulus of approximately 3.5% of the elastic modulus.

Using modal tests, approximate elastic stiffness characteristics of the abutments were identified. Three loaded trucks, each weighing 142 kN were placed on the bridge deck in six different configurations and vertical deflection profiles of the deck slab measured. Destructive tests were undertaken with four hydraulic servo-controlled actuators to simulate the footprint of a tandem semi-trailer. Failure occurred in a brittle manner at a total load of 3200 kN. First yield of reinforcing bars had occurred at a total load of 2893 kN.

Prior to the testing, predictive analyses were carried out with a range of methods from simple yield line analysis to linear and nonlinear finite element analysis.

A close match between measured failure load and that predicted by yield line analysis was considered as coincidental because the bridge did not fail in a flexural mode. Finite element

analysis demonstrated an important role of slab membrane force, which is directly affected by assumed horizontal support conditions.

5.2.11 Bearing Restraint in Slab-on-Girder Bridges (Bakht and Jaeger, 1988)

Tests on a large number of bridges in Ontario have shown that slab-on-girder bridges are usually significantly stiffer in flexure that is predicted by analysis. The tests have also shown that, in a single-span right bridge, the total longitudinal moment across a transverse section, as calculated by measured girder strains, is nearly always less than the total moment at the transverse section as calculated by treating the whole bridge as a simply supported beam.

From a systematic study of the problem, it has been concluded that slab-on-girder bridges are stiffer mainly because of horizontal restraint provided by the girder bearings. The restraint can reduce live load moments in existing single-span slab-on-girder bridges by up to 20%.

It was suggested that bearings, of a type that permits horizontal support movement, were not needed in short-span bridges.

While the reduction in live load effects due to the restraint for new bridges was open to question, the beneficial effects could be used to advantage in the evaluation of existing structures.

5.2.12 Simulation of Dynamic Load for Bridges (Hwang and Nowak, 1991)

The objectives of the study were to develop a procedure for calculation of the dynamic load and to determine statistical parameters of the dynamic load to be used in the development of a reliability-based bridge design code (the Ontario Highway Bridge Design Code 1983).

Models were developed for trucks, comprising body, tyres and suspension system, composite steel girder and prestressed concrete bridges with simply supported spans between 12m and 30m, and the road surface.

A large number of computer simulations were undertaken.

The study concluded that:

- the dynamic load factor decreases as the gross vehicle mass increases
- the maximum midspan dynamic deflection is however almost constant regardless of the wieght of the truck, meaning that dynamic and static loads could be considered uncorrelated except 30m spans, for which a low degree of correlation was observed
- the dynamic load factor was higher for 30m and 12m spans than for 24m and 18m spans
- the coefficients of variation ranged from 40% to 70%, depending on the span length of the bridge, indicating significant scatter in the dynamic effects
- the dynamic load factors for two side-by-side trucks were lower than for one truck
- dynamic load factors varied from 0.09 to 0.21.

5.2.13 Modal Analysis for Damage Detection in Structures (Hearn and Testa, 1991)

Natural frequencies, mode shapes and modal damping coefficients in structures are affected by changes in condition, providing opportunities for inspection and monitoring of structures. The nature of the effects is dependent upon the element affected and the nature of the deterioration.

Experiments were undertaken on a welded steel frame and a wire rope to validate dynamic monitoring as a method of structural inspection.

5.2.14 Bridge Assessment Using Forced-Vibration Testing (Salawu and Williams, 1995)

Full-scale forced vibration tests were carried out on a multispan reinforced concrete highway bridge before and after repairs for structural cracking caused by alkali aggregate reaction

and to address changes in design requirements since the bridge was built in the 1960's. The bridge was excited using an hydraulic actuator, and the bridge response measured using accelerometers. As a result of the test program, it was concluded that:

- the natural frequencies of the bridge did not change significantly as a result of structural repairs
- comparison of the components of the normalised cumulative frequency-response function was able to give an indication of the changes to the bridge's condition
- changes in mode shapes were found to give a good indication of the presence and location of repairs
- a procedure to assess the condition of bridge structures was proposed, although it was recognised that there were limitations.

5.2.15 Dynamic Assessment of Bridge Load-Carrying Capacities I and II (Law, Ward, Shi, Chen, Waldron and Taylor)

A one-fifth model of a reinforced concrete T-beam bridge was tested to destruction, with the vibrational response to ambient excitation measured at different stages of cracking and spalling. Parametric studies were undertaken of the effects of different boundary conditions on the fundamental modal frequency.

Principles from the model testing were subsequently used for measuring responses of 13 full-scale bridge decks. It was concluded that it was feasible to use the method to assess the structural condition of bridge decks.

5.2.16 Membrane Action, and Design Against Punching Shear (Chana and Desai, 1992)

The paper discusses a test program to study and quantify the effect of membrane action on the punching shear resistance of slabs and to provide design recommendations.

Five reinforced concrete slabs 9m x 9m plan dimensions and 250mm thick, representing areas of slab surrounding internal columns of continuous flat slabs, were tested.

All specimens failed in a brittle manner in a punching shear mode. The extent of cracking on the tension face and the crack widths were reduced compared to conventional punching shear specimens.

It was concluded that there was a significant increase in shear capacity attributable to membrane action developed by the extent of slab outside the failure zone.

5.2.17 Punching Capacity of Deck Slabs in Girder-Slab Bridges (Azad, Baluch, Abbasi and Kareem, 1994)

Static tests were conducted on a series of simulated deck panels of girder-slab bridges to determine the punching resistance of the reinforced slabs, with the aim of generating reliable test data from representative large-scale models. Three sets of four identical panels, with varying amounts of reinforcement, were cast with testing involving loads applied over four different load areas. Sudden push-out type failure occurred in all cases, with the top surface of the displaced concrete cone equal to the load area and the bottom encompassing a larger area. Code provisions for punching shear failure are generally based on a slip plane at an angle of 45^0. The experimental work described in the paper, and previous work, have indicated that the angle of the slip plane is expected to lie within the range of 20^0 to 35^0 to the horizontal, meaning that codes yield conservative results, particularly for small patch loads, and providing scope for refinement.

5.2.18 Strength Evaluation of M-beam Bridge Deck Slabs (Kirkpatrick, Rankin and Long, 1984)

The paper discusses the testing of a 1/3 scale model of a bridge deck to assess the possibility of reducing bridge costs by increasing the spacing of the British standard prestressed M-beams from 1m to 2m.

Analysis using the equations of Westergaard had shown that an area of steel reinforcement of the order of 1.7% of the cross-sectional area of the deck was required. For test purposes, areas of 0.25%, 0.49%, 1.19% and 1.68% were provided.

While bridge deck slabs are commonly designed by flexural methods, all twenty test panels failed by punching shear.

It was concluded that the existing British bridge codes did not provide an accurate prediction of the ultimate load capacity of the M-beam deck slab, as no account was taken of the considerable enhancement in capacity from the in-plane restraint of the deck. A simplified design method was proposed. Observations from the model tests indicated that an isotropic mesh of 0.5% area of deformed bars would provide an adequate level of serviceability.

5.2.19 The Influence of Compressive Membrane Action on the Serviceability of Beam and Slab Bridge Decks (Kirkpatrick, Rankin and Long, 1986)
The paper discusses the testing of a full-scale bridge which was built with beam spacings up to twice normal to establish serviceability criteria and other performance characteristics that could not be properly assessed with the third scale model. It was found that contemporary methods of calculating crack widths based on flexural analysis were not applicable to bridge decks where the development of compressive membrane action resulted in improved serviceability characteristics. It also found that compressive membrane forces played an important part in the control of cracking in the slab even at relatively low levels of load, and that all test panels were uncracked at the service load.

5.2.20 Compressive membrane action strength enhancement in uniformly loaded, laterally restrained slabs (Rankin, Niblock, Skates and Long, 1991)
The paper follows the investigation of membrane action in M-beam bridge decks and examines the effect in uniformly loaded, laterally restrained rectangular reinforced concrete slabs.

Seven rigidly restrained and four unrestrained slab models, all 0.95m square and isotropically reinforced with 0% to 1.57% reinforcement were tested for the effects of compressive membrane action.

Compressive membrane action applies to transient or short-term loadings because creep of concrete will increase deflections and reduce the arching moment lever arm for long-term loadings.

The combined experimental and analytical study found that the ultimate capacities and post-cracking stiffnesses of uniformly loaded, laterally restrained slabs were considerably enhanced by the effects of compressive membrane action. A simple analytical method was developed to predict the strength of restrained slabs.

5.2.21 The Global and Local Behaviour of Bridge Deck Slabs (Jackson, 1990)
In bridge design, the global and local behaviours of bridge decks are generally considered separately. Research has however shown that bridge deck slabs are able to resist very much higher wheel loads than is implied by conventional design methods. As a result, empirical design methods for deck slab reinforcement have been incorporated in codes such as the Ontario Highway Bridge Design Code.

Non-linear analysis shows that global transverse moments could significantly reduce the local strength of bridge deck slabs, and this was confirmed by tests on two half-scale model bridge decks. Brittle punching shear type failures occurred in the models; these were considered to be primarily brittle bending compression failures. Despite the reductions in

strength due to global transverse moments and the brittle nature of the failures, capacities of the deck slabs were nevertheless high and the empirical design rules considered to result in acceptable designs.

5.2.22 Punching Shear Behaviour of Restrained Reinforced Concrete Slabs (Kuang, 1991)
When a slab is restrained against lateral expansion, membrane compressive forces are developed. Membrane action is generally considered as a secondary effect which occurs after cracking of the concrete or yielding of the reinforcement, and has been found to result in substantial enhancements in the load carrying capacity of restrained concrete slabs. The report presents the results of a number of tests on concrete slabs. Conclusions include the failure of all the slabs in punching mode, the development of compressive membrane forces, greater restraint resulting in greater enhancement in load capacity, and the strength of the slabs being greater than that predicted by Johansen's yield-line theory and code provisions.

5.2.23 Behaviour of Isotropic R/C Bridge Decks on Steel Girders (Fang I K, Worley J, Burns N H and Klingner R E)
The paper describes an experimental and analytical investigation into the behaviour of reinforced concrete bridge decks designed to Ontario Code provisions, with about 60% of the reinforcement required by the AASHTO Code. It concludes that the bridge decks behave satisfactorily under design loadings, that behaviour of the slab was essentially linear under overload conditions, significant compressive forces were present in the deck after cracking, and that there was good correlation between analytical predictions and experimental observations using a smeared cracking model.

5.2.24 Cracking, Serviceability and Strength of Concrete Bridge Decks (Allen, 1991)
The paper discusses extensively a number of aspects of the behaviour of isotropic and orthotropic bridge decks, including shrinkage cracking, compression membrane action and live and fatigue load behaviour.

The following conclusions are drawn from the work:
- high collapse strength, or punch-out strength, of a bridge deck does not assure adequate serviceability
- isotropic decks which have transverse-through-shrinkage cracking exhibit serious serviceability problems
- vehicle loads are sufficient to cause flexural cracking in many isotropic or conventional bridge decks
- strength of isotropic bridge decks after cracking is not adequate
- the load regime under moving loads is more severe than fixed position loads
- flexural moments in the negative moment region over the interior girders are well below the flexural cracking strength of the concrete
- decks with full flexural positive moment reinforcing according to AASHTO provide satisfactory strength
- a bottom-layer only AASHTO deck will not suffer degradation from corrosion of top reinforcing bars and can be expected to have superior durability compared to two layers with either isotropic or AASHTO reinforcing
- the greatest efficiency and economy of reinforcement placement for a specified strength is achieved when reinforcing is confined to the bottom mat.

5.2.25 Assessment Implications from Tests on a Model Concrete Beam and Slab Bridge (Daly and Cullington, 1991)
A half-scale model prestressed concrete bridge deck was tested to collapse in the Transport and Road Research Laboratory Structures Laboratory. The deck was tested under dead load, superimposed dead load and live load, as specified in BS 5400: Part 2, with the HB component of live load increased until failure.

Member forces calculated from a linear grillage analysis were compared with test results.

The study concluded that the design, which complied with BS 5400, was conservative but that the overall margin was not large. The model failed at 3.17 times the HB load factored for the ultimate limit state. The unfactored code calculation indicated failure at 2.8 times the HB load.

In some areas there were reserves of strength which could possibly be used in the assessment of similar structures. Examples are flexure in the slab, torsion in the beams and end diaphragms, interfacial shear, web crushing, combined shear and torsion, and shear strength close to the support.

5.2.26 Tests on a Half-Scale Prestressed Beam and Slab Bridge Deck (Withey, 1989)
The report describes the testing of half-scale model bridges and section of bridges and comparisons with results from elastic and nonlinear models of analysis.

The model was loaded by means of single acting hydraulic jacks. Instrumentation comprised linear variable differential transformer transducers and electrical resistance strain gauges.

Eventual failure of the model was shear dominated, but did not occur in a brittle manner because of yielding of elements and redistribution.

Elastic methods predicted behaviour well at lower loads, although there is difficulty in predicting the properties of materials. At higher loads, elastic methods were unsatisfactory. Mechanism methods were even less satisfactory because of inadequate modelling of the beam and slab configuration.

A finite element model with a fine mesh predicted behaviour well up to the point where bending was no longer the major mode of displacement.

The mode of failure emphasised that if arbitrarily large factors of safety are applied to the principal or desired mode of failure, then other modes of failure, such as shear, will become more likely. Similarly the effect of extra strengthening can change failure modes from ductile to brittle.

5.2.27 Strength of Concrete T-Beam Bridges (Beal, 1985)
A series of static load tests were performed on two concrete T-beam bridges, both built in 1931, to evaluate the stresses induced in tensile reinforcement and transverse load distribution factors. While the two structures were similar in dimensions and reinforcing, they had markedly different qualities of concrete. The load tests showed no difference in bridge behaviour attributable to concrete condition.

To obtain data on failure capacity, testing was performed on two single and one double T segment taken from the deteriorated structure. The measured failure moments exceeded the nominal flexural strength as given by ordinary ultimate strength design methods.

5.2.28 Application of Field Testing to Bridge Evaluation (Moses, Lebet and Bez, 1994)
The paper explores bridge testing as a specific part of the evaluation and assessment of bridges, especially for cases in which a safe capacity evaluation or bridge capacity rating must be carried out.

Extensive programs of bridge testing have been undertaken in Switzerland, where all structures are tested before going into service, and in Ontario as part of a program of verifying capacities of older bridges. In other cases, bridges have been tested at loads much below service loads to diagnose bridge behaviour, particularly load distribution, and under normal traffic loadings to assess dynamic responses and spectra for fatigue estimates.

The Swiss bridge test consists of about one day of placement of four to eight heavy dump-truck types vehicles in different positions on the bridge to simulate longitudinal centre moments, torsional effects and support negative moments. Each test vehicle has a gross mass of approximately 250kN. The major concerns during the tests are as follows:

- obtain agreement for each load case between computed and measured displacements at a number of locations along the girders
- behaviour should be linear so that displacements return to zero when the load is removed
- crack opening during load application should be within acceptable limits.

In addition, dynamic responses are measured to provide a record of bridge displacements, impacts, frequencies and crack widths.

The author considers an extension of the Swiss technique to the evaluation of existing bridges. Such evaluations may be necessary for a number of reasons:

- calculations have shown that a structure is not capable of meeting present standards
- inspections have revealed a loss of capacity such that the strength may have fallen below the level needed for meeting the load criteria
- to measure directly the stress spectra to evaluate a possible fatigue prone detail.

It was concluded that field testing provides a number of benefits from a safety point of view. The use of load levels of about 0.85 times the design load includes both benefits of diagnostic testing and proof loading in bridge evaluation. The tests are relatively simple to perform and give information about serviceability performance for long term durability, behaviour data for the bridge to verify the prediction model, and a significant degree of strength uncertainty truncation.

For reliability analysis, bridge testing may result in higher safety indices because or reduced behaviour uncertainty and truncation of the lower section of the resistance curve.

5.2.29 The AASHO Road Test, Report 4, Bridge Research (Highway Research Board, 1962)

The AASHO Road Test was a study of the performance and capabilities of highway pavement and bridge structures under moving loads of known magnitude and frequency. Eighteen beam and slab bridges, comprising ten with steel beams, four with prestressed concrete beams and four reinforced concrete T-beams, were included in the program. The testing was undertaken in Ottawa, Illinois between 1958 and 1961, with construction of the bridges having commenced in 1956. The program involved trucks of known configurations travelling on specially built loops to test both pavement and structures. The bridges were instrumented for strain and deflection.

Five types of tests were conducted, with the principal tests being concerned with the behaviour and life of the bridges under repeated high overstress. Discussion in this report focuses on the reinforced concrete bridges.

Before traffic began using the bridges, dead load stresses in the bottom bars of the beams at midspan were lower than those predicted by straightline cracked section theory. The stresses remained essentially the same until traffic commenced, when there was a rapid growth in cracking of the reinforced concrete, resulting in a progressive increase in stresses to those calculated by straightline theory. The slabs resisted 2% to 13% of external moments from vehicles in addition to their role as top flanges of the reinforced concrete beams. There was good agreement between calculated and measured stresses in interior beams, but exterior beams carried higher stresses. Under repeated loadings, tension cracking in all of the reinforced concrete beams increased. In the lower stressed beams, the increase consisted primarily of new vertical cracks and extensions of the cracks existing before the commencement of traffic. In the higher stressed bridges, numerous inclined cracks formed in

the outer 4.5m of the beams and a considerable amount of irregular cracking occurred near the level of the reinforcement. Live load deflections increased with time because of lower stiffness. All four reinforced concrete bridges survived the 556,000 trips of regular test vehicles. Accelerated fatigue tests were conducted with three of the bridges, proceeding without change in the response or general behaviour of the bridges until bars fractured or the tests were discontinued. In the two bridges stressed to higher levels, two bars in the exterior beam fractured after approximately 730,000 cycles. In the lower stressed bridge, a total of 1,500,000 stress cycles was reached without failure. Two bridges were tested to failure, which occurred by yielding of the tension reinforcement followed by crushing of the slab.

For estimating the limit of elastic behaviour, the moment at first yielding of the reinforcement computed from the ordinary straightline cracked-section theory and from the yield point of the reinforcing bars was found satisfactory. The maximum static moment applied in the ultimate strength test exceeded the computed strength, calculated from commonly accepted formulae based on beam tests, by 4 percent. Comparisons between laboratory fatigue tests on beams and the life determined by Miner's hypothesis of cumulative damage for applied loads suggested that the test bridges were slightly weaker in fatigue than indicated by the lower limit of the laboratory data.

5.2.30 Strength Evaluation by Testing of an Old T-Beam Bridge (Mufti and Bakht, 1991)
The paper discusses the testing of a rigid frame reinforced concrete T-beam bridge which had deteriorated extensively and was posted for a load limit of 5 tonnes, with the two outer lanes blocked to traffic. It was likely that the bridge had been built in either 1912 or 1926, with testing undertaken in 1991. The clear span of the bridge was 9.8m and the overall width 20.1m.

Although drawings were not available, a pretest analysis was undertaken using the semicontinuum analysis computer program SECANI with assumptions that the span was 9.75m, all girders were of equal stiffness, the deck slab was 200mm thick and that each girder had a width of 460mm and depth of 690mm below the deck slab. While the computer program can only analyse simply supported bridges, it has been shown by Jaeger and Bakht (1989) that the semicontinuum method of analysis can be applied to the positive moment region of rigid frame bridges by using a simply supported span length of L/1.5, where L is the span of the rigid frame bridge. The analysis found that distribution factors for deflections and moments were within 5% of each other.

Instrumentation was primarily with deflection transducers, although some strain gauges were fitted. The bridge was tested with two special vehicles, and loads increased by adding concrete blocks. The vehicles were placed at a number of longitudinal and transverse positions.

The allowable loading was calculated from the 1983 Ontario Highway Bridge Design Code, using appropriate capacity reduction, dynamic load and multiple lane loading factors. As a result of the testing it was recommended that the posting of 5 tonnes be upgraded to a single posting of 19 tonnes or triple posting of 19, 26 and 35 tonnes.

5.2.31 Old Concrete Slab Bridges, Experimental Investigation and Analysis (Azizinamini A, Boothby T E and Shekar Y, 1994)
The papers report on a program of testing of a number of reinforced concrete slab bridges. Six of the bridges were tested under truck loadings, with the weight of each truck selected to ensure that the response of each bridge was confined to the elastic range only. Another five span bridge, built in 1938 and decommissioned since 1972, was subjected to a range of tests including ultimate load tests.

The experimental work showed tensile strains in the bottoms of slabs to be higher than compressive strains at the tops of the slabs, attributable to the opening of cracks which open as the structure is loaded. The bridges behaved in a linear elastic manner under truck loading, with principles of superposition applying. Kerbs were found to contribute significantly to load capacity. Dynamic tests found good correlation between impact factors derived from slab tensile strains and deflections. Impact factors derived from compressive strains at the top of the slab were consistently higher. The use of a board fixed to the ground at bridge abutments did not necessarily increase the impact factor. No apparent correlation was found between span length and impact factor.

A number of tests were conducted on the bridge tested to failure. Behaviour was found to be linear at lower loads, with no damage observed. At higher loads, permanent deformations occurred, but behaviour was linear elastic for subsequent loadings less than the previously applied load. Failure of the continuous span was ductile, with a maximum observed deflection in excess of 127mm. For the simple span, yielding of bars and a deflection of more than 25mm occurred prior to failure, which resulted from punching shear failure over one of the loading rams. The testing showed the bridge capacity to be significantly higher than predicted by the current rating procedures.

Finite element and yield line analyses of the bridges were undertaken. Displacement results from the three-dimensional analyses were in good agreement with the test results. Analytical studies incorporating a moment-curvature analysis approach, together with actual material properties, found that the higher observed capacity of the bridges could be attributed to the actual rather than assumed material properties and the participation of kerbs in load carrying capacity. The studies also indicated that there were significant differences between the maximum bending moments obtained from two- and three-dimensional analyses because of the participation of non-structural elements, such as kerbs. It was concluded that old concrete slab bridges have significant reserves of capacity and that yield-line analysis and three-dimensional finite element analysis could be used to address the strength capacity and load effect aspects of bridge rating. Adequate strength reduction and load factors however need to be developed for the rating process.

5.2.32 Destructive Testing of Decommissioned Concrete Slab Bridge (Miller, Aktan and Shahrooz, 1994)

The paper describes the destructive testing of a 38-year old deteriorated concrete slab bridge, with the goal of observing the behaviour of the bridge at various load levels and using the information to verify analytical bridge evaluation techniques.

The loading system was designed to simulate the footprint of a HS20-44 truck, and used hydraulic cylinders and rock anchors to apply the load

Approximately 150 instruments were used to measure displacements, rotations, distortions and reinforcement strains.

Final failure was by punching shear of the slab.

Modelling of behaviour used an effective strip model, linear finite element analysis and nonlinear finite element analysis.

The following conclusions were drawn:

- the total failure load of 3200kN was equivalent to 22 HS20-44 trucks, indicating that decommissioning on the basis of inadequate load capacity was not warranted
- the response of the bridge was marked by behavioural changes (limit states) that occurred in various parts of the structure at different times. Since no single instrument could capture a complete response, it was necessary to interpret instrument response as a whole. The boundary conditions greatly affected bridge response.

- failure began in the deteriorated shoulder region over the piers, progressively shifting, with eventual failure by punching shear. The final failure load of 3200kN was 40% below the load value for punching predicted by the AASHTO Standard of 1989. The failure surface was not the usual one for punching shear, indicating that damage had affected the final failure.
- the effective-strip model was found to give an overly conservative estimate of bridge capacity. Linear finite element analysis was able to account for some of the mechanisms of load redistribution in the slab. Nonlinear analysis provided a further improvement, although failure occurred before many on the nonlinear mechanisms occurred.
- deterioration of the slab greatly reduced shear capacity, leading to an unexpected failure, and demonstrating the difficulty in understanding and incorporating the effects of local deterioration on structural response.

5.2.33 Ultimate Load Test of Slab-on-Girder Bridge (Bakht and Jaeger, 1992)

The paper reports on the ultimate load test of a skewless two-span, two-lane bridge having a clear span of 13.72m with six rolled steel girders and non-composite concrete deck in London, Ontario, Canada.

The bridge was instrumented with strain gauges on the bridge at midspan and loaded with concrete blocks.

Conclusions from the testing were as follows:

- girders continued to carry loads long after the formation of first yield and the bridge as a whole continued to carry loads long after the failure of the first girder reached its ultimate load
- bearing restraint forces reduced the applied moments by a minimum of about 11%. The effective coefficient of friction between the somewhat rusted bottom flanges of the girders and the concrete abutment was found to be nearly 1.0 at the ultimate limit state.
- for loads within the linear range of behaviour, the load distribution characteristics of the bridge appeared to deteriorate slightly with load.
- in the absence of mechanical shear connection between the deck slab and the girders, any composite action between these two components that may exist at service loads deteriorates rapidly as the load approaches the failure load for the girder.

5.2.34 Test Loading of a Full Scale Bridge (Gosbell and Stevens, 1968)

The construction of the Nillhacootie dam in Victoria led to the inundation of a section of highway, including a bridge over Sandy Creek. The bridge was built in 1961-62, and consisted of seven precast prestressed concrete beams spanning 58'10" with a 6" reinforced concrete deck slab.

Loads were applied with rock anchors grouted into the stream bed, and double I section beams used to form a grillage to apply the loads to the deck through hydraulic jacks.

Two independent scaffolding systems were built under the bridge; one for access and the second to provide a rigid datum for deflection measurements.

Deflections were measured with vernier scales, dial gauges and levels. Strains were measured with Demec mechanical gauges of 8" gauge length.

Average test results of concrete cores taken from the bridge were as follows:

Sample Position	Equivalent Cylinder Strength	Modulus of Elasticity
Deck	5300 psi (37 MPa)	4.1×10^6 psi (28GPa)
Beams	8750 psi (60 MPa)	6.58×10^6 psi (45 GPa)

Estimated loss of prestress was 29%, compared with the design value of 20%.

There were a number of conclusions drawn from the extensive range of testing undertaken:

- The condition of the bridge after 6 years of service was excellent, with no visible signs of deterioration.
- Concrete strengths were well above design values.
- The longitudinal flexural rigidity of the deck varied significantly across the width. Integral action between the deck, the precast kerbing and the hand rails increased the edge beam rigidity considerably.
- The midspan diaphragm was ineffective in the transverse distribution of loads. Separation between the diaphragm and the beam webs occurred at very low loads.
- The limited correlation between strains and deflections for single concentrated loads was significantly improved with multiple loadings.
- The action of the bridge under simulated design loads was essentially linearly elastic.
- The distributions predicted by the NAASRA Bridge Design Code were shown to be conservative.
- Cracking of the longitudinal beams produced little change in the form of distribution coefficients at midspan.
- A load over three times that required to initiate cracking was applied without producing complete failure.
- The bridge showed excellent recovery after overloading, with most cracks closing almost completely.
- No signs of shear failure were detected in the deck slab or beams during the main flexure tests.
- Local flexural effects in the slab were adequately predicted by Westergaard's method, with the NAASRA recommendations being generally found conservative.
- The ultimate punching shear strength of the slab was adequately predicted by the methods available at the time of testing.
- The predicted and measured frequencies of vibration of the bridge were in good agreement, at about 7Hz with an average logarithmic decrement of about 0.07.
- At low speeds the bridge was forced into oscillations at the frequency of the vehicle, but at higher speeds the natural frequency of the bridge predominated.
- The impact factor was found to be dependent on the vehicle speed, with maximum values at about 10 mph and 25 mph.
- The NAASRA impact factor was found to be generally conservative for the bridge with no induced roughness.
- The introduction of induced roughness near midspan increased the impact factor to about three and a half times the maximum obtained without induced roughness.

5.2.35 Destructive Testing of Two 80-year-old Truss Bridges (Aktan, Lee, Naghavi and Hebbar)

Two decommissioned 80-year-old truss bridges were subjected to a series of nondestructive and destructive tests with the following objectives:

- to evaluate whether many bridges dating from the early 1900's having similar design and construction characteristics pose a safety hazard
- to explore cost-effective and unobtrusive methods of upgrading deteriorated steel truss bridges
- to explore the measurement of truss behaviour by nondestructive and destructive methods and correlate experimentally measured responses with corresponding analytical predictions, to address the difficulties in detecting damage and deterioration in hidden and obscured components and the lack of reliable procedures for analytical modelling.

The two bridges were subject to detailed inspections and then loaded with trucks and with a servo-controlled electro-hydraulic system with the reaction provided by rock anchors. Instrumentation included wire potentiometer and linear variable displacement transducers, strain gauges and thermocouples. The test results showed that serviceability, damageability

and failure behaviour of steel truss bridges possessing built-up members rigidly connected by gusset plates are not adversely affected by local deterioration. The built-up members and the connections possessed adequate deformability permitting extensive redistribution. Connection retrofit by welding plates was feasible and successful.

5.2.36 Destructive Testing of Deteriorated Prestressed Box Bridge Beam (Miller and Parekh, 1994)

A prestressed concrete beam that had been located beneath the footway of a road bridge was removed because of severe corrosion of prestressing strand in one corner and subsequently tested to failure by loading with two point loads. The beam failed suddenly at a load 8% less than calculated capacity; with the likely mode of failure being lateral instability. By comparison, a new beam constructed for comparison purposes behaved in a ductile manner, and did not fail at an applied load 15% greater than the ultimate capacity predicted by the 1989 AASHTO Code.

5.2.37 Calibration of Bridge-Strength Evaluation Code (Verma and Moses, 1989)

The process of determining the live load capacity of existing bridges is distinct from the design procedure, which is necessarily generalised for applicability to a wide range of structures. Many of the bridges were designed for vehicles which do not represent current configurations and may have reduced load capacity due to deterioration.

The paper presents a comprehensive evaluation specification, with the following constraints:

- it is limited to the evaluation of existing steel and prestressed concrete bridges
- the only limit state recognised is the ultimate limit state; serviceability limit states were not considered
- fatigue life of steel bridges was not discussed in the paper
- nominal live loads were chosen to match existing vehicle loads and configurations
- a load factor was prescribed to account for uncertainties in actual live loads and static and dynamic load effects.

A load factor method is used, with the load and resistance factors based on providing a uniform safety level for all structures, with the target safety level being that implicit in existing rating practices.

Statistical data is used to determine dead load, live load, headway, coincidence, load distribution, impact and resistance effects.

An analysis of safety indices for bridges using existing procedures showed significant variability with span length, traffic category and structure type. Target values of 2.3 for redundant members and 3.5 for non-redundant members were adopted.

Calibrated live load and capacity reduction factors are detailed below:

Category of traffic	Live load factor
Enforced, light volume	1.30
Enforced, heavy volume	1.45
Unenforced, light volume	1.65
Unenforced, heavy volume	1.80

Bridge condition	Capacity reduction factor
Slight corrosion	0.85
Severe corrosion	0.75
Prestressed concrete	0.95
Nonredundant elements	0.80

5.2.38 Reliability of Highway Girder Bridges (Tabsh and Nowak, 1991)
Load and resistance parameters for bridges are random variables and deterministic approaches thus do not usually reveal the actual safety reserve. Probabilistic methods have however been developed since the 1970's and can be used for reliability calculations for bridges.

The paper describes the analysis of available statistical data on bridge loads and resistances to calculate reliability indices for a range of span lengths of composite and non-composite steel girder, reinforced concrete T-beam and prestressed concrete girder bridges. Moment-curvature relationships are developed using incremental load techniques. Live load models are based on the maximum 75-year live load, with two trucks side by side.

Reliability calculations were undertaken for bridge girders and bridge systems, with system reliability higher because of redundancy. Sensitivity analyses indicated the importance of resistance parameters such as the yield stress of steel or the steel area.

5.2.39 Probabilistic Assessment of Prestressed Concrete Bridge (Sobrino and Casas, 1995)
The parameters used for the design of new bridges are not appropriate for the assessment of existing structures, because the uncertainties involved in load and resistance values are usually lower. Accurate estimations can be made using information from inspections, experimental tests, traffic measurements and other supplementary data. A full probabilistic analysis can then be performed to determine the reliability index for a particular structure.

The paper describes a structural assessment procedure and illustrates it with a case study for a prestressed concrete voided slab bridge.

5.2.40 Calibration of LRFD Bridge Code (Nowak, 1995)
Bridge codes are now being written in terms of load and resistance factor design to provide a consistent safety margin for different types of bridges over a wide variety of spans. The paper discusses the development of the AASHTO LRFD bridge code, which involved the following steps:

- the selection of representative bridges
- the establishment of a statistical database for load and resistance parameters
- the development of load and resistance models
- the development of a reliability analysis procedure
- the selection of a target reliability index
- the calculation of load and resistance factors.

It is noted that contemporary codes (AASHTO, 1992) show a considerable variation in the value of the reliability index, β. Recommended values for a uniform safety level are presented.

5.2.41 Risk-Based Proof-Load Requirements for Bridge Evaluation (Fu and Tang, 1995)
Proof loading can provide a reliable approach to evaluating the load capacity of an existing structure, especially where analytical rating is not feasible. Proof-load factors in design and evaluation codes however vary, and there is a need to develop consistency in methods for determining target proof-loads and resulting load ratings. The paper discusses structural

reliability theory and makes recommendations for proposed factors in proof-load requirements.

5.3 Discussion

The Princess River Bridge testing included the review of a range of literature relating to the program.

While dimensional tolerances are routinely included in specifications for structures, compliance with those tolerances has been shown to depend on a number of factors. Marrosszeky and Chew (1989) found that no single factor could be identified as dominant in the accuracy of reinforcement placement, although the accuracy was better in bridges than buildings. This is likely to be consistent with the conclusion of Udoeyo and Ugbem (1995) that variation in member sizes was reduced by increased levels of inspection.

The assessment of load distribution is an important element of bridge design and a number of techniques are available, ranging from simplified distribution formulae, through grillage and yield line analysis, to non-linear finite element analysis. Simplified distribution formulae were developed some 60 years ago, prior to the advent of electronic calculation tools, for non-skewed simply supported bridges. Contemporary practice however means that a large proportion of bridges are curved, skewed and/or continuous. While increased sophistication leads to improved accuracy, it is at the expense of calculation time and computing power. Accurate results from finite element analysis require care to be taken with the preparation of the model and the selection of the software. Bridge designers and assessors require an appropriate balance, and the National Co-operative Research Program (1992) showed that grillage analysis and enhanced distribution formulae can provide acceptable results and reasonable amounts of calculation.

Bridge dynamics are of relevance for both assessing the effective increase in static load effects of vehicles and as a means to assess damage to and deterioration of structures. Simulations by Hwang and Nowak (1991) show no or low correlation between static and dynamic vehicle loads and a high variability in dynamic load effects. A number of investigators have found that dynamic techniques have the potential to monitor damage and deterioration, but that there are limitations.

Researchers, including Chana and Desai (1992), Azad et al (1994), Kirkpatrick et al (1984, 1986), Rankin et al (1991) and Jackson (1990), have found high load capacities in reinforced concrete bridge decks. Bridge decks are conventionally designed by flexural methods, although failure is typically by punching shear at loads substantially higher that those predicted by design. The increased capacity is generally attributed to the lateral restraint provided by supporting beams and the membrane action which occurs with transient loads. Recognition of those effects has led to the incorporation of empirical design methods for bridge deck slabs in the Ontario Highway Bridge Design Code (Jackson, 1990).

Testing of model and full-size bridges has been reported on a number of occasions in the literature. The testing has covered a range of aspects of bridge behaviour at both working and ultimate loads. Extensive testing programs have occurred in Switzerland, where all bridges are tested before entering service, and Ontario as part of a program of verifying capacities of older bridges (Moses et al, 1994). The AASHO Road Test involved the testing of eighteen bridges (Highway Research Board, 1962). Other testing has generally involved individual bridges. A number of principles emerge consistently from the test programs:

- elastic prediction of bridge behaviour is good at lower loads, but unsatisfactory at higher loads
- design methods are generally conservative, with high reserves of strength in tested bridges
- failure modes are generally ductile, although there are some reported cases of shear failure

- large factors of safety for desired ductile modes can lead to other modes of failure, including shear, becoming more likely
- the reduced uncertainty about bridge behaviour resulting from bridge testing can lead to higher safety indices in assessment.

Probabilistic methods for the design and evaluation of bridges have been developed since the 1970's and are now generally incorporated in codes. Historic design methods for different materials and structural forms have however led to a considerable variation in the reliability index, β. Additionally, different parameters are appropriate for design and for evaluation due to the reduced uncertainty with existing bridges. The needs for broad statistical databases for load and resistance parameters and to provide a basis for consistent approaches to bridge design and rating are highlighted.

6. CLIMATE AND HYDROLOGY

6.1 General

The Princess River is located within the King River Power Development catchment on Tasmania's west coast, at a latitude between 42° and 43° south. The area is subject to Southern Ocean depressions and their associated frontal systems.

The climate over the area is generally mild with cool and wet conditions prevailing for the greater part of the year. Frosts are general in winter. Snow did not normally lie at the bridge site, which was located approximately 215 metres above sea level.

The Hydro-Electric Commission undertook a detailed assessment of the area which includes the Princess River Bridge as part of their design of the King River Power Development. The following climatic data is drawn from their assessment.

6.2 Air Temperatures

Likely maximum and minimum average temperatures were assessed for the Crotty Dam, based on records from Queenstown, Zeehan, Murchison River and the Franklin River below the Jane River. The estimated accuracy of the figures is ±1°C for September and ±2°C for the other months. Estimated temperatures are shown in Table 6.1 and Figure 6.1, with extreme temperatures at Queenstown based on records from 1965 to 1983.

Month	Air Temperatures - Degrees Celsius			
	Likely Average Daily Temperatures		Extreme Daily Temperatures at Queenstown	
	Maximum	Minimum	Maximum	Minimum
January	21.0	8.8	37.3	0.0
February	21.4	9.2	36.3	0.0
March	18.9	8.1	35.6	-1.1
April	15.3	6.9	28.7	-2.6
May	12.5	5.2	25.0	-6.0
June	10.2	3.6	19.5	-6.2
July	9.9	3.3	19.5	-6.7
August	11.0	3.4	21.0	-5.5
September	12.8	4.3	26.4	-3.9
October	15.3	5.1	27.8	-3.3
November	17.0	6.7	33.3	-1.5
December	18.7	7.8	35.3	-0.6

Table 6.1 - Temperatures

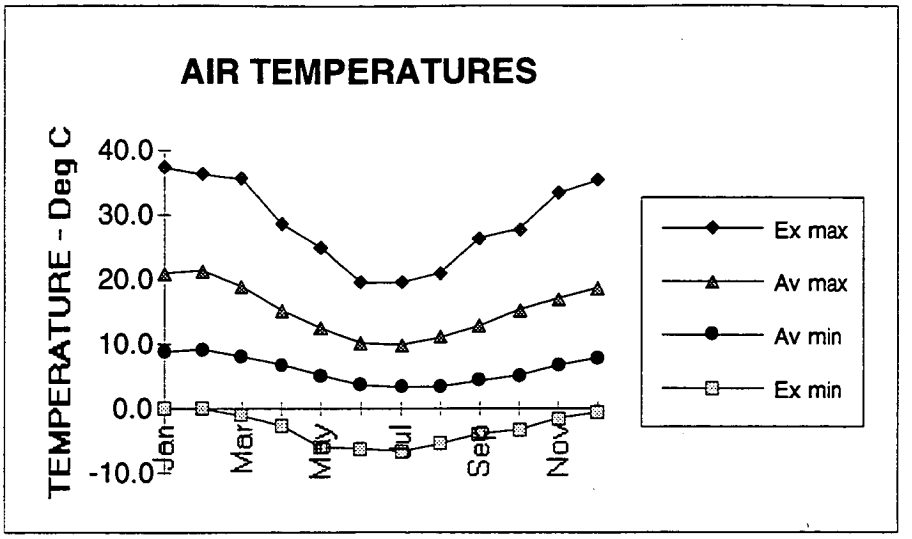

Figure 6.1 - Temperatures

6.3 Humidity

Mean relative humidity varies little between stations on Tasmania's west coast, and data for Zeehan is used to give an indication of monthly mean relative humidities near the bridge site. Local effects from the river are not included, although measured relative humidities measured under the bridge during the period of testing were of the order of 95% with temperatures from 3° to 5°C.

Month	Relative Humidities	
	9am	3pm
January	68	61
February	70	61
March	75	65
April	81	70
May	85	74
June	86	74
July	86	74
August	83	72
September	78	68
October	71	64
November	68	64
December	68	65

Zeehan - Elevation 592 ft (180m)
Period of Record : 51 Years (1909-1959)

Table 6.2 - Mean Daily Relative Humidity

6.4 Sunshine

Average hours of sunshine provide an inverse measure of the cloud cover experienced at a site. Date from five locations in Tasmania are given in Table 6.3, with the record from Lake St Clair being indicative of conditions at Princess River.

Month	Strathgordon	Lake St Clair	Hobart	Bushy Park	Burnie
January	238	263	239	243	257
February	190	220	200	212	204
March	146	166	197	203	198
April	98	98	149	143	174
May	79	82	137	115	143
June	50	69	119	87	111
July	63	74	135	104	127
August	95	93	158	144	155
September	87	107	178	174	183
October	139	182	188	195	220
November	172	174	214	219	252
December	171	199	228	234	273
Totals					
Annual	1528	1740	2143	2075	2297
Winter	513	620	916	821	939
Summer	1015	1120	1227	1254	1358

Winter = May to October
Summer = November to April

Table 6.3 - Average Hours of Sunshine per Month

6.5 Precipitation

Rainfall data from 37 stations in the vicinity of the King River is shown in Table 6.4.

Station	Period use in Calculating Mean	No of full Years	Long Term Mean (mm)
King River at Crotty	1958-1985	25	2788
Franklin River below Jane	1957-1979	22	2751
Narcissus River	1964-1982	17	2290
Franklin Track Hill 4	1968-1984	15	2853
Andrew Divide	1960-1972	10	3483
Franklin at Fincham	1953-1976	18	2612
King William Creek	1965-1984	18	2185
Frenchmans Cap Track	1968-1972	3	1851
Zeehan Post Office	1890-1967	75	2448
Lake St Clair	1937-1977	39	1520
Cuvier River	1942-1950	8	1989
Princess River	1948-1951	3	2304
Franklin Camp	1972-1974	2	2985
Surprise Valley	1954-1958	1	2126
Butlers Gorge	1941-1982	41	1691
Queenstown	1906-1968	59	2526
Regatta Point	1908-1946	30	1662
Bills Creek	1954-1956	1	2653
Crotty	1917-1929	11	3057
Cardigan Flats	1968-1985	15	2817
Burns Dam	1966-1967	0	1932
Arrowsmith Divide	1968-1969	0	2288
Murchison River	1956-1972	5	2033
Strahan	1882-1935	29	1609
Pillinger	1907-1924	16	1963
Gormanston	1895-1976	78	2973
West Lyell	1945-1975	29	2684
Lake Margaret Dam	1912-1973	60	3577
Lake Margaret Power Station	1944-1982	37	2974
Renison Bell	1911-1973	37	2279
Cape Sorell	1899-1970	71	1352
Comstock	1926-1944	18	2938
Koyule	1914-1943	21	1540
Rosebery	1918-1979	60	2117
Williamsford	1956-1972	8	3183
Mt Reid	1901-1920	20	3073
King at Tofft	1960-1971	12	3420

Table 6.4 - West Coast Rainfalls

Mean monthly rainfalls at Crotty and Queenstown are shown in Table 6.5.

Month	Crotty Pluviograph 1952-1985	Queenstown 1907-1965
January	146	149
February	120	128
March	164	171
April	252	222
May	291	242
June	270	240
July	310	252
August	291	264
September	315	243
October	220	229
November	210	204
December	208	180
TOTAL	**2797**	**2524**

Table 6.5 - Mean Monthly Rainfalls

6.6 Storage Filling

The Hydro-Electric Commission developed predicted storage filling curves for Lake Burbury for diversion tunnel closure on the first of each calendar month based on 56 years of historical records and on 2000 years of synthetically generated data.

Curves for closure on 1st July and 1st August are shown below. The actual closure date of 24 July 1991 with the actual filling curve is shown for comparison.

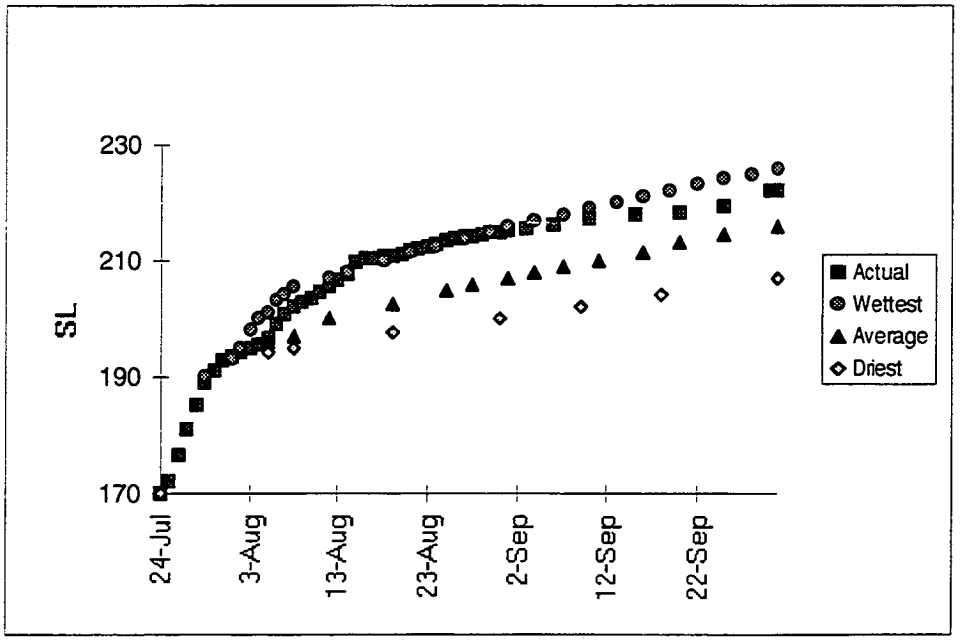

Figure 6.2 - Actual and Predicted Lake Burbury Filling Rates

6.7 Water Quality

A sample of water from the River was tested by the Tasmanian Government Analyst. Its chemical composition is detailed in Table 6.6.

pH	6.9
Conductivity @ 25°C	114 uS/cm
Total dissolved solids	68 mg/l
Total alkalinity (as $CaCO_3$)	33 mg/l
Hardness (as $CaCO_3$)	52 mg/l
Chloride (Cl)	9.9 mg/l
Sulphate (SO_4)	8.5 mg/l
Calcium (Ca)	16.1 mg/l
Magnesium (Mg)	2.9 mg/l
Potassium (K)	0.43 mg/l
Sodium (Na)	7.1 mg/l

Table 6.6 - Chemical Composition of Water

6.8 Catchment Hydrology

The Princess River catchment upstream of the bridge had the following characteristics:

Catchment area	32km^2
River length	10km
Maximum elevation	765m
River invert level at bridge	212m
Average river slope	5.5%
River slope at bridge	0.64%

The average stream velocity for normal flows at the bridge is assessed to be 1.1 to 1.2m/s.

Stream discharges at the bridge are calculated using the Rational Method from Australian Rainfall and Runoff, based on 41 years of records for the King River at Crotty.

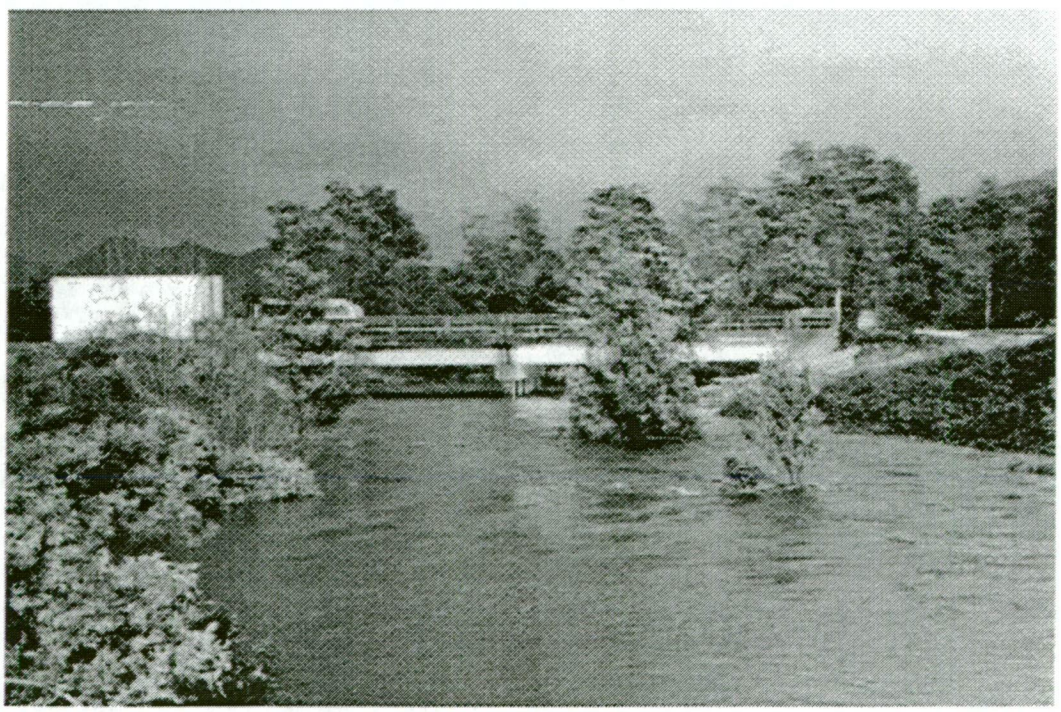

Figure 6.3 - Princess River in Flood During Bridge Testing

For western Tasmania,

$Q_2 = C_2 A^{0.79}$

For the catchment,

C_2=3.05

Skew = 1.05

Standard deviation, S = 0.14

Q_2 = 47 cumec

For an annual frequency, Y,

$\log Q_Y = \log Q_2 + K_Y.S$

From Australian Rainfall and Runoff,

Y	2	5	10	20	50	100	200
K_Y	-0.17	0.75	1.34	1.885	2.56	3.05	3.54
Q	47	60	72	86	107	126	147

Table 6.7 - Frequency-Discharge Relationship

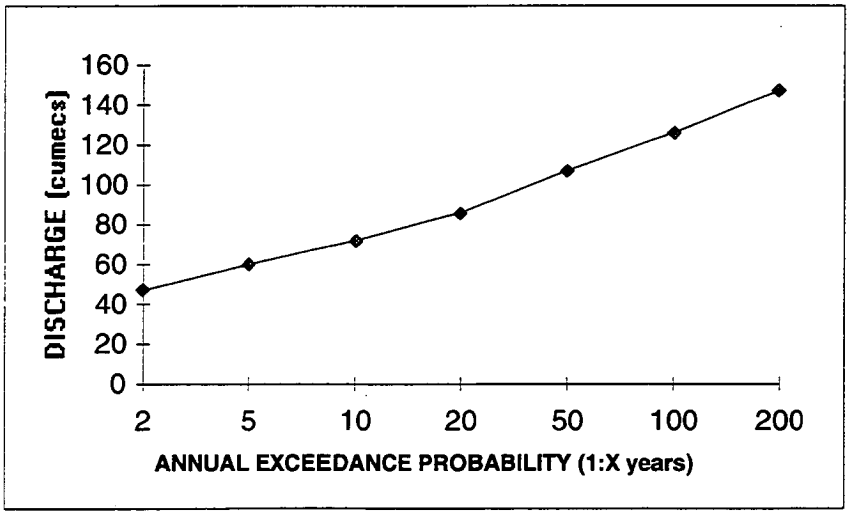

Figure 6.4 - Discharge Exceedance Probabilities

The stage- discharge relationship was determined as detailed in Table 6.8.

Y	2	5	10	20	50	100	200
Q	47	60	72	86	107	126	147
Depth	1.9	2.1	2.2	2.4	2.6	2.8	3.0
Area	17.6	20.6	23.2	25.9	30.0	33.5	37.2
Velocity	2.67	2.92	3.10	3.31	3.56	3.76	3.95

Table 6.8 - Stage - Discharge Relationship

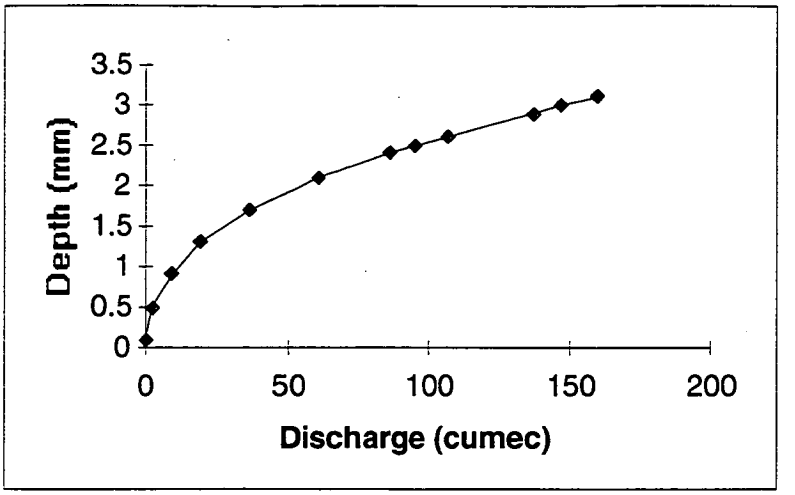

Figure 6.5 - Stage - Discharge Relationship

6.9 Discussion

Conditions at the bridge site are generally mild, with cool and wet conditions prevailing for much of the year. The average maximum temperature is likely to vary from 21°C in the summer to 10°C in winter, with minimum average temperatures ranging from 9°C to 3°C. The humidity in the area is high, with mean values likely to range from 60% to 90%. The presence of the river would be expected to increase the relative humidities at the bridge. Average annual hours of sunshine are likely to be about 1600 to 1700, with an average annual rainfall of the order of 2300 mm. The water in the river can be considered as benign.

An hydraulic analysis showed that the bridge had a capacity to carry floods of the order of 0.5% to 1% annual probability.

Weather during the testing period was severe, resulting in extremely rapid early filling of the King River storage. Two significant floods, of 20 to 50 year return interval, were experienced during the four week period.

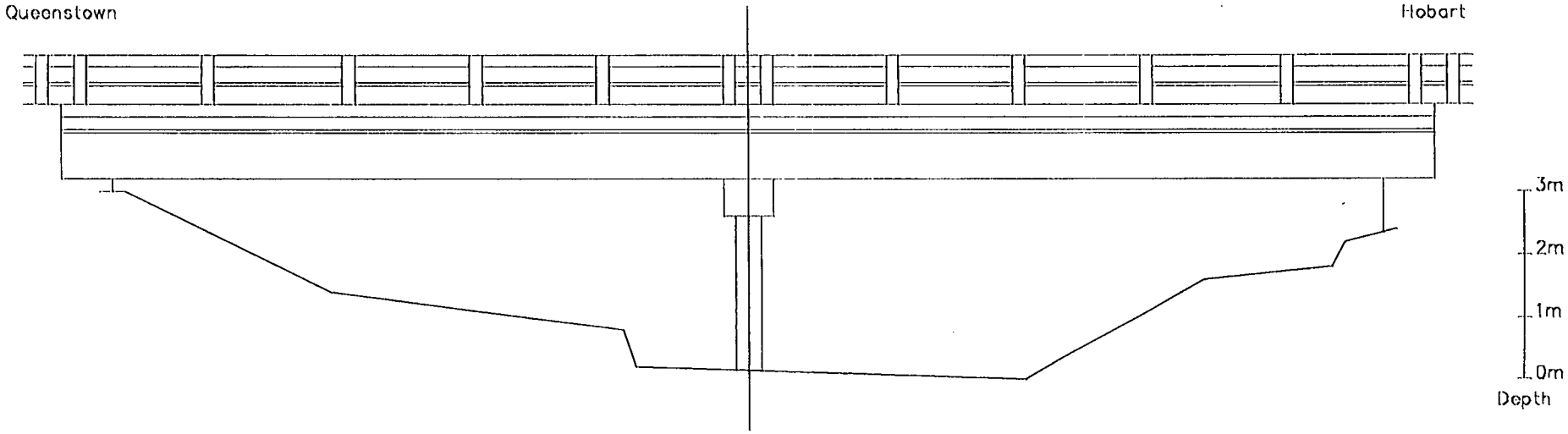

Figure 6.6 - Channel Cross-Section

7. INSTRUMENTATION

7.1 Cover

Reinforcement covers were measured with a Profometer 3 cover meter, serial number 2189.34.

Calibration of indicated covers against those measured where reinforcement was exposed showed a consistent under-indication of 10%, and indicated covers have been increased by 10% for the reporting of covers. The calibration factor has subsequently confirmed with measurements of actual cover on a number of other structures.

7.2 Strain, Linear Displacement and Acceleration

The Department of Roads and Transport's General Purpose Data Logger was used for the measurement of strain, linear displacement and acceleration.

Strains were measured with mechanical strain gauge amplifiers of gauge length 300mm developed by the Australian Road Research Board.

Linear displacements were measured with RDP Electronics linear variable displacement transducers with a capacity of 2".

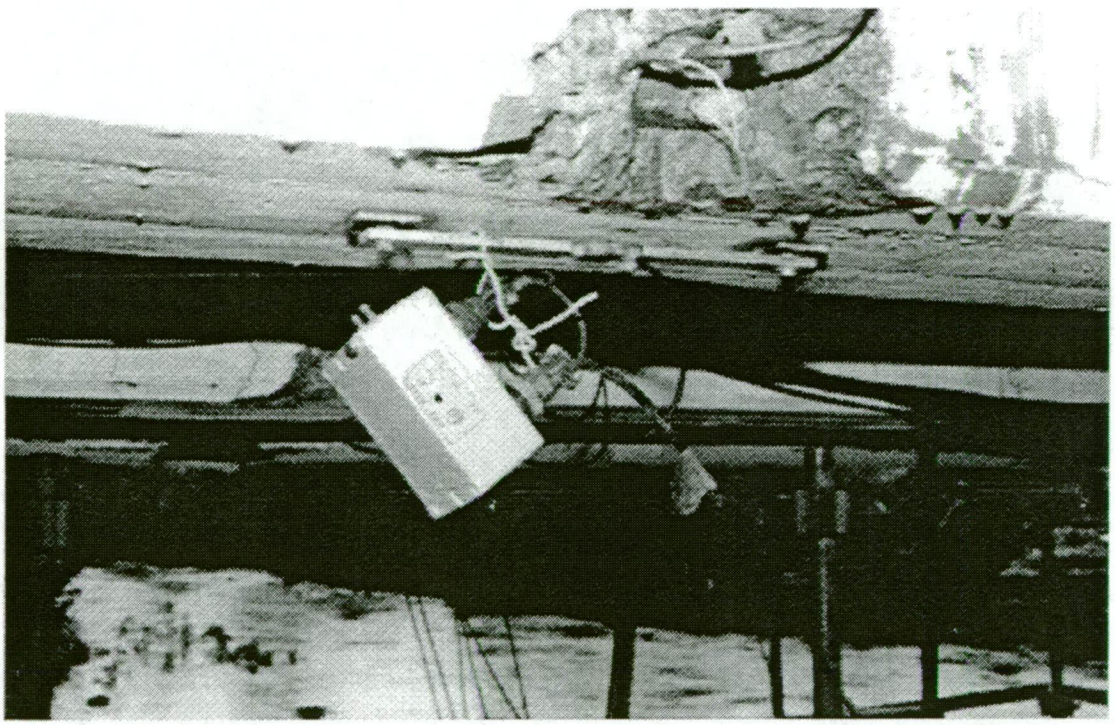

Figure 7.1 - Strain Gauges (Mechanical strain gauge amplifier with signal conditioner at bottom, strain gauge welded to reinforcement)

Accelerations were measured using Minebea strain gauge accelerometers.

Strains were also measured with Micro-Measurements electrical resistance strain gauges connected to an ORION data logger provided by ETRS Consultants. Linear displacement transducers with a capacity of 58mm were also constructed from linear resistance, linear dimension audio potentiometers connected to the data logger in a Wheatstone Bridge configuration. Calibrations for the linear displacement transducers are shown in Table 7.1, with a typical calibration curve shown in Figure 7.2.

S22		S23		S24		S25		S26		S27	
x (mm)	R (Ω)	x (mm)	R (Ω)	x (mm)	R (Ω)	x (mm)	R (Ω)	x (mm)	R (Ω)	x (mm)	R (Ω)
32.18	134	33.82	200	33.15	11	34.03	171	33.62	162	33.00	188
34.17	1934	36.19	1890	35.25	1865	35.81	778	35.14	1380	34.67	1815
38.83	6300	38.24	4250	36.06	2920	36.56	2380	37.37	3830	36.77	3860
46.18	13200	44.78	9800	39.50	6250	39.44	5340	43.00	9440	40.47	7630
53.63	19440	50.38	15470	45.43	12050	44.14	9880	50.85	16560	44.38	11460
60.60	25200	54.85	19570	51.70	17790	50.81	16420	54.31	19870	52.99	19280
71.22	33800	61.75	26200	57.37	23700	56.64	23100	62.08	26700	60.59	25800
76.58	38000	71.53	34500	64.05	30100	60.30	26800	75.12	37500	67.72	32200
79.27	40100			71.80	36400	67.27	33100	81.58	43100	76.35	39100
				79.87	42900	74.98	39000			82.15	44200
						80.52	43400				

Table 7.1 - Linear Displacement Transducer Calibrations

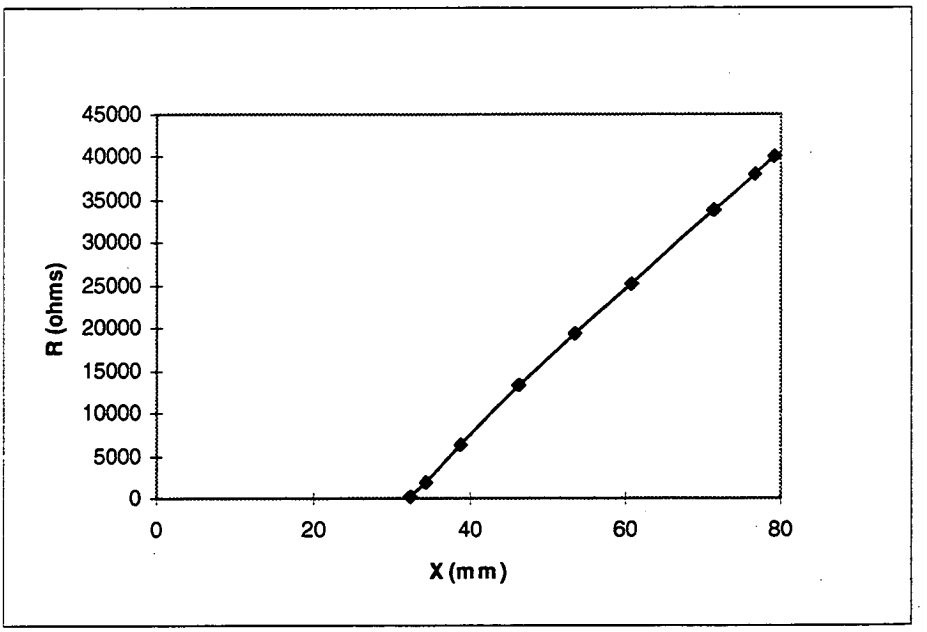

Figure 7.2 - Linear Displacement Transducer Calibration (S22)

The locations of the various transducers on the bridge are shown in Figure 7.3.

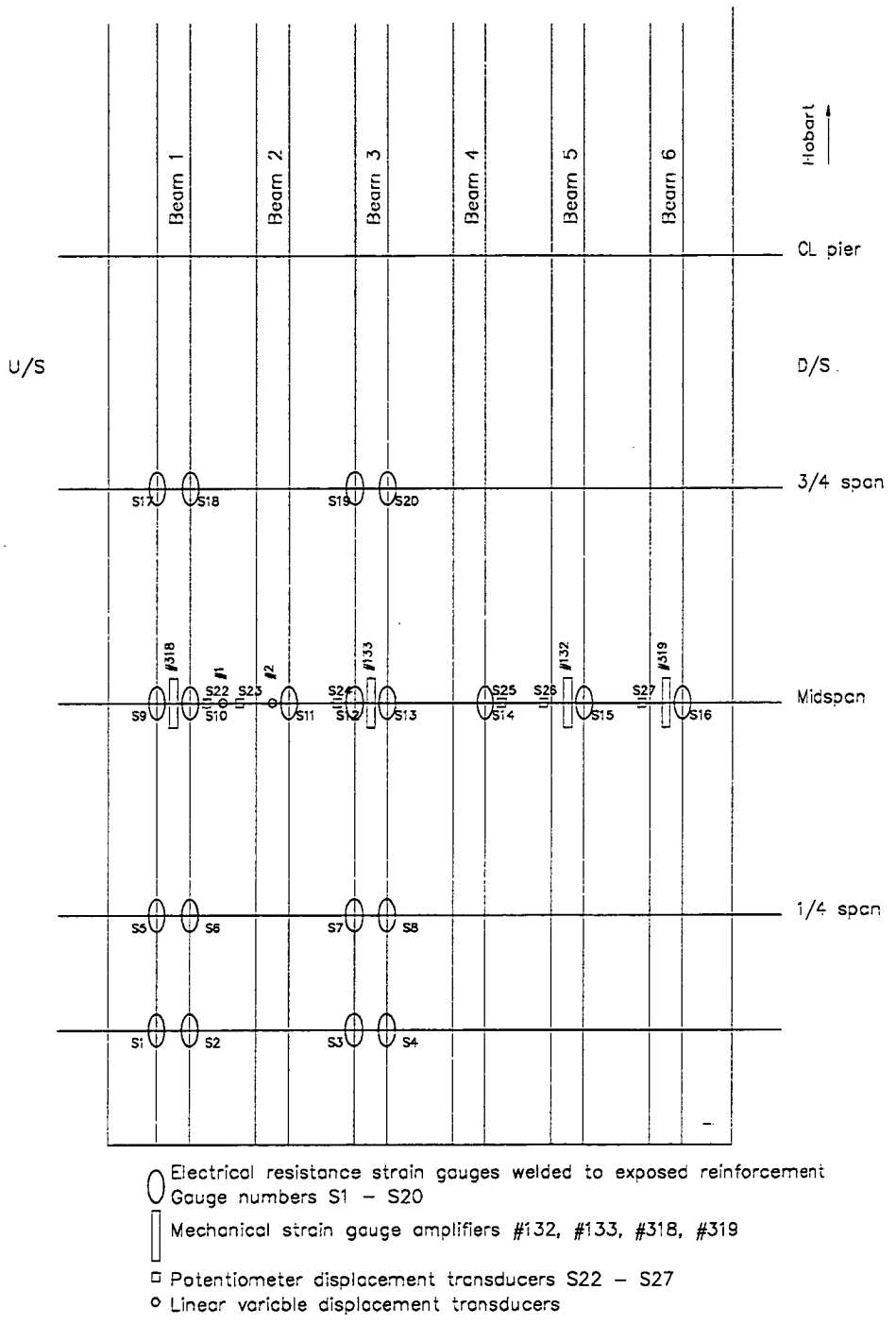

Figure 7.3 - Gauge Positions

7.3 Vicroads testing

The Vicroads test program involved three organisations, each with their own instrumentation and data acquisition systems, as described below.

The ETRS system involved:

- sixteen low cost velocity transducers located on the bridge deck
- a sixteen channel computer based high speed data acquisition system
- ETRS developed software
- analysis software (FFT) for data reduction and plotting of results.

The University of Melbourne system used:

- five servo-accelerometers
- eleven velocity transducers
- a multi-channel computer based data acquisition system.

The Structural Dynamics Group in the Civil and Mining Engineering Department of University of Wollongong used accelerometers with a four channel Tektronix 2630 spectrum analyser.

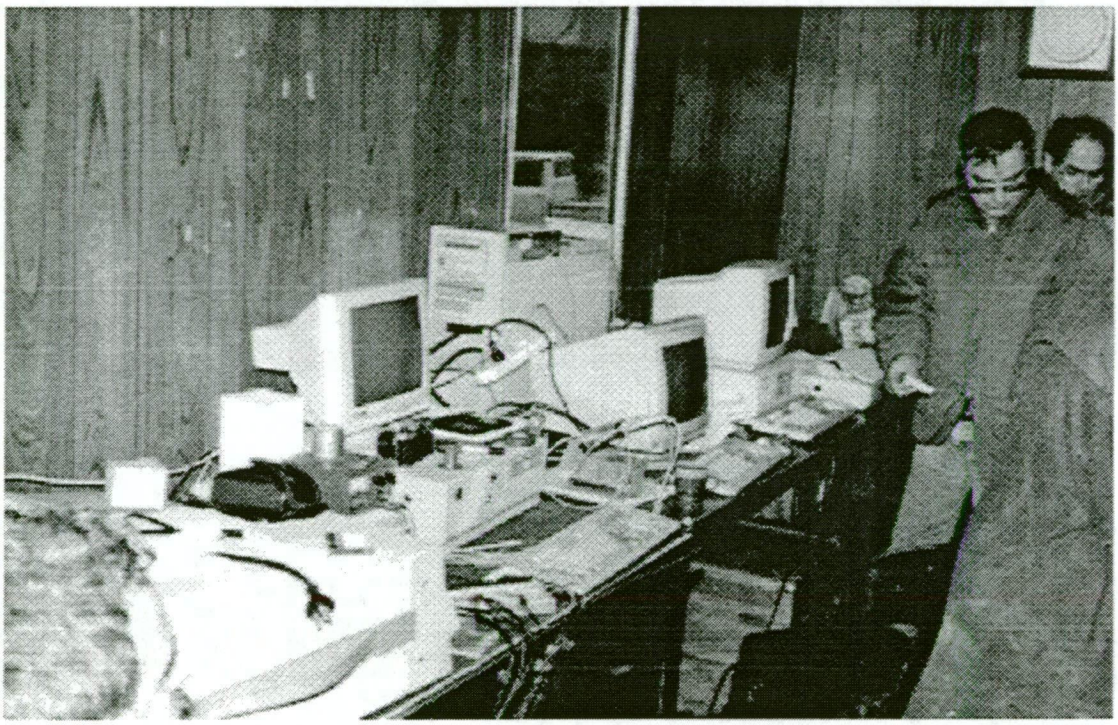

Figure 7.4 - Data Acquisition Equipment

8. BRIDGE LOADING

8.1 Introduction

A range of loads were applied to the bridge during the testing to assess load distribution, static and dynamic responses, and ultimate capacity.

Two precast beams, which had apparently been rejected during construction, were located near the bridge. They nevertheless appeared to be in good condition and were thus transported to Hobart for static load testing.

8.2 Bridge Truck Loading

Specific measurements were taken using a 7.5 m^3 capacity Department of Construction gravel truck with a Batchelor's weighbridge certificate from Queenstown. Uncalibrated truck loadings used passing semi-trailer trucks recovering gravel from the King River bed before its inundation.

The footprint of the Department of Construction gravel truck is shown in Figure 8.1.

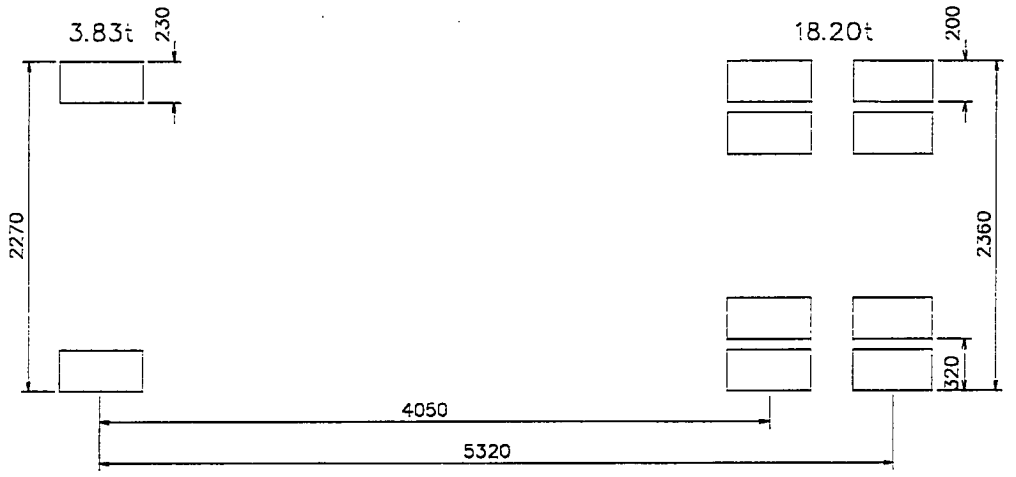

Figure 8.1 - Department of Construction Gravel Truck

8.3 Bridge Dynamic Loading

While it was recognised that the ideal form of excitation for the bridge for the dynamic testing would have been an electrodynamic or hydraulic shaker, the equipment was not available and an alternative form of excitation was required.

A number of attempts to excite the bridge were made using the instantaneous release of a mass of approximately 1t of steel suspended by a steel cable through a cored hole in the deck at midspan. This method however proved unsuccessful in imparting sufficient energy to the bridge for meaningful dynamic measurements.

Subsequently an impact weight, of approximately 75 kg mass, free falling a height of 0.9m onto a rubber pad lying on the bridge deck was found to produce a clean impact signal, and this method of excitation was used for the majority of tests.

A number of tests were also carried out using gravel trucks, including semi-trailers and tandem axle tippers, traversing the downstream lane at speeds between 30 km/h and 60 km/h.

8.4 Bridge Loading

Ultimate load testing was undertaken using the loading rig shown in Figure 8.2.

Loads were applied to the bridge through loading feet and elastomeric pads, to simulate tyre footprints, reacting against jacking beams, thence the launching nose from the new King River Bridge and finally to the ground through ground anchors.

Details of the loading rig and the calculations used to determine member sizes are included in Appendix A.

Appendix A also includes details of the loading arrangements for the individual beam tests.

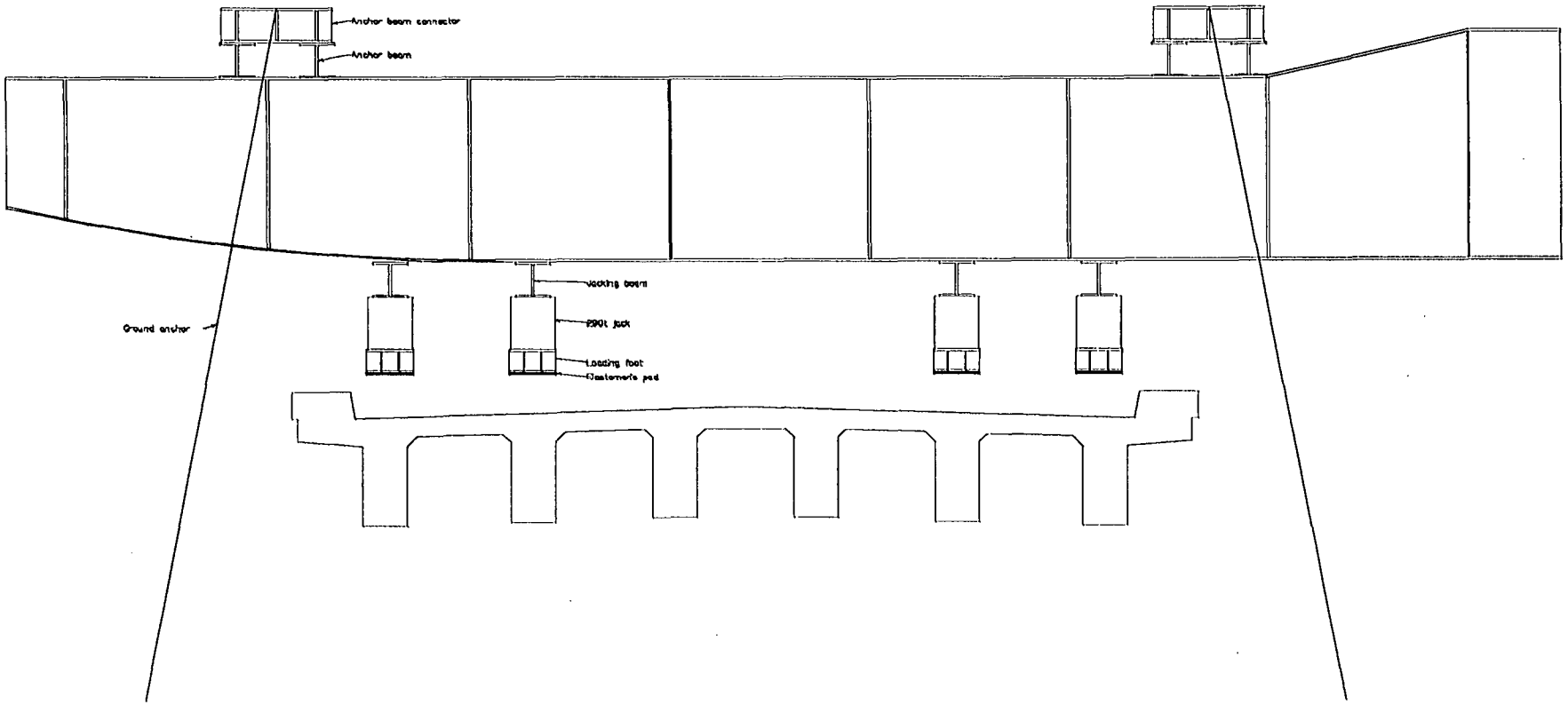

Figure 8.2 - Loading Rig Configuration

9. DIMENSIONAL SURVEY

9.1 Introduction

Detailed measurements of the deck and two Queenstown span cross-sections were taken to assess the accuracy of construction of the bridge and the compliance with contemporary tolerances.

Detailed measurements were also taken as part of the precast beam testing.

9.2 Dimensions

Measured cross-sections and deck plan dimensions are shown in Figures 9.1 and 9.2.

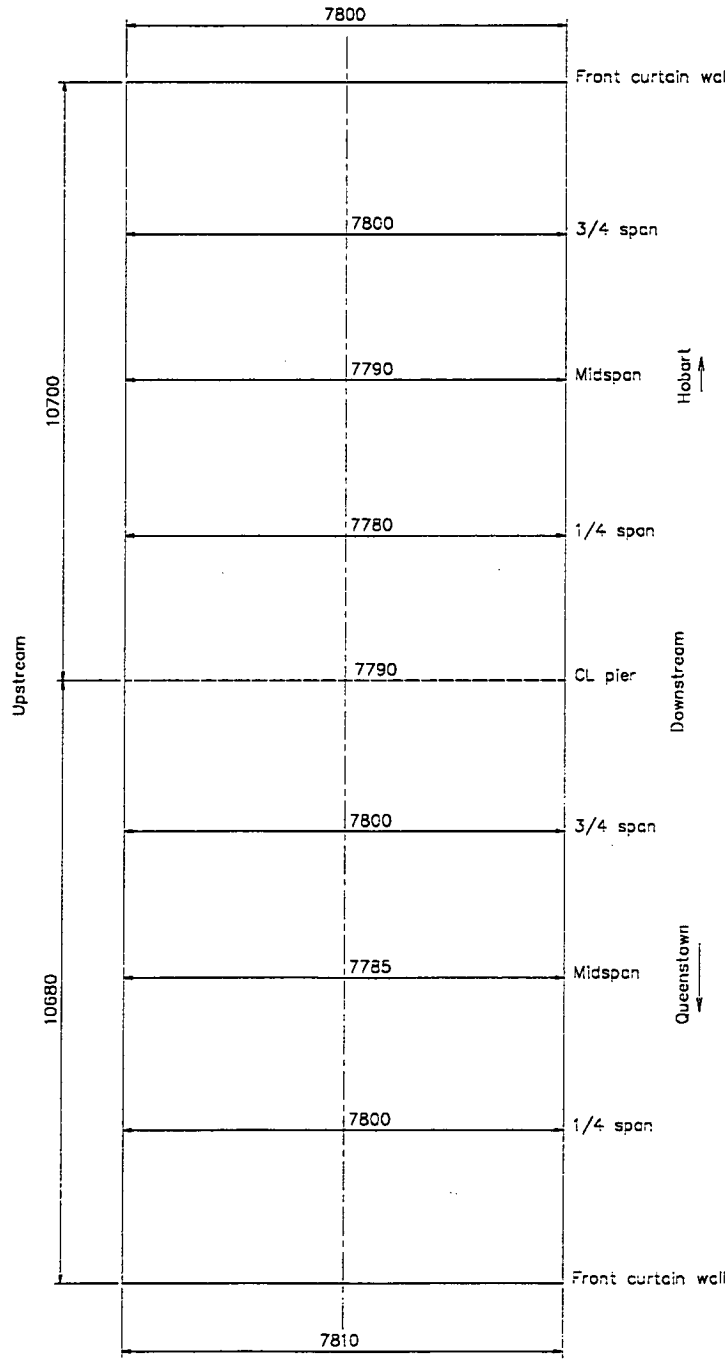

Figure 9.1 - Bridge Plan

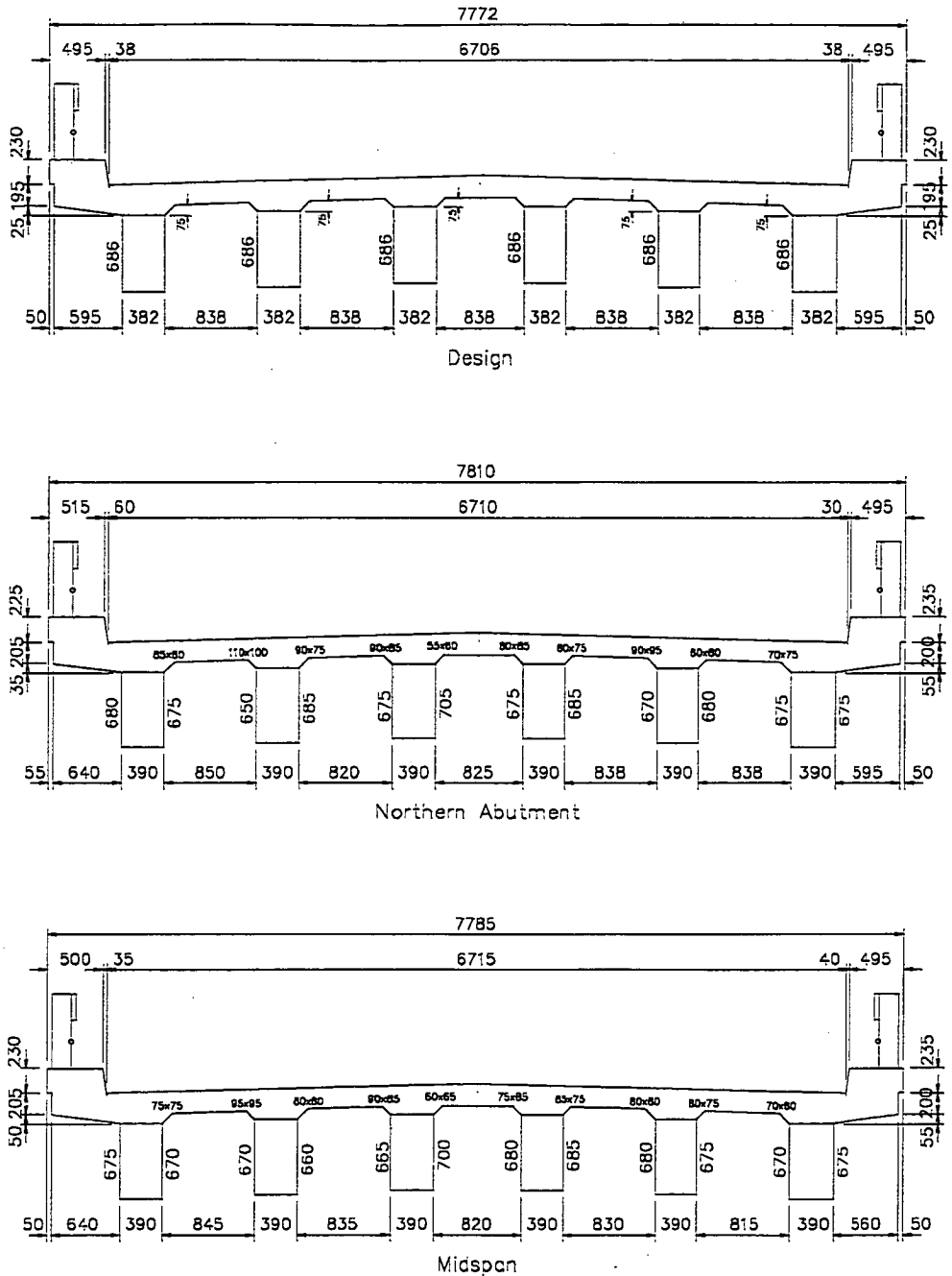

Figure 9.2 - Bridge Cross-Sections

Dimensions of the two precast beams removed from site are discussed in Chapter 14.

9.3 Precast Element Tolerances

A summary of precast beam dimensions is detailed in Table 9.1.

	Depth	Width
Average	684	380
Minimum	674	376
Maximum	700	382
Specified	686	381

Table 9.1 Beam Dimensions

9.4 Superstructure Dimension Tolerances

Superstructure dimensions for analysis are detailed in Table 9.2.

	Deck Width	Span Length	Beam Spacings
Average	7795	10690	1222
Maximum	7780	10700	1240
Minimum	7810	10680	1205
Specified	7772	10668	1220

Table 9.2 - Structure Dimensions

9.5 Deviations from Specified Locations

Deviations from specified locations are detailed below in Tables 9.3 and 9.4, with the normalised values shown in Figures 9.3 and 9.4. Data and analysis of the accuracy of reinforcement placement are included in a subsequent chapter. The numbers of measurements taken were limited by the focus on structural and durability aspects and the severe weather, including flooding, during the period of testing. Precast beam depths are not included due to the variability resulting from the roughened surface required for shear transfer in the completed structure.

Description	Measured location			Specified location			Departure		
	Trans.	Long.	Vector	Trans.	Long.	Vector	Trans.	Vector	Normalised
From plan									
Queenstown curtain wall									
Upstream	3905	10680	11371.5	3886	10668	11353.7	-19.0	-17.8	-0.0049
Centreline	0	10680	10680.0	0	10668	10668.0	0	-12.0	N/A
Downstream	3905	10680	11371.5	3886	10668	11353.7	-19.0	-17.8	-0.0049
Quarter span									
Upstream	3900	8010	8909.0	3886	8001	8894.8	-14.0	-14.2	-0.0036
Centreline	0	8010	8010.0	0	8001	8001.0	0	-9.0	N/A
Downstream	3900	8010	8909.0	3886	8001	8894.8	-14.0	-14.2	-0.0036
Midspan									
Upstream	3893	5340	6608.4	3886	5334	6599.4	-7.0	-9.0	-0.0018
Centreline	0	5340	5340.0	0	5334	5334.0	0	-6.0	N/A
Downstream	3893	5340	6608.4	3886	5334	6599.4	-7.0	-9.0	-0.0018
Three-quarter span									
Upstream	3900	2670	4726.4	3886	2667	4713.2	-14.0	-13.2	-0.0036
Centreline	0	2670	2670.0	0	2667	2667.0	0	-3.0	N/A
Downstream	3900	2670	4726.4	3886	2667	4713.2	-14.0	-13.2	-0.0036
Pier centreline									
Upstream	3895	0	3895.0	3886	0	3886.0	-9.0	-9.0	-0.0023
Centreline	0	0	0.0	0	0	0.0	0	0.0	N/A
Downstream	3895	0	3895.0	3886	0	3886.0	-9.0	-9.0	-0.0023
Quarter span									
Upstream	3890	2675	4721.0	3886	2667	4713.2	-4.0	-7.8	-0.0010
Centreline	0	2675	2675.0	0	2667	2667.0	0	-8.0	N/A/
Downstream	3890	2675	4721.0	3886	2667	4713.2	-4.0	-7.8	-0.0010
Midspan									
Upstream	3895	5350	6617.7	3886	5334	6599.4	-9.0	-18.2	-0.0023
Centreline	0	5350	5350.0	0	5334	5334.0	0	-16.0	N/A
Downstream	3895	5350	6617.7	3886	5334	6599.4	-9.0	-18.2	-0.0023
Three-quarter span									
Upstream	3900	8025	8922.5	3886	8001	8894.8	-14.0	-27.7	-0.0036
Centreline	0	8025	8025.0	0	8001	8001.0	0	-24.0	N/A
Downstream	3900	8025	8922.5	3886	8001	8894.8	-14.0	-27.7	-0.0036
Hobart curtain wall									
Upstream	3900	10700	11388.6	3886	10668	11353.7	-14.0	-34.9	-0.0036
Centreline	0	10700	10700.0	0	10668	10668.0	0	-32.0	N/A
Downstream	3900	10700	11388.6	3886	10668	11353.7	-14.0	-34.9	-0.0036

Note: Normalised departures are for transverse measurements.

Table 9.3 - Bridge Dimensional Survey

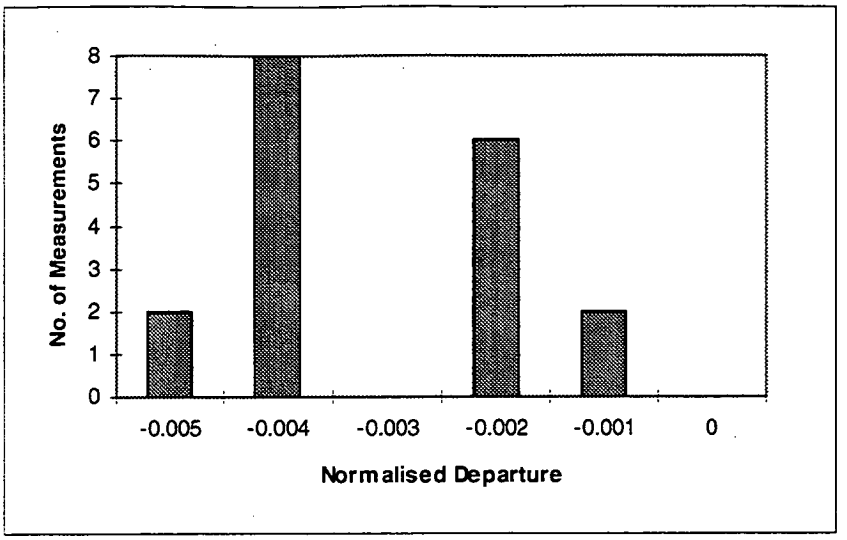

Figure 9.3 - Bridge Dimensional Survey

Measurement	Proportion of specified	Measurement	Proportion of specified
Structure			
Northern abutment		**Midspan**	
390	1.021	390	1.021
390	1.021	390	1.021
390	1.021	390	1.021
390	1.021	390	1.021
390	1.021	390	1.021
390	1.021	390	1.021
Precast beams			
378	0.990	381	0.997
381	0.997	381	0.997
381	0.997	380	0.995
377	0.987	380	0.995
378	0.990	381	0.997
381	0.997	380	0.995
377	0.987	381	0.997
376	0.984	381	0.997
379	0.992	382	1.000
379	0.992	381	0.997

Table 9.4 - Beam Width Measurements

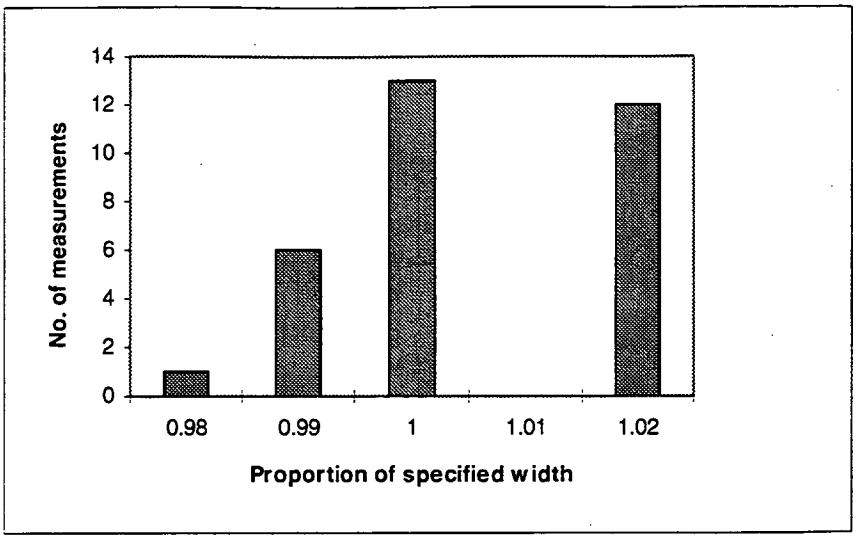

Figure 9.4 - Beam Width Distribution

Statistical analyses are shown in Table 9.5.

	Mean	Standard deviation
Beam width	1.004	0.0137
Transverse departure	-0.00297	0.00115

Table 9.5 - Statistical Analysis for Normalised Measurements

9.6 Specified Tolerances

Specified tolerances by the Department of Transport (September 1994) for cast in place concrete are:

(i) Reinforcement

(a)	Placing of reinforcement, from position shown on drawings	10mm
(b)	Concrete cover (measured at reinforcement supports	+5,-0mm
(c)	Concrete cover (measured anywhere other than supports)	+10,-5mm

(iv) Columns, crossheads, slabs, walls and similar parts

(a)	Variation in cross section	
	(1) Less than 3 metres	-5 to +15mm
	(2) Greater than 3 metres	-10 to +25mm
(b)	Variation from vertical or specified batter	
	(1) Unexposed concrete	10mm in 2.5m
	(2) Exposed concrete	5mm in 2.5m
(c)	Reduced level of tops of walls and crossheads	-5mm to +5mm
(d)	Difference in level across width of abutment and crosshead shall not exceed	5mm
(e)	Departure from plan position at any level	25mm
(f)	Relative displacement of adjoining components shall not exceed	10mm
(g)	Departure from alignment	10mm
(h)	Seatings for pretensioned beam bearings	
	(1) Departure from specified grade	1 in 200
	(2) Depth of depressions from true line	1mm
(i)	Reduced level of mortar bearing pads	-2.5mm to +2.5mm

(v) Deck

(a)	Variation in thickness (excluding allowance for correction of camber or hog)	-5 to +15mm
(b)	Deck joints - width of slot	-3 to +3mm
(c)	Deck surface finish	5mm in 2.5m
(d)	Deck surface reduced level	-5 to +5mm
(vi)	Kerbs and arrises	
(a)	Variation from grades	2.5mm in 2.5m
(b)	Section dimensions of kerbs and channels	-5 to +5mm
(c)	Departure from plan position shall not exceed	10mm
(vii)	Exposed concrete surfaces, maximum allowance for irregularities	
(a)	Sections less than 1m in dimension when measured with a straightedge across the dimension of the section	2.5mm
(b)	Sections greater than 1m in dimension when measured with a straightedge across the dimensions of the section, except that when sections are greater than 2.5m in dimension, a 2.5m straightedge shall be used	5mm

For precast beams, the relevant tolerances are:

(a)	Variations in cross section	
(1)	Dimensions up to 200mm	-4 to 0mm
(2)	200mm and above	-7 to 0mm
(b)	Variation in length or -0.06% to +0.06% of the length of the beam, whichever is the greater	-7 to +7mm
(c)	Twist	0.5° per length of beam
(d)	Straightness of edges and flatness of surfaces	$\frac{\text{Length}}{1000}$
(g)	Maximum deviation in the horizontal plane (bow) or -0.06% to +0.06% of the length of the beam, whichever is the greater	-7 to +7mm
(h)	Warp	
(1)	Up to 5m diagonal	7mm
(2)	Over 5m diagonal	10mm
(i)	Accuracy of corners	
(1)	Up to 2m	4mm
(2)	Over 2m and up to 4m	5mm
(3)	Over 4m	7mm

9.7 Discussion

While the sample is small, the measurements do provide a number of indications:

- locations of points within the finished structure were generally within the tolerance of 25mm permitted in contemporary specifications
- a number of measurements of the widths of the precast beams were outside the permitted tolerance of -7 to 0 mm. The non-complying measurements were however on the built structure, with the accuracy of measurement having potentially been affected by the difficulties associated with site measurement
- the results indicate that normal distributions are likely to be valid in the analysis of structures.

10. REINFORCEMENT COVERS

10.1 Scope of Survey

The survey was undertaken over the Queenstown end of the Queenstown span, with one measurement taken for the beams at each ligature, at approximately mid-height of the beam sides and on the centreline of the soffit, and on transverse bars in the deck slab adjacent to each fillet at the beam-slab junction.

Covers were measured with a Profometer 3 cover meter.

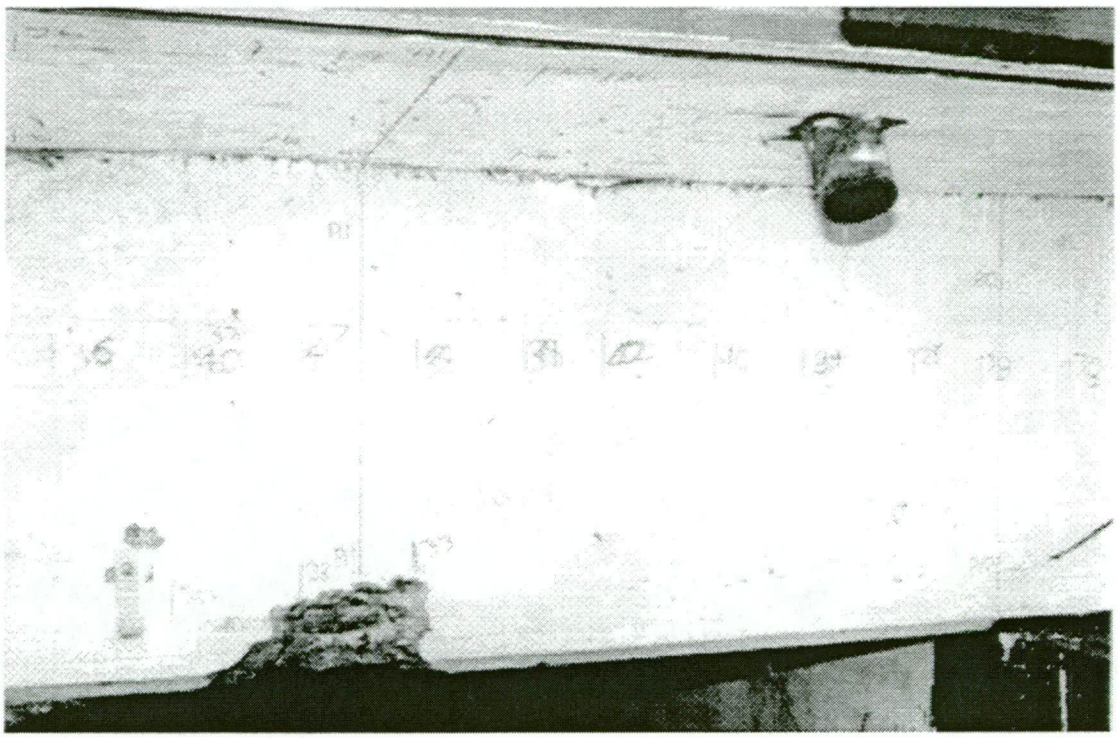

Figure 10.1 - Covers on Exterior Beam and Deck Soffit

The extent of the survey was dictated by time and access considerations. The extent of cover survey, the number of readings and cover statistics for each location are shown in Table 10.1.

Location	Extent of survey (m)	No. of readings	Min cover (mm)	Max. cover (mm)	Average cover (mm)	Standard deviation (mm)
Downstream beam						
- soffit	2.1	8	20	33	26.4	4.4
- upstream	4.6	20	45	62	52.3	3.9
Slab soffit						
- downstream	5.2	28	33	45	39.9	3.6
- upstream	5.2	27	25	43	35.4	4.0
Fifth beam						
- downstream	5.3	22	44	64	51.7	4.6
- soffit	2.8	15	26	33	29.8	2.2
- upstream	5.4	26	32	46	39.7	4.8
Slab soffit						
- downstream	5.3	38	41	56	47.2	3.8
- upstream	5.3	36	29	45	36.2	4.5
Fourth beam						
- downstream	5.6	28	33	62	49.1	6.9
- soffit	3.4	19	19	43	27.2	7.9
- upstream	3.2	21	32	44	37.0	3.6
Slab soffit						
- downstream	2.8	20	33	44	39.4	2.7
- upstream	2.8	21	32	52	45	4.8
Third beam						
- downstream	2.6	18	33	51	43.5	5.2
- soffit	3.4	4	21	23	22	0.9
- upstream	6.1	28	33	50	37.9	4.0
Slab soffit						
- downstream	5.9	31	32	53	45.8	5.6
- upstream	5.7	29	43	68	56.2	6.7
Second beam						
- downstream	6.2	30	40	62	51.2	5.2
- soffit	3.2	17	26	50	37.0	7.7
- upstream	4.2	25	24	48	35.2	5.5
Slab soffit						
- downstream	3.4	26	10	57	41.5	10.9
- upstream	3.4	25	23	66	38.9	10.0
Upstream beam						
- downstream	3.8	23	41	50	45.4	2.6
- soffit	6.4	20	24.2	38.5	30.6	3.8
- upstream	6.2	39	31	49.5	42.9	4.1
Kerb overhang						
- downstream	7.9	24	25	68	46.4	11.9
- upstream	8.1	25	21	50	30.6	7.6

Table 10.1 - Cover Measurements

10.2 Statistical Analysis

A statistical analysis of the cover measurements shows the following results:

	Beams	Slab	Overall
Specified cover (mm)	38	32	-
Average cover (mm)	40.9	42.1	-
Median cover (mm)	41.8	41.8	-
Standard deviation (mm)	9.4	9.4	-
Minimum cover (mm)	19	10	10
Maximum cover (mm)	64	68	68
Number of measurements	363	330	693

Table 10.2 - Cover Statistical Analysis

The distribution of covers in 5mm groupings is shown in Figure 10.2.

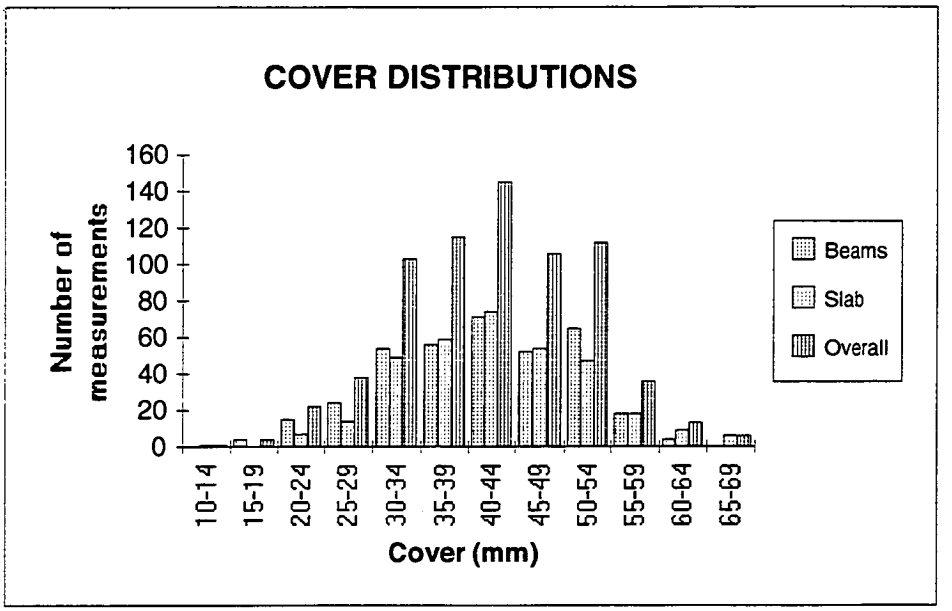

Figure 10.2 - Cover Distributions

The covers are also considered in terms of the proportions complying with the Department of Transport specification requirements at the time of testing of within 5mm of specified cover and with the AS3600 and more recent Departmental requirements of -5mm,+10mm of specified cover.

	Beams	Slab	Overall
DoT specification			
Number below	63	16	79
Number above	157	228	385
Number complying	143	86	229
% complying	43	26	33
AS3600			
Number below	63	16	79
Number above	96	157	253
Number complying	204	157	361
% complying	56	48	52

Table 10.3 - Cover Compliances

10.3 Comparative Results

Measured covers from Princess River Bridge are compared with those reported by Marrosszeky and Chew (1989) for a number of bridges in the Sydney area. Results are reported in terms of the percentages of measurements exceeding proportions of the nominal cover, N.

	Percentages of cover exceeding thresholds			
	Beams	Slab	Overall	M&C
>0.6N	96.7	99.7	98.1	96
>0.7N	93.7	99.1	96.3	95
>0.8N	86.5	96.2	91.2	93
>0.9N	73.3	95	83.7	87
>1.0N	61.2	87	73.6	51

Table 10.4 - Cover Comparisons

The comparisons are shown graphically in Figure 10.3.

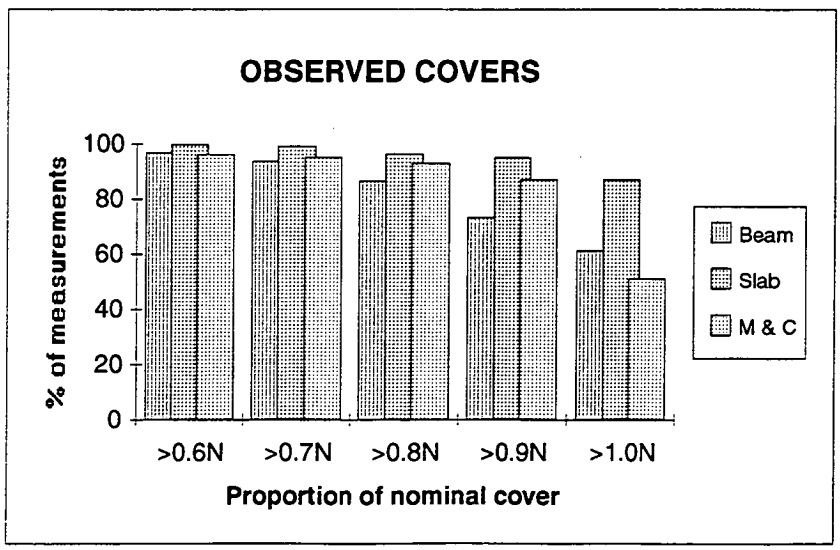

Figure 10.3 - Cover Comparisons

10.4 Comparison with other Tasmanian bridges

A comparison of the results of the Princess River cover survey with a more general survey of Tasmanian bridges, encompassing 10313 measurement on 49 structures built between 1932 and 1996, and Marrosszeky and Chew's results is shown in Figure 10.4. The overall distribution of cover measurements for the Tasmanian bridges is shown in Figure 10.5.

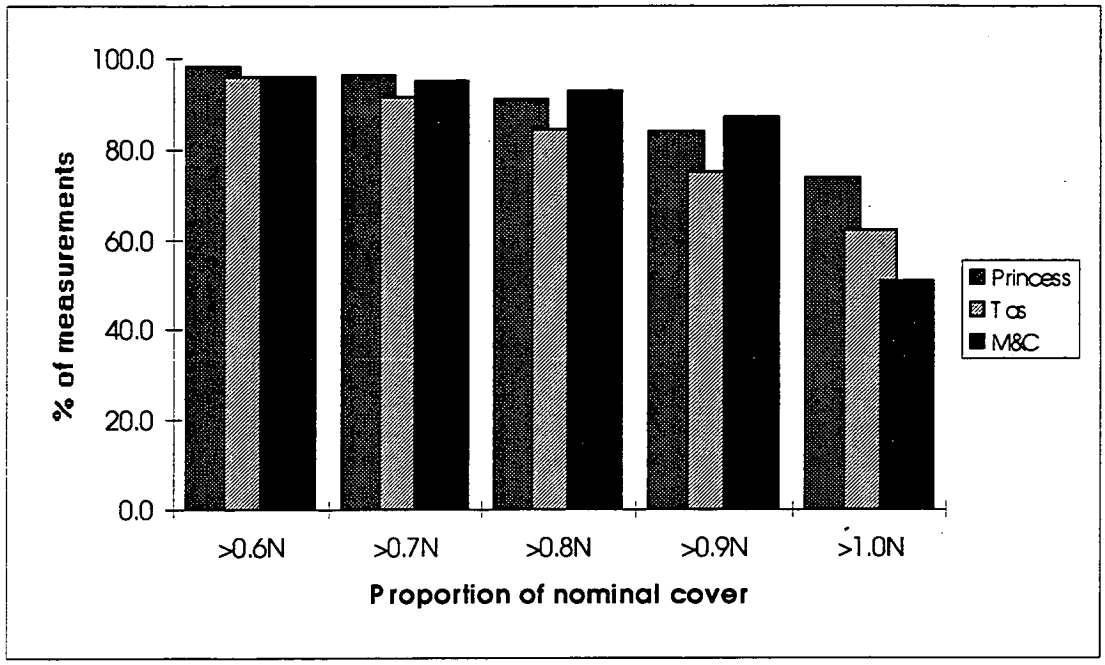

Figure 10.4 - Cover Comparisons

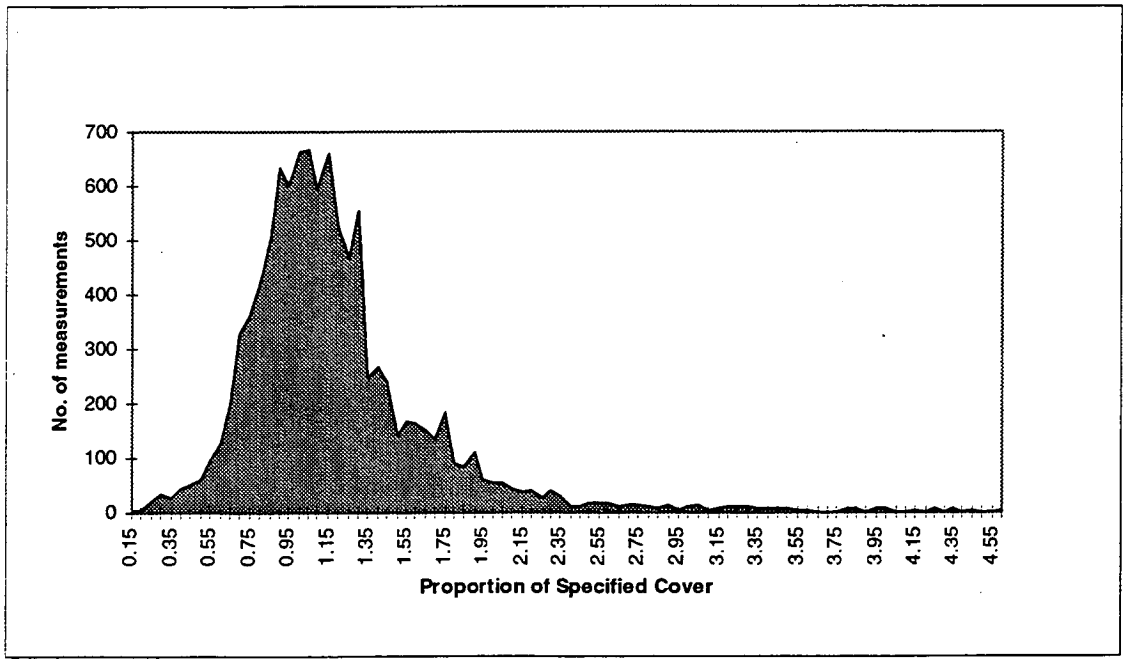

Figure 10.5 - Cover Distributions for Tasmanian Bridges

Proportions of cover measurements complying with the AS3600 tolerance of -5+10mm for the 49 Tasmanian bridges by decade and those for Princess River Bridge are detailed in Table 10.5.

	1930's	1940's	1950's	1960'	1970'	1980's	1990's	Overall	Princess
No. bridges	4	8	13	7	4	3	10	49	1
No. measurements	1252	1533	3062	1644	833	468	1501	10313	693
% complying	44.1	48.6	38.2	54.7	64.9	75.6	57.3	49.6	52

Table 10.5 - Comparisons of Cover Measurements

10.5 Discussion

The overall distribution of measurements shows an approximately normal distribution, with the peak of the curve at a cover slightly greater than that specified.

The distributions of cover measurements are consistent with those reported by Marrosszeky and Chew and those for a number of other Tasmanian bridges.

The benign environment at Princess River meant that the low recorded covers did not cause durability problems in the structural members. Low covers and porous concrete in the railings had however led to corrosion in those elements.

The cover variabilities and the large proportion of measurements outside specified tolerances indicate a need to review specification requirements and construction practices.

11. PRE-EXISTING CRACKING

11.1 Introduction

An extensive survey of pre-existing cracking was undertaken as part of the survey of the condition of the bridge prior to the full-scale load testing to give an indication of construction deficiencies, loading history and serviceability and durability defects.

11.2 Pre-existing crack patterns

The underside of the bridge was painted prior to load testing with a single coat of an isocyanate cured polyurethane paint to highlight cracks, both pre-existing and those that developed during the testing program. The paint also provided a surface suitable for felt tip pens for marking the cracks.

Figure 11.1 - Marking of Pre-Existing Cracks

Pre-existing cracking in the bridge was extensive, particularly in the deck soffit, and consisted generally of a random pattern of fine cracks (<0.1mm). Little flexural cracking of the beams was evident, with many of the near-vertical cracks in the beam webs being discontinuous and starting above the beam soffit. Typical crack patterns are shown in Figures 11.2 to 11.6.

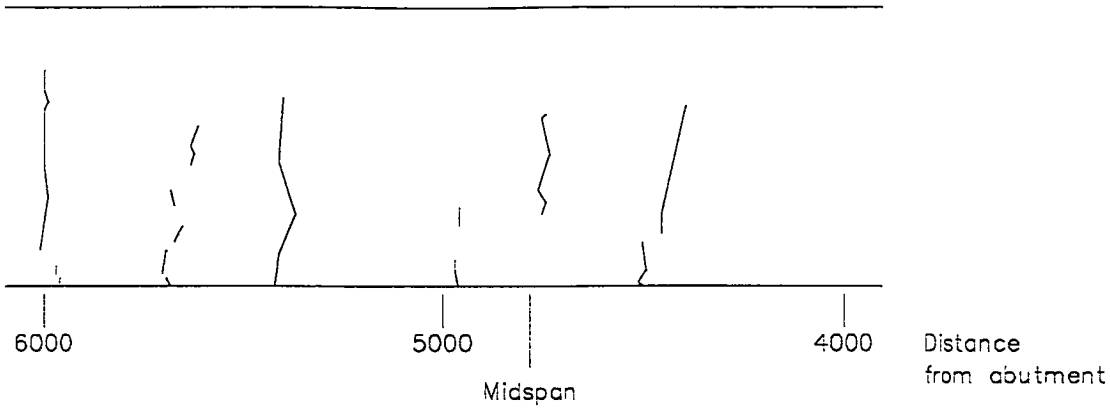

Figure 11.2 - Pre-existing cracks, exterior face of upstream beam

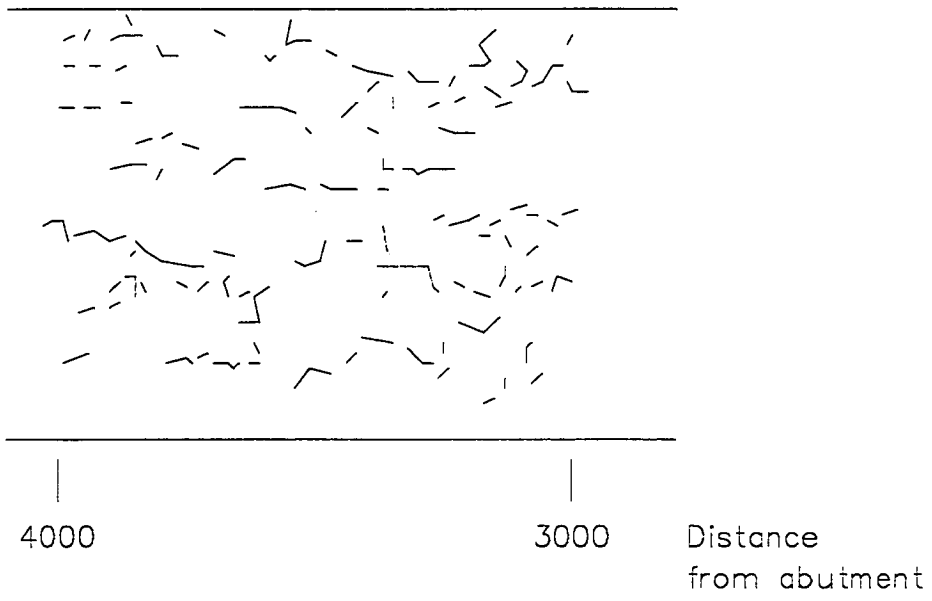

Figure 11.3 - Deck soffit between second and third beams from upstream

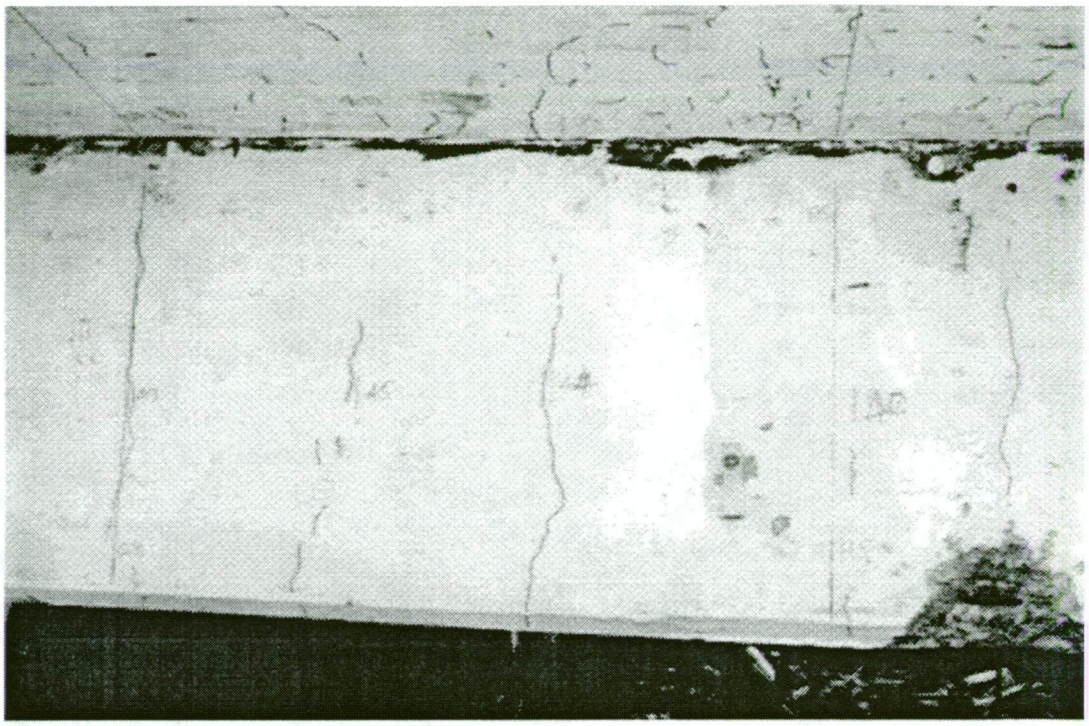

Figure 11.4 - Pre-existing Beam Cracking

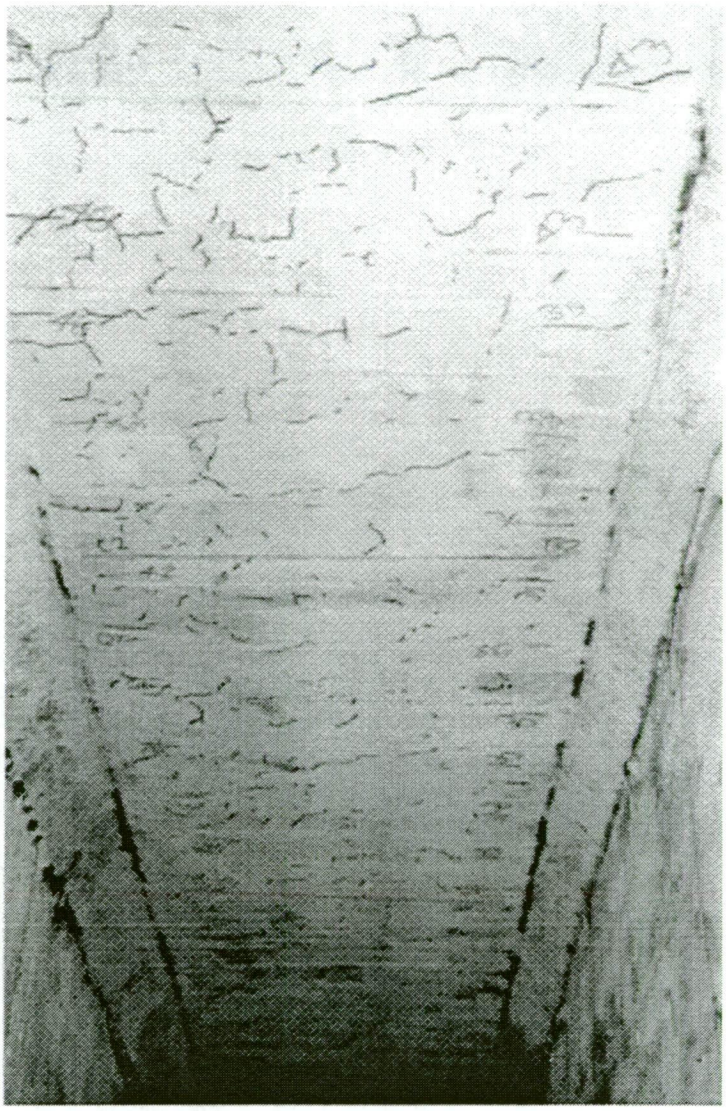

Figure 11.5 - Pre-existing Deck Soffit Cracking

Figure 11.6 - Pre-existing Deck Soffit and Diaphragm Cracking

11.3 Discussion

While pre-existing cracking in the soffit of the deck and in the beams was extensive, there was no evidence of durability having been adversely affected. There was little or no efflorescence, despite the high rainfall at the site, indicating that cracking was not continuous through the deck. Vertical cracking in the beams may or may not have been flexural, because of the irregular nature and limited amount of cracking and the relatively high stiffness of the bridge. It would be expected that flexural cracking, in accordance with St Venant's principle, would take the form of a primary pattern of cracks at a spacing between one and two times the height of the neutral axis (320 to 640 mm for the non-composite section, 640 to 1280 mm for the composite interior beam section) extending from the soffit of the beam to the neutral axis, with a secondary pattern of more closely spaced shorter cracks extending from the beam soffit.

The regular pattern of lines on the concrete surfaces indicates that tongue and groove flooring was used as formwork. It is unlikely that effective sealing compounds were available at the time of the bridge's construction and it is thus concluded that the cracks were principally caused by drying shrinkage resulting from ineffective curing. The lesser amount of cracking in the beams may have been attributable to the fact that they were precast and had better curing; the insitu deck by contrast had higher cement contents, with consequent higher shrinkage, and is likely to have had less effective curing leading to the more extensive crack patterns.

Notwithstanding the extensive pre-existing cracking, the lack of durability related distress in the structure, except for the railings, can be attributed to the high humidities at the site and the resultant low rates of carbonation.

The lack of flexural cracking in the beams and the absence of longitudinal cracking in the deck indicate that the bridge had not been subject to any significant overload.

12. CONCRETE PERFORMANCE

12.1 Introduction

A number of cores were taken from the bridge deck and the Hobart abutment during the on-site work and subsequently tested to assess the quality and performance of the concrete in the structure.

Cores were also taken from the two beams transported to Lutana for testing.

It had originally been intended to take a large number of cores from deck, beams, pier crosshead and piles, and abutments to investigate the effects of microclimate on concrete performance, but this was not possible due to high water levels in the Princess River and a number of closures of the Lyell Highway from ice and snow during the period of testing and the consequent inability of Materials and Research personnel to reach the site.

12.2 Concrete Specification

Drawings specified Class A concrete in the structure, with the exception of the piles which were to be Class AA.

For a Class A concrete, Taylor (1969) reports that the Commonwealth Department of Works method for designing a suitable mix was based on a water/cement ratio of 0.5 by weight and a mean 28 day compressive strength of 4400 psi (30.4 MPa). For site batching and 95% of tests above the nominal minimum, a control factor of 70% to 75% would be applied, giving a characteristic strength of 3080 psi (21.3 MPa) to 3300 psi (22.8 MPa). It is thus assumed that the Class A concrete corresponded to a characteristic strength of 3000 psi (20.7 MPa).

12.3 Cement Composition

It is probable that Goliath cement was used in the construction of the bridge. Average results from weekly testing of cement at the time of construction of the bridge are detailed in Table 12.1.

Item	Six months 01.07.58 to 31.12.58	Year 01.07.58 to 30.06.59	Six months 01.07.59 to 31.12.59
%CaO	63.4	63.4	63.5
$\%SiO_2$	21.3	21.4	21.0
$\%Al_2O_3$	5.70	5.68	5.96
$\%Fe_2O_3$	3.44	3.40	3.30
$\%SO_3$	1.91	1.91	1.96
% Freelime	1.3	1.3	1.2
% Loss on ignition	1.4	1.4	1.3
Surface area (m^2/kg)	307	307	305
C_3S	47.5	47.0	48.5
C_2S	25.2	26.0	23.8
C_3A	9.3	9.3	10.2
C_4AF	10.4	10.4	10.0

Table 12.1 - Cement Composition

12.4 Concrete Strength Testing

Compressive tests were made on 75mm diameter cores from midspan of the Hobart and Queenstown spans upstream of the bridge centreline and two specimens cut from a 50mm diameter horizontal core from the Hobart abutment.

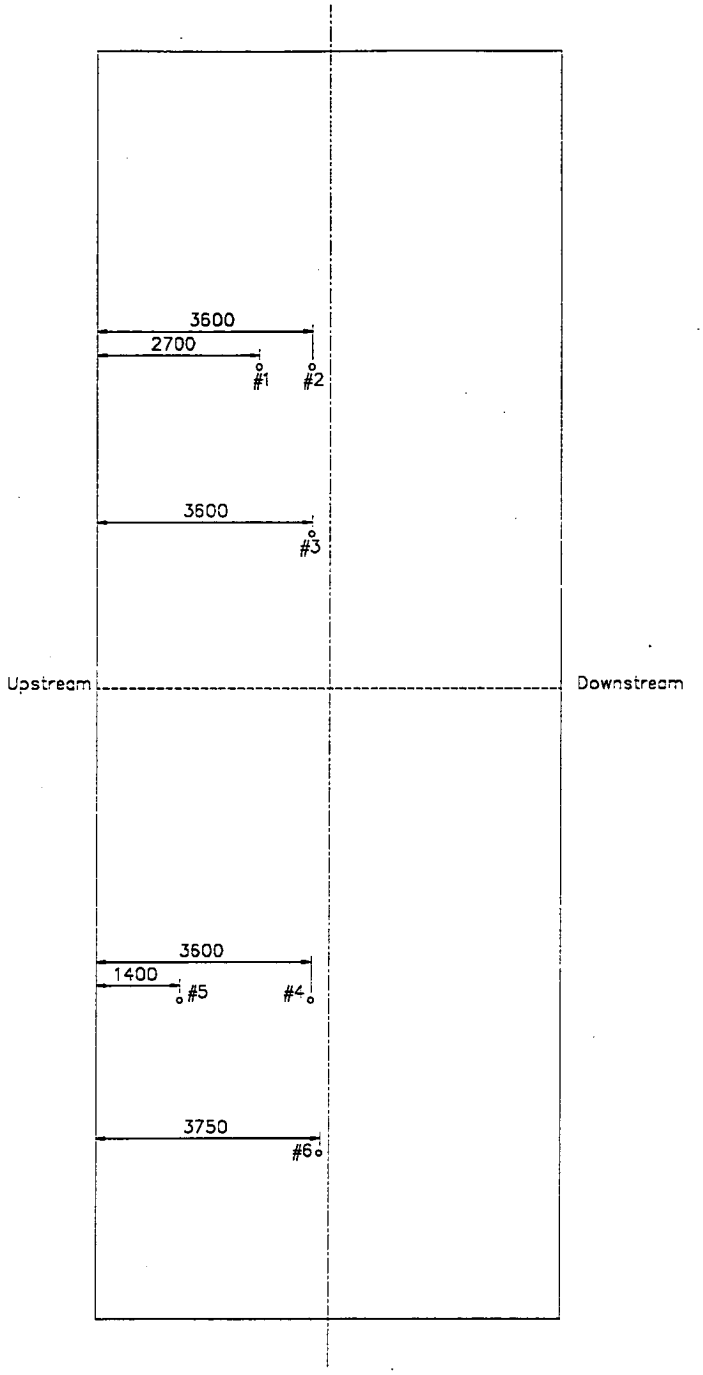

Figure 12.2 - Deck Core Locations

The Hobart span deck core was tested by the University of Tasmania with strains being measured by Huggenberger tensometers of 50mm gauge length, and the remainder at the Department of Transport's Materials and Research Laboratory using a 50mm Demec gauge to measure strains.

Young's Modulus calculations are based on the method described in AS1012 Part 17 - 1976, but without the initial loading and unloading cycles, and the Modulus calculated between the strain measurement closest to 50 microstrain and the measurement closest to 40% of the ultimate compressive strength.

Results are detailed in Table 12.2 and stress-strain curves plotted in Figures 12.3 and 12.4.

	Deck		Abutment	
	Hobart	Queenstown	1X	1Y
Core length (mm)	132	109.5	97.2	97.9
Core diameter (mm)	74	75	49.9	49.8
Density (kg/m^3)	2590	2550	2550	2450
Compressive strength (MPa)	60.5	53.4	47.6	43.6
Young's Modulus (MPa)	35200	35100	32300	36000

Table 12.2 - Bridge Cores

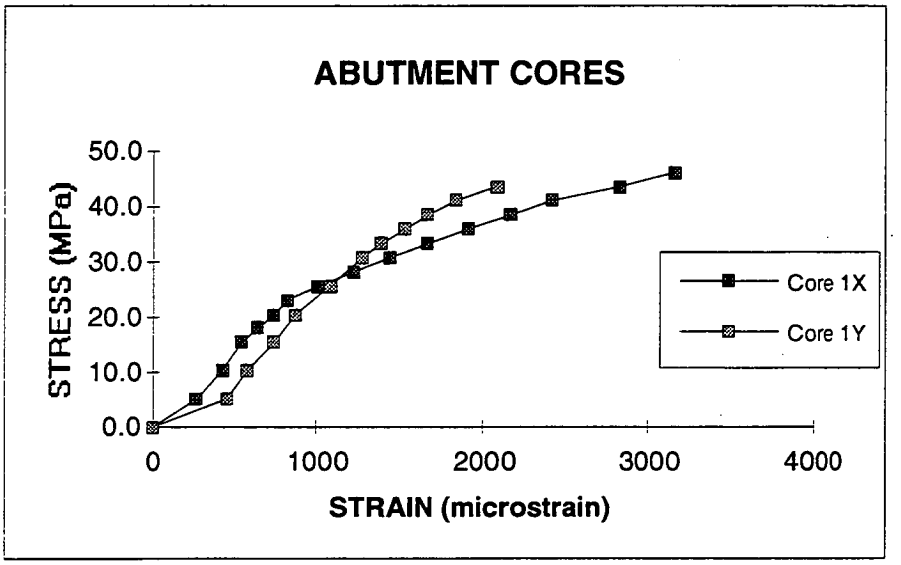

Figure 12.3 - Abutment Cores

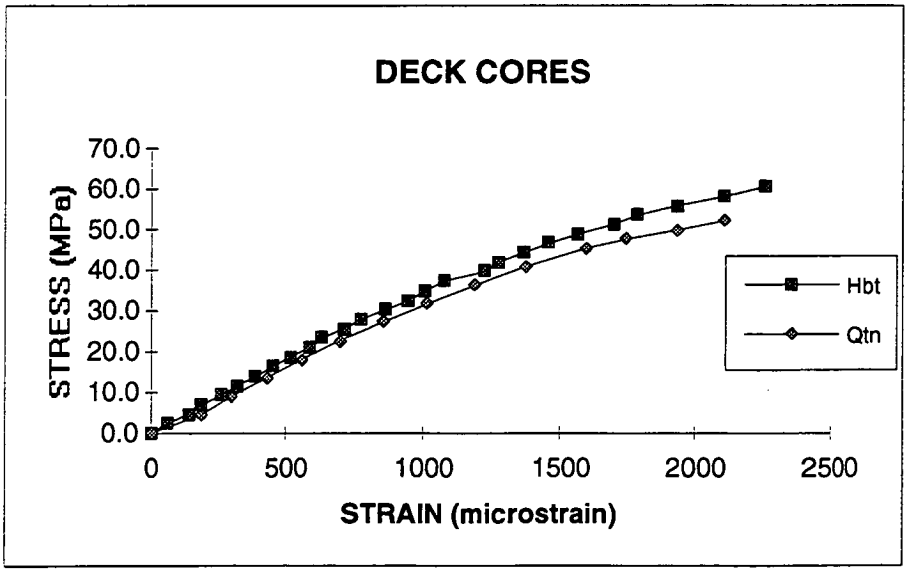

Figure 12.4 - Deck Cores

A further three cores were taken from the two beams transported to the Lutana Quarry for testing. Coring occurred on 20 August 1992, almost exactly twelve months after the beams were transported from Princess River to Hobart.

Cores were each cut into three approximately equal lengths, with the outer sections being subject to testing for carbonation, cement content and water cement ratio, and the inner sections subject to compression testing. The compression cores were conditioned for 17 hours in lime water prior to testing.

	Beam		
	Flexural	Flexural	Shear
Distance from beam end (m)	0.39	8.14	5.36
Height above soffit (m)	0.49	0.42	0.36
Total core length (mm)	378	379	381
Compression core length (mm)	131.9	136.2	116.4
Core diameter (mm)	68.6	68.1	68.3
Dry density (kg/m^3)	2670	2560	2510
Conditioned density (kg/m^3)	2680	2580	2520
Compressive strength (MPa)	75.8	57.4	76.4
Maximum strain (με)	1400	1300	1800
Young's Modulus (MPa)	66800	51300	41300
Chemical analysis samples			
Oven dry density (kg/m^3)	2420	2420	2400
Saturated surface dry density (kg/m^3)	2600	2600	2580
Cement content (kg/m^3)	370	330	360
Water cement ratio	0.44	0.48	0.46
Carbonation depth (mm)	<1	<1	<1

Table 12.3 - Beam Cores

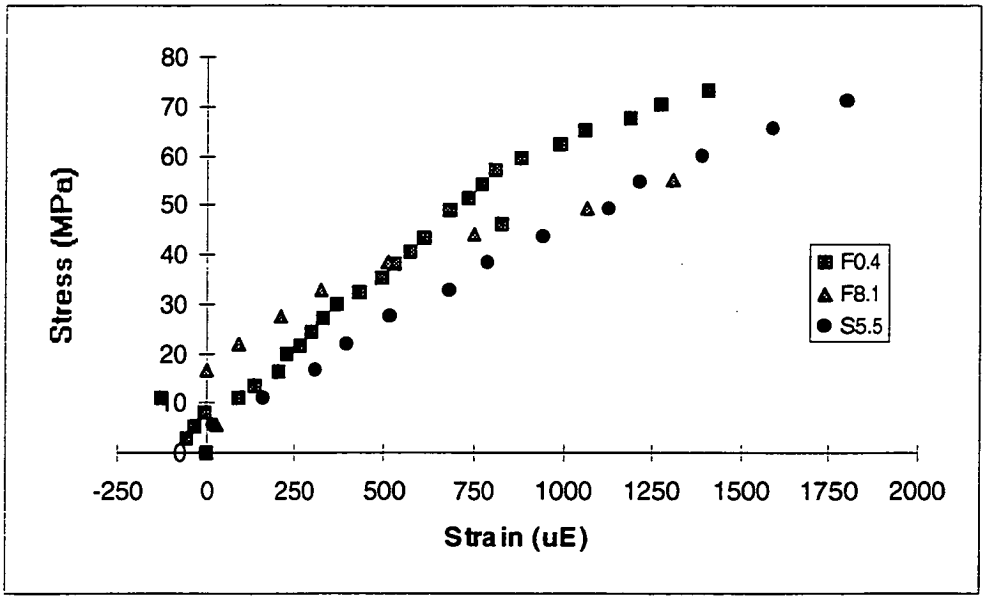

Figure 12.5 - Beam Cores

12.5 Carbonation

Depths of carbonation were measured on a core from the Hobart span deck upstream of the road centreline at the span quarter point and on the core from the top abutment core using phenolpthalein solution.

No carbonation could be detected in either core.

As shown in Table 12.3, carbonation depths in the cores taken from the two precast beams were less than 1mm a year after they were transported to Hobart.

12.6 Cement Content

Cement contents were determined in accordance with AS1012 Part 15 - 1979 EDTA titrimetric method (acid extractable calcium) for the two cores tested for carbonation.

Results are presented in Table 12.4.

Core	Oven dry density (kg/m³)	Cement content (kg/m³)
Deck	2540	450
Abutment	2380	490
Beams	2420	370
	2420	330
	2400	360

Table 12.4 - Concrete Properties

12.7 Water Cement Ratio

Water cement ratios were determined for the three cores from the two precast beams by determining the original water content of the concrete at the time of hardening . The method involved immersing the sample of hardened concrete in water for 24 hours and dehydrating at 593°C for 2 hours. The resulting % total moulding water was converted to kg/m³ using the mass per unit volume of the concrete, correcting for aggregate absorption (assumed at 1%), and using the previously determined cement content.

Ratios are detailed in Table 12.5.

Location	Cement Content (kg/m³)	Water cement ratio
Flexural beam 0.4m	370	0.44
Flexural beam 8.1m	330	0.48
Shear beam 5.5m	360	0.46

Table 12.5 - Water cement ratios

12.8 Chloride Profile

The concentration of chloride ions at various depths was determined on a core from the deck of the Queenstown span at the quarter point on the road centreline by extraction with 1M nitric acid and using a mercuric thiocyanate spectrophotometric method.

The chloride profile is detailed in Table 12.6.

Distance from deck surface (mm)	%Cl by mass of concrete
0-20	0.010
20-40	0.011
40-60	0.007
60-80	0.005
80-100	0.007
100-120	0.010
120-140	0.007
140-160	0.005
160-180	0.005
180-210	0.004

Table 12.6 - Chloride Profile

As expected in the west coast environment, chloride concentrations are significantly lower than the 0.8 kg/m^3 (corresponding to 0.03% by mass for a density of 2600 kg/m^3) generally permitted for new construction. The values also indicate that calcium chloride was not used as an accelerator for the concrete.

12.9 Sulphate Profile

The sulphate profile was measured for a core from the Hobart span at midspan on the road centreline by determining sulphur trioxide contents after extraction with 1M hydrochloric acid, using the classic gravimetric procedure of precipitation with barium chloride solution, filtration, washing and ignition of the barium sulphate precipitate.

Distance from deck surface (mm)	%SO_3 by mass of concrete
0-20	0.40
20-40	0.33
40-60	0.32
60-80	0.33
80-100	0.33
100-120	0.33
120-140	0.33
140-160	0.40
160-180	0.43
180-202	0.50

Table 12.7 - Sulphate Profile

For a 1.91% SO_3 content, a cement content of 450kg/m^3 and concrete density of 2550 kg/m^3, the concrete SO_3 content is calculated to be 0.34% correlating with the measured content in the body of the concrete.

12.10 Young' Modulus

Core	Compressive Strength (MPa)	Density (kg/m3)	Young's Modulus (MPa)	$E/\{\sqrt{(w^3F'_c)}\}$	$0.043\{\sqrt{(w^3F'_c)}\}$
Deck - Hobart	60.5	2590	35200	0.0343	44100
Deck - Queenstown	53.4	2550	35100	0.0342	40500
Abutment - 1X	47.6	2550	32300	0.0364	38200
Abutment 1Y	43.6	2450	36000	0.0450	34400
Flexural - 0.39m	75.8	2670	66800	0.0556	51600
Flexural - 8.14m	57.4	2560	51300	0.0523	42200
Shear - 5.36m	76.4	2510	41300	0.0376	47300
Mean	59.2	2550	42600	0.0422	42600
Std. deviation	12.8	70	12400	0.0089	5700

Table 12.8 - Comparative Concrete Properties

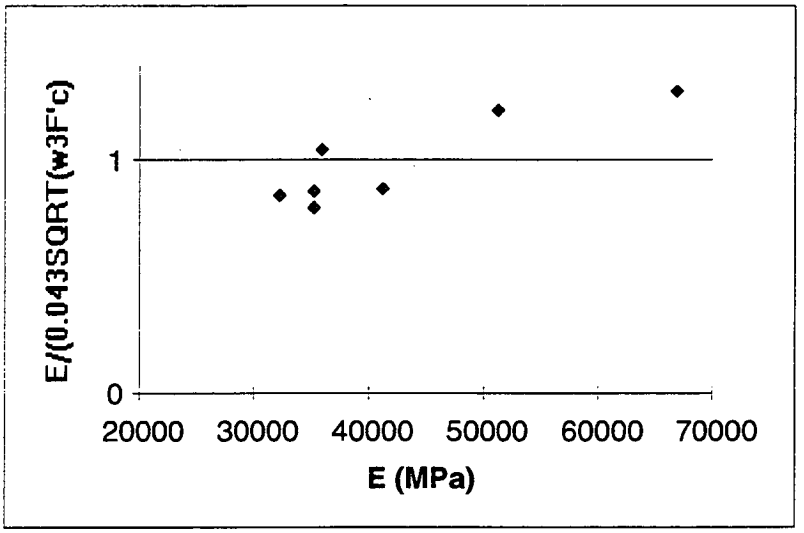

Figure 12.9 - Young's Modulus Comparison

12.11 Long Term Strength Gain

No compressive test results from the time of construction of the bridge could be located, and it has thus not been possible to assess long term strength gain in the concrete.

Washa and Wendt (1975) have reported results of testing on United States concretes up to 50 years old. For 18 concretes, the ratio of compressive strength at 25 years to that at 1 month ranged from 1.27 to 3.26. If the 15 results where the 25 years strength exceeded 45 MPa (6500 psi) are considered, the mean ratio is 1.8. On that basis, mean strength of concrete used in the structure would have been of the order of 33 MPa, corresponding closely to the target mean compressive strength of 30.4 MPa from Taylor. Mean cement content of the United States concretes was 320 kg/m^3 and water/cement ratio 0.47. The mean 28 day compressive strength was 4750 psi (33 MPa). It is of interest to note that the surface areas of the cements ranged from 105 to 180 m^2/kg, compared to the 305 to 307 m^2/kg for Goliath cement. C_2S contents were however generally higher than the 25% of Goliath, ranging from 23.2% to 44.4%.

12.12 Discussion

It is likely that the quality of the concrete used in the construction of Princess River Bridge is significantly better than for other structures around the State constructed at about that time.

Using all compression test results,

mean strength	=	59.2 MPa
standard deviation	=	12.8 MPa
F'_c	=	59.2 - 1.65*12.8
	=	38 MPa

Using superstructure results only

mean strength	=	64.7 MPa
standard deviation	=	10.7 MPa
F'_c	=	64.7 - 1.65*10.7
	=	47 MPa

The large standard deviations result from the small number of samples. The 1965 Highway Bridge Design Specification requires F'c for reinforced concrete not to exceed 4500 psi (31 MPa), although the modular ratio is given in Codes from 1958 to 1970 for F'_c of 5000 psi (45 MPa) or more. F'_c is thus taken to be 35 MPa for subsequent analysis.

With an characteristic compressive strength of 35 MPa, cement content of 400 kg/m^3 and water cement ratio of 0.46, and the bridge in a relatively benign environment with high humidity, no corrosion was evident in the main structural members notwithstanding the existence of covers as low as 10mm.

Current concrete mixes of a similar design to that in the preceding paragraph would typically result in an average 28 day strength of 50 MPa.

While no samples were taken from the handrails, it is likely that corrosion resulted from a lower quality of concrete and minimal cover.

There is significant variability in the measured values of Young's Modulus for the various concrete cores. The 1976 NAASRA Bridge Design Specification specified value of $0.043\sqrt{(w^3F'_c)}$ provides reasonable correlation with the measured values and has been used for structural analysis.

12.13 Properties for Structural Analysis

The following concrete properties have been adopted for structural analysis.

Density, ω	2580 kg/m^3
F'_c	35 MPa
E_c	33 GPa
n	6.0
Beam width	380 mm
Beam depth	685 mm

13. STEEL PERFORMANCE

13.1 Introduction

Reinforcement samples were taken from the Queenstown end upstream and downstream kerb overhangs, the Hobart span beam subject to artificial deterioration (refer chapter on dynamic response), and from each of the two beams transported to Lutana.

13.2 Tensile Testing

The kerb bars were tested by the Civil Engineering Department of the University of Tasmania, and the remaining three by the Engineering and Scientific Services Department of the Hydro-Electric Commission.

Test results are summarised in Table 13.1.

Bar location	Bar diameter	Yield Stress (MPa)	Ultimate Tensile Stress (MPa)	% Elongation $5.65\sqrt{(s_0)}$	Young's Modulus (GPa)
Upstream kerb	12.62 mm	300.6	474.1	-	-
Downstream kerb	12.6 mm	301.5	474	-	-
Hobart span	1.25"	300	440	33	214
Flexural beam	1.25"	280	460	33	-
Shear beam	1.25"	280	420	39	-

s_0 = cross-sectional area

Table 13.1 - Tensile Test Results

13.3 Properties for Analysis

The reinforcing steel properties adopted for analysis are detailed in Table 13.2.

Yield Stress	290 MPa
Young's Modulus	200 GPa

Table 13.2 - Steel Properties for Analysis

14. BEAM TESTING

14.1 Introduction

Two precast beams had been condemned during construction, and placed on the ground some 50 metres from the bridge with the area, at the time of bridge testing, overgrown with blackberries.

Anecdotal evidence was that the beams had been dropped in transit. A close inspection of the bridge however showed only evidence of local honeycombing in the lower part of the beams and no significant cracking.

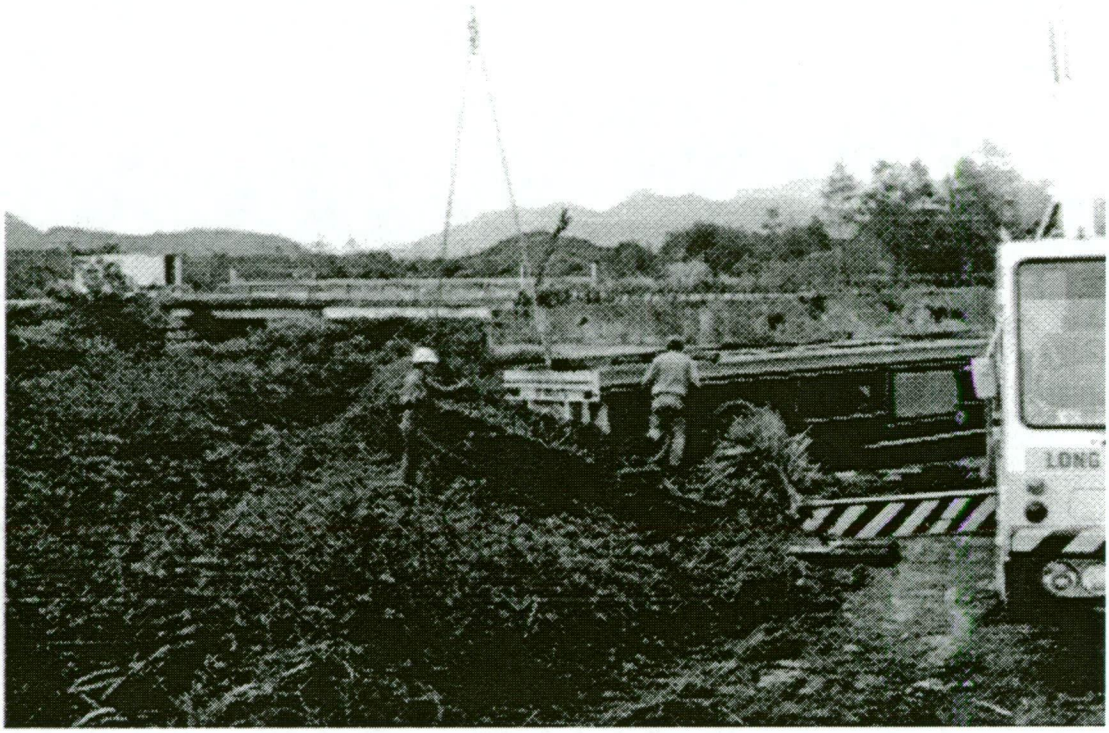

Figure 14.1 - Recovery of Precast Beams from Site

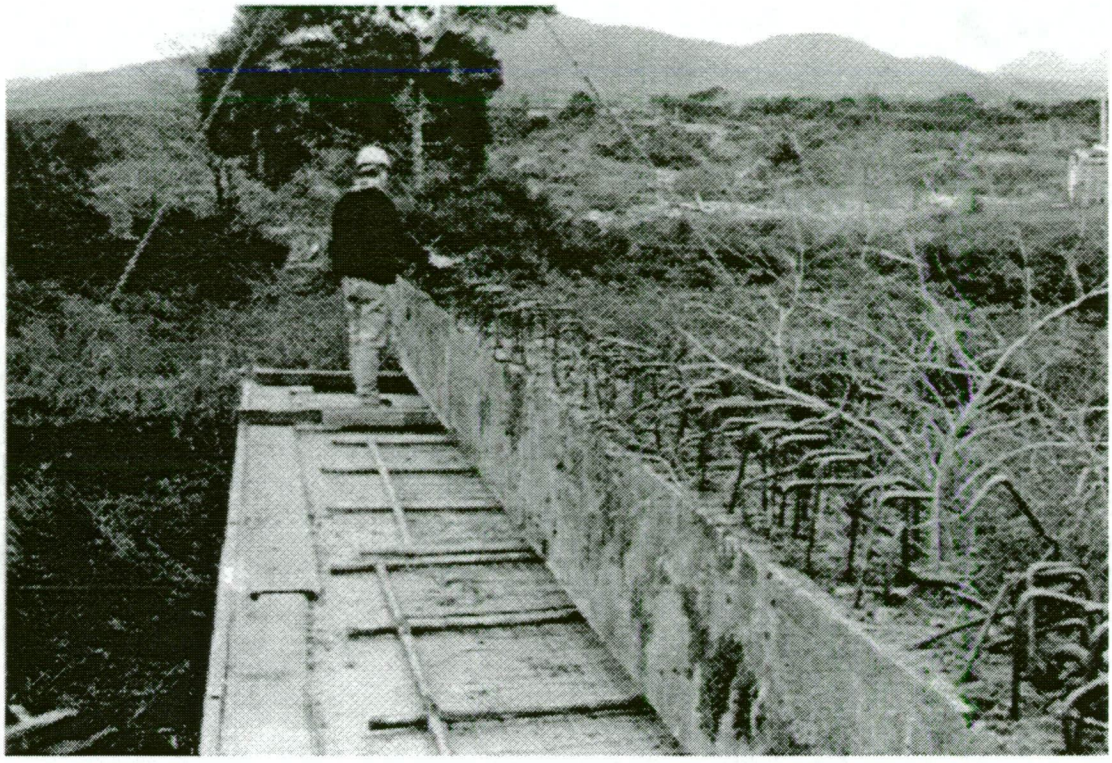

Figure 14.2 - Recovery of Precast Beams from Site

The beams were transported to the Department of Construction's Lutana Quarry and tested in June 1992. One beam was loaded in flexure and the other in shear.

The beams were painted with one coat of white two-pack polyurethane paint prior to testing to highlight pre-existing cracks and cracks which developed under load. The only pre-existing cracks evident were short cracks at the top of the beam likely to have resulted from corrosion of the top sections of the ligatures.

14.2 Beam Dimensions

Beam dimensions were measured at 1 metre intervals along the two beams. Measurements are tabulated in Table 14.1.

	Flexural Beam		Shear Beam	
Overall length	10660		10625	
Distance along beam (m)	**Depth**	**Width**	**Depth**	**Width**
1.0	674	378	700	381
2.0	680	381	685	381
3.0	682	381	685	380
4.0	682	377	690	380
5.0	675	378	688	381
6.0	677	381	680	380
7.0	675	377	682	381
8.0	680	376	690	381
9.0	690	379	693	382
10.0	685	379	686	381
Mean	680	379	688	381
Standard deviation	5.0	1.8	5.8	0.6

Table 14.1 - Beam Dimensions (mm)

	Depth	Width
Specified	686	381
Permitted tolerance	-5, +15	-5, +15
Mean	684	380
Standard deviation	6.6	1.7

Table 14.2 - Dimensional Summary

The permitted tolerance is taken from the current Department of Transport bridge construction specification and is not necessarily that applying at the time of construction. The higher variability in the depth dimension is expected because of the requirement to leave the top surface rough for subsequent casting of the insitu deck. Because of the casting of insitu concrete and the large fillets in the design, greater variability in the dimension is acceptable.

The mean measured dimensions are within 0.3% of the specified depth and width. All width measurements were within the specified tolerance. Five of the twenty depth measurements were outside the permissible deviation in the Department's current specification. The dimensional accuracy of the members is nevertheless considered acceptable.

14.3 Beam Flexural Test

The beam selected for testing was loaded at two points to give a uniform bending moment over a distance of 3.3m. The beam was supported on elastomeric bearing pads 400mm x 200mm x 25mm located 0.15m from each end of the 10.68m long beam.

The loading was applied through 50t capacity hand operated hydraulic jacks with the reaction being supplied through the transverse beams used for the full-scale bridge test with 3 no. 12.7mm diameter prestressing strands at each end grouted 5m into the floor of the quarry.

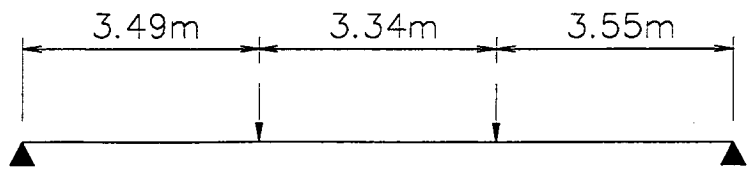

Figure 14.3 - Beam Loading Configuration

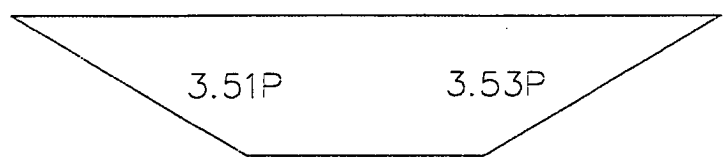

Figure 14.4 - Bending Moment Diagram

Strains were measured at midspan. The range of the gauges was exceeded at a load P approaching 125kN, and thus the only strain measurement is 84.5 microstrain for P=62.1 kN.

Photographs of the beam at the conclusion of the testing are included as Figures 14.5 to 14.20. Beams are marked at 1m intervals so that '5A' for example refers to a location 5m from the end of the beam on side A. The marks on the cracks refer to gauge pressures on the hydraulic jacks.

At midspan, there were a small number of vertical cracks to the full depth of the beam, with further and more frequent to and spaced at the calculated depth of the neutral axis. At the ends of the beams the cracks were inclined.

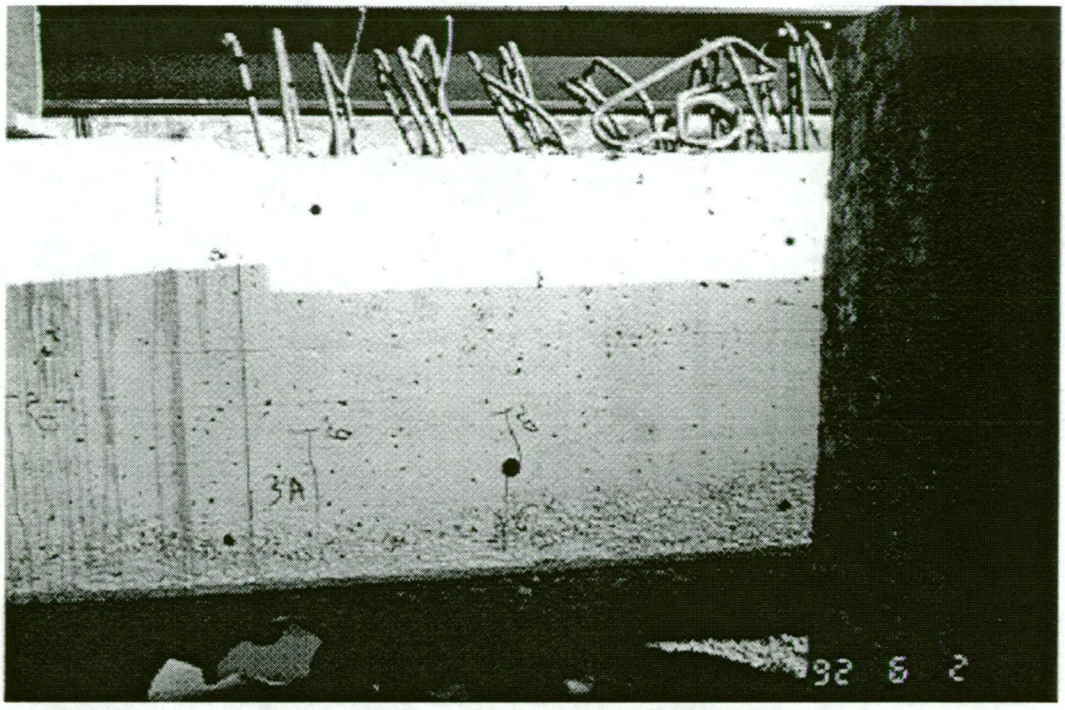

Figure 14.5 - Flexural Beam Crack Patterns

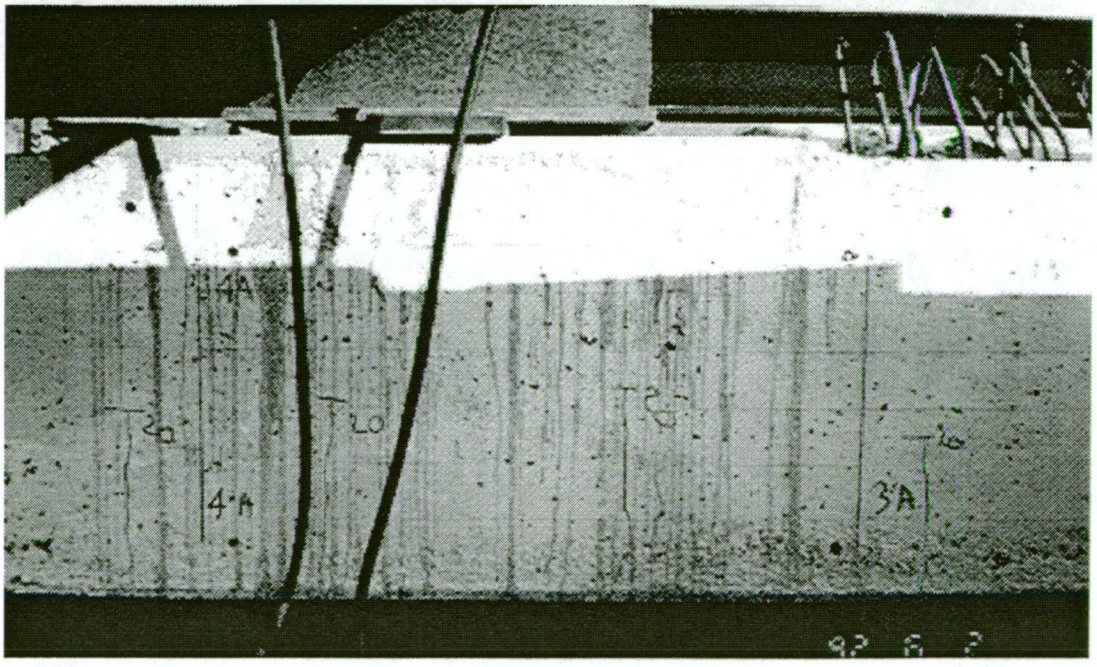

Figure 14.6 - Flexural Beam Crack Patterns

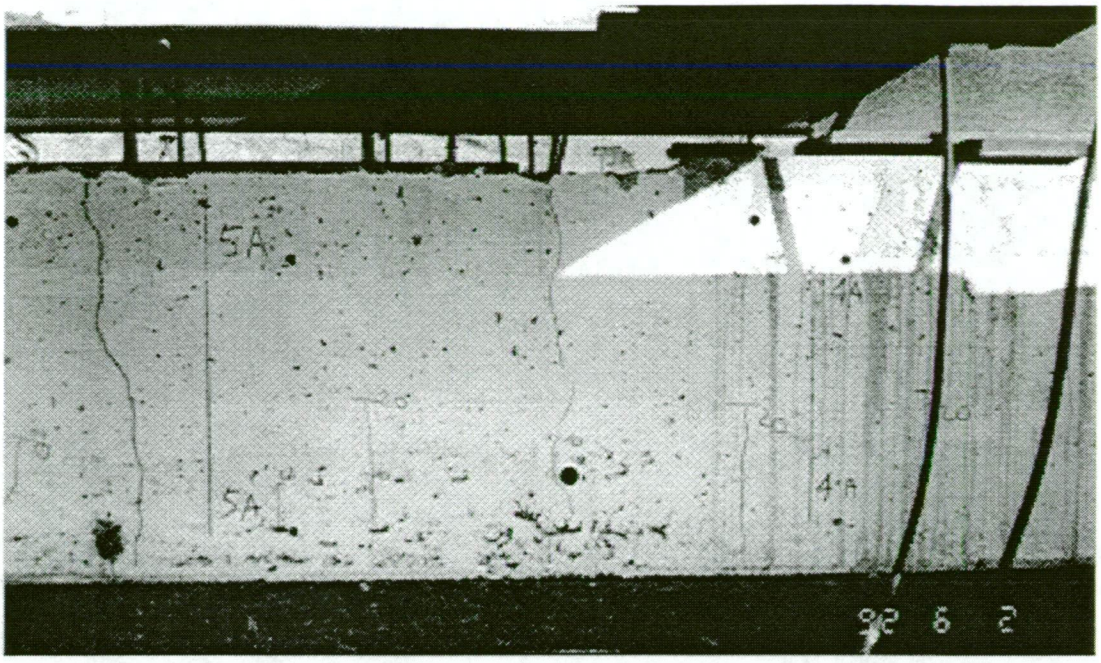

Figure 14.7 - Flexural Beam Crack Patterns
(Note area of honeycombing in soffit of beam at centre of photograph)

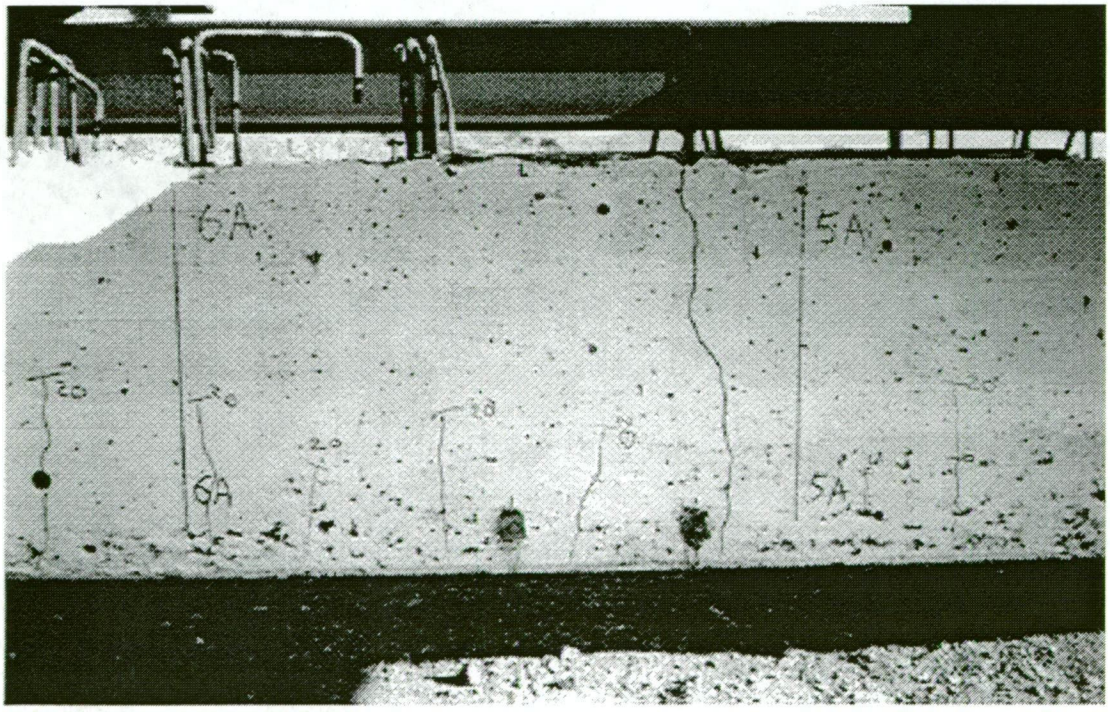

Figure 14.8 - Flexural Beam Crack Patterns

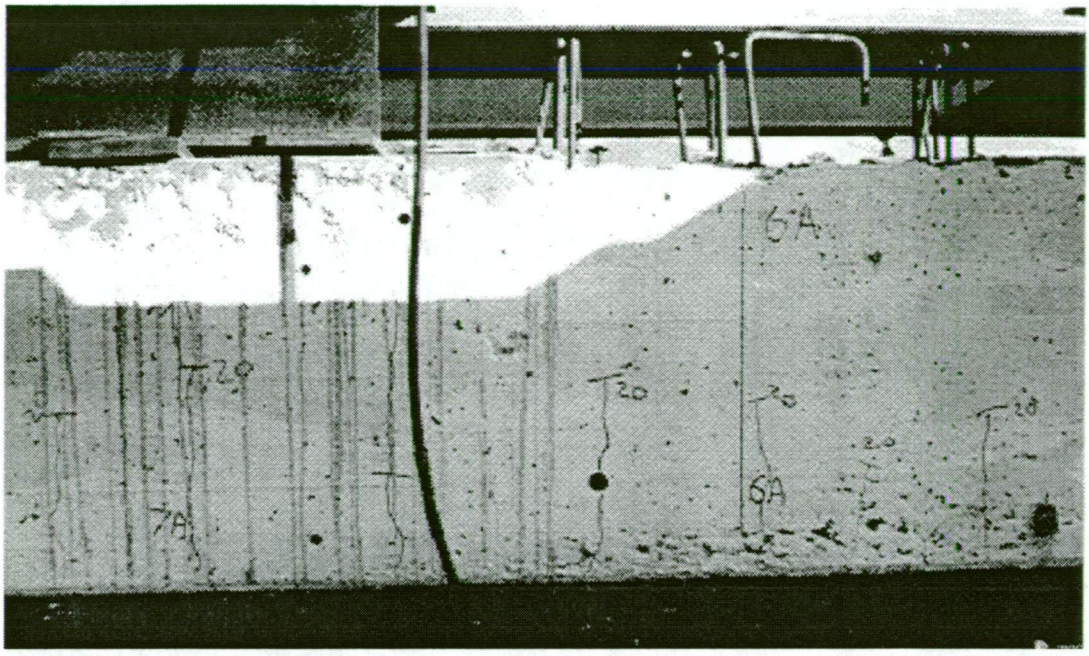

Figure 14.9 - Flexural Beam Crack Patterns

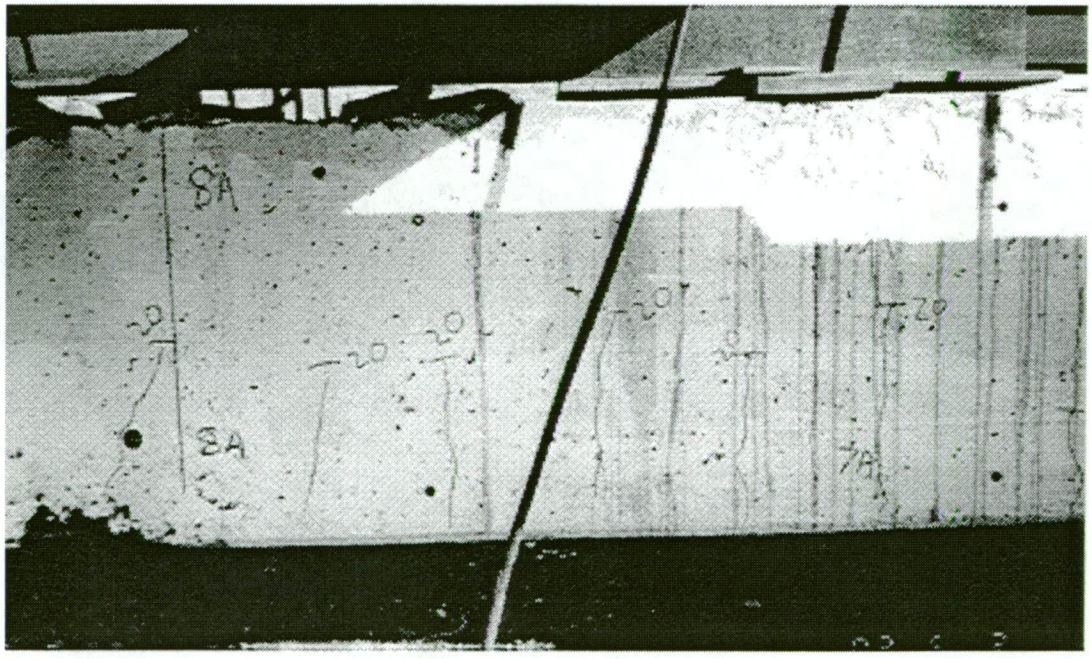

Figure 14.10 - Flexural Beam Crack Patterns

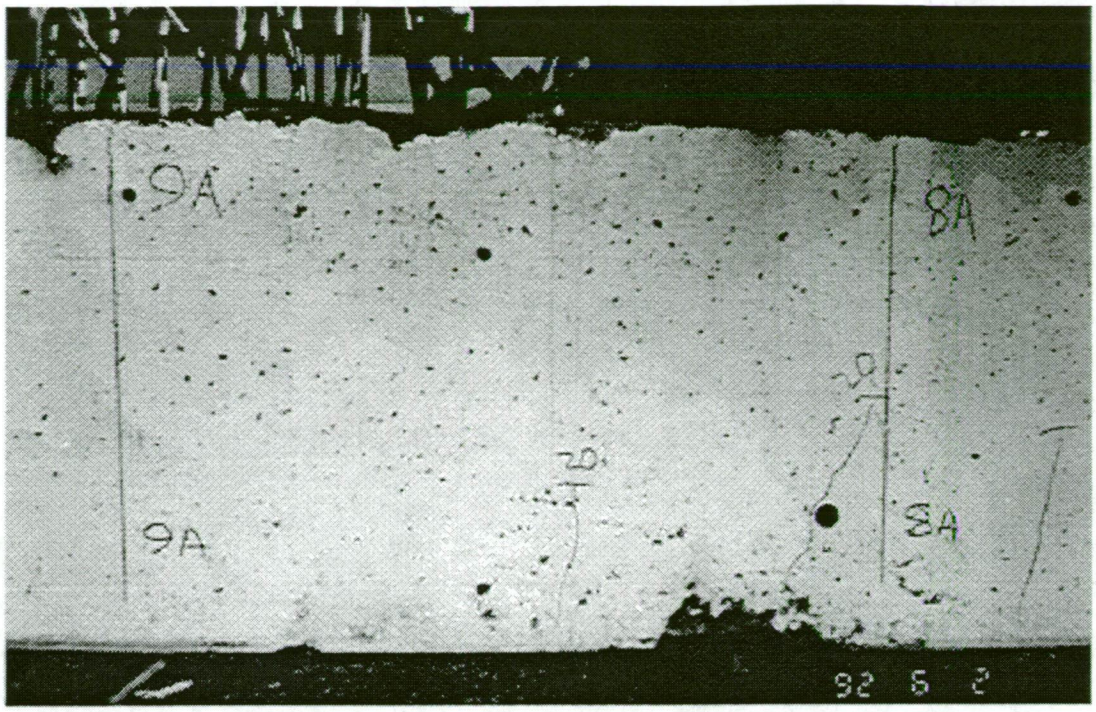

Figure 14.11 - Flexural Beam Crack Patterns

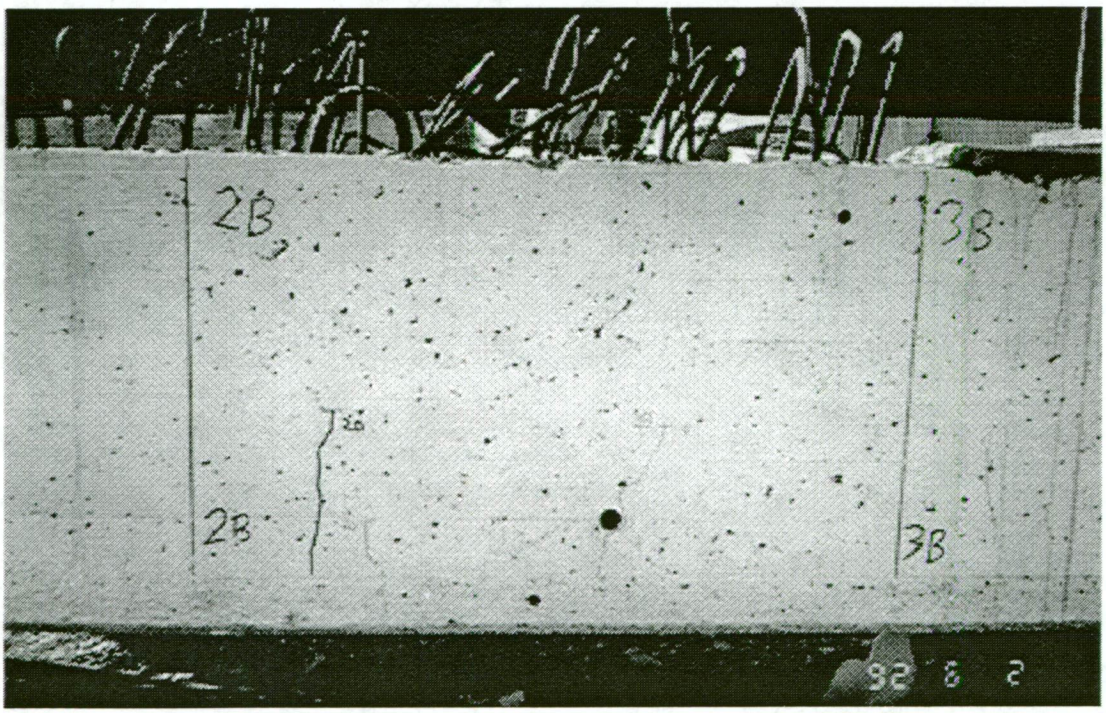

Figure 14.12 - Flexural Beam Crack Patterns

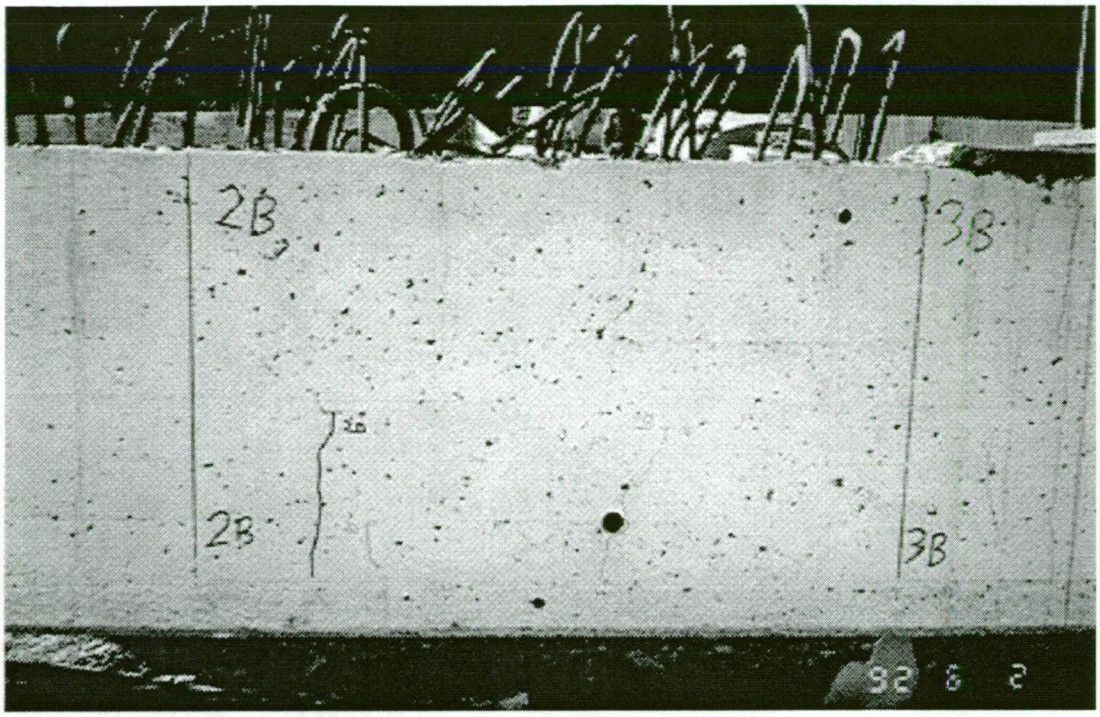

Figure 14.13 - Flexural Beam Crack Patterns

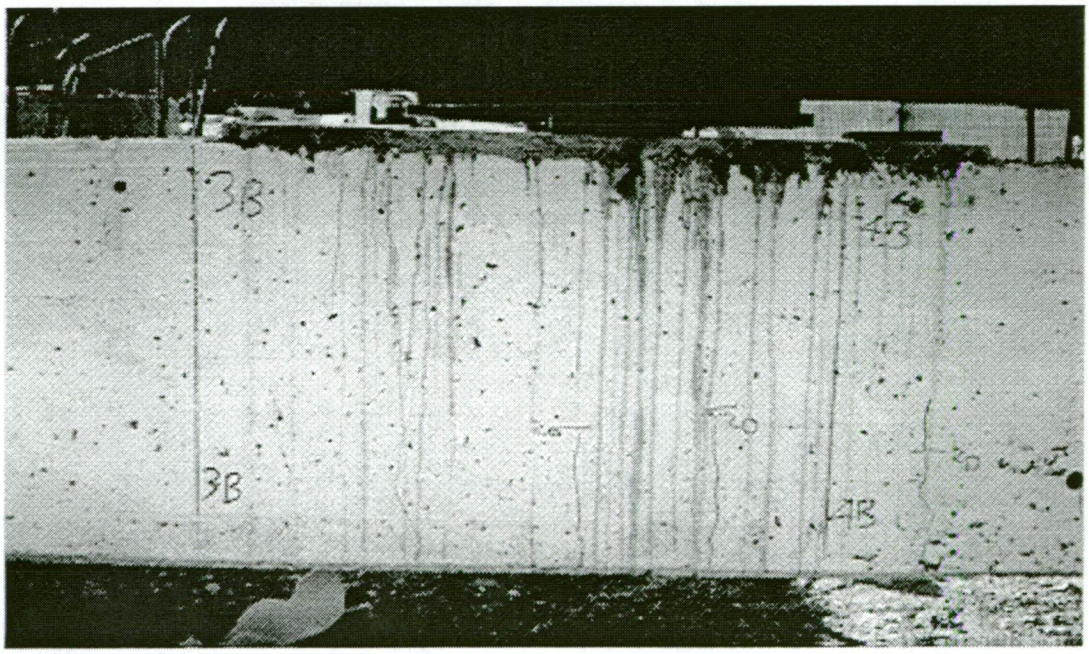

Figure 14.14 - Flexural Beam Crack Patterns

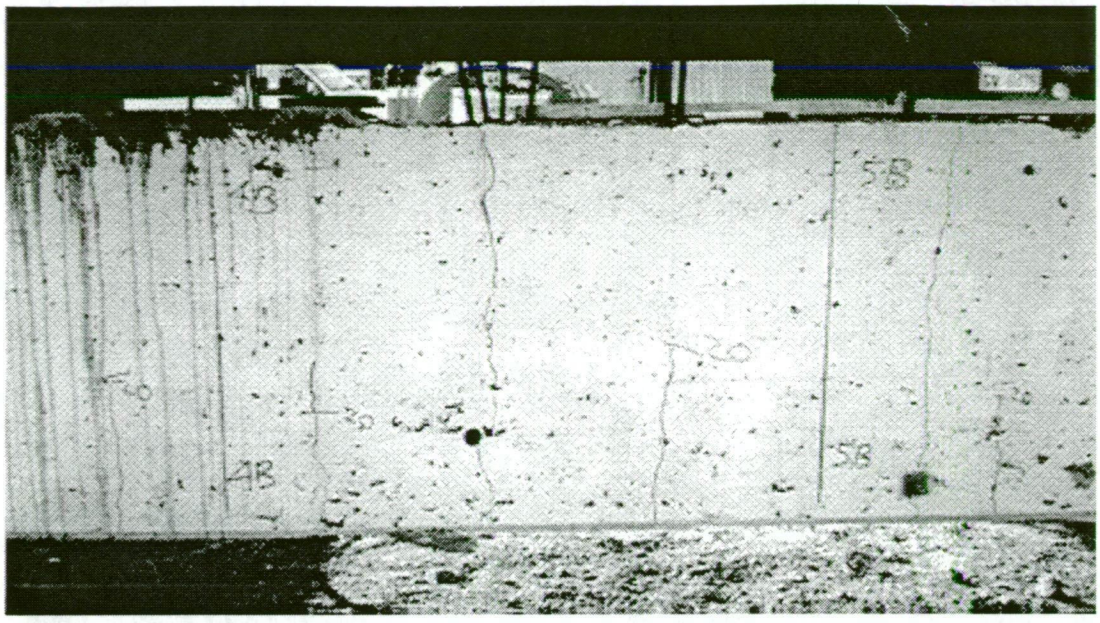

Figure 14.15 - Flexural Beam Crack Patterns

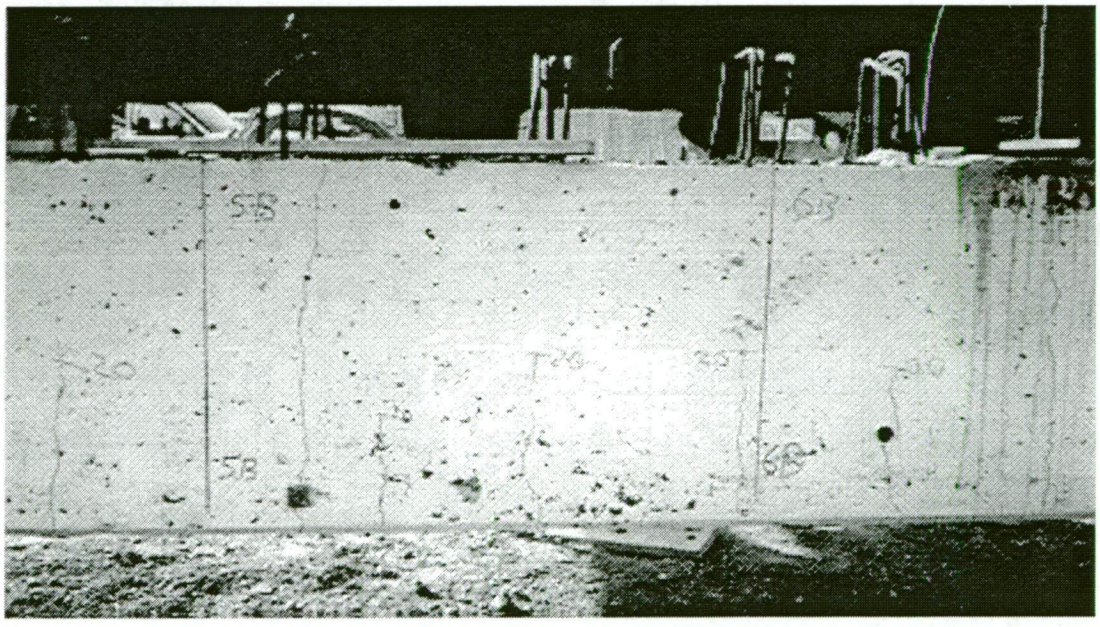

Figure 14.16 - Flexural Beam Crack Patterns

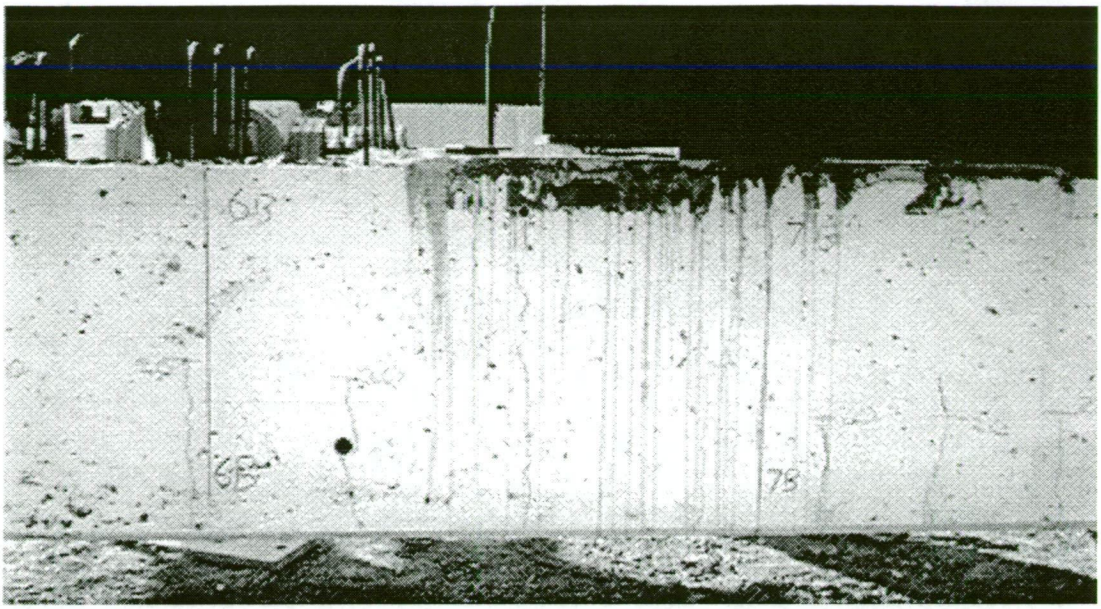

Figure 14.17 - Flexural Beam Crack Patterns

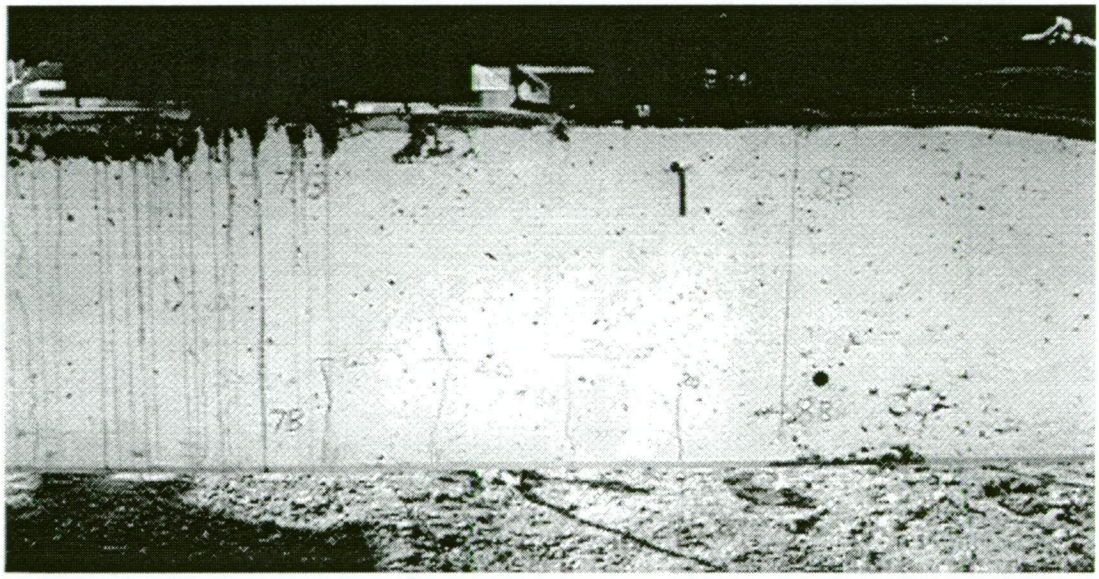

Figure 14.18 - Flexural Beam Crack Patterns

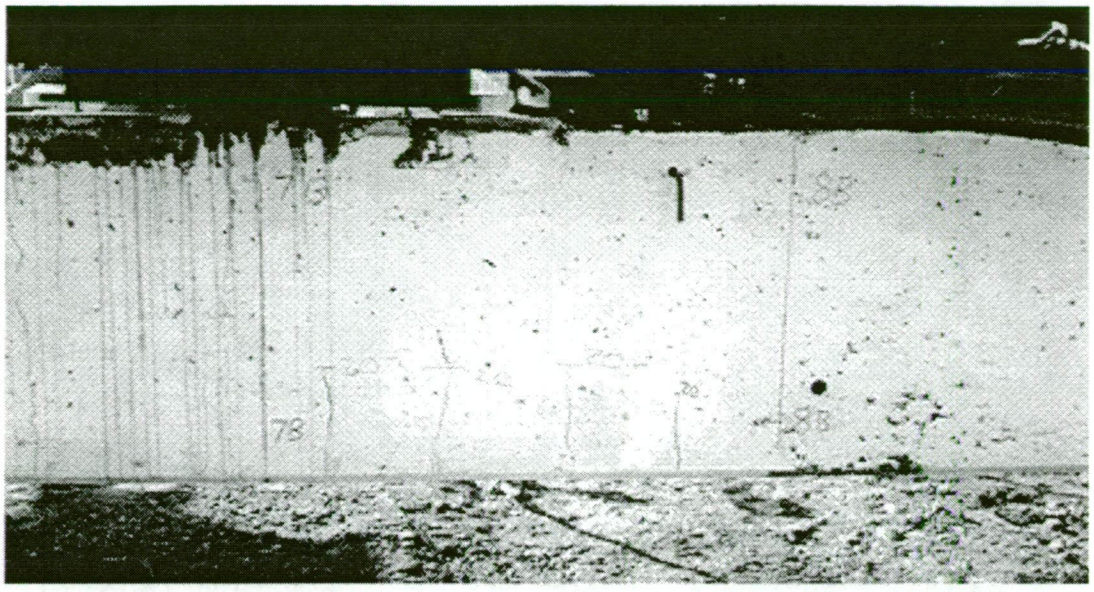

Figure 14.19 - Flexural Beam Crack Patterns

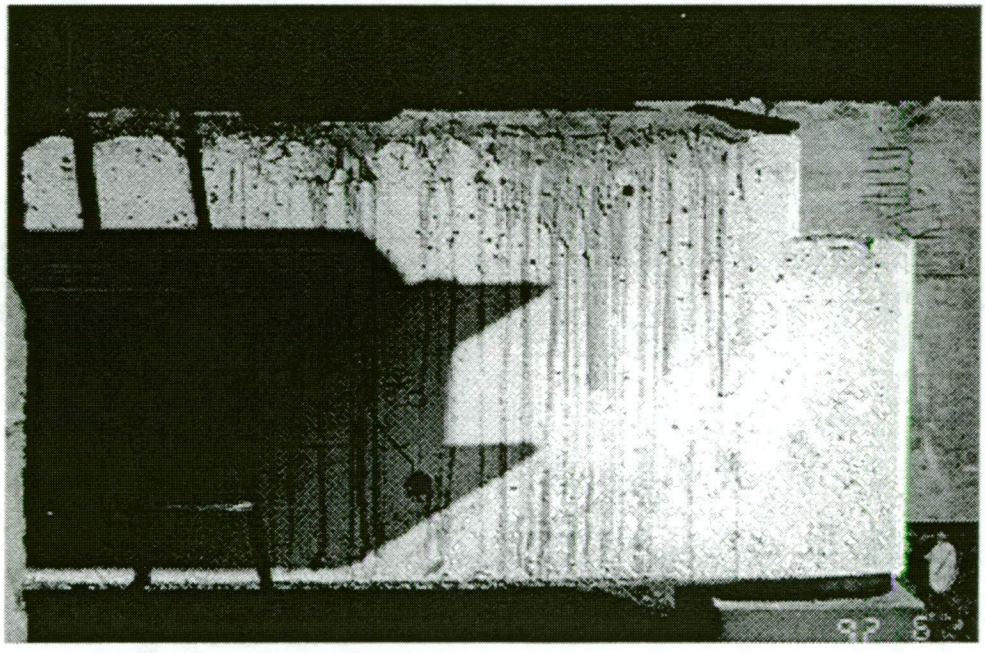

Figure 14.20 - Flexural Beam Crack Patterns

The load-deflection response was measured with a survey staff and level. The response is detailed in Table 14.3. Net deflections remove the effects of bearing compression.

Load P (kN)	Total deflection (mm) at distance from support (m)			
	-0.06	1.47	5.19	10.36
0	0	0	0	0
62	2	2	6	1
125	3	5	11	2
190	3	6	13	3
250	4	9	20	3
250	7	13	32	4

Table 14.3 - Beam Deflections

Load P (kN)	Net deflection (mm) at distance from support (m)			
	-0.06	1.47	5.19	10.36
0	0	0	0	0
62	0	0	3	0
125	0	2	9	0
190	0	3	10	0
250	0	5	17	0
250	0	11	27	0

Table 14.4 - Net Beam Deflections

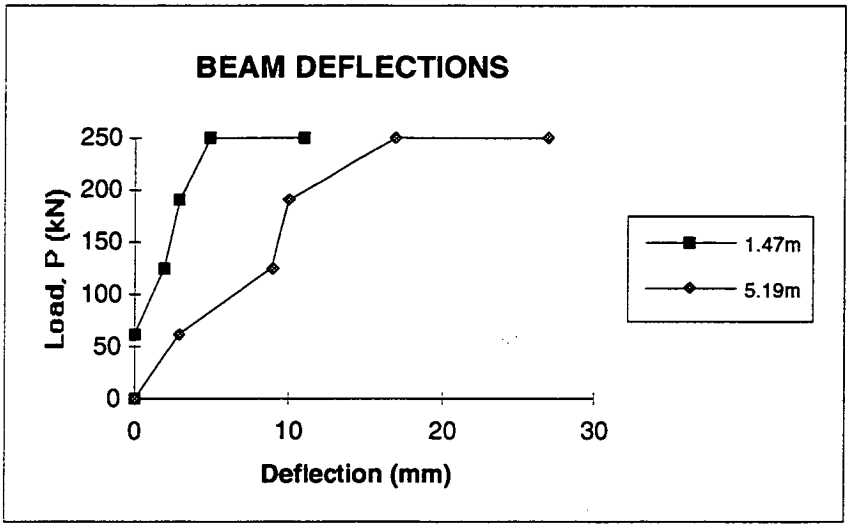

Figure 14.21 - Beam Deflections

The maximum crack width was 0.2mm at the conclusion of testing.

14.4 Correlation of Predicted and Observed Flexural Response

The derivation of concrete properties for analysis is described in the chapter on concrete performance.

Properties are:

Density, ω	2580 kg/m^3
F'_c	35 MPa
E_c	33000 MPa

From the chapter on steel properties,

Yield stress	290 MPa		
Youngs' Modulus	200 GPa		
n	6.0		
A_{st}		=	6334 mm^2
b		=	380 mm
d		=	685-99
		=	586 mm
p		=	0.0284
n		=	6.0
k		=	0.438
j		=	0.854

At steel yield,

M_y		=	$6334*290*0.854*586*10^{-6}$
		=	919 kN
f_c		=	290*0.438/(6.0*(1-0.438))
		=	37.7MPa, approx F'_c
Self weight, ω		=	0.685*0.380*2.58*9.81
		=	6.59 kN/m
Midspan self weight moment, M_{sw}		=	$6.59*10.38^2/8$
		=	89 kNm

For the beam loading configuration in Figure 14.3,

R_A		=	P(3.55+6.89)/10.38
		=	1.006P
R_B		=	0.994P
At midspan, M		=	1.006P*5.19-1.70P
		=	3.52P
Load at yield		=	(919-89)/3.52
		=	236 kN

This is in close agreement with the measured load of 250kN, and within the tolerances of calibration and reading of the jack gauges.

At the load of 62.1 kN,

Moment at centreline		=	3.52P
		=	219 kN.m
Steel stress, f_s		=	$219_{10}3/(6334 * 0.854 * 586)$
		=	69 MPa
Predicted strain, ε_s		=	69/200000
		=	345 με
Measured strain		=	85 με

The measured strain is thus significantly lower than the calculated strain and may be attributable to the limited depth of cracking in the section so that it was acting more as a gross section.

For the cracked section,

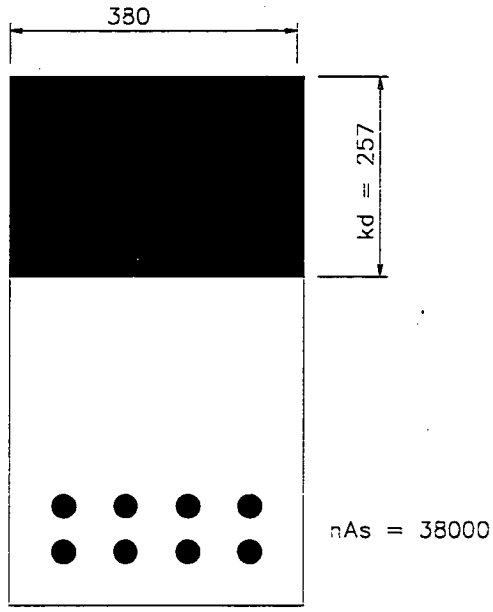

Figure 14.22 - Beam Cross-Section for Analysis

Part	A	y	Ay	A(y-y_c)2	I_{self}
Steel	38000	0	0	$4.12_{10}9$	$0.13_{10}9$
Concrete	97660	458	$44.7_{10}6$	$1.62_{10}9$	$0.54_{10}9$
	135660		**$44.7_{10}6$**	**$5.74_{10}9$**	**$0.67_{10}9$**

y_c = 329mm
I_{xx} = $6.41_{10}9mm^4$
E_c = 33000MPa
EI = $2.11_{10}14Nmm^2$

The bending moment diagram is shown in Figure 14.23.

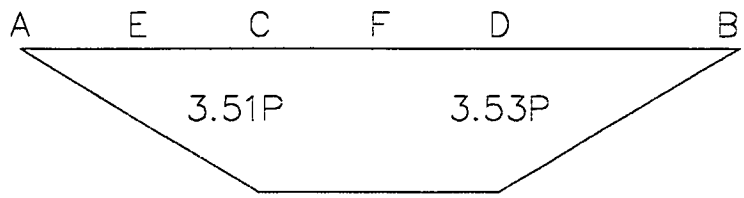

Figure 14.23 - Bending Moment Diagram

d_{BA} = {(3.49*3.51/2)*8.053 + (3.34*3.51)*5.22
+(3.34*0.02/2)*4.663
+(3.55*3.53/2)*2.367}*P/EI
= 125.5P/EI

t_A = 125.5P/EI/10.38
= 12.09P/EI

At distance 1.47m from A,

d_{EA} = {(1.47*1.48/2)*0.49}P/EI
= 0.53P/EI

ie deflection at E = (12.09*1.47-0.53)P/EI
= 17.2P/EI

At distance 5.19m from A,

d_{FA} = {(3.49*3.51/2)*2.863 + (1.7*3.51)*0.85
+(1.7*0.001)*1.13}P/EI
= 22.6P/EI

ie deflection at F = (12.09*5.19-22.6)P/EI
= 40.1P/EI

Calculated deflections are detailed in Table 14.5.

Load (kN)	Deflection (mm)	
	1.47m	5.19m
0	0	0
62	5.0	11.8
125	10.2	23.8
190	15.5	36.1
250	20.3	47.5

Table 14.5 - Calculated Deflections

For an uncracked section, neglecting reinforcement

I_g = 380*685³/12
= $10.2_{10}9$ mm⁴

E_c = 33 000 MPa

E_cI_g = $3.36_{10}14$ N mm²

AS1480 permitted the use of an effective moment of inertia

I_e = $[M_c/M]^3(I_g-I_{cr}) + I_{cr}$

F_t = $0.62\sqrt{(F'_c)}$
= $0.62\sqrt{(35)}$
= 3.67

y_t = 685/2
= 343

M_c = F_tI_g/y_t
= $3.67*10.2_{10}9/343_{10}6$
= 109 kN.m

I_e = $([109/M]^3(10.2_{10}9-6.41_{10}9)$
$+ 6.41_{10}9)$
= $(3.79_{10}9[128/M]^3 + 6.41_{10}9)$ mm⁴

Calculated deflections using the effective moment of inertia are detailed in Table 14.6.

Load (kN)	1.47m			5.19m		
	Moment (kN.m)	I_e ($10^9 mm^4$)	Deflection (mm)	Moment (kN.m)	I_e ($10^9 mm^4$)	Deflection (mm)
0	0	9.93	0	0	9.93	0
62	92	17.3	1.5	218	6.45	9.6
125	185	7.01	7.7	440	5.68	22.1
190	281	5.98	13.7	669	5.60	34.0
250	370	5.75	18.7	880	5.58	44.9

Table 14.6 - Deflections using Effective Moment of Inertia

Measured and calculated deflections are summarised in Table 14.7.

Load (kN)	1.47m			5.19m		
	Cracked section	I_e	Measured	Cracked section	I_e	Measured
0	0	0	0	0	0	0
62	5.0	1.5	0	11.8	9.6	3
125	10.2	7.7	2	23.8	22.1	9
190	15.5	13.7	3	36.1	34.0	10
250	20.3	18.7	5	47.5	44.9	17

Table 14.7 - Summary of Beam Deflections

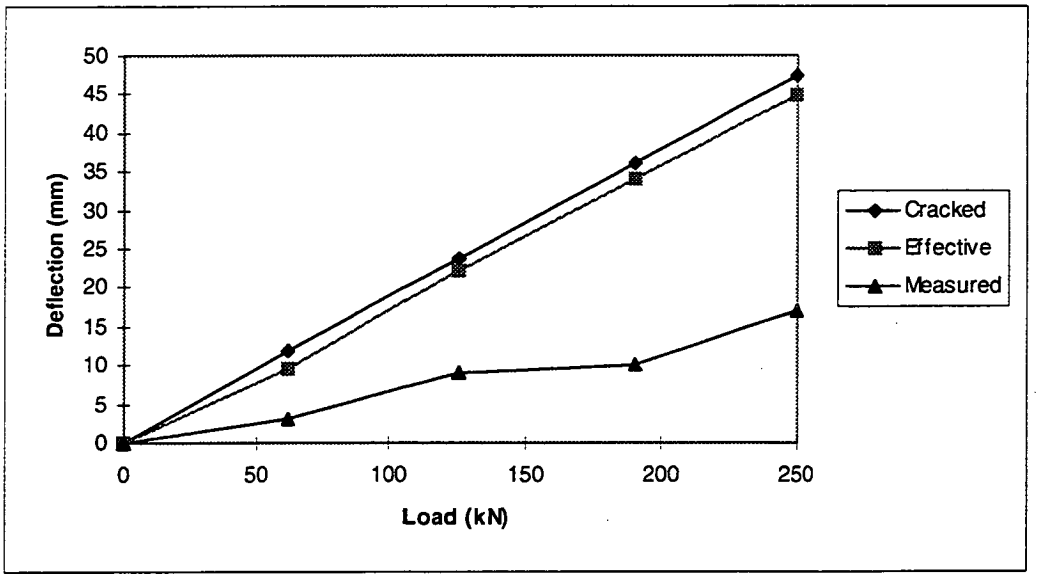

Figure 14.24 - Measured and Calculated Beam Deflections

As with the strains, analytical methods underestimate the actual performance of the beam.

14.5 Beam Shear Test

The beam tested in shear was 10.64m long with supports 0.15m and 10.50m from one end. Loads were applied at distances of 0.89m and 8.69m to approximate one and two times the effective depth from the support.

Crack patterns at the conclusion of the shear testing are shown in Figures 14.25 to 14.46. Patterns in the flexural section of the beam are similar to those in the flexural test. The ends

of the beams showed inclined cracks starting at approximately the effective depth of the beam from the support.

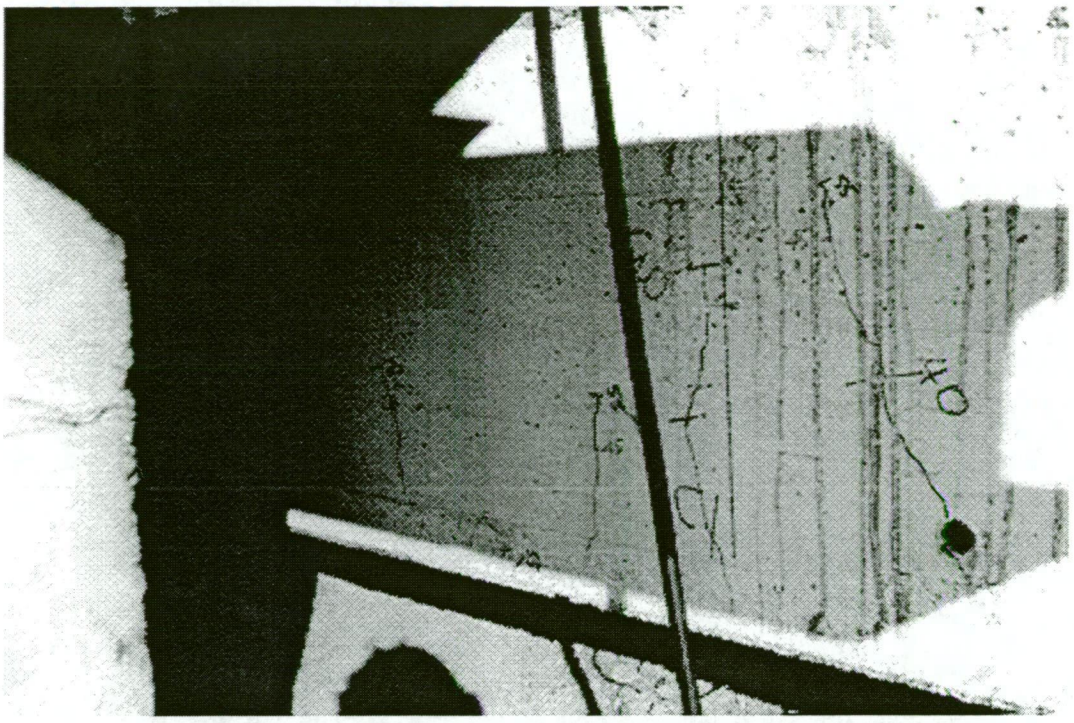

Figure 14.25 - Shear Beam Crack Patterns

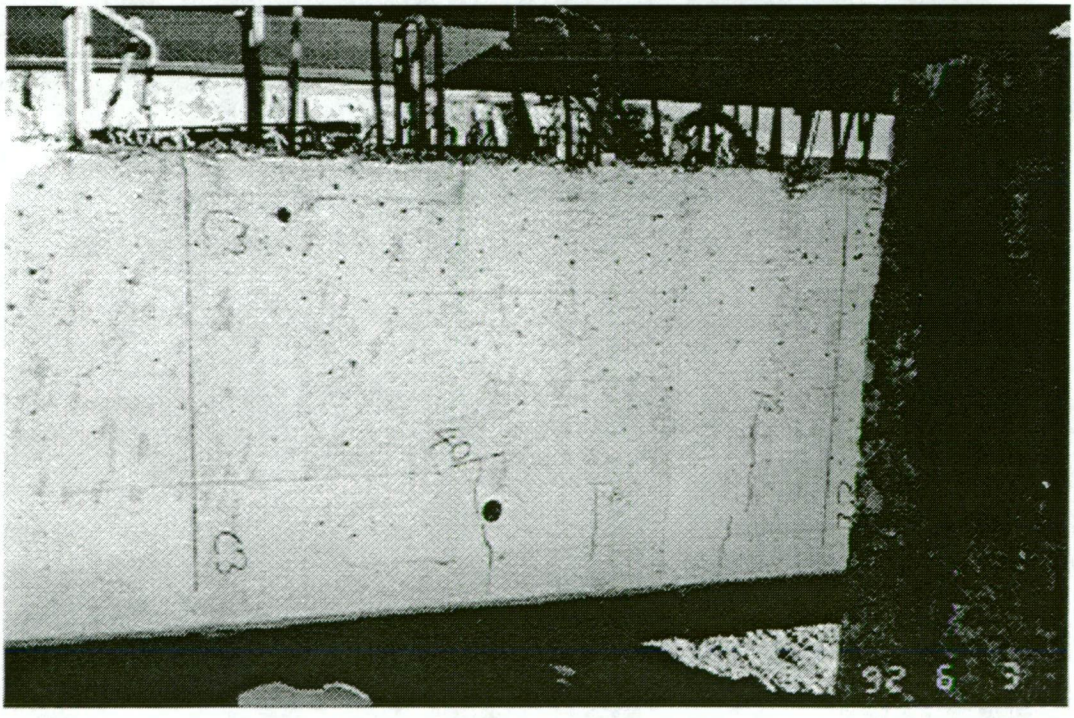

Figure 14.26 - Shear Beam Crack Patterns

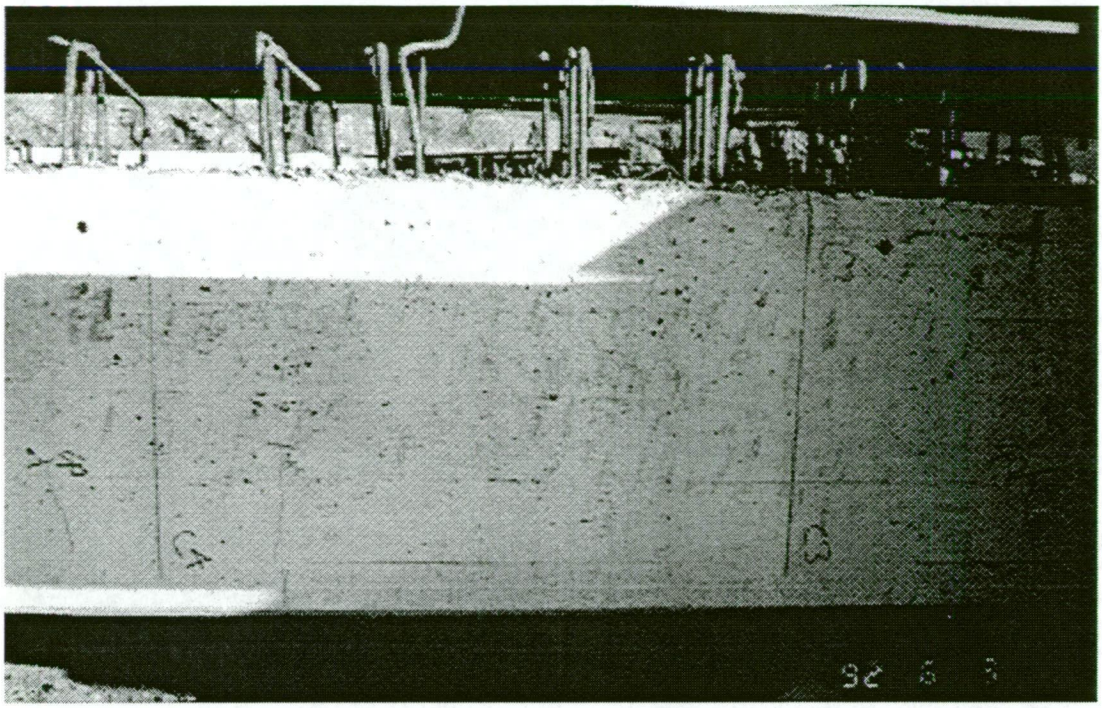

Figure 14.27 - Shear Beam Crack Patterns

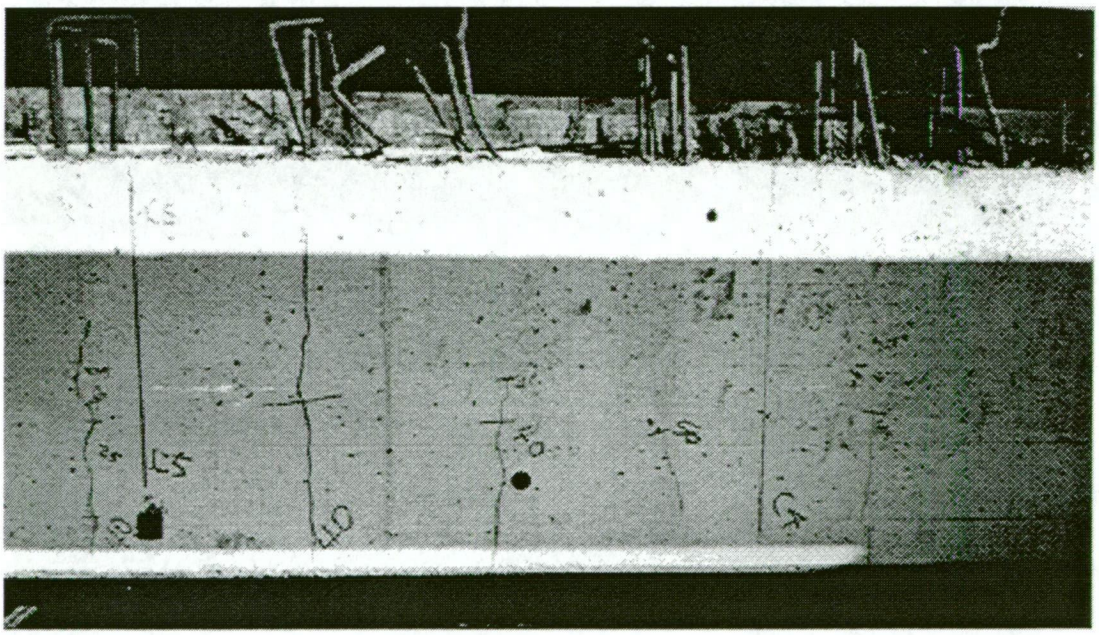

Figure 14.28 - Shear Beam Crack Patterns

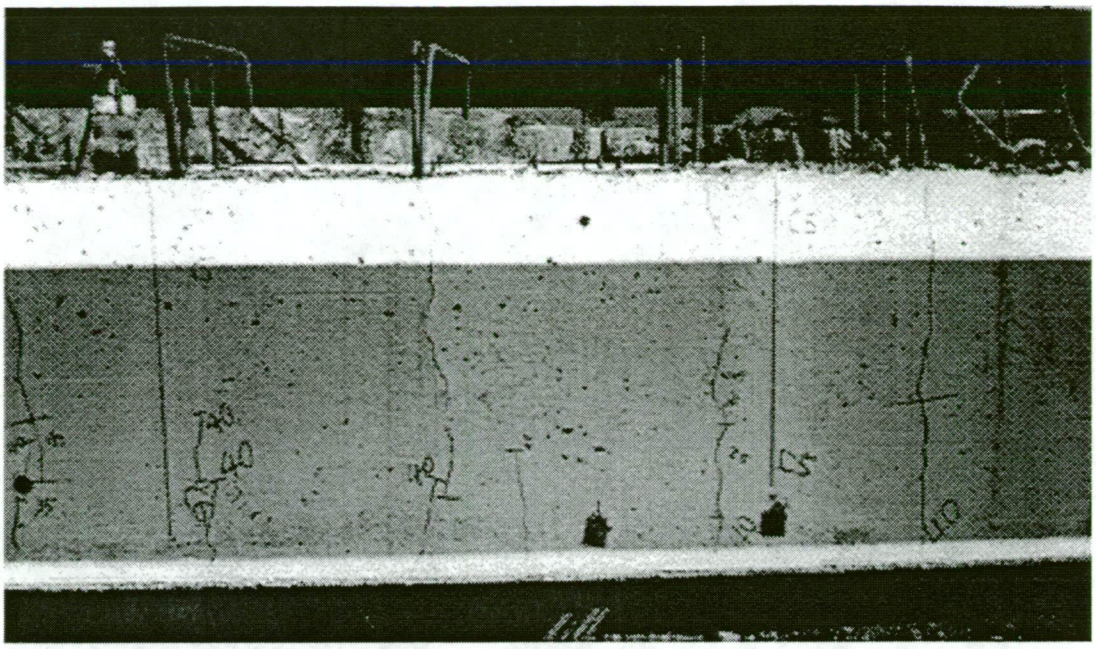

Figure 14.29 - Shear Beam Crack Patterns

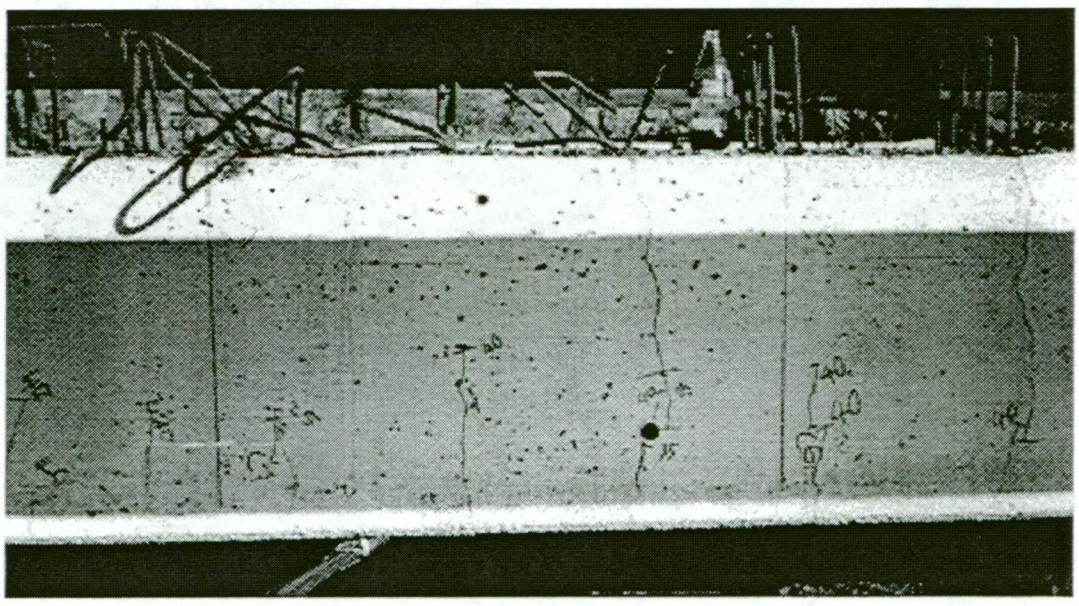

Figure 14.30 - Shear Beam Crack Patterns

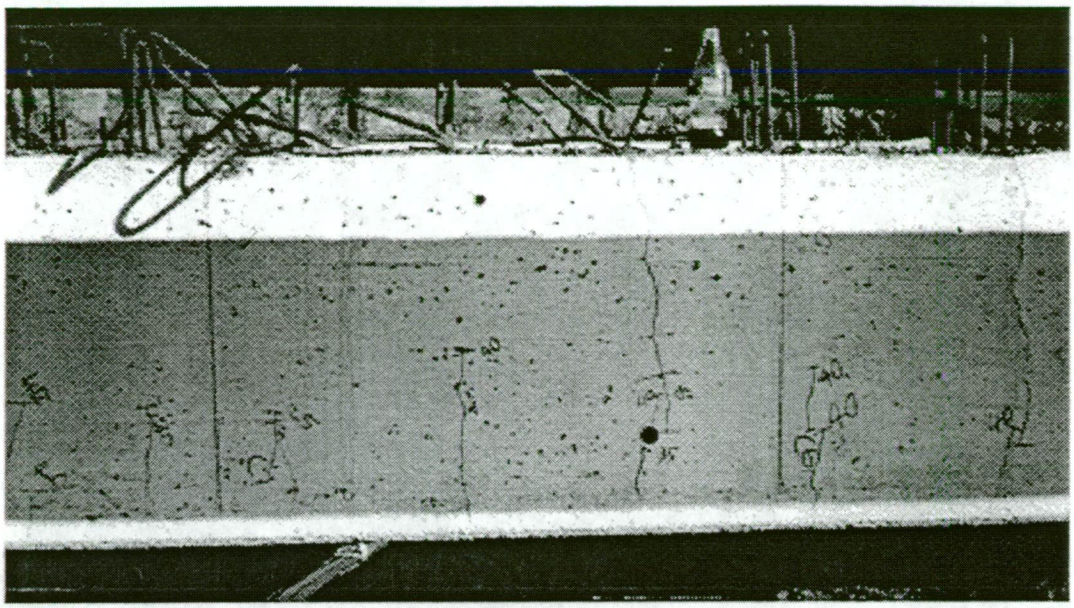

Figure 14.31 - Shear Beam Crack Patterns

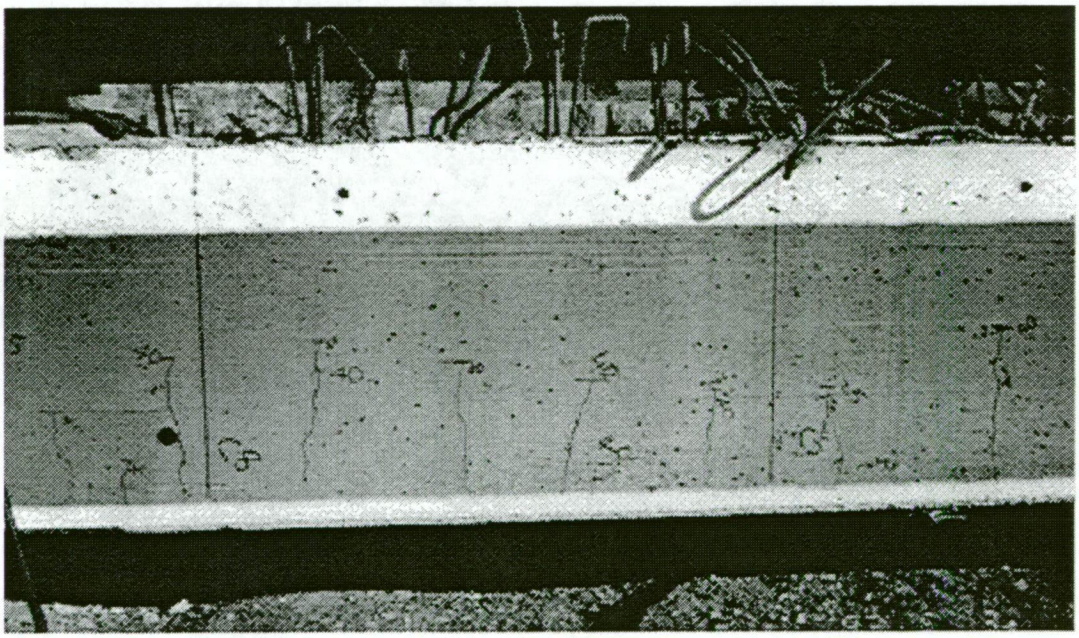

Figure 14.32 - Shear Beam Crack Patterns

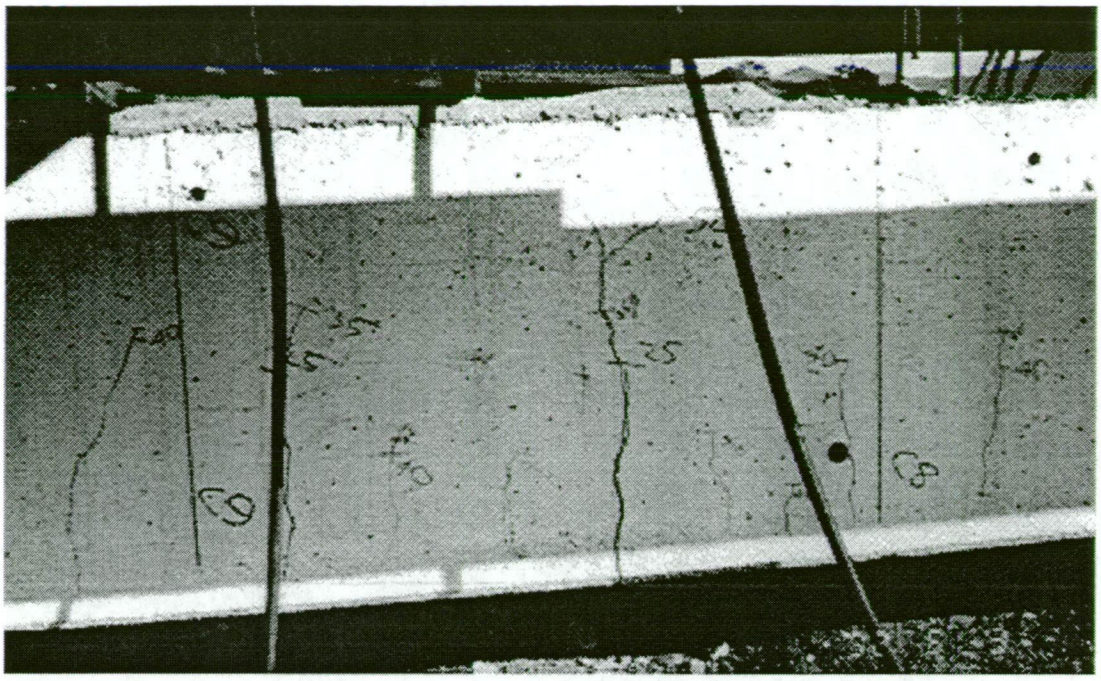

Figure 14.33 - Shear Beam Crack Patterns

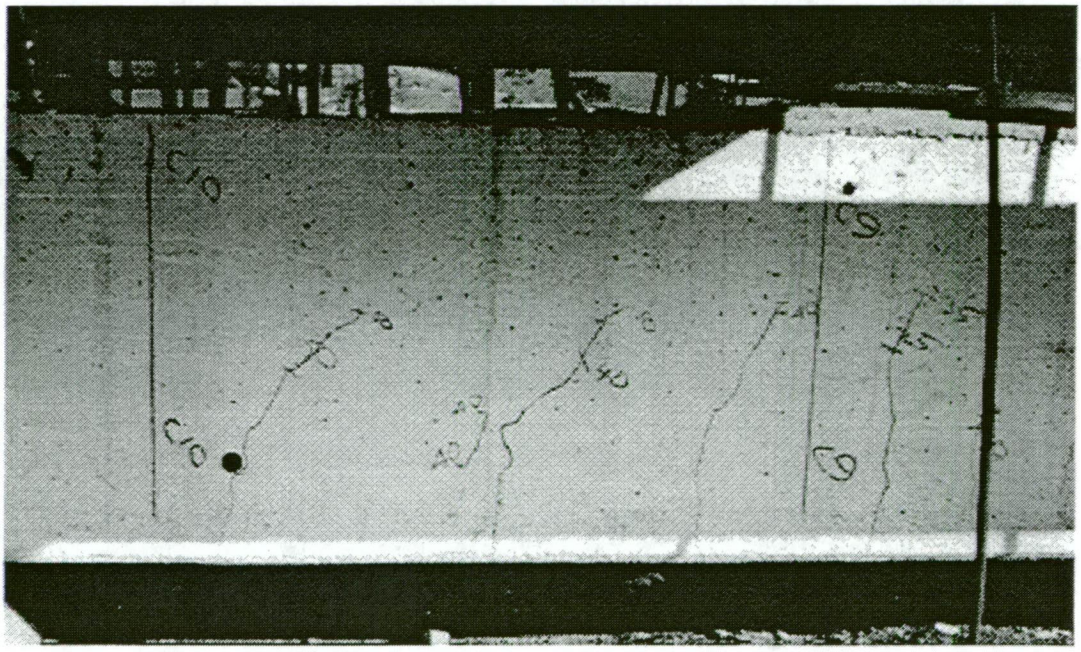

Figure 14.34 - Shear Beam Crack Patterns

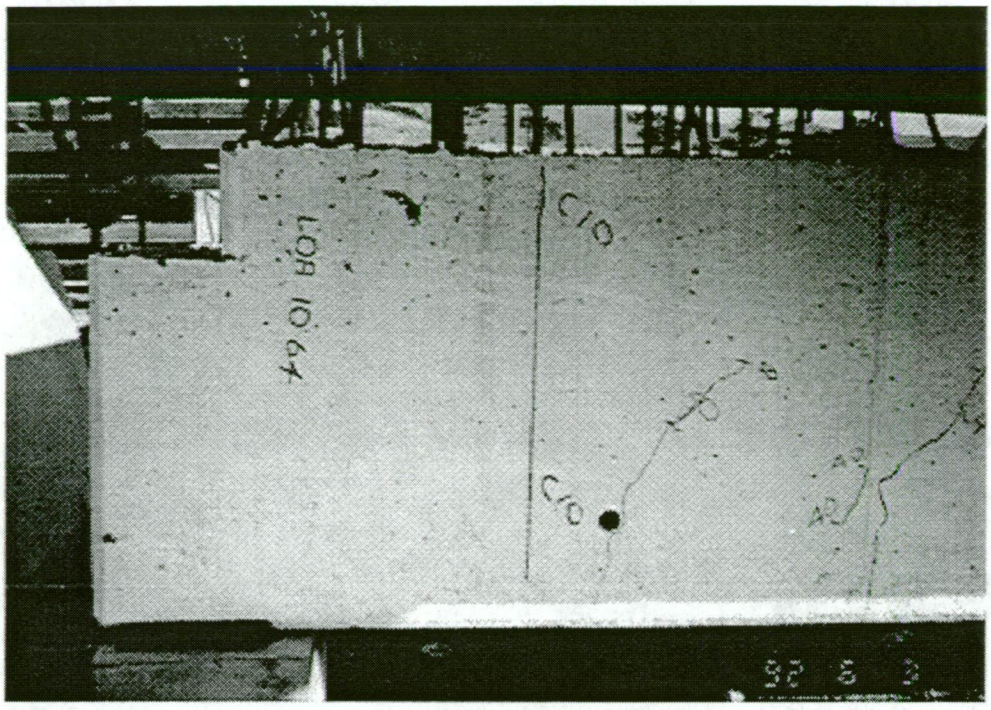

Figure 14.35 - Shear Beam Crack Patterns

Figure 14.36 - Shear Beam Crack Patterns

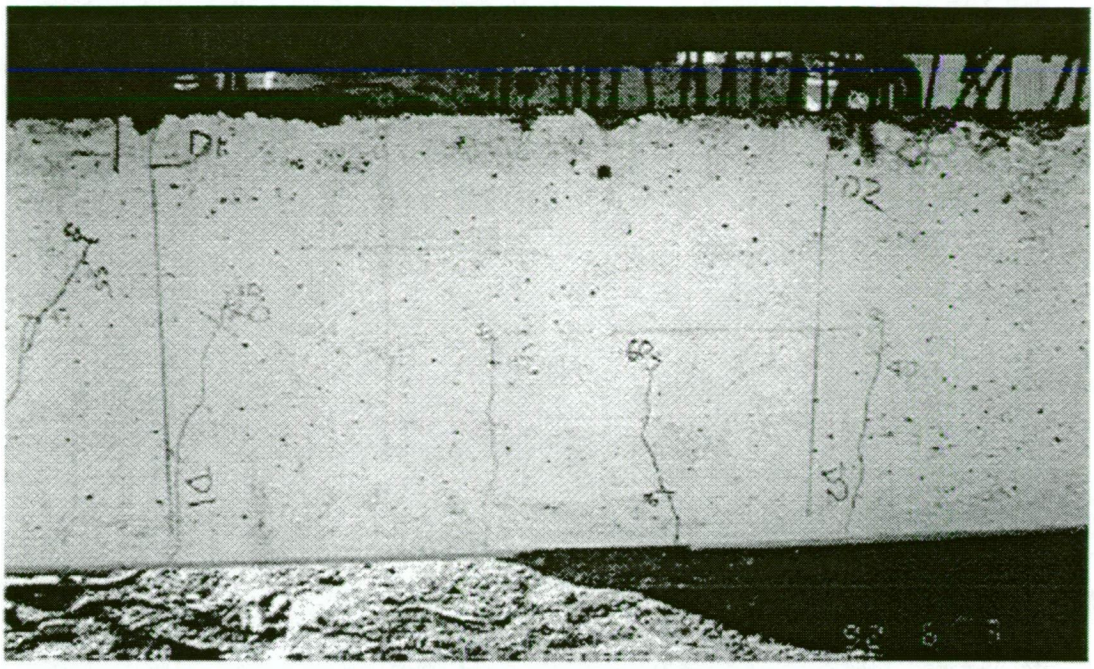

Figure 14.37 - Shear Beam Crack Patterns

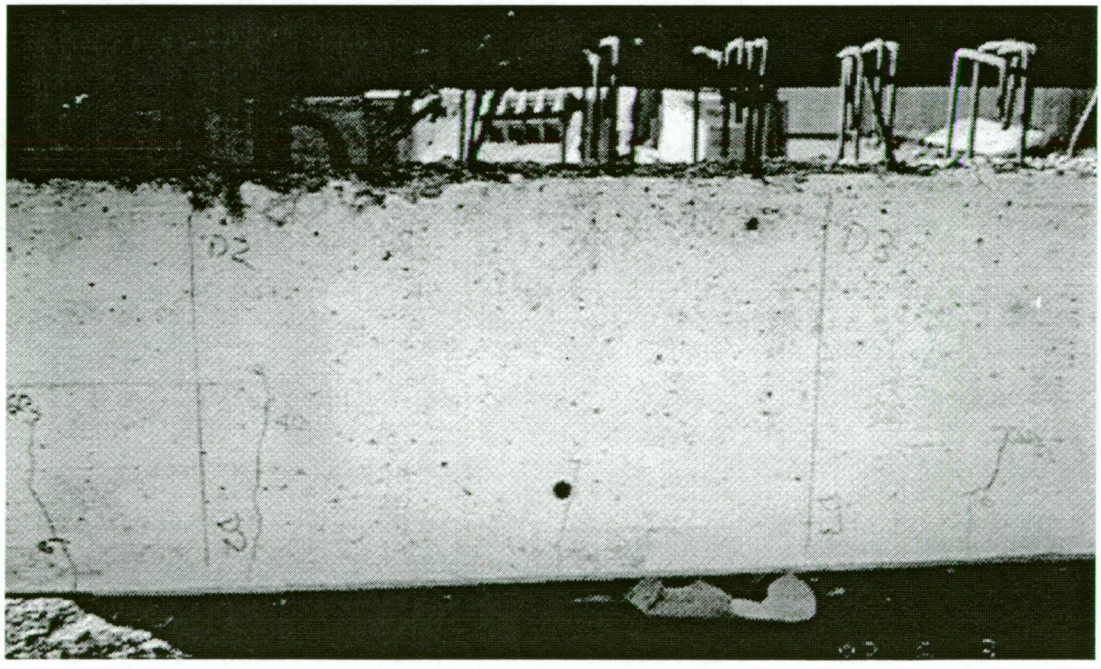

Figure 14.38 - Shear Beam Crack Patterns

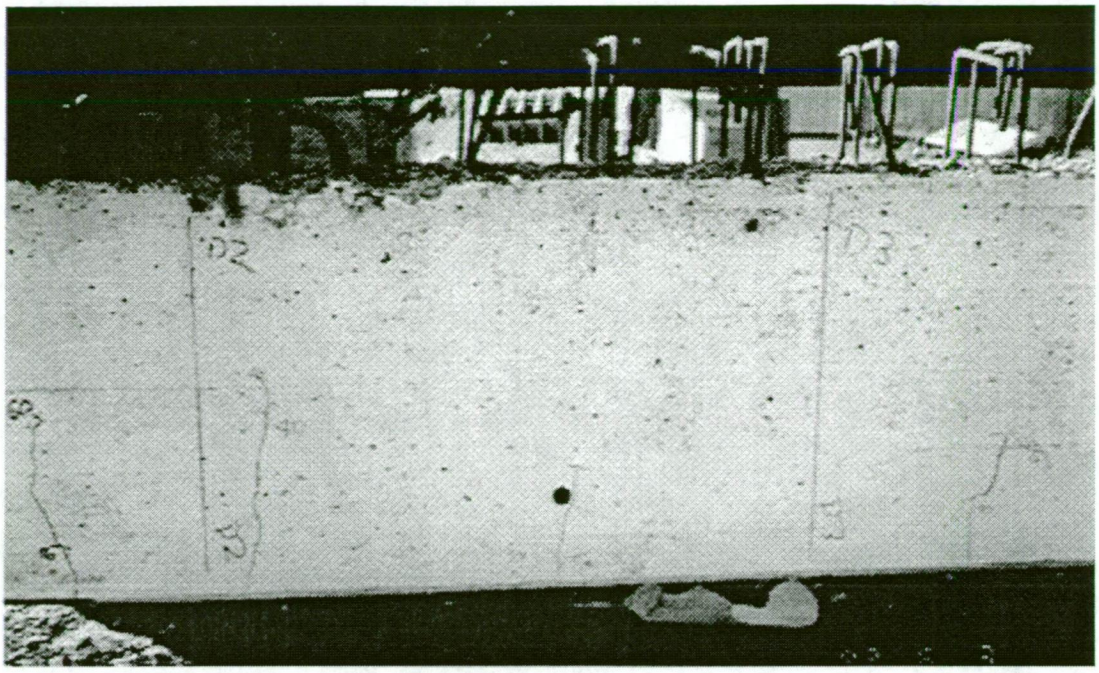

Figure 14.39 - Shear Beam Crack Patterns

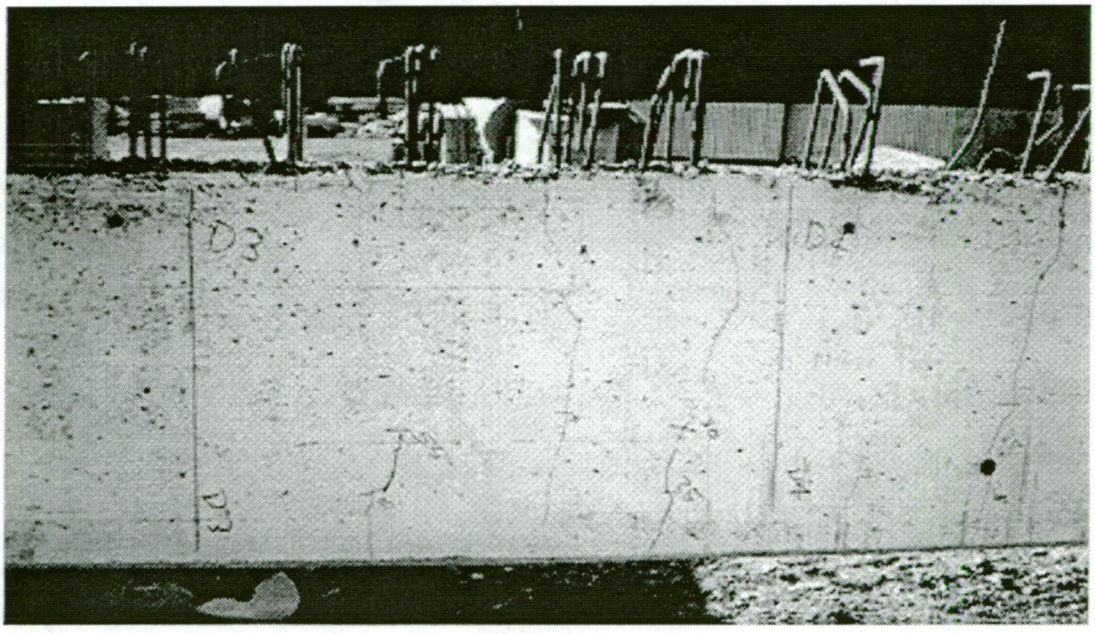

Figure 14.40 - Shear Beam Crack Patterns

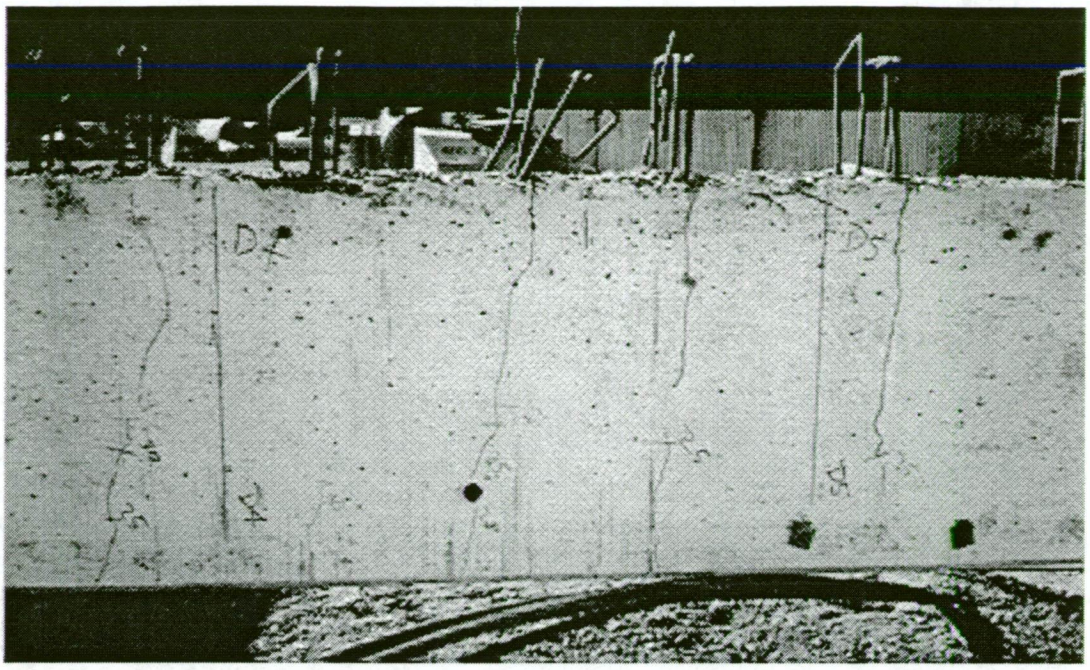

Figure 14.41 - Shear Beam Crack Patterns

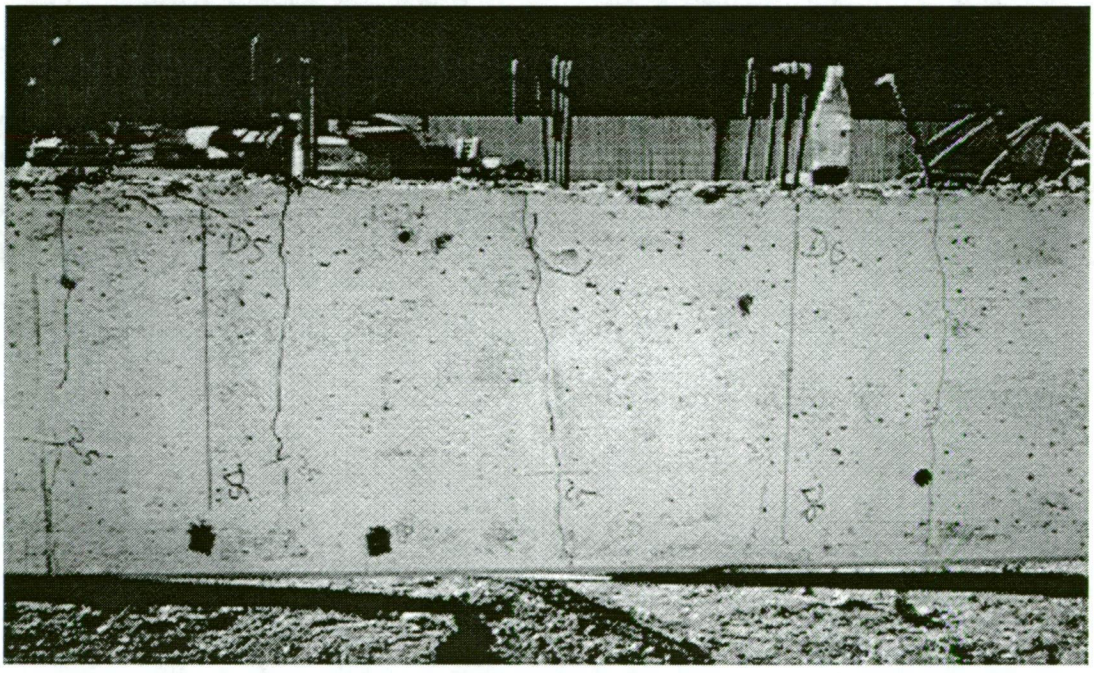

Figure 14.42 - Shear Beam Crack Patterns

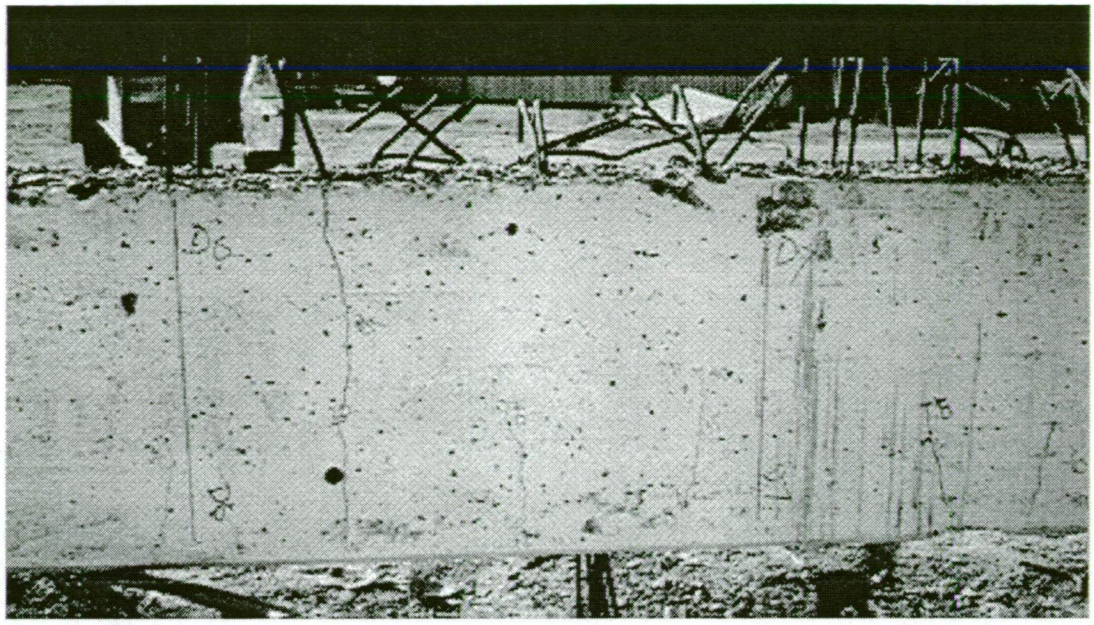

Figure 14.43 - Shear Beam Crack Patterns

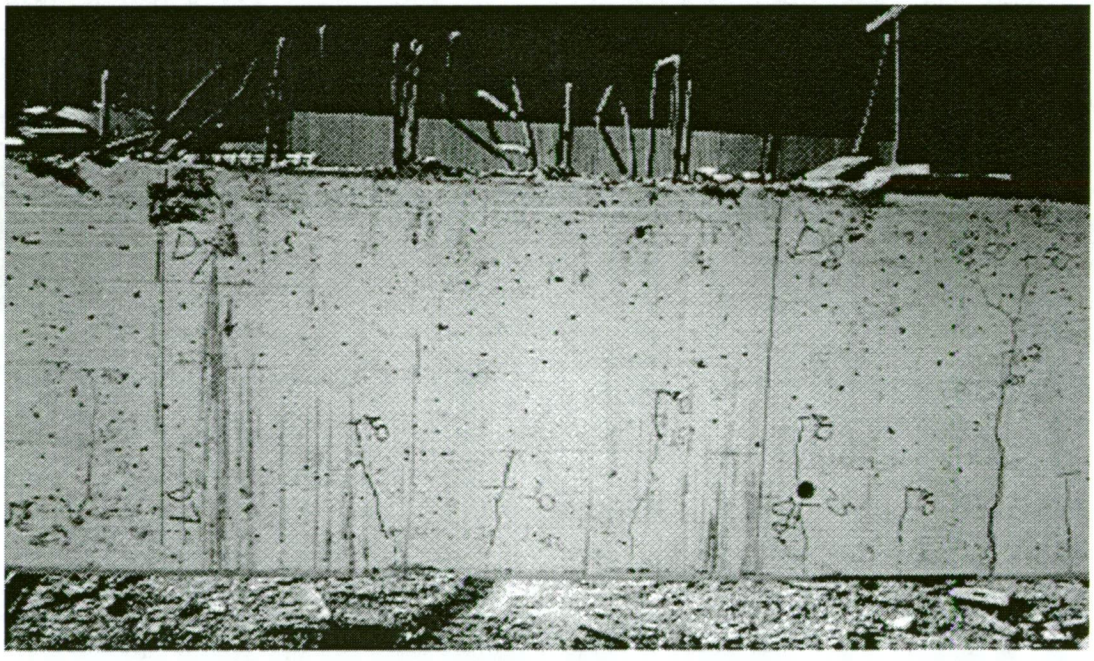

Figure 14.44 - Shear Beam Crack Patterns

Figure 14.45 - Shear Beam Crack Patterns

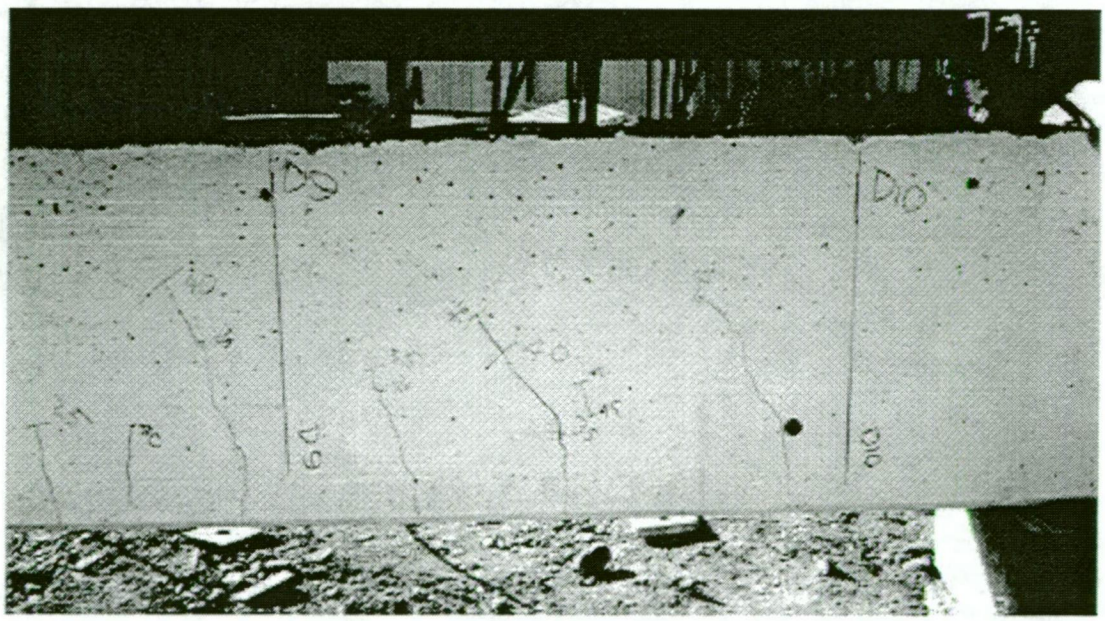

Figure 14.46 - Shear Beam Crack Patterns

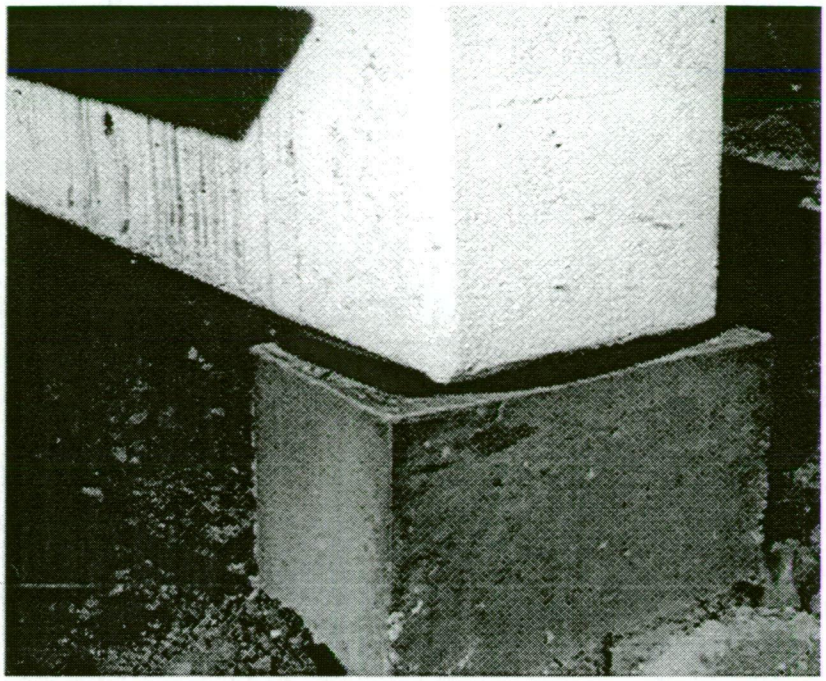

Figure 47 - Bearing Distortion during Loading

The load deflection response is detailed in Table 14.8.

Load	Deflection (mm) at distance from support			Remarks
(kN)	1.99m	5.25m	6.45m	
0	0	0	0	
125	11	4	6	
250	12	3	3	
310	7	2	4	
495	9	10	5	
620	15	16	16	
870	20	21	21	
995	13	23	19	Flexure and shear cracks 0.1mm
1115	17	23	17	Flexure and shear cracks 0.15mm
1155	22	31	27	4mm wide crack at 8.4m

Table 14.8 - Load-Deflection Response for Shear Test

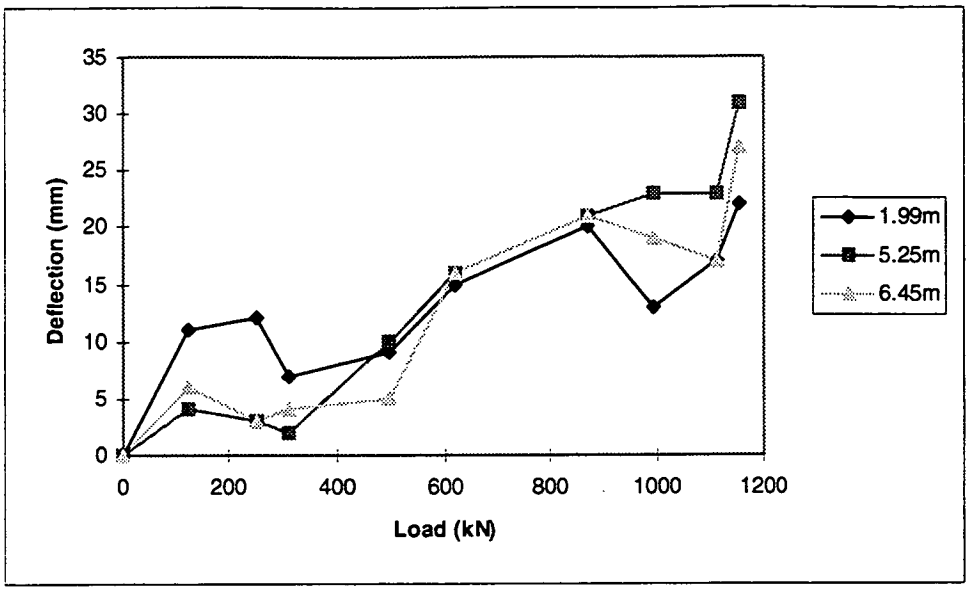

Figure 14.48 - Beam Deflections during Shear Test

14.6 Allowable Shear Stress

Calculations are based on the 1976 NAASRA Highway Bridge Design Specification for 35 MPa concrete.

Critical cross-section is a distance, d, from the support
The upper layers of reinforcement are terminated approximately 4' and 8' from the support.
For the lower layer of reinforcement,

d	=	2'3" - 2 5/8" - 5'8"
	=	603 mm
A_{ts}	=	4 no. 1.25" bars
	=	3167 mm^2
A_{ts}/bd	=	3167/(603*381)
	=	0.0138
Basic allowable shear stress	=	0.433 MPa
Basic allowable shear force	=	0.433*603*381/1000
	=	101 kN

Shear reinforcement at critical cross-section is 4 legs of 0.5" bars at 6" spaces

A_v	=	3.32 mm^2/mm

For an allowable reinforcing stress of 125 MPa

V'_s	=	$3.32 * 125 * 603/10^3$
	=	251 kN
Permissible shear force on beam	=	251 + 101
	=	352 kN

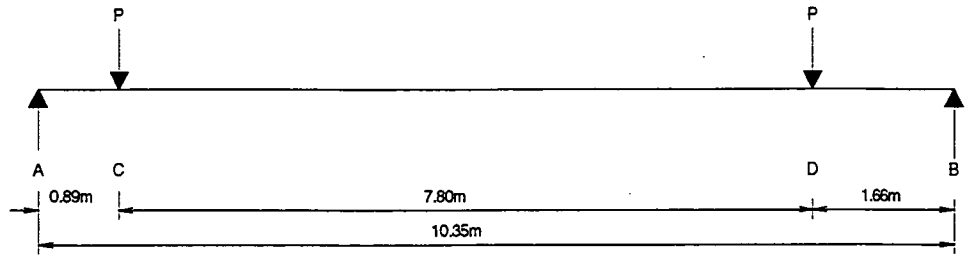

Figure 14.49 - Beam Shear Test Configuration

For the beam loading configuration,

$$R_B = P(0.89+8.69)/10.35 = 0.926P$$

$$R_A = 2P - 0.926P = 1.074P$$

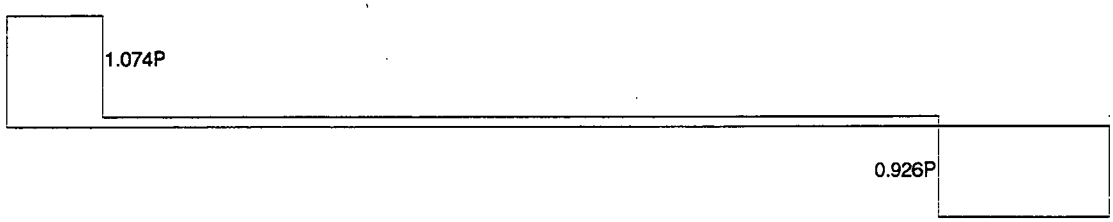

Figure 14.50 - Shear Force Diagram

$$M_C = 1.074P * 0.89 = 0.956P$$

$$M_D = 0.926P * 1.66 = 1.537P$$

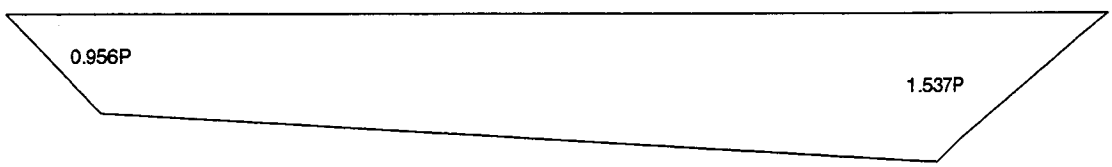

Figure 14.51 - Bending Moment Diagram

Maximum shear force = 1.074P

Maximum permissible working load = 352/1.074 = 328 kN

This compares to the maximum applied load of 1155 kN, and the load of 995 kN at which cracks appeared.

14.7 Discussion

Two precast beams were tested subsequent to the main testing program. While anectodal evidence was that they had been dropped during construction and subsequently rejected, they both performed satisfactorily in the testing.

Width measurements were within current dimensional tolerances. Variations in depth measurements can be attributed to the roughened surface for casting of the insitu deck and could be considered acceptable.

For the flexural test, the calculated yield point is in close agreement with that measured. Deflections and strains in the elastic range are however underestimated, possibly because the section remained relatively uncracked until yield.

The shear capacity was adequate, with a maximum load of approximately 3.5 times the permissible load calculated by the Bridge Design Specification without brittle failure.

15. DYNAMIC RESPONSE

15.1 Introduction

The use of dynamic response measurements to assess bridge load capacity and the existence or development of defects has been investigated by a number of researchers.

The determination of live loads for the design of bridges requires an assessment of the dynamic effects associated with the interaction between the bridge and the vehicle. A number of researchers have found dynamic increments in some structures to be higher than those included in design codes.

The test program provided an opportunity to evaluate both aspects of dynamic behaviour of the bridge.

15.2 Vicroads Research Project

At the time of the Princess River bridge testing, ETRS Pty Ltd in association with Melbourne University were undertaking Stage III of a Vicroads research and development project on the 'Load Capacity of In-Service Bridges'. The project was based on the use of dynamic response to determine bridge load capacity.

Figure 15.1 - Raising Weight for Excitation of Span

The equipment used by ETRS was an enhancement of that used in earlier stages of the project. It comprised a 386/33 MHz IBM compatible computer with expanded memory equipped with a 100 kHz analogue-digital card linked to 16 low cost electrical seismic type velocity transducers. Software and hardware modifications provided the capacity to capture bridge vibration response over a time period of 10.5 seconds at a rate of 1024 points per second for each of the 16 channels following the triggering of the record. Software transformed the time domain based data into the frequency domain using a Fast Fourier Transform algorithm, giving a frequency spectrum where power spectral density is plotted against frequency. With some further processing, response shapes for particular frequencies can be displayed. Raw data, including velocity vs time traces and displacement response shapes, can also be reviewed.

University of Melbourne used a multi-channel computer based data capture system with five servo-accelerometers and eleven velocity transducers, with data acquisition generally being undertaken in tandem with ETRS to facilitate comparison of results.

The Structural Dynamics Group of the Civil and Mining Engineering Department of the University of Wollongong also collected data on the dynamic response of the bridge to assist with calibration of the ETRS dynamic response technique. Data acquisition used a four channel Tektronix 2630 spectrum analyser to identify frequency and modal responses for the bridge.

ETRS transducers were initially placed in five rows of five transducers on each of the kerbs and on the centreline of the bridge, with the sixteenth transducer being positioned on the adjacent span as a reference and to establish any inter-relationship that may exist between spans. The end transducer in each row was placed 1.0m from the supports, with the remaining transducers equally spaced between. The row of transducers on the centreline of the bridge was subsequently moved to the centreline of the upstream lane to assist with the measurements of the effects of defects introduced into the bridge.

Dynamic testing was undertaken between 6 August and 15 August 1991. Excitation primarily used an impact weight, of approximately 75kg mass, free falling onto a rubber pad on the bridge deck.

Defects introduced into the Hobart span to assess the ability of dynamic measurement to detect them were:

- removal of a section of concrete handrail
- cutting of a single reinforcing bar in one beam at midspan
- cutting of the remaining bars in the bottom layer of reinforcement of the beam
- partial removal of abutment seating of one beam
- cutting of the bottom layer of reinforcement at midspan in another beam.

A dynamic finite element analysis of the bridge was undertaken to determine the first few mode shapes and corresponding frequencies. The first analysis used simple beams and plates, but results were inaccurate in comparison with the experimental results. Trials with T-beams were also carried out, but further refinement of the models was considered necessary.

The undamaged structure had a natural frequency of 17.6 Hz for the first bending mode of the Queenstown span, corresponding to a high stiffness of the bridge. Numerous flapping and twisting or torsional modes were measured, including modes at 22.0 Hz and 28.8 Hz. The second bending mode of the span proved difficult to identify from an initial analysis of the test data, although higher harmonics of this mode were noted at 66.0 Hz and 95.2 Hz.

The removal of the upper rail of the second bay from the Hobart end of the upstream side of the Hobart span did not affect the dynamic behaviour of the bridge as a whole. High deflections were however noted in the bridge response at a frequency of 43.0 Hz, and the mode shape exhibited the induced defect clearly at 59.0 Hz where the adjacent transducer vibration was out of phase with the remainder of the bridge deck.

The removal of 300 mm of one beam reinforcing bar at midspan in the second beam from the upstream side of the Hobart span caused no noticeable variations in the frequency response spectra when compared with only handrail damage. The cutting of the remaining three bars in the lower layer of reinforcement however caused a shift in the frequency of the first bending mode of the defective beam from 17.6 Hz to 16.6 Hz. Allowing for the resolution of the analysis software, the shift was considered to be between 0.5 Hz and 1.0 Hz. The mode shape at 58.1 Hz also exhibited noticeable changes, with increased deformations occurring at the transducer located nearest to the defect.

Partial removal of the abutment seating of one beam caused no noticeable changes to the dynamic response.

Cutting of the lower four reinforcing bars in the upstream beam of the Hobart span caused increased beam responses to occur at higher frequencies with associated changes in the mode shape. At 77.6 Hz, a new peak was visible on a number of spectra and increased deformations were visible on the edge of the bridge in the vicinity of the two transducers adjacent to the defect.

15.3 Departmental Testing

Dr Rob Heywood of Queensland University of Technology and Infratech Systems and Services analysed one set of data for frequency. Transducer responses and power spectral densities are shown in Figures 15.2 to 15.7 inclusive.

The ability to analyse the data was affected by the sampling frequency of 250 Hz and duration of 1.2 s, which was considered too slow and/or too short for confident analysis, and the presence of the vehicle on the bridge which meant that frequencies are for the bridge/vehicle system rather than for the free vibration of the bridge.

The power spectral density plots for the accelerometers nevertheless show significant peaks at around 22 Hz corresponding to the second mode of vibration identified by the Vicroads study.

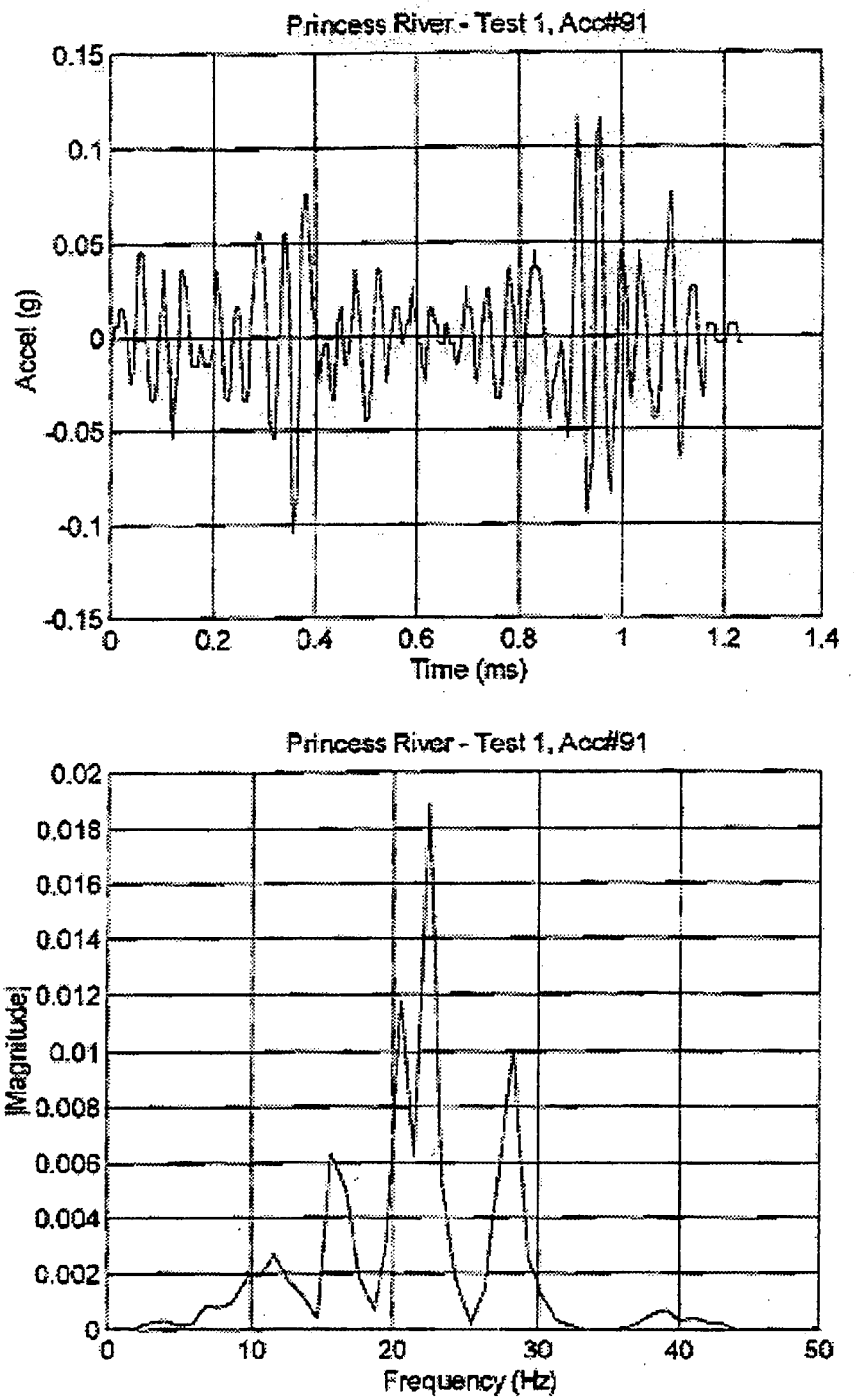

Figure 15.2 - Accelerometer Response and Power Spectral Densities

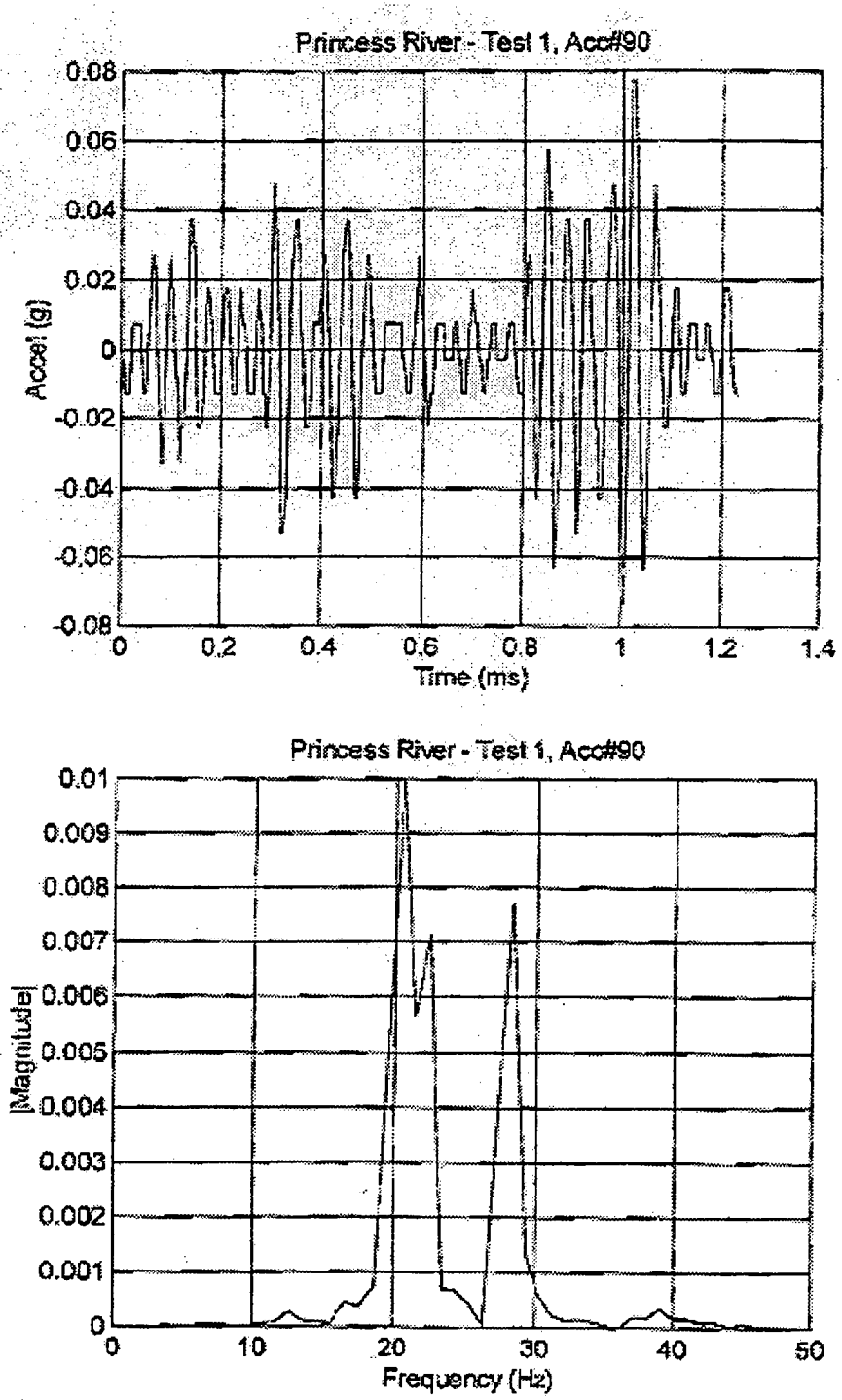

Figure 15.3 - Accelerometer Response and Power Spectral Densities

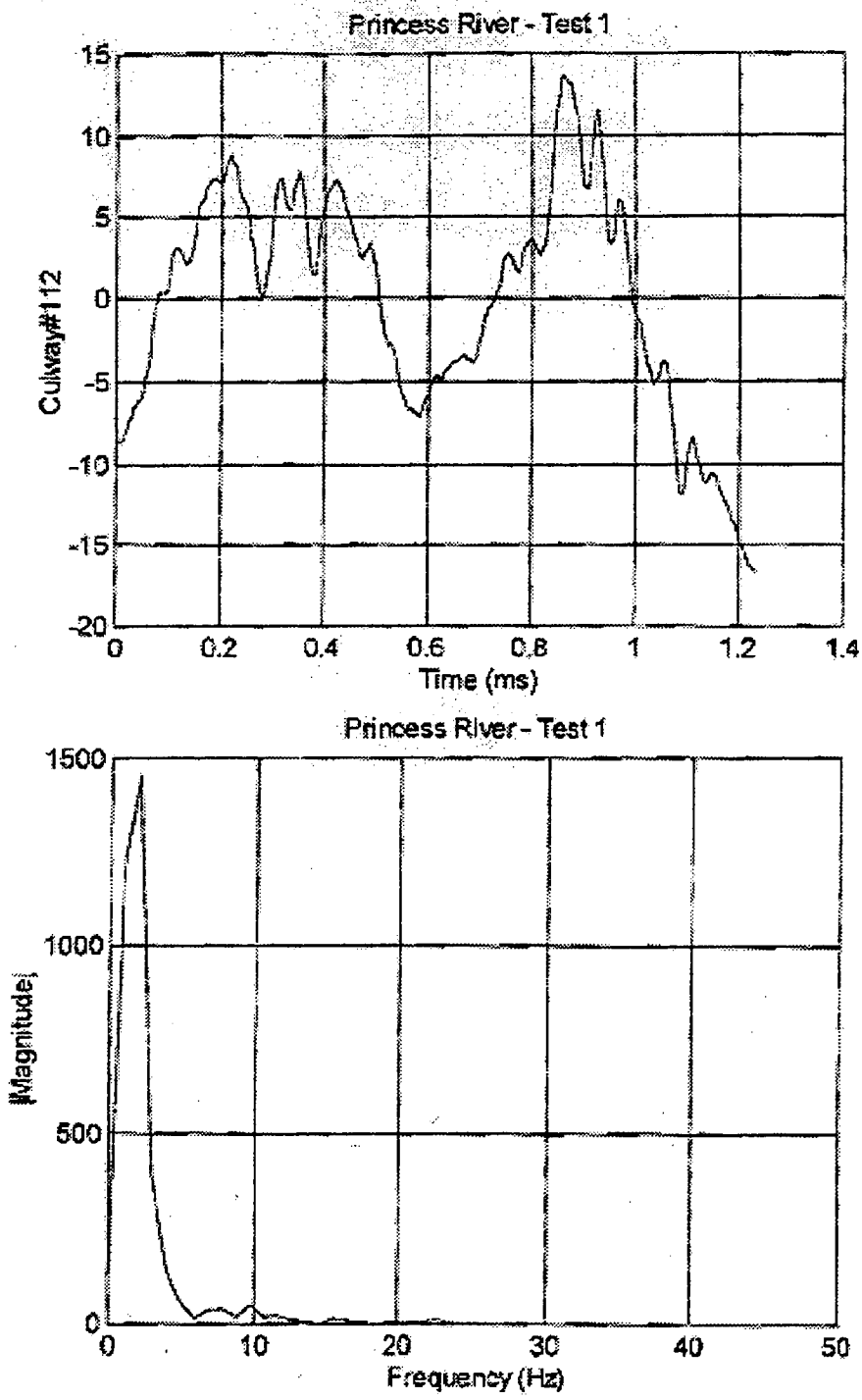

Figure 15.4 - Strain Response and Power Spectral Densities

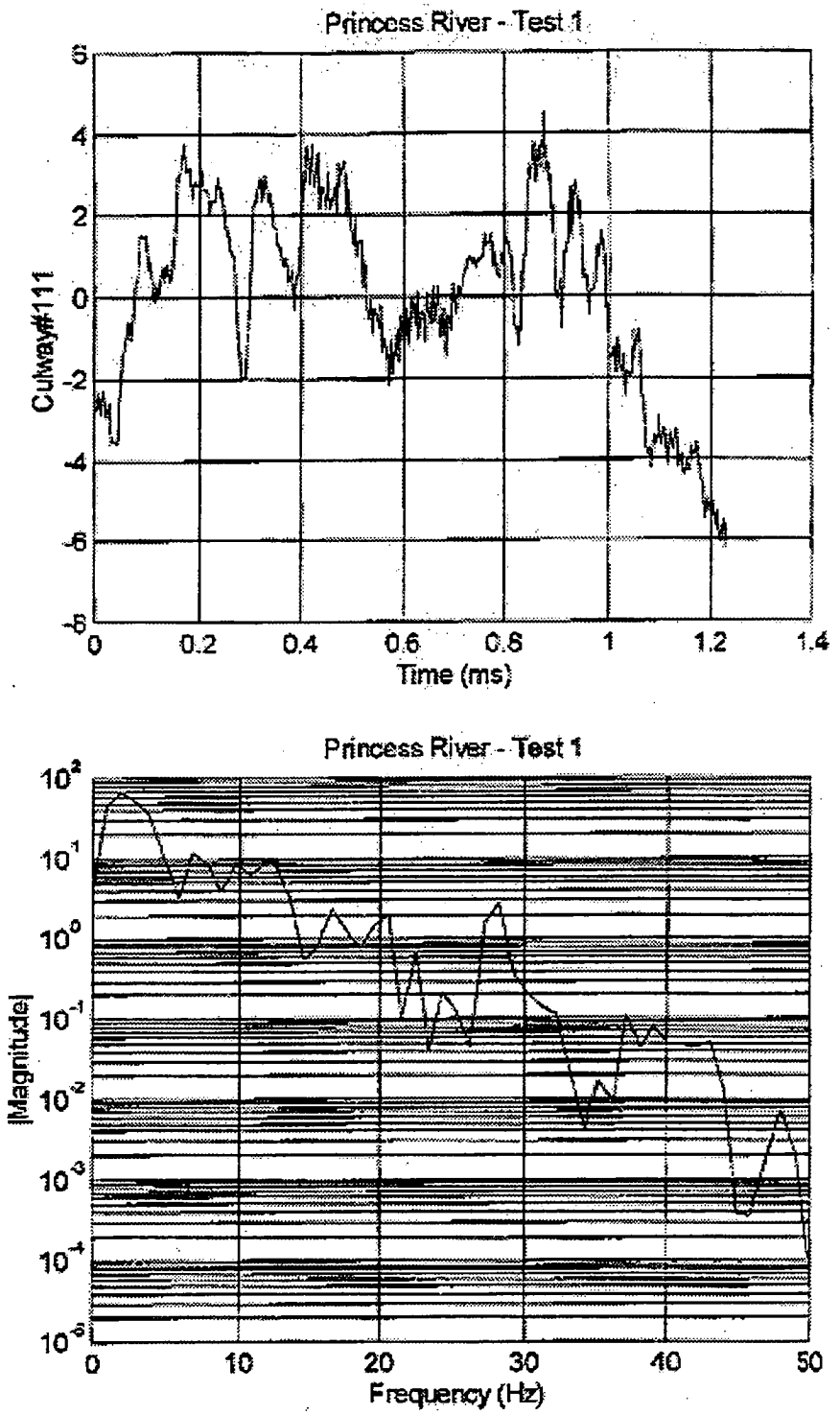

Figure 15.5 - Strain Response and Power Spectral Densities

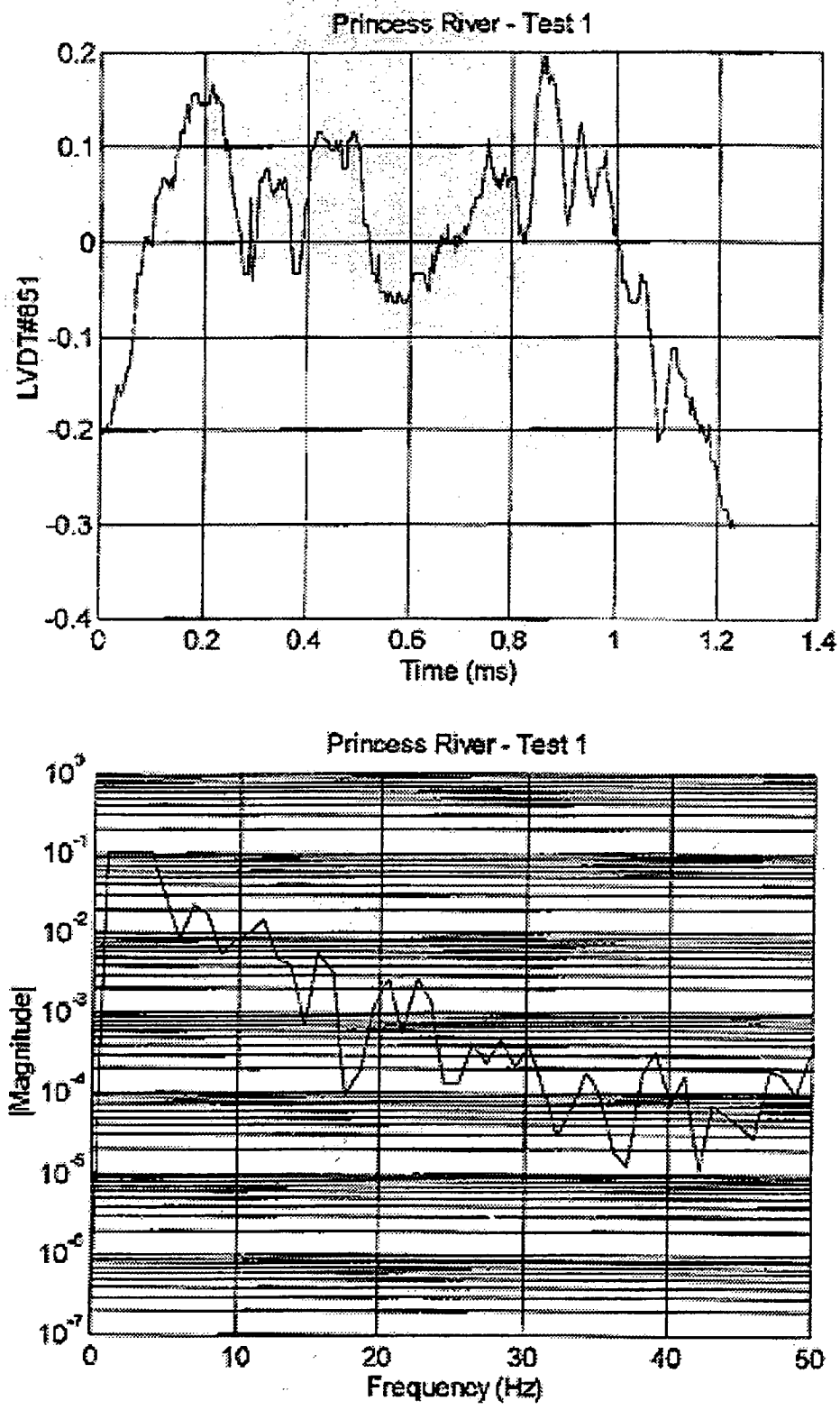

Figure 15.6 - Strain Response and Power Spectral Densities

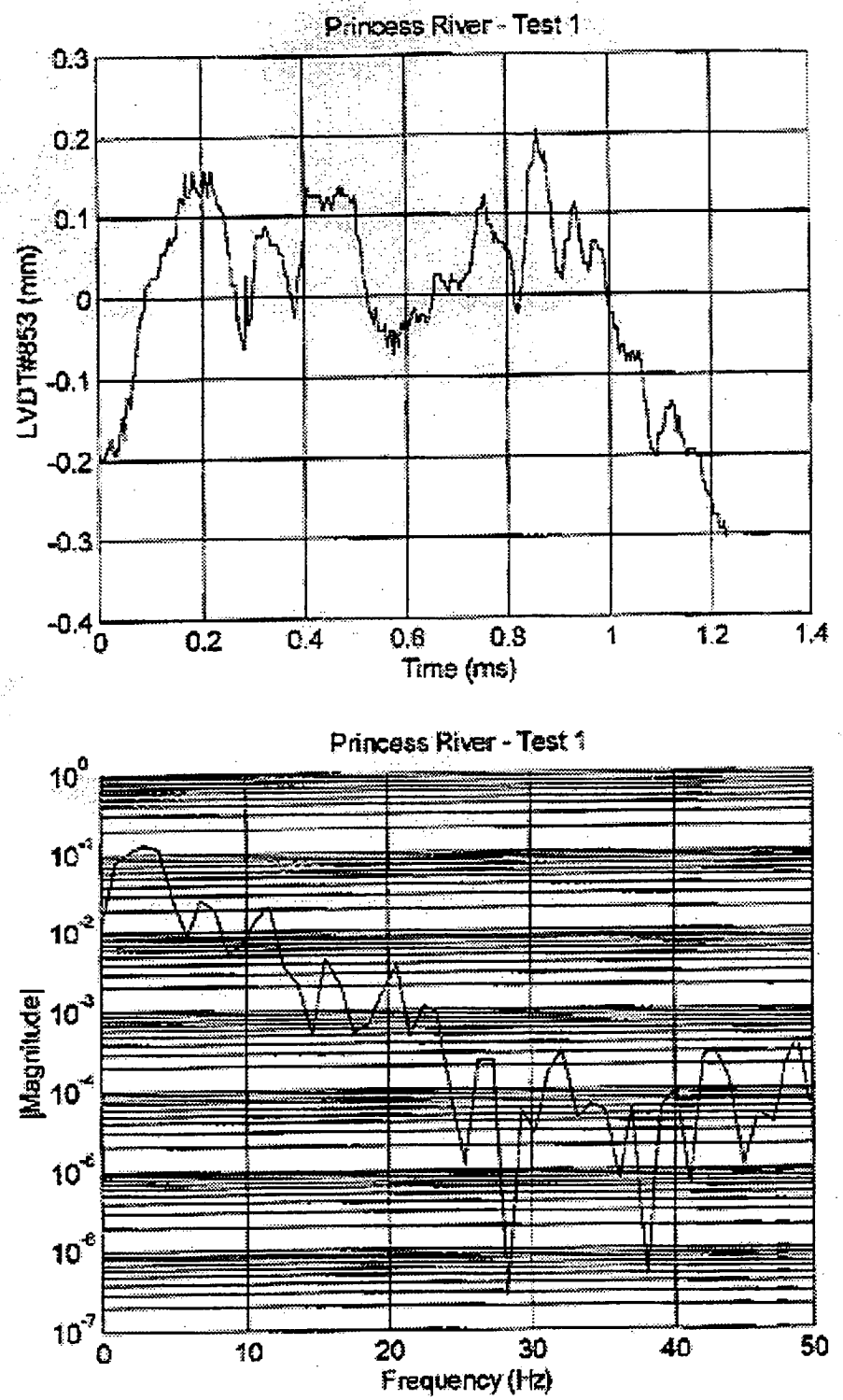

Figure 15.7 - Displacement Response and Power Spectral Densities

15.4 Dynamic Load Allowance

In the 1976 Bridge Design Specification, live load impact was determined using an expression based on span length.

$I = 1600/(L + 40)$, where I = impact percentage, L = length (m)

The permissible range of values is from 10% to 30%.

For a span of 10.364m,

$I = 1600/(10.364 + 40)$

$= 31.8\%$, but not > 30%

$\therefore \quad I = 30\%$

The 1992 AUSTROADS Bridge Design Code specifies a dynamic load allowance based on the first flexural frequency of the superstructure in accorance with Figure 15.8. The relationship is drawn from the 1982 Ontario Highway Bridge Design Code.

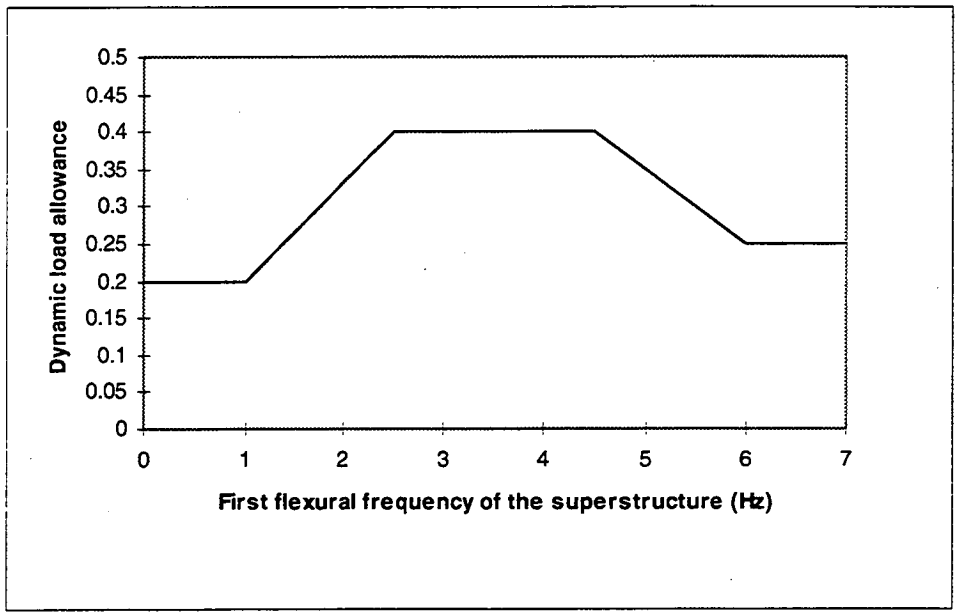

Figure 15.8 - AUSTROADS Dynamic Load Allowance

For preliminary analysis of spans less than 22.5m, the dynamic load allowance can be taken as 0.3.

For more detailed analysis, the first natural frequency in Hertz can be estimated from

$f_1 = \omega_1/(2\pi)$

where $\omega_1 = (\pi/l)^2 \sqrt{(EI\ 10^6/m)}$ $\sec^{-1}$

l = span length
= 10.364 m

E = elastic modulus
= 33,000 MPa

I = second moment of area of section (m^4)

Using the section properties calculated for the load distribution analysis,

Part	A	y	Ay	A(y-yc)2	Iself
Interior beams	2029200	582	$1.181_{10}9$	$3.009_{10}9$	$168.4_{10}9$
Exterior beams	1313400	680	$0.893_{10}9$	$4.649_{10}9$	$130.0_{10}9$
Total	**3342600**		**$2.074_{10}9$**	**$7.658_{10}9$**	**$298.4_{10}9$**

y_c = $2.074_{10}9/3342600$
= 621 mm

I = $306_{10}9$ mm^4

m = 3.343 * 2580
= 8625 kg/m

ω_1 = $(\pi/10.364)^2 \sqrt{(33000 * 0.306 * 10^6/8625)}$ sec^{-1}
= 99.4 sec^{-1}

f_1 = 99.2/(2π)
= 15.8 Hz

From Figure 15.8, the dynamic load allowance is 0.25 or 25%.

The calculated first flexural frequency is in reasonable agreement with the ETRS measured natural frequency of 17.6 Hz for the first bending mode.

In his paper on 60 years experience of dynamic load testing of bridges in Switzerland, Cantieni (1983) discusses the use of empirical formulae to calculate bridge natural frequencies. While the formula

f = 100/L where L = span length

is attractive, he considers that it yields fundamental frequencies which are too low and recommends, as a first estimate, the function g(L) as follows:

f = $95.4\ L^{-0.933}$

For a span length of 10.364m, the function gives a value of

f = 10.8 Hz

By comparison, the formula 100/L gives an estimated fundamental frequency of 9.65 Hz.

Cantieni also presents envelopes showing the maximum dynamic effects measured for bridges over a period of 25 years with both undisturbed pavements and with the axle hop vibration mode for trucks excited by a plank 40 to 60mm thick. The envelopes are shown in Figures 15.9 and 15.10.

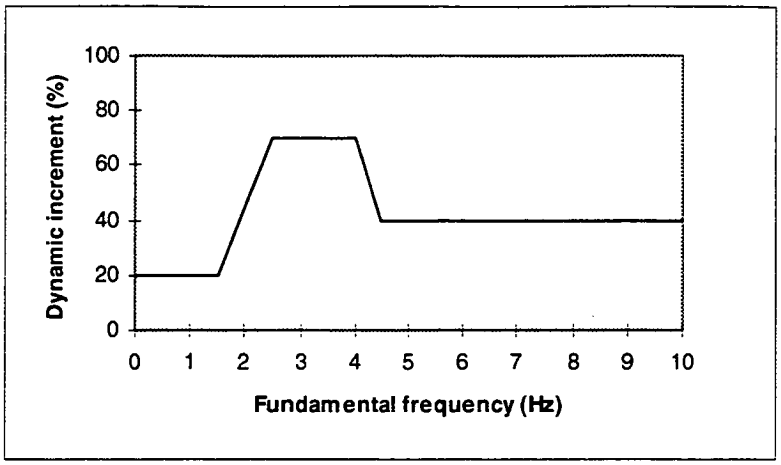

Figure 15.9 - Dynamic Effects with Undisturbed Pavements

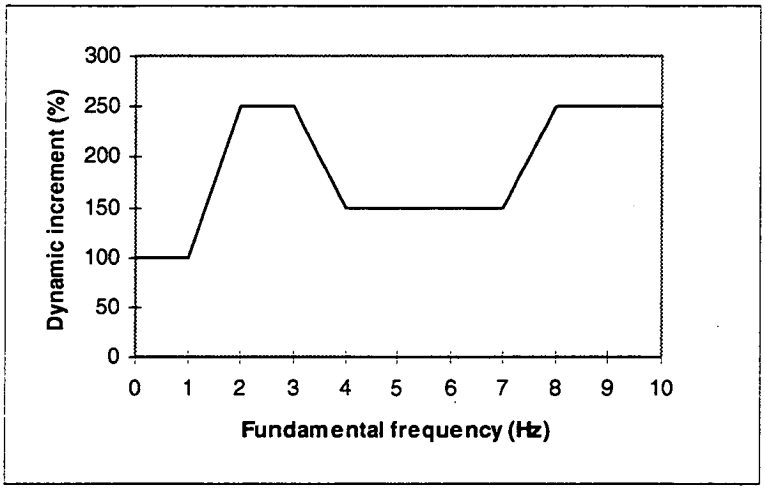

Figure 15.10 - Dynamic Effects with Plank on Pavement

Figure 15.11 shows strain, acceleration and displacement responses of Princess River Bridge, with a plank placed on the approaches. Raw data only is shown, with the actual values of strain, displacement and acceleration determined using the appropriate calibration factors.

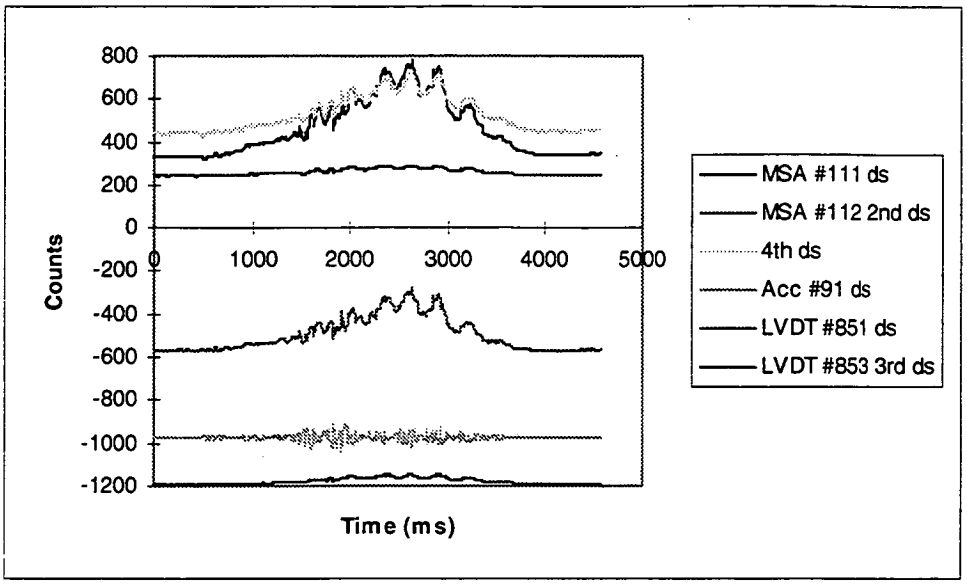

Figure 15.11 - Bridge Responses with DOC Truck Crossing at 10km/h with Plank

As outlined above, a definitive assessment of dynamic effects cannot be made because of the sampling frequency and duration. Indicative effects are however estimated by fitting a polynomial curve to a section of the strain response at around the maximum response corresponding to the passage of a particular axle group, as shown in Figure 15.12.

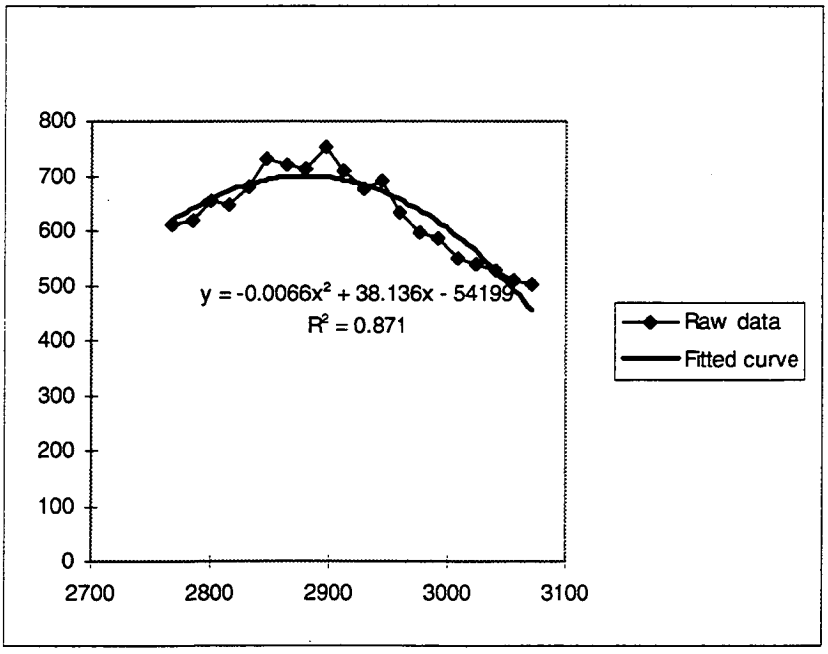

Figure 15.12 - Sample of Strain Response (MSA #111)

For a base reading with the truck of the bridge of 340 counts, the maximum measured response of 752 counts, and the maximum value of the fitted curve being 700 counts, the estimated impact factor is given by:

$$I = (752-700)*100/(700-340)$$
$$= 14.4\%, \text{ say } 15\%$$

15.5 Discussion

Dynamic measurements were made on the bridge for a range of excitation mechanisms to assess the ability to identify structural damage and impact effects.

While the removal of sections of bridge railing was readily identifiable at higher frequencies, it was not possible to discern damage to the beam reinforcing until a substantial proportion of the reinforcement in a beam had been cut.

The natural frequency of the bridge for the first mode of vibration was measured at 17.6 Hz, which corresponds approximately to the 15.8 Hz calculated by elastic theory. Simplified methods, based on the reciprocal of span length, underestimate the natural frequency of the bridge. This may be in part due to the close spacing and large number of the T-beams resulting in a comparatively high flexural stiffness for the bridge.

The ability to investigate dynamic load effects was constrained by the relatively low sampling frequency and limited duration of measurements. Impact factors for the bridge are estimated to be of the order of 15%, compared to the 25% to 30% calculated in accordance with the 1976 NAASRA and 1992 AUSTROADS Codes and the higher values measured by Cantieni for trucks passing over a plank. The natural frequency of the bridge is higher than the typical body bounce frequencies of 1 to 4 Hz and axle hop frequencies of 8 to 15 Hz for heavy vehicles meaning that resonance does not occur, and thus limiting dynamic effects.

16. LOAD DISTRIBUTION

16.1 Introduction

A series of measurements were taken with the bridge loaded with a gravel truck to determine the distribution of live load between the six beams in the bridge and to assess the accuracy of various analytical methods in predicting the load distribution.

Strain and deflection measurements were taken with both the ORION data logger and the Department of Roads and Transport's data acquisition system.

Average strains are generally used where measurements were taken on both sides of a beam.

16.2 Loading

The bridge was loaded with a Department of Construction 7.5 cubic metre capacity truck carrying King River gravel, with axle loads as shown below.

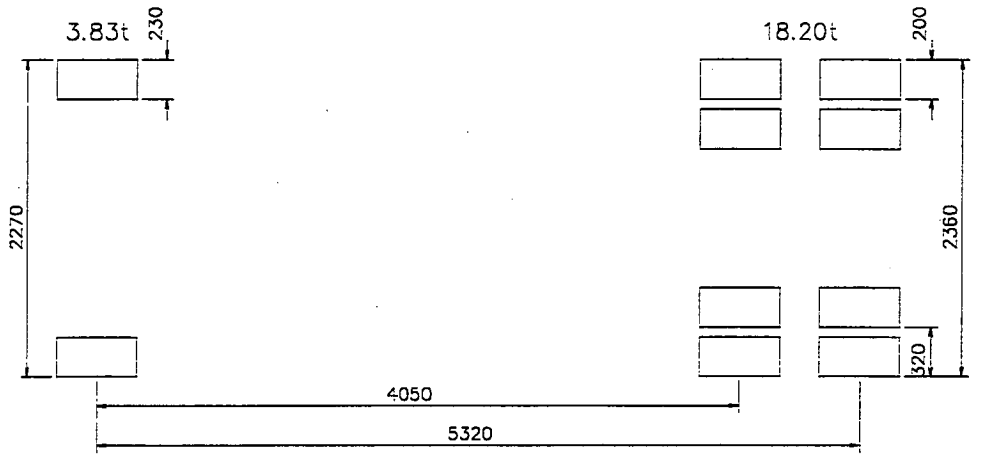

Figure 16.1 - Department of Construction Truck

16.3 Measured Strain Distributions

Measured strains and the offsets from the face of the downstream kerb to the face of the upstream tyre are given in Table 16.1.

Distance from d/s kerb	Midspan strain (με)						
	D/s beam	5th beam	4th beam	3rd beam	2nd beam	U/s beam	Total strain
170	42	36	24	8	5	3	118
530	9	9	8	3	-6	2	25
1070	27	37	33	19	9	7	132
1130	24	33	33	18	4	6	118
1470	16	34	30	15	8	7	110
2050	13	15	27	30	24	13	122
2140	13	24	30	26	18	9	120
2750	8	15	29	27	21	18	118
3700	4	8	17	27	29	37	122

Table 16.1 - Strain Distributions

Table 16.2 shows the proportions of the total load taken by each beam, based on the strain distributions and neglecting the variation in section properties between interior and exterior

beams. The maximum distribution factor excludes the results for the 530mm offset because of the apparently anomalous strains. Results are shown graphically in Figure 16.2.

Distance from d/s kerb (mm)	Proportion of axle load					
	D/s beam	5th beam	4th beam	3rd beam	2nd beam	U/s beam
170	0.356	0.305	0.203	0.068	0.042	0.025
530	0.360	0.360	0.320	0.120	-0.240	0.080
1070	0.205	0.280	0.250	0.144	0.068	0.053
1130	0.203	0.280	0.280	0.153	0.034	0.051
1470	0.145	0.309	0.273	0.136	0.073	0.064
2050	0.107	0.123	0.221	0.246	0.197	0.107
2140	0.108	0.200	0.250	0.217	0.150	0.075
2750	0.068	0.127	0.246	0.229	0.178	0.153
3700	0.033	0.066	0.139	0.221	0.238	0.303
Maximum	0.356	0.309	0.280	0.246	0.238	0.303

Table 16.2 - Measured Load Distributions

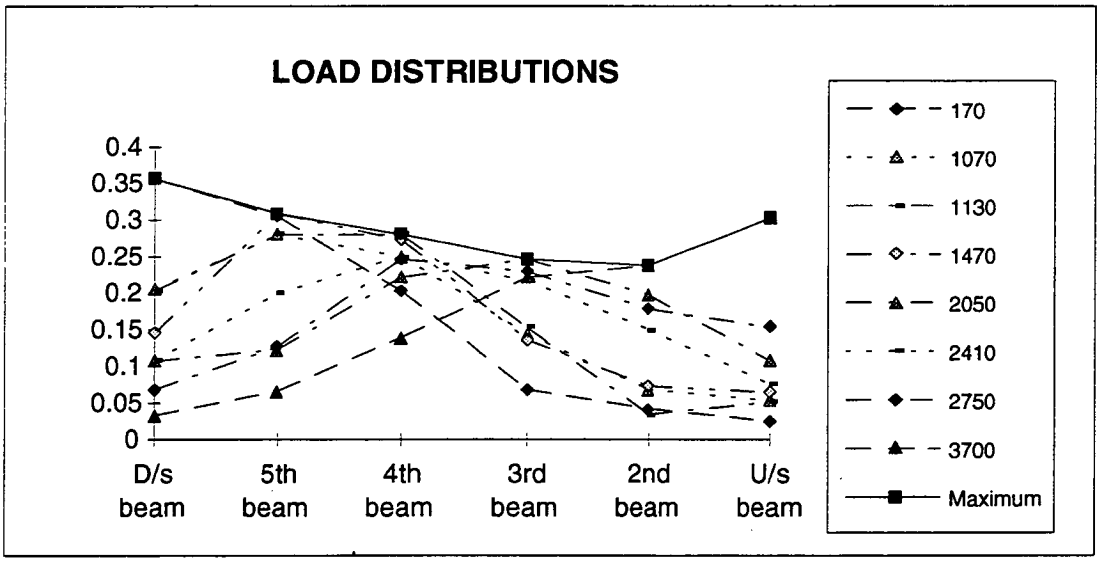

Figure 16.2 - Measured Load Distributions

16.4 Load Distribution by Grillage Analysis

Grillage analysis used the computer program 'GROPER' developed by Technical Systems Australia of Melbourne. Varying coarsenesses of meshes were used to assess the convergence of the program and compare measured distributions with measured distributions.

Section properties for the interior beams are determined as follows:

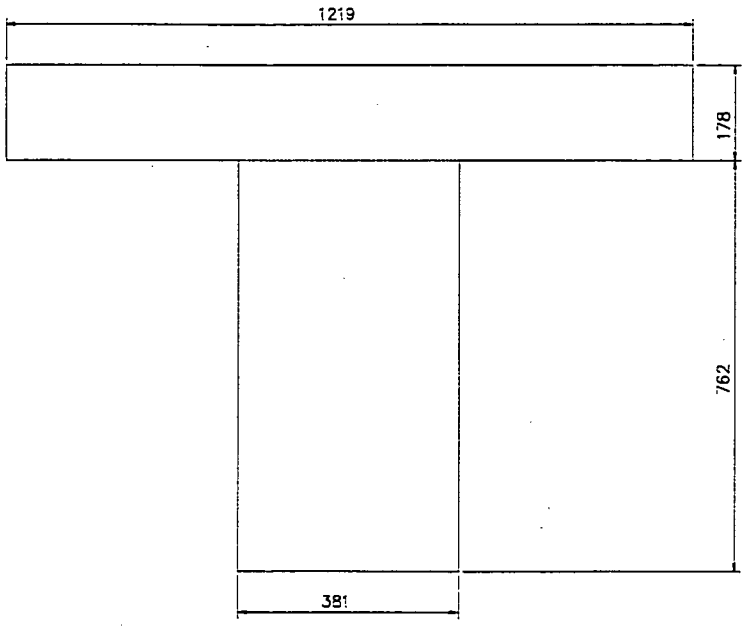

Figure 16.3 - Interior Beam

Part	A	y	Ay	A(y-yc)2	Iself
Beam	290320	381	$111_{10}6$	$11.7_{10}9$	$14.1_{10}9$
Deck	216980	851	$185_{10}6$	$15.7_{10}9$	$0.6_{10}9$
Total	**507300**		**$295_{10}6$**	**$27.4_{10}9$**	**$14.6_{10}9$**

y_c = $295_{10}6/507300$
= 582

I_{xx} = $42.1_{10}9$ mm⁴

For grillage analysis,

J = $J_{beam} + J'_{slab}$
= $762*381^3/3 + 1219 * 178^3/6$
= $15.2_{10}9$ mm⁴

For the exterior beam,

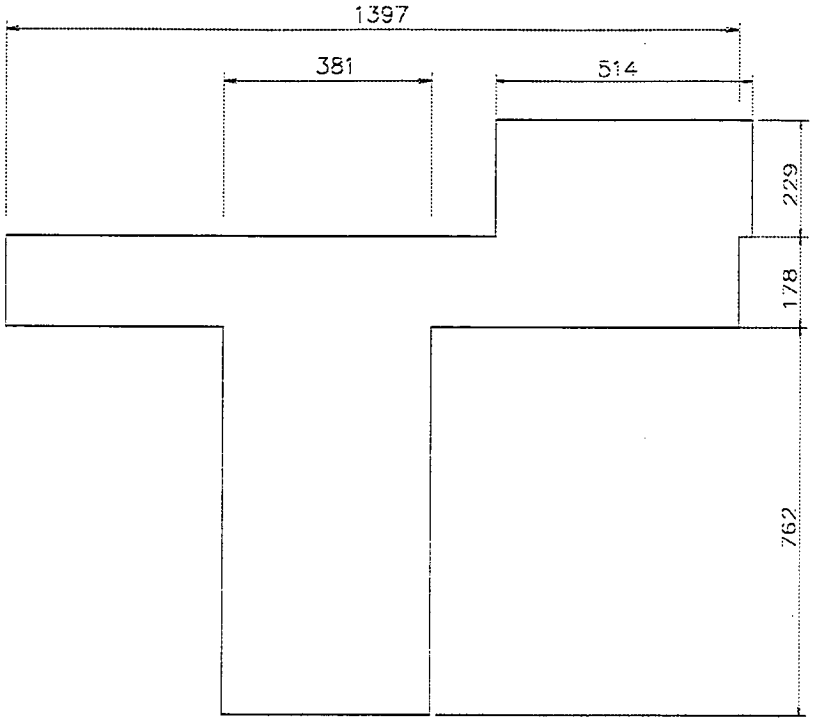

Figure 16.4 - Exterior Beam

Part	A	y	Ay	A(y-yc)2	Iself
Kerb	117710	1055	$124_{10}6$	$16.5_{10}9$	$0.5_{10}9$
Slab	248670	851	$212_{10}6$	$7.3_{10}9$	$0.7_{10}9$
Beam	290320	381	$111_{10}6$	$25.8_{10}9$	$14.1_{10}9$
Total	**656700**		**$446_{10}6$**	**$49.8_{10}9$**	**$15.2_{10}9$**

$y_c = 446_{10}6/656700$
$= 680$

$I_{xx} = 65.0_{10}9\ mm^4$

For grillage analysis,

$J = J_{kerb} + J_{beam} + J'_{slab}$
$= 514*229^3/3 + 762 * 381^3/3 + 1397*178^3/3$
$= 17.4_{10}9\ mm^4$

From testing of deck concrete,

Youngs Modulus, E = 35000 MPa
Density = 25 kN/m³

Poissons Ratio = 0.2
Shear modulus, G = 35000/2(1+0.2)
= 14500 MPa

The program documentation recommends a maximum aspect ratio for plate elements of 3, requiring a minimum of 3 divisions along the bridge. Four divisions were adopted to provide output at midspan.

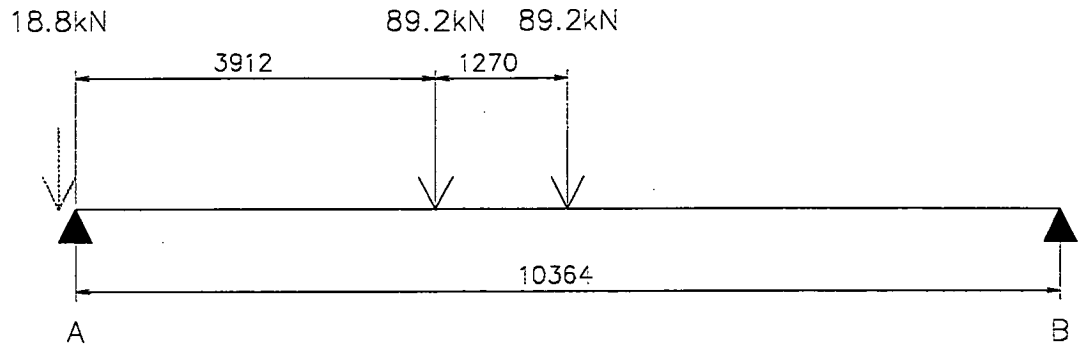

Figure 16.5 - Vehicle Loading

Figure 16.5 shows the position of the DOC truck on the bridge. The total bending moment calculated for a simply supported beam is determined as follows:

$$R_A = 89.2(5.182+6.452)/10.364$$
$$= 100.1 \text{ kN}$$

$$R_B = 78.3 \text{ kN}$$

$$M_C = 78.3 * 5.182$$
$$= 405.8 \text{ kN.m}$$

Beam midspan bending moments from GROPER, using four lengthwise divisions, are shown in Table 16.3.

Distance from d/s kerb		Bending moment (kN.m)						Total moment (kN.m)
		D/s beam	5th beam	4th beam	3rd beam	2nd beam	U/s beam	
170	M	171.7	96.8	76.8	37.3	14.4	4.4	401.4
	%	42.8	24.1	19.1	9.3	3.6	1.1	
530	M	138.1	95.6	92.9	47.8	19.4	6.8	400.6
	%	34.5	23.9	23.2	11.9	4.8	1.7	
1070	M	95.4	97.3	95.7	66.5	30.4	14.3	399.6
	%	23.9	24.3	23.9	16.6	7.6	3.6	
1130	M	90.9	97.6	95.3	68.7	31.7	15.3	399.5
	%	22.8	24.4	23.9	17.2	7.9	3.8	
1470	M	71.1	89.4	94.6	82.4	40.2	21.5	399.2
	%	17.8	22.4	23.7	20.6	10.1	5.4	
2050	M	45.5	66.0	96.1	97.9	57.4	36.2	399.1
	%	11.4	16.5	24.1	24.5	14.4	9.1	
2140	M	42.1	62.8	96.7	97.2	60.5	39.6	398.9
	%	10.6	15.7	24.2	24.4	15.2	9.9	
2750	M	24.0	43.6	87.8	94.7	84.0	65.1	399.2
	%	6.0	10.9	22.0	23.7	21.0	16.3	
3700	M	7.5	21.1	51.1	97.9	95.3	127.3	400.2
	%	1.9	5.3	12.8	24.5	23.8	31.8	

Table 16.3 - Beam Bending Moments with 4 Longitudinal Divisions

Using six lengthwise divisions, midspan bending moments from GROPER are detailed in Table 16.4.

Distance from d/s kerb		Bending moment (kN.m)						Total moment (kN.m)
		D/s beam	5th beam	4th beam	3rd beam	2nd beam	U/s beam	
170	M	172.5	97.1	77.1	37.0	14.0	3.7	401.4
	%	43.0	24.2	19.2	9.2	3.5	0.9	
530	M	138.2	96.1	93.8	47.6	19.0	5.9	400.6
	%	34.5	24.0	23.4	11.9	4.7	1.5	
1070	M	94.6	98.2	96.5	66.8	30.1	13.4	399.6
	%	23.7	24.6	24.1	16.7	7.5	3.4	
1130	M	90.0	98.6	96.2	69.0	31.5	14.3	399.6
	%	22.5	24.7	24.1	17.3	7.9	3.6	
1470	M	69.9	90.3	95.4	83.1	40.1	20.4	399.2
	%	17.5	22.6	23.9	20.8	10.0	5.1	
2050	M	44.3	66.3	97.0	99.0	57.5	35.0	399.1
	%	11.1	16.6	24.3	24.8	14.4	8.8	
2140	M	40.9	63.1	97.7	98.3	60.7	38.4	399.1
	%	10.2	15.8	24.5	24.6	15.2	9.6	
2750	M	22.8	43.5	88.7	95.5	88.8	64.0	403.3
	%	5.7	10.8	22.0	23.7	22.0	15.9	
3700	M	6.7	20.7	51.0	99.0	95.8	127.1	400.3
	%	1.7	5.2	12.7	24.7	23.9	31.8	

Table 16.4 - Beam Bending Moments with 6 Longitudinal Divisions

With eight lengthwise divisions, the midspan bending moments from GROPER are detailed in Table 16.5.

Distance from d/s kerb		Bending moment (kN.m)						Total moment (kN.m)
		D/s beam	5th beam	4th beam	3rd beam	2nd beam	U/s beam	
170	M	173.0	97.1	77.2	36.9	13.9	3.4	401.5
	%	43.1	24.2	19.2	9.2	3.5	0.8	
530	M	138.4	96.2	93.9	47.7	18.9	5.6	400.7
	%	34.5	24.0	23.4	11.9	4.7	1.4	
1070	M	94.6	98.4	96.8	67.0	30.1	13.0	399.9
	%	23.7	24.6	24.2	16.8	7.5	3.3	
1130	M	89.9	98.8	96.5	69.2	31.5	13.9	399.8
	%	22.5	24.7	24.1	17.3	7.9	3.5	
1470	M	69.8	90.5	95.8	83.3	40.2	20.0	399.6
	%	17.5	22.6	24.0	20.8	10.1	5.0	
2050	M	44.0	66.4	97.4	99.3	57.7	34.6	399.4
	%	11.0	16.6	24.4	24.9	14.4	8.7	
2140	M	40.5	63.2	98.1	98.6	60.9	38.0	399.3
	%	10.1	15.8	24.6	24.7	15.3	9.5	
2750	M	22.4	43.5	88.9	95.8	85.0	63.8	399.4
	%	5.6	10.9	22.3	24.0	21.3	16.0	
3700	M	6.3	20.6	51.1	99.2	96.0	127.3	400.5
	%	1.6	5.1	12.8	24.8	24.0	31.8	

Table 16.5 - Beam Bending Moments with 8 Longitudinal Divisions

The distributions show only minimal changes in calculated bending moments for an increasing fineness of mesh, and the results for six longitudinal divisions are used for subsequent analysis.

Calculated Strains

The concrete properties used for the analysis are derived in the chapter on concrete performance.

For the interior beams, neglecting compression reinforcement

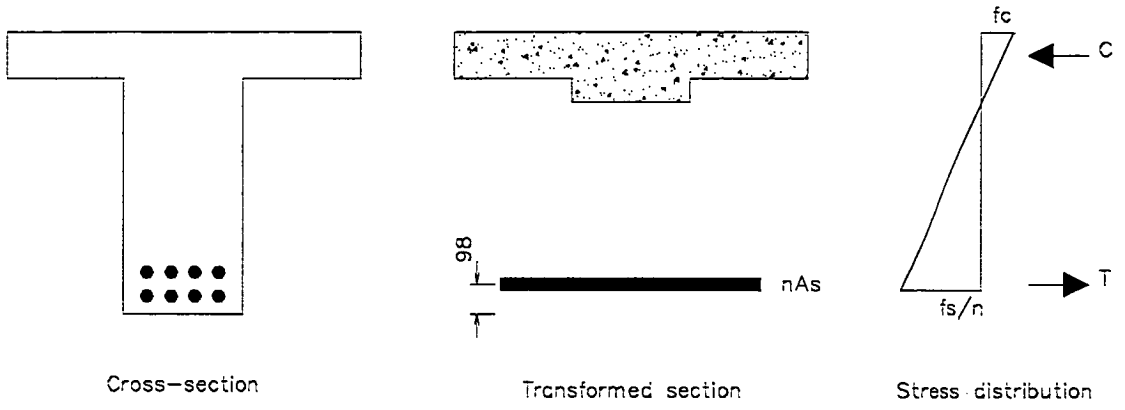

Figure 16.6 - T-beam Properties

For neutral axis in flange,

A_{st}	=	$8(\pi/4)*31.8^2$
	=	6334
n	=	6
p	=	6334/(1219*842)
	=	0.0062
np	=	0.0370
k	=	0.238
j	=	0.921
kd	=	0.238*842
	=	200

ie neutral axis in web

C	=	$f_c*381*kd/2 + (kd-89)*fc*838*178/kd$
T	=	$6334f_s$
f_s	=	$nf_c(d-kd)/kd$

Solving,

T	=	C
k	=	0.240
kd	=	201

The inaccuracies introduced by treating the section as rectangular are thus negligible.

f_c	=	$f_sk/(1-k)n$
	=	$f_s*0.238/(1-0.238)6$
	=	$0.0519f_s$
f_s	=	M*1000/(6334*0.921*0.842)
	=	0.240M

For Young's modulus of steel of 200000 MPa

$\varepsilon_s = f_s/200000$

For the exterior beams, neglecting compression reinforcement

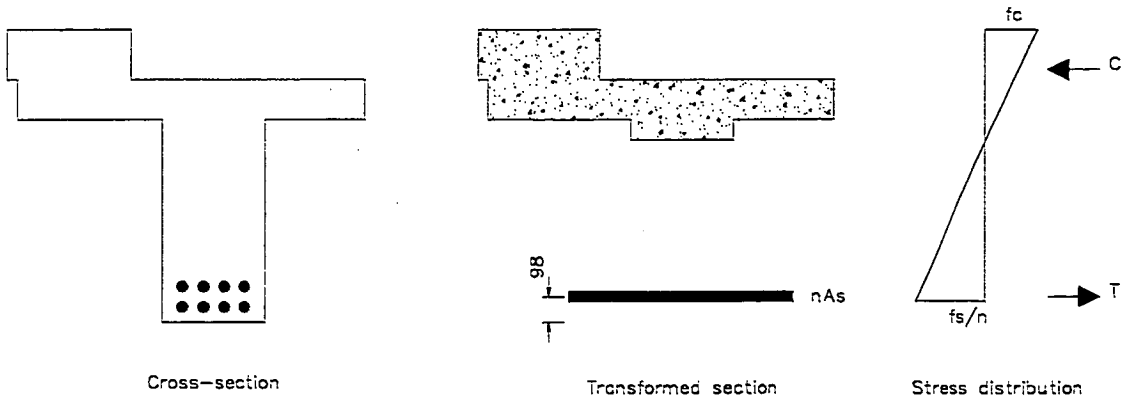

Figure 16.7 - Exterior Beam Properties

For neutral axis in deck slab

A_{st} = 6334
n = 6
d = 762+178+229-98
= 1071

C = $(f_c(1+(kd-229)/kd)*514*229)/2 + f_c(kd-229)^2*1397/2kd$

T = $6334f_s$
= $6334*nf_c(1-k)/k$

Solving, k = 0.294
kd = 315

Element	Force		Lever arm	Moment
Deck	85.9*1397*85.9/315/2	=16360	57.2	936,500
Kerb	514*229*85.9/315	=32100	200.4	6,432,000
	+514*229*229/315/2	=42800	238.5	10,210,000
Total		**91260**		**17,579,000**

Height of centroid = 193
Lever arm = 1071-315+193
= 949

f_s = M*1000/(6334*0.949)
= 0.166M

f_c = $f_sk/(1-k)/n$
= f_s*0.294/(1-0.294)/6
= $0.0694f_s$

ε_s = $f_s/200000$

Distance from d/s kerb		D/s beam	5th beam	4th beam	3rd beam	2nd beam	U/s beam
170	M (kNm)	173	97	77	37	14	3.7
	f_s (MPa)	28.7	19.8	15.7	7.5	2.9	0.61
	f_r (MPa)	2.0	1.0	0.82	0.39	0.15	0.04
	ε_s (uE)	144	99	79	38	14	3.1
530	M (kNm)	138	96	94	48	19	5.9
	f_s (MPa)	22.9	19.6	19.2	9.8	3.9	1.0
	f_r (MPa)	1.6	1.0	1.0	0.51	0.20	0.07
	ε_s (uE)	115	98	96	49	19	5
1070	M (kNm)	95	98	97	67	30	13
	f_s (MPa)	15.8	20.0	19.8	13.7	6.1	2.2
	f_r (MPa)	1.1	1.0	1.0	0.71	0.32	0.15
	ε_s (uE)	79	100	99	68	31	11
1130	M (kNm)	90	99	96	69	32	14
	f_s (MPa)	14.9	20.2	19.6	14.1	6.5	2.3
	f_r (MPa)	1.0	1.0	1.0	0.73	0.34	0.16
	ε_s (uE)	75	101	98	70	33	12
1470	M (kNm)	70	90	95	83	40	20
	f_s (MPa)	11.6	18.4	19.4	16.9	8.2	3.3
	f_r (MPa)	0.81	0.95	1.1	0.88	0.42	0.23
	ε_s (uE)	58	92	97	85	41	17
2050	M (kNm)	44	66	97	99	58	35
	f_s (MPa)	7.3	13.5	19.8	20.2	11.8	5.8
	f_r (MPa)	0.51	0.70	1.0	1.0	0.61	0.40
	ε_s (uE)	37	67	99	101	59	29
2140	M (kNm)	41	63	98	98	61	38
	f_s (MPa)	6.8	12.9	20.0	20.0	12.4	6.3
	f_r (MPa)	0.47	0.67	1.0	1.0	0.65	0.44
	ε_s (uE)	34	64	100	100	62	32
2750	M (kNm)	23	44	89	96	89	64
	f_s (MPa)	3.8	9.0	18.2	19.6	18.2	10.6
	f_r (MPa)	0.26	0.49	0.94	1.0	0.94	0.74
	ε_s (uE)	19	45	91	98	91	53
3700	M (kNm)	6.7	21	51	99	96	127
	f_s (MPa)	1.1	4.3	10.4	20.2	19.6	21.1
	f_r (MPa)	0.08	0.22	0.54	1.0	1.0	1.5
	ε_s (uE)	6	21	52	101	98	105

Table 16.6 - Beam Stresses and Strains

Converting strains to proportions of axle load, neglecting the differences in section properties between interior and exterior beams, proportions of load carried by each beam are detailed in Table 16.7.

Distance from d/s kerb (mm)	Proportion of axle load					
	D/s beam	5th beam	4th beam	3rd beam	2nd beam	U/s beam
170	0.382	0.263	0.209	0.101	0.037	0.008
530	0.301	0.257	0.251	0.128	0.050	0.013
1070	0.204	0.258	0.255	0.175	0.080	0.028
1130	0.193	0.260	0.252	0.180	0.085	0.031
1470	0.149	0.236	0.249	0.218	0.105	0.044
2050	0.094	0.171	0.253	0.258	0.151	0.074
2140	0.087	0.163	0.255	0.255	0.158	0.082
2750	0.048	0.113	0.229	0.247	0.229	0.134
3700	0.016	0.055	0.136	0.264	0.256	0.274
Maximum	0.382	0.263	0.255	0.258	0.256	0.274

Table 16.7 - Calculated Load Distributions

16.6 Predicted Load Distribution by 1965 NAASRA Bridge Design Specification

For a bridge designed for two traffic lanes, and an average beam spacing, S, of 4', the 1965 Bridge Design Specification requires the live load bending moment for each girder to be determined by applying the following fraction of the wheel load:

$$S/6.0 = 4.0/6.0 = 0.667$$

This corresponds to 0.333 of the total load, compared with the maximum measured distribution factor of 0.309.

The proportion of load carried by the outer beam is determined by applying to the stringer the reaction of the wheel load obtained by assuming the decking to act as a simple beam between the stringers.

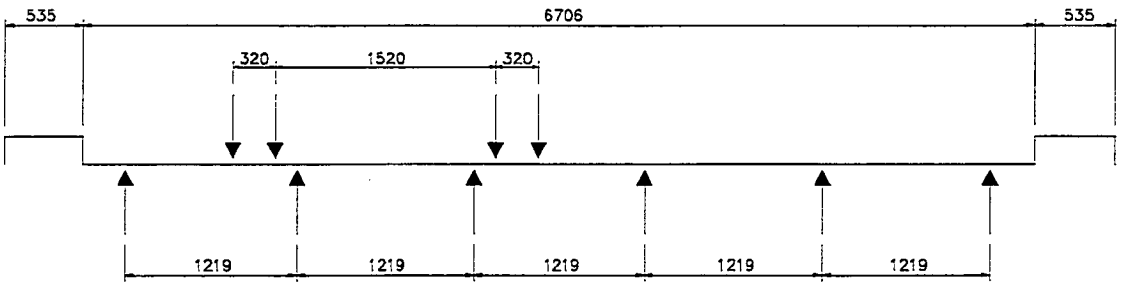

Figure 16.8 - Dual Tyre Vehicle Load Distribution

Distance from d/s kerb (mm)	Proportion of axle load					
	D/s beam	5th beam	4th beam	3rd beam	2nd beam	U/s beam
170	0.454	0.279	0.315	-0.061	0.015	-0.003
530	0.293	0.328	0.400	-0.026	0.007	-0.001
1070	0.091	0.414	0.360	0.166	-0.037	0.006
1130	0.073	0.421	0.347	0.194	-0.042	0.007
1470	-0.003	0.423	0.286	0.340	-0.055	0.009
2050	-0.032	0.246	0.324	0.416	0.055	-0.009
2140	-0.029	0.206	0.344	0.403	0.089	-0.014
2750	0.003	-0.019	0.419	0.282	0.347	-0.033
3700	0.003	-0.016	0.068	0.400	0.378	0.168
Maximum	0.454	0.423	0.419	0.416	0.378	0.168

Table 16.8 - Calculated Load Distribution by Simple Beam (Dual Tyre)

The load distributions are calculated alternately with the dual tyres equated to a single tyre.

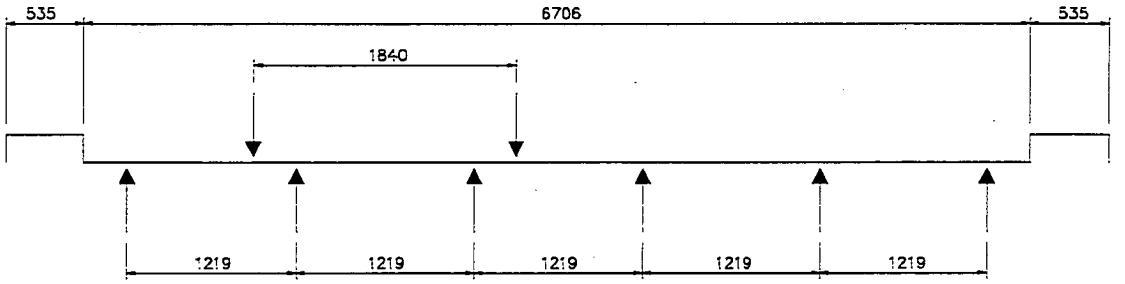

Figure 16.9 - Single Tyre Vehicle Load Distribution

Distance from d/s kerb (mm)	Proportion of axle load					
	D/s beam	5th beam	4th beam	3rd beam	2nd beam	U/s beam
170	0.523	0.259	0.267	-0.062	0.016	-0.003
530	0.353	0.308	0.382	-0.055	0.014	-0.002
1070	0.136	0.393	0.395	0.095	-0.023	0.004
1130	0.115	0.404	0.383	0.123	-0.030	0.005
1470	0.018	0.442	0.301	0.288	-0.058	0.010
2050	-0.038	0.313	0.288	0.438	-0.001	0.000
2140	-0.037	0.277	0.292	0.432	0.037	-0.006
2750	-0.002	0.009	0.437	0.294	0.299	-0.038
3700	0.005	-0.003	0.125	0.381	0.405	0.114
Maximum	0.523	0.442	0.437	0.438	0.405	0.114

Table 16.9 - Calculated Load Distribution by Simple Beam (Single Tyre)

For the interior beam, using a distribution factor of 0.333 of the total load and section properties from the grillage analysis

M_{beam} = 0.333*405.8

= 135 kN.m

f_s = 0.204M
= 27.5 MPa

f_c = $0.0519f_s$
= 1.43 MPa

ε_s = $f_s/200000$
= 138 με

For the exterior beam, using the maximum distribution factor of 0.454 from the analysis using dual tyres

M_{beam} = 0.454*405.8
= 184 kN.m

f_s = 0.166M
= 30.5 MPa

f_c = $0.0694f_s$
= 2.1 MPa

ε_s = $f_s/200000$
= 153 με

16.7 Comparison of Measured and Calculated Strains

Maximum values of measured and calculated strains and distribution factors, neglecting differences in section properties between beams, are detailed in Table 16.10.

	Interior Beams		Exterior Beams	
	Distribution Factor	Strain	Distribution Factor	Strain
Measured	0.309	37	0.356	42
Grillage	0.263	101	0.382	144
BDS (1976)	0.333	138	0.454	153

Table 16.10 - Comparison of Strains and Load Distributions

16.8 Longitudinal Load Distribution

In addition to strains at midspan, strain gauges were fixed to beam reinforcement on the upstream beam and on the third beam from upstream 1m from the Queenstown abutment and at the quarter and three-quarter points to measure longitudinal strain distribution.

Measured strains from the load distribution testing are detailed in Table 16.11.

Distance from	Upstream beam				3rd beam			
d/s kerb	1m	1/4 point	Midspan	3/4 point	1m	1/4 point	Midspan	3/4 point
170	5	5	4	4	5	11	9	7
530	1	2	2	2	1	4	0	4
1070	6	7	7	7	8	17	19	10
1130	4	4	7	4	4	13	17	8
1470	3	4	3	4	7	11	6	8
2050	6	8	14	8	8	20	27	11
2140	6	8	10	9	8	21	26	10
2750	8	11	18	12	8	21	25	12
3700	10	18	38	18	5	17	24	12

Table 16.11 - Longitudinal Strain Distribution

The strains are recalculated as proportions of the midspan strain in Table 16.12. Averages are calculated from the measured strains with the truck at distances of 2050, 2140, 2750 and 3700 from the downstream kerb because of the higher strains.

Distance from	Upstream beam				3rd beam			
d/s kerb	1m	1/4 point	Midspan	3/4 point	1m	1/4 point	Midspan	3/4 point
170	1.25	1.25	1.0	1.0	0.56	1.22	1.0	0.78
530	0.5	1.0	1.0	1.0	-	-	-	-
1070	0.86	1.0	1.0	1.0	0.42	0.89	1.0	0.53
1130	0.57	0.57	1.0	0.57	0.24	0.76	1.0	0.47
1470	1.0	1.33	1.0	1.33	1.17	1.83	1.0	1.33
2050	0.43	0.57	1.0	0.57	0.30	0.74	1.0	0.41
2140	0.6	0.8	1.0	0.9	0.31	0.81	1.0	0.38
2750	0.44	0.61	1.0	0.67	0.32	0.84	1.0	0.48
3700	0.26	0.47	1.0	0.47	0.21	0.71	1.0	0.5
Average	0.43	0.61	1.0	0.65	0.29	0.78	1.0	0.44

Table 16.12 - Longitudinal Strain Ratios

Calculating moments for a wheel line of the truck on a simply supported span, with the steer axle being off the span

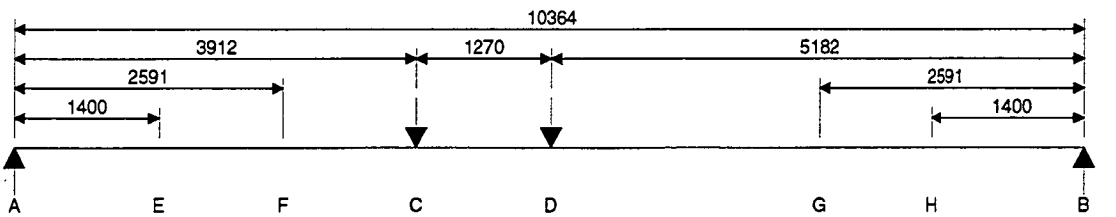

Figure 16.10 - Beam Loading

R_B = P(5.182+3.912)/10.364
= 0.877P

R_A = P(2-0.877)
= 1.123P

M_C = 1.123P*3.912
= 4.39P

M_D = 0.877P*5.182
= 4.55P

For points E and F 1.4m from the centrelines of the supports

M_E = 1.123P*1.4
= 1.57P

M_H = 0.877P*1.4
= 1.23P

At the quarter points

M_F = 1.123P*2.6
= 2.92P

M_G = 0.877P*2.6
= 2.28P

The calculated proportions of the maximum midspan moment are detailed in Table 16.13.

Location	Proportion of maximum moment
1m	0.35
1/4 point	0.64
Midspan	1.00
3/4 point	0.50
1m	0.27

Table 16.13 - Proportions of Midspan Moment for Simple Beam

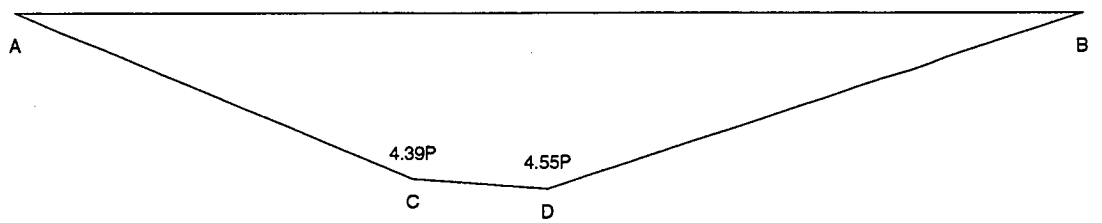

Figure 16.11 - Simply Supported Beam

For the encastre beam

EId_{BA} = {(4.55*5.182/2)*3.455 + 4.39*1.270*5.187
+(0.16*1.27/2)*5.605 +(3.912*4.39/2)*7.756}P
- M_B*10.364²/2 - (M_A-M_B)*)10.364/2)*6.909

ie 0 = 140P - 35.8M_A - 17.9M_B

EId_{AB} = {(3.912*4.39/2)*2.608 + 4.39*1.270*4.547
+(0.16*1.27/2)*4.759 +(5.182*4.55/2)*6.909}P
- M_B*10.364²/2 - (M_A-M_B)*)10.364/2)*3.455

ie 0 = 129.7P - 17.9M_A - 35.8M_B

$2M_A + M_B$= 7.82
$M_A + 2M_B$= 7.24

M_B = 2.22P

M_A = 2.80P

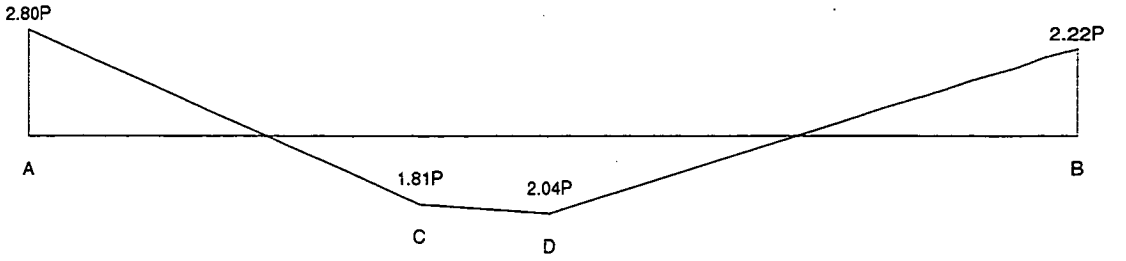

Figure 16.12 - Encastré Beam

Moments are expressed in terms of the midspan moment in Table 16.14.

Location	Moment	Proportion of Midspan Moment
Abutment A	-2.80P	-1.37
1m	-1.62P	-0.79
1/4 point	0.27P	0.13
Midspan	2.04P	1.00
3/4 point	-0.09P	-0.04
1m	-1.40P	-0.69
Abutment B	-2.22P	-1.09

Table 16.14 - Proportions of Midspan Moment for Encastré Beam

16.9 Comparison of measured and calculated longitudinal strain distributions

The average measured longitudinal strain distributions and those calculated for simply supported and encastré beams are summarised in Table 16.15.

Location	Proportion of misdpan strain			
	1m	1/4 point	Midspan	3/4 point
Measured				
- upstream beam	0.43	0.61	1.00	0.65
- 3rd beam	0.29	0.78	1.00	0.44
Calculated				
- simply supported	0.35	0.64	1.00	0.50
- encastré	-0.79	0.13	1.00	-0.04

Table 16.15 - Comparison of Longitudinal Strain Distributions

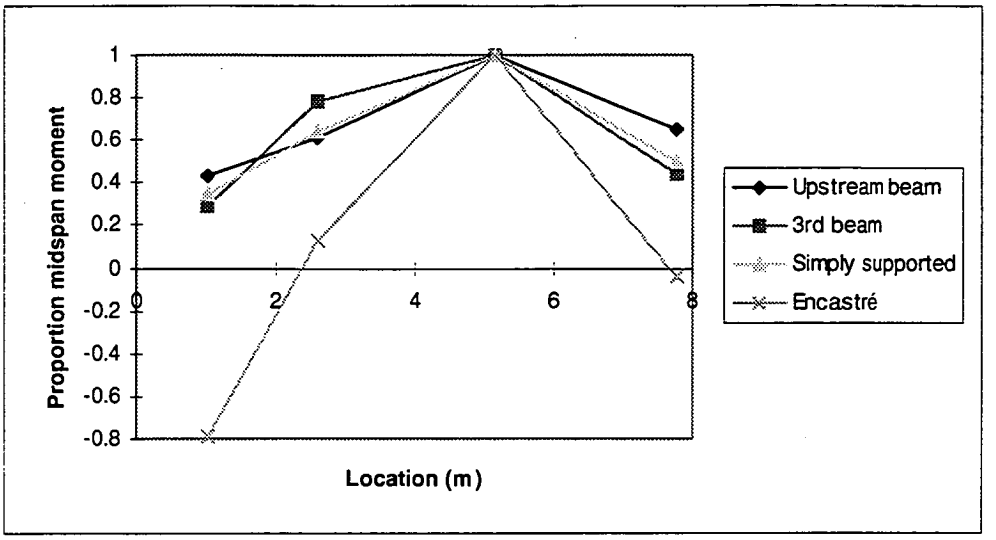

Figure 16.13 - Comparison of Longitudinal Strain Distributions

The longitudinal strain distributions indicate that the beams are acting as simply supported elements rather than as encastré beams.

16.10 Point Load Distribution

The bridge was loaded with a 'point load' at mid-span midway between the second and third beams from upstream for the purpose of assessing punching shear behaviour of the bridge deck. The measurements also provided information on load distribution.

The measured lateral strain distribution is detailed in Table 16.16 and shown in Figure 16.14.

Jack Gauge (MPa)	Load (kN)	Midspan Strains (με)					
		D/s	5th	4th	3rd	2nd	U/s
0	0	0	0	0	0	0	0
8	400	88	83	99	140	97	102
12.5	630	106	107	138	209	163	150
15	750	118	122	161	263	223	183
19	950	154	166	226	403	400	272
21	1050	184	202	269	478	489	331
23	1150	247	270	360	615	627	444
25	1250	269	299	402	681	696	497
28	1400	349	388	525	838	839	646
0	0	201	198	156	210	210	242

Table 16.16 - Lateral Strain Distribution

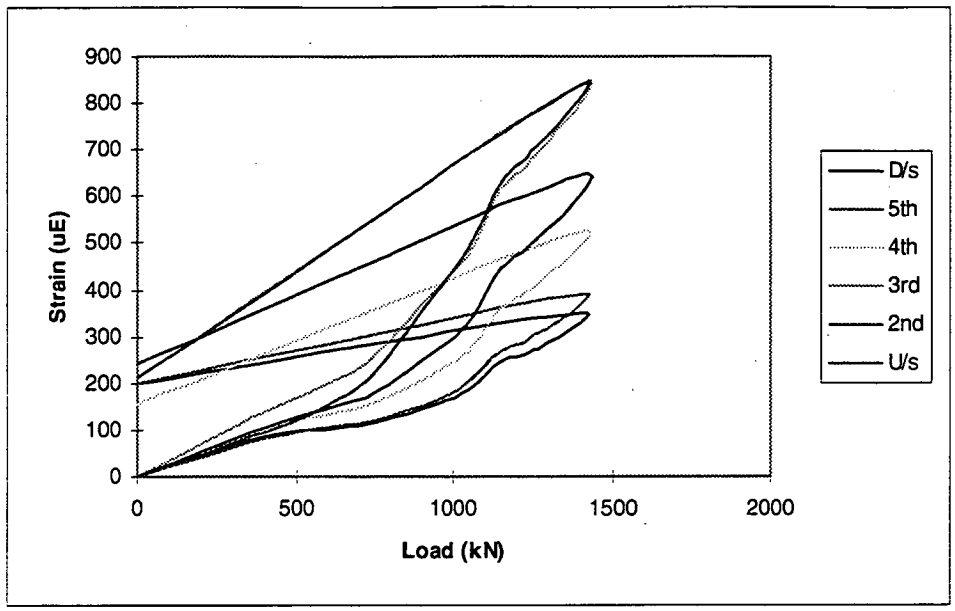

Figure 16.14 - Load~strain Relationship

Figure 16.14 indicates that yield occurred at a load of approximately 750 kN, and that comparisons between measured and theoretical distributions should be for loads not greater than that value. The yield is confirmed by the plastic strains in the reinforcement. Axes are translated from the usual convention for simplicity with the computer software.

Longitudinal strain distributions for the upstream and third beam from upstream are detailed in Tables 16.17 and 16.18 and Figures 16.15 and 16.16.

Jack Gauge (MPa)	Load (kN)	Strains (με)			
		1m from abut	1/4 point	Midspan	3/4 point
0	0	0	0	0	0
8	400	66	90	102	99
12.5	630	85	115	150	129
15	750	100	135	183	151
19	950	141	188	272	208
21	1050	174	223	331	248
23	1150	244	302	444	324
25	1250	270	334	497	359
28	1400	353	425	646	466
0	0	94	127	242	155

Table 16.17 - Longitudinal Strains in Upstream Beam

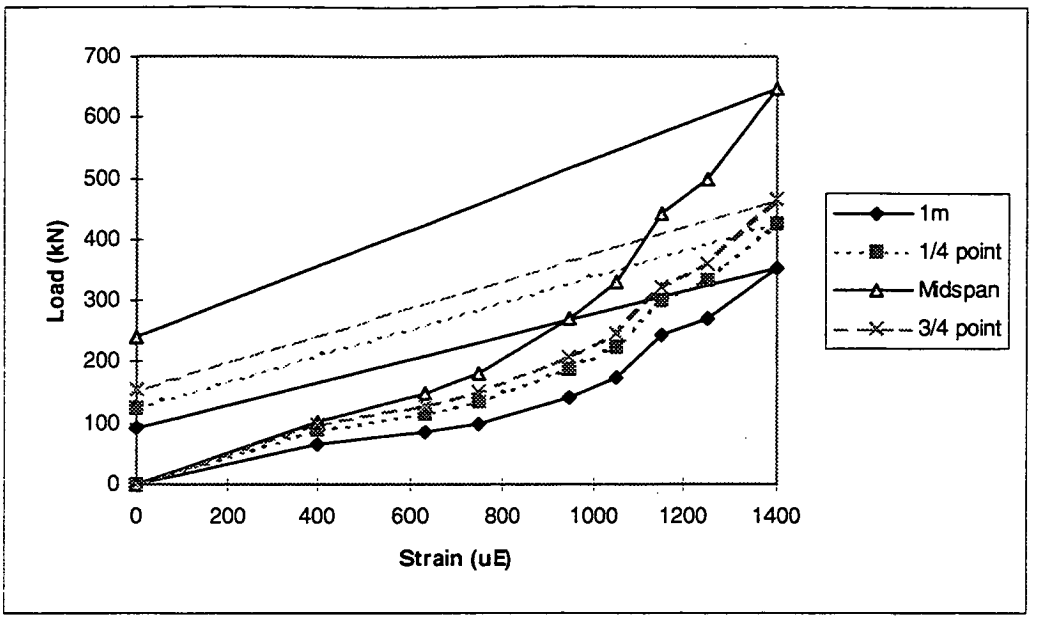

Figure 16.15 - Longitudinal Strains in Upstream Beam

Jack Gauge (MPa)	Load (kN)	Strains (με)			
		1m from abut	1/4 point	Midspan	3/4 point
0	0	0	0	0	0
8	400	72	99	140	88
12.5	630	89	127	209	121
15	750	107	150	263	141
19	950	145	205	403	189
21	1050	173	237	478	227
23	1150	245	310	615	295
25	1250	273	339	681	324
28	1400	348	424	838	407
0	0	103	121	210	116

Table 16.18 - Longitudinal Strains in Third Beam from Upstream

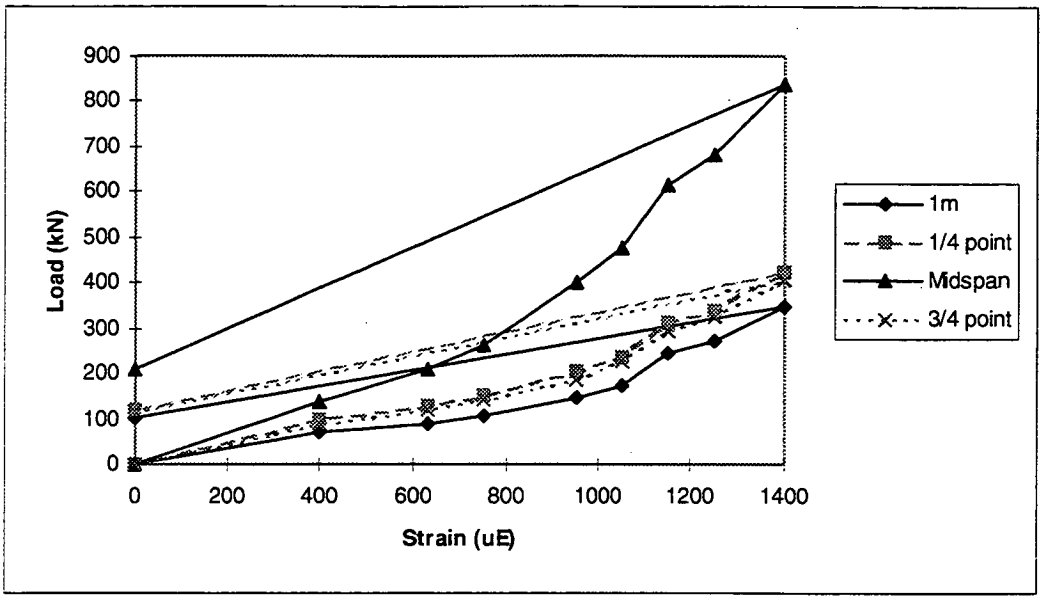

Figure 16.16 - Longitudinal Strains in Third Beam from Upstream

The following results were calculated from the moments determined by GROPER for a 1000kN load placed midway between the second and third beams from upstream.

Previously calculated section properties were used to determine the stresses and strains.

	D/s beam	5th beam	4th beam	3rd beam	2nd beam	U/s beam
M (kN.m)	44	138	346	749	742	528
f_s (MPa)	5.8	27.9	69.9	151	150	69.2
f_c (MPa)	0.4	1.5	3.7	8.1	8.0	4.6
ε_s (uE)	29	139	349	756	749	346

Table 16.19 - Transverse Load Distribution by GROPER

Longitudinal distributions for the upstream beam and the third beam from upstream are detailed in Table 16.20.

		1m from abutment	1/4 point	Midspan	3/4 point
Upstream beam	M (kN.m)	115	317	528	324
	f_s (MPa)	15.0	41.5	69.2	42.4
	f_c (MPa)	1.0	2.8	4.6	2.8
	ε_s (uE)	75	207	346	212
Third beam	M (kN.m)	124	314	749	311
	f_s (MPa)	25.0	63.3	151	62.8
	f_c (MPa)	1.3	3.4	8.1	3.4
	ε_s (uE)	125	317	756	314

Table 16.20 - Calculated Longitudinal Load Distribution

Comparisons between calculated and measured strains for a load of 750 kN are detailed below.

	D/s beam	5th beam	4th beam	3rd beam	2nd beam	U/s beam
Calculated	22	104	262	567	562	260
Measured	118	122	161	263	223	183

Table 16.21 - Comparison of Lateral Strain Distributions

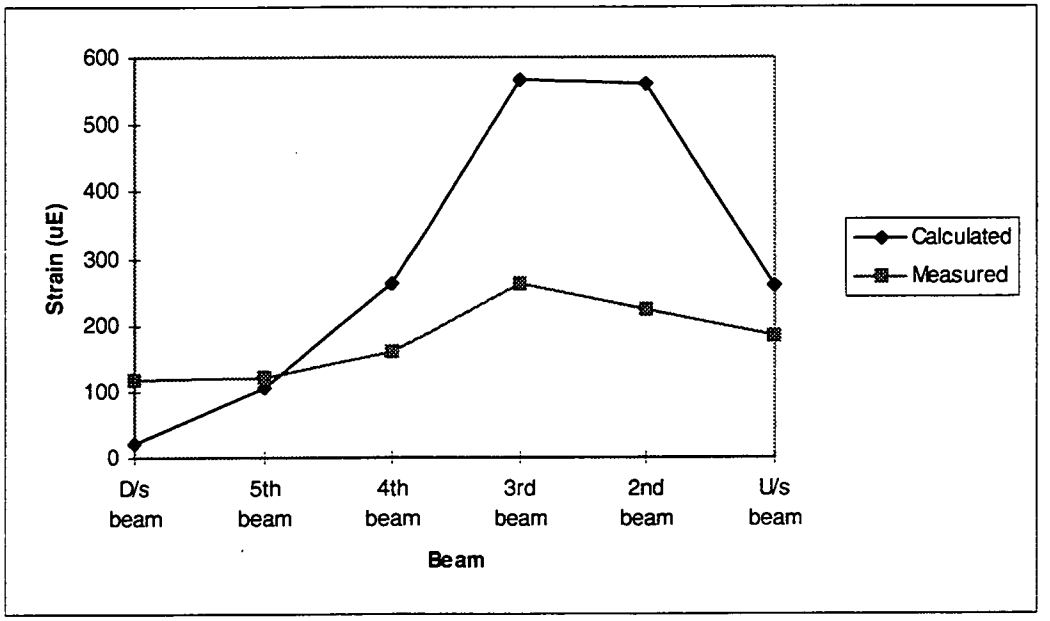

Figure 16.17 - Comparison of Lateral Strain Distributions

	1m from abutment	1/4 point	Midspan	3/4 point
Upstream beam				
- calculated	56	155	260	159
- measured	100	135	183	151
3rd beam				
- calculated	94	238	567	236
- measured	107	150	263	141

Table 16.22 - Comparison of Longitudinal Strain Distribution

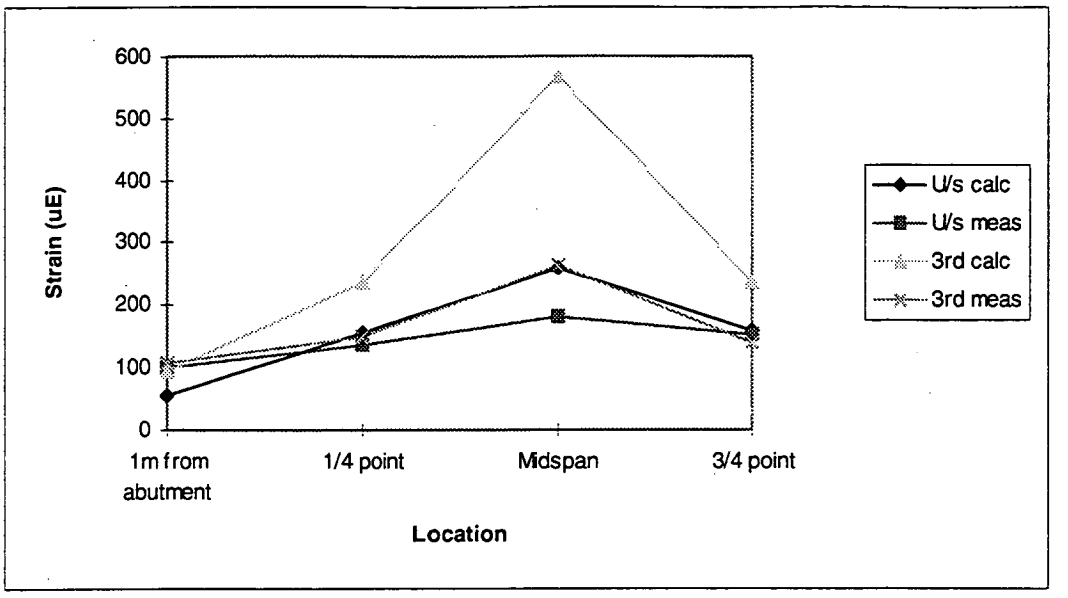

Figure 16.18 - Comparison of Longitudinal Strain Distribution

16.11 Ultimate Load Test Distributions

Strain measurements were also taken during the ultimate load testing, with loads applied to the exterior pairs of beams.

The measured strain distribution at midspan is detailed in Table 16.23.

Jack Gauge Reading (MPa)	Load (kN)	Strains (με)					
		D/s beam	5th beam	4th beam	3rd beam	2nd beam	U/s beam
Prior to testing	0	0	0	0	0	0	0
After punching shear							
Nose	230	326	313	312	363	364	358
0	60	201	198	156	219	248	242
10	1900	504	633	302	342	531	615
15	2900	1002	1062	648	582	885	1629
20	3900	5089	8938	1026	965	1512	9167
23/24	4600	O'load	14879	17001	2319	12569	O'load

Table 16.23 - Ultimate Load Strain Distribution

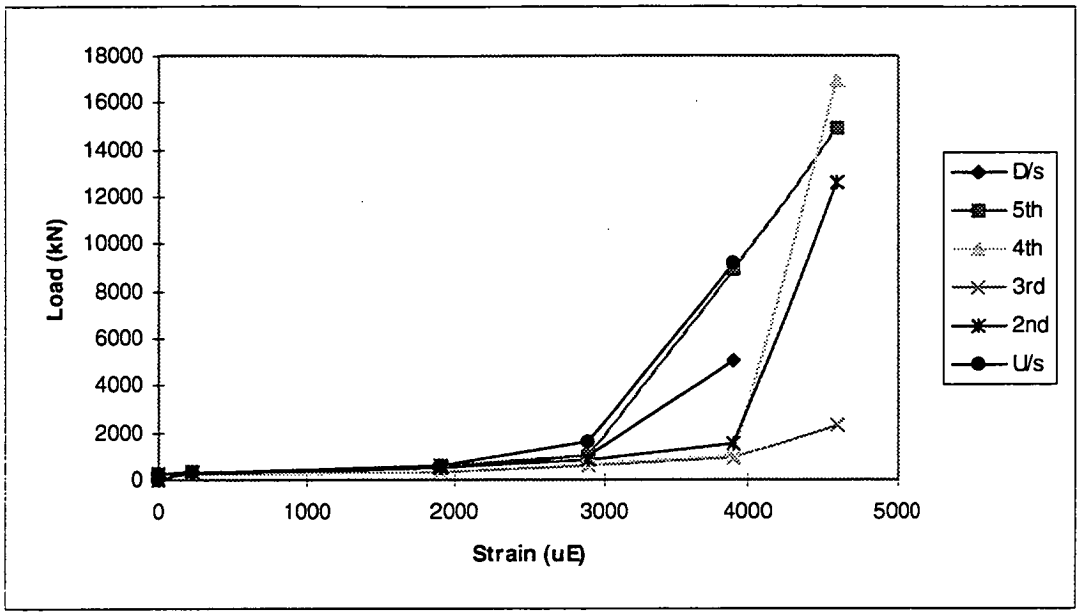

Figure 16.19 - Ultimate Load Strain Distribution

The measured longitudinal strain distributions are detailed in Table 16.24.

		1m from abutment	1/4 point	Midspan	3/4 point
Prior to testing	0	0	0	0	0
After punching shear					
Nose	230	260	299	358	318
0	60	94	127	242	155
10	1900	99	176	615	219
15	2900	114	316	1629	326
20	3900	64	353	9167	312
23/24	4600	45	341	O'load	271

Table 16.24 - Strain Distributions in Upstream Beam

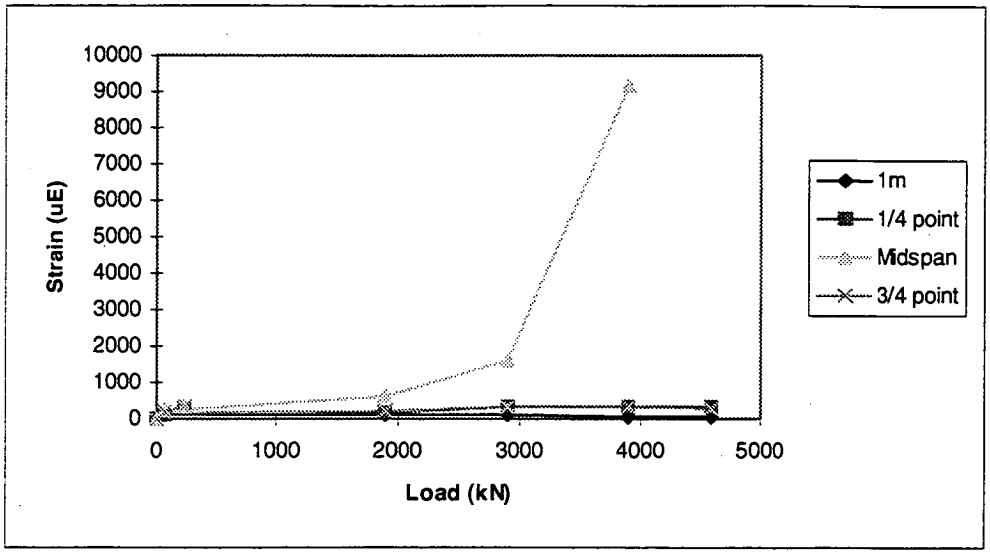

Figure 16.20 - Strain Distributions in Upstream Beam

		1m from abutment	1/4 point	Midspan	3/4 point
Prior to testing	0	0	0	0	0
After punching shear					
Nose	230	327	327	363	308
0	60	182	177	219	156
10	1900	153	192	342	183
15	2900	151	251	582	290
20	3900	224	505	965	622
23/24	4600	454	766	2319	903

Table 16.25 - Strain Distributions in Third Beam from Upstream

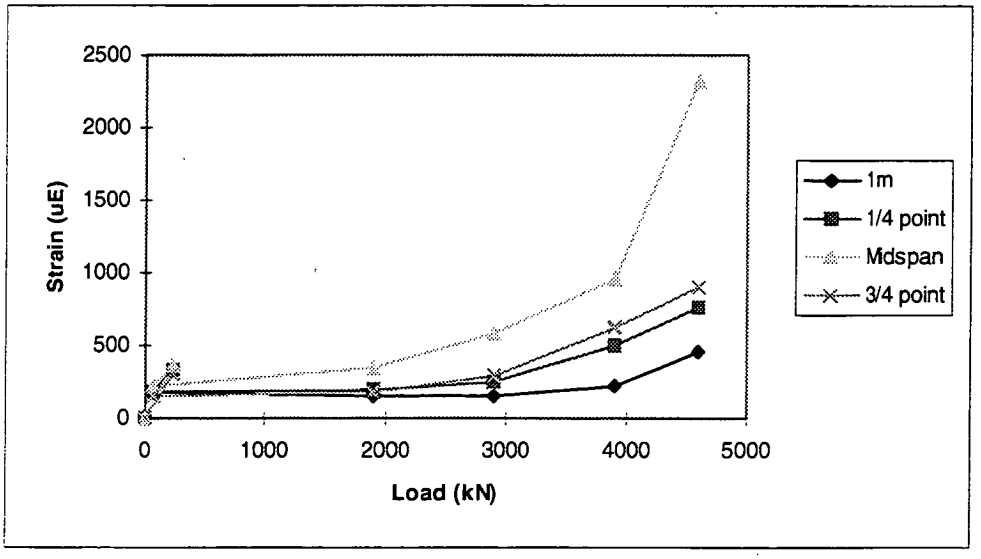

Figure 16.21 - Strain Distributions in Third Beam from Upstream

Comparisons of measured and calculated strains for a load of 1900 kN are detailed in Tables 16.26 and 16.27. The load of 1900 kN has been selected because it is likely to be within the region of elastic behaviour.

	D/s beam	5th beam	4th beam	3rd beam	2nd beam	U/s beam
Calculated	799	750	483	483	750	799
Measured	504	633	302	342	531	615

Table 16.26 - Comparison of Lateral Strain Distributions

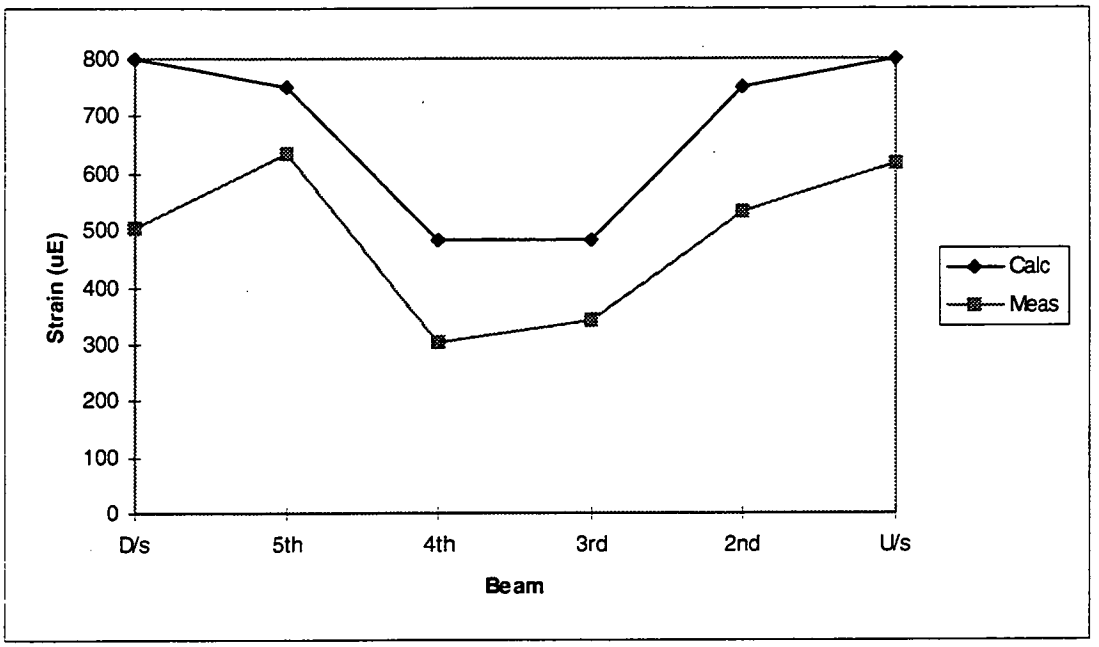

Figure 16.22 - Comparison of Lateral Strain Distributions

	1m from abutment	1/4 point	Midspan	3/4 point
Upstream beam				
- calculated				
- measured	99	176	615	219
3rd beam				
- calculated				
- measured	153	192	342	183

Table 16.27 - Comparison of Longitudinal Strain Distribution

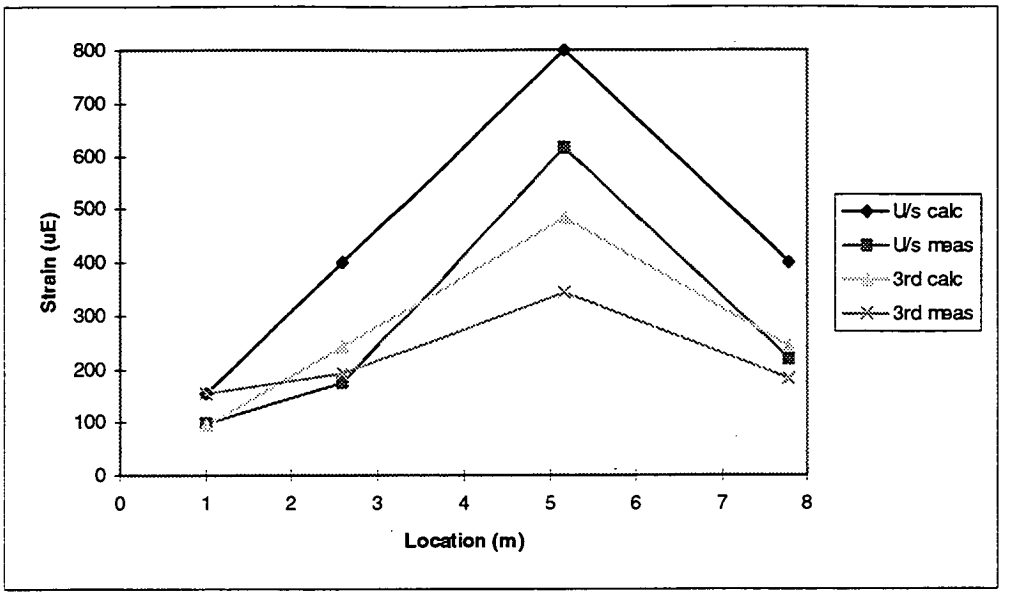

Figure 16.23 - Comparison of Longitudinal Strain Distribution

16.12 Discussion

Load distributions were calculated by grillage analysis and in accordance with the 1965 NAASRA Bridge Design Specification and compared with the measured behaviour of the bridge.

There was little difference in the grillage analysis results for an increasing fineness of mesh, between four and eight longitudinal divisions, and six divisions were used for subsequent analysis.

There was reasonable correlation between the measured load distributions and those predicted by the two methods, but strains were overestimated by analytical techniques for both working loads and those applied during the ultimate load testing.

The possibility of bearing rotational restraint causing the low strains was assessed by evaluating longitudinal strain distributions. These however showed that the bridge was behaving as a simply supported structure.

Darvall and Brown (1976) discuss the effects of arching action in beams producing a vertical component of compressive normal stress, thus reducing the principal tensile stress near a support and explaining why the critical section for shear is some distance from the support. As with the behaviour of the deck, arching effects may have had the effect of reducing the strains from those predicted by the structural analysis.

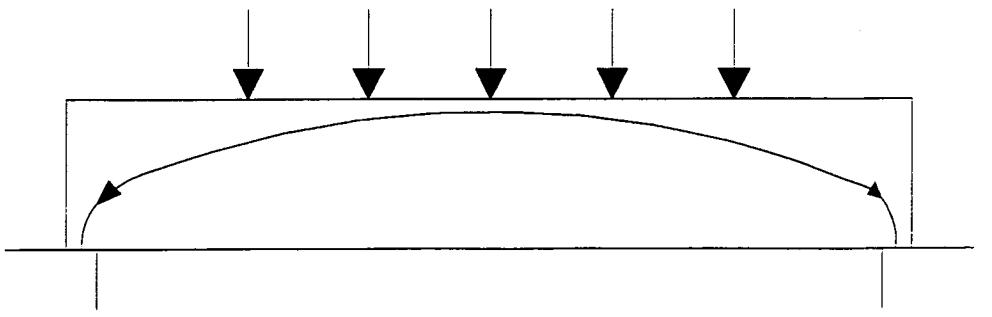

Figure 16.24 - Arching Action in Beams

17. PUNCHING SHEAR IN DECK

17.1 General

The bridge was loaded prior to the ultimate capacity test to assess the load-deflection response of a portion of the deck slab.

Extensive laboratory and field testing of deck slabs of slab-on-girder bridges in Ontario and New York has shown that the slabs possess far more strength than could be possible if transverse moments as predicted by conventional analyses did really exist.

The testing was intended to further validate the results of that testing.

17.2 Loading and Instrumentation

The bridge was loaded immediately prior to the ultimate load capacity test with a single hydraulic jack acting through a 400mm x 200mm universal beam and elastomeric pad placed transversely at midspan centrally between the second and third beams from upstream.

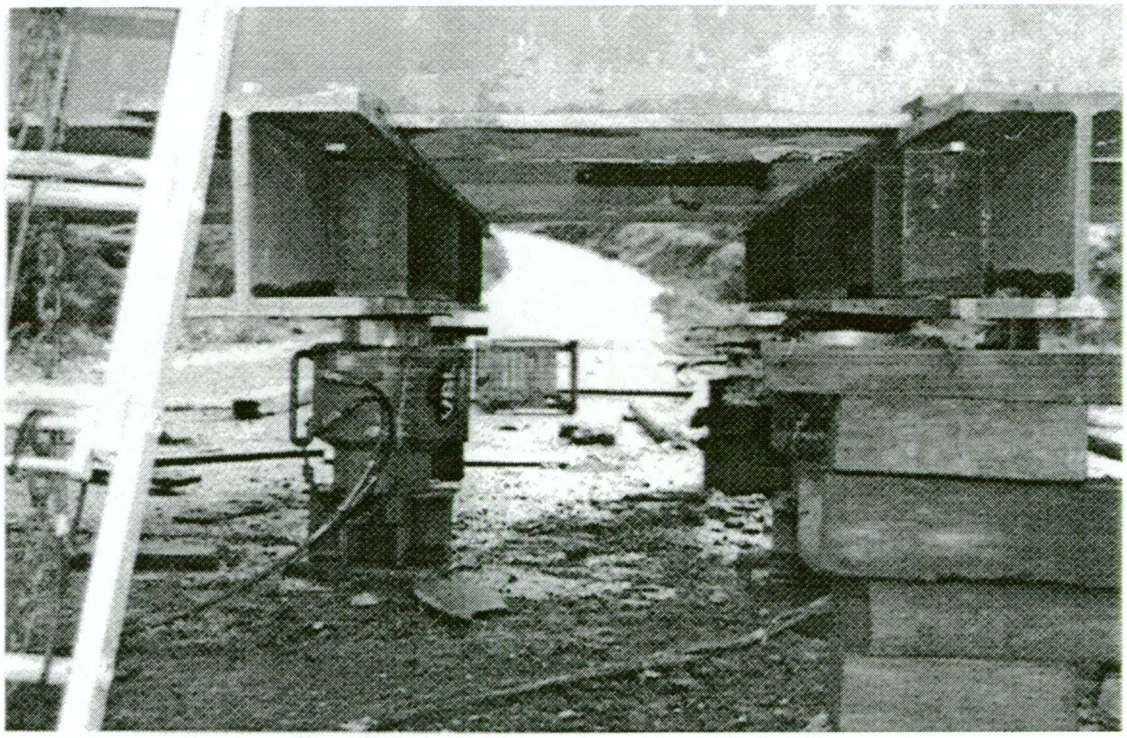

Figure 17.1 - Loading of Bridge

Relative deflection of the slab was measured with a linear variable displacement transducer supported on a steel angle fixed to the sides of the adjacent beams. The deflection of the third beam from upstream was measured with another displacement transducer supported on scaffolding.

Strains were measured with electrical resistance strain gauges connected to the ORION data logger and with CULWAY strain gauges fixed to a number of the beams.

17.3 Load-Deflection Response

The load-deflection response is detailed in Table 17.1 and Figure 17.2. Deflections were measured with the linear variable displacement transducers.

Jack Gauge (MPa)	Load (kN)	Slab Deflection (mm)	Beam Deflection (mm)	Remarks
0	0	0	0	
8	400	0.17	0.44	
12.5	630	0.32	0.92	
15	750	0.43	1.37	First cracks
19	950	0.64	1.93	
21	1050	0.79	2.38	
23	1150	0.81	3.21	
25	1250	0.97	3.67	Crack widths 0.2mm slab, 0.15mm beams
28	1400	1.47	4.43	
0	0	0.16	1.4	

Table 17.1 - Load-Deflection Response

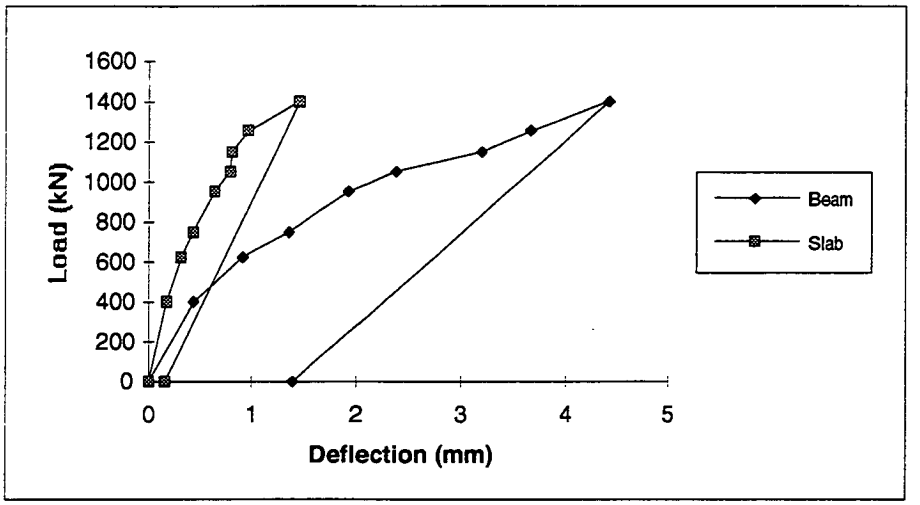

Figure 17.2 - Load-Deflection Response

The load-deflection response for the beams is detailed in Table 17.2. Deflections in this case were measured with the audio potentiometer displacement transducers, resulting in the differences from the measurements in the previous table.

Jack Gauge (MPa)	Load (kN)	Deflection (mm)					
		D/s beam	5th beam	4th beam	3rd beam	2nd beam	U/s beam
0	0	0	0	0	0	0	0
8	400	-0.04	0.00	-0.02	0.64	0.53	0.26
12.5	630	-0.10	0.05	0.31	1.51	1.39	0.88
15	750	-0.10	0.21	0.53	1.27	1.21	0.86
19	950	0.02	0.46	1.05	2.88	2.39	1.51
21	1050	-0.03	0.51	1.22	3.65	3.14	1.65
23	1150	0.04	0.69	1.50	4.30	3.85	2.34
25	1250	0.06	0.78	1.68	5.06	4.49	2.67
28	1400	0.10	1.01	2.07	6.27	5.74	3.38
0	0	-0.12	0.24	1.02	2.16	2.07	1.53

Table 17.2 - Beam Load-Deflection Response

17.4 Crack Development

The development of cracks in the deck soffit with the increasing loads is shown in Figures 17.3 to 17.9.

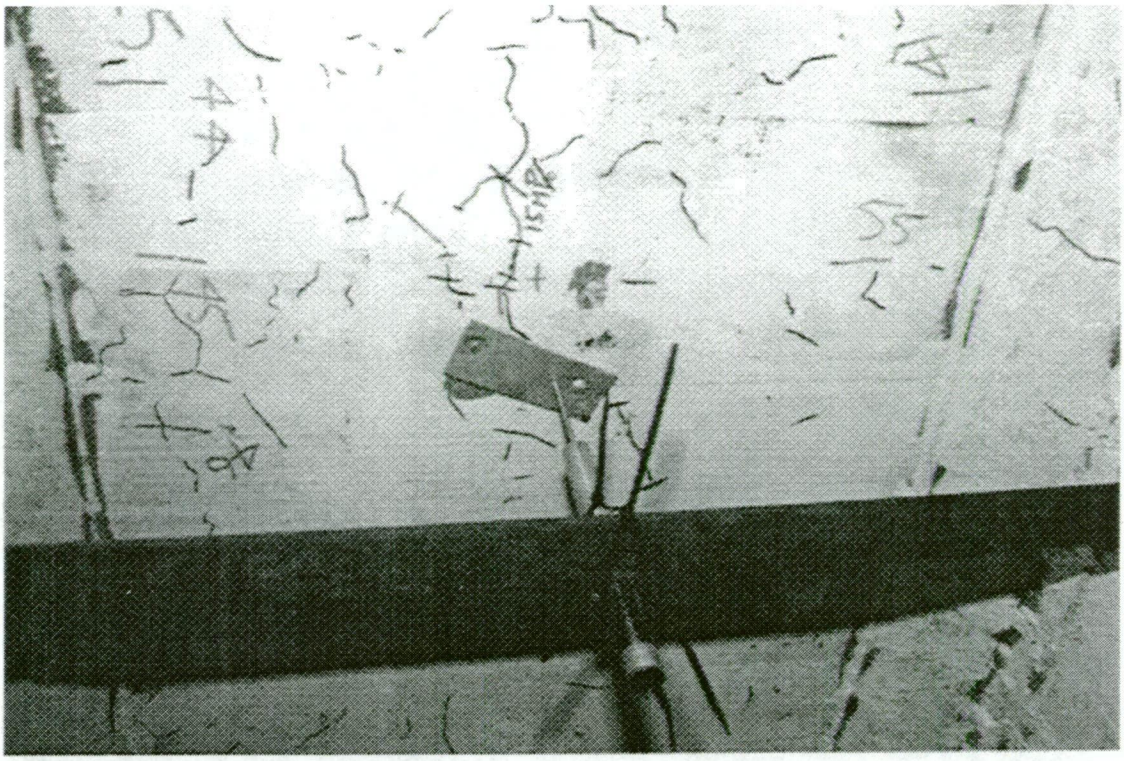

Figure 17.3 - Cracking at 750 kN Load

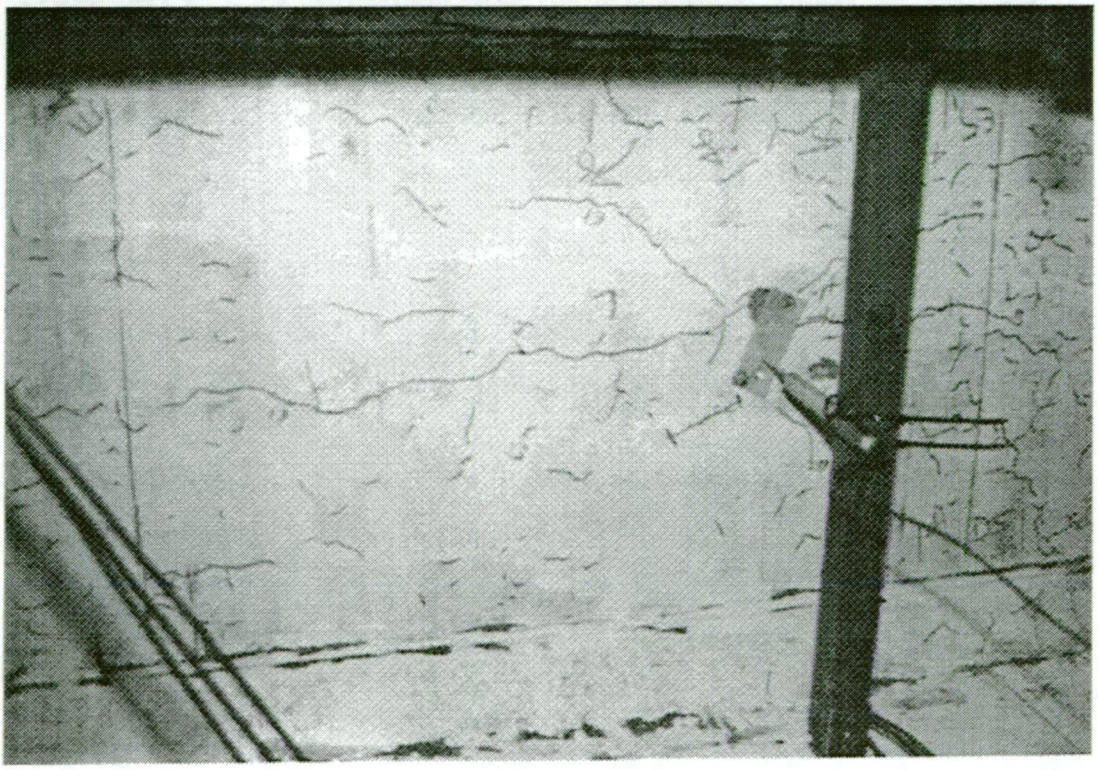

Figure 17.4 - Cracking at 950 kN Load

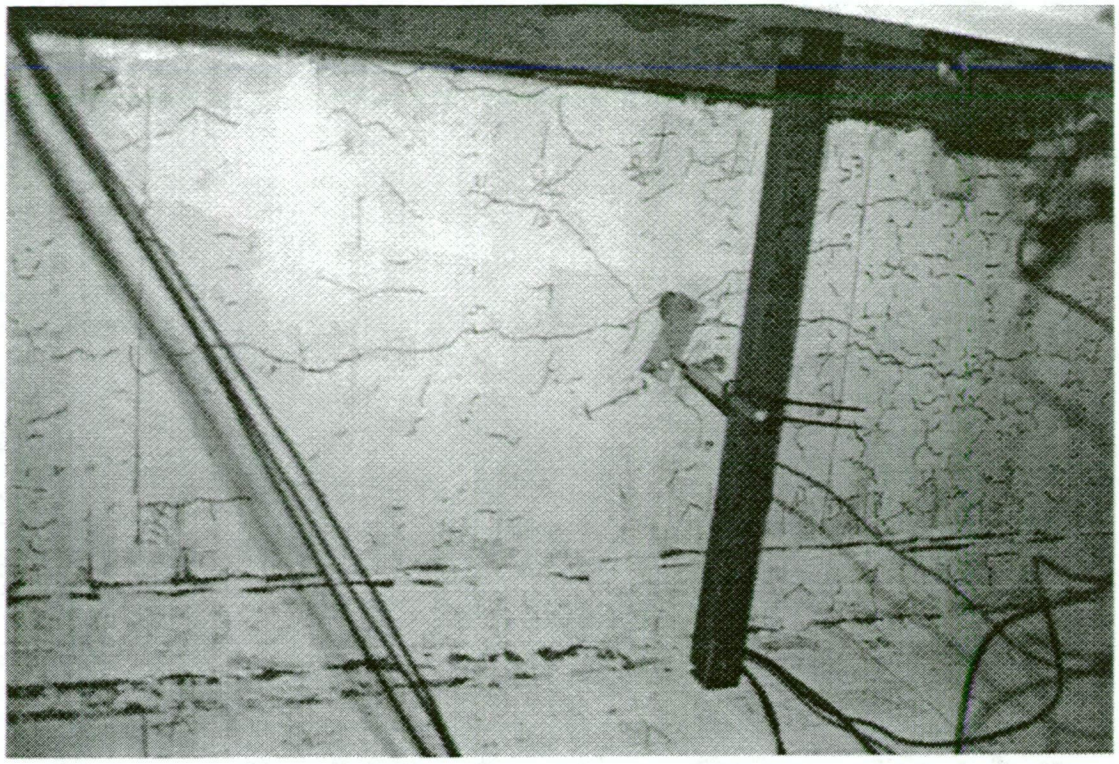

Figure 17.5 - Cracking at 1050 kN Load

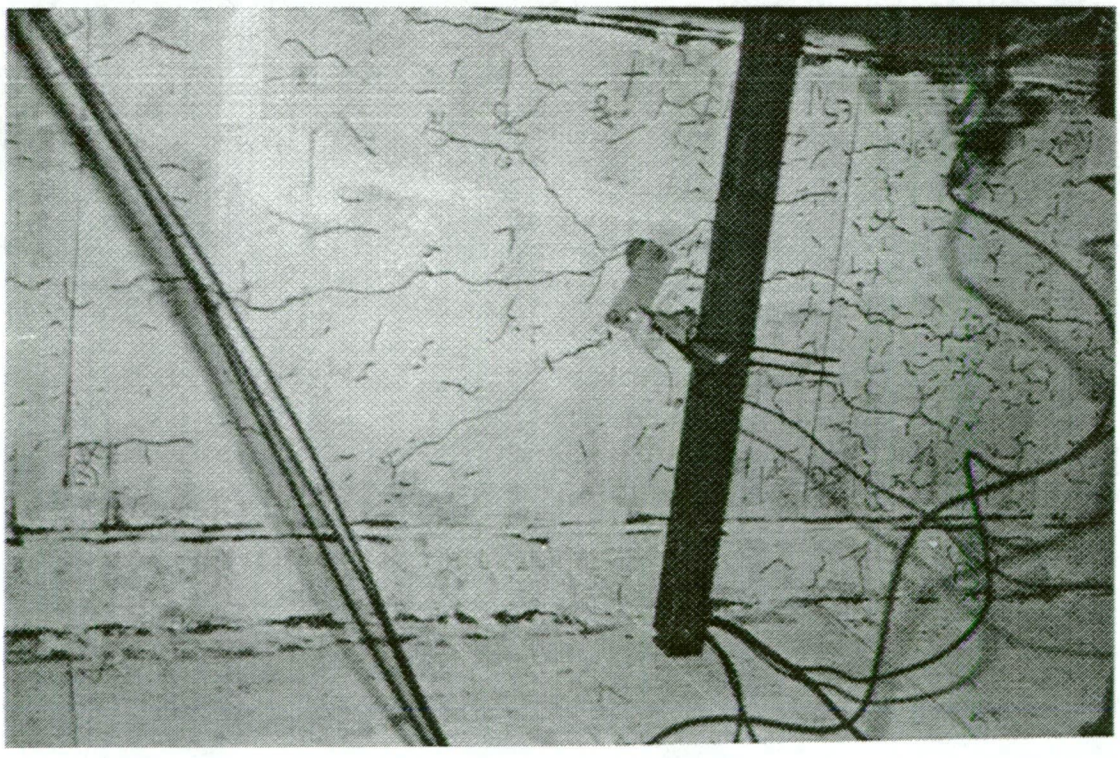

Figure 17.6 - Cracking at 1150 kN Load

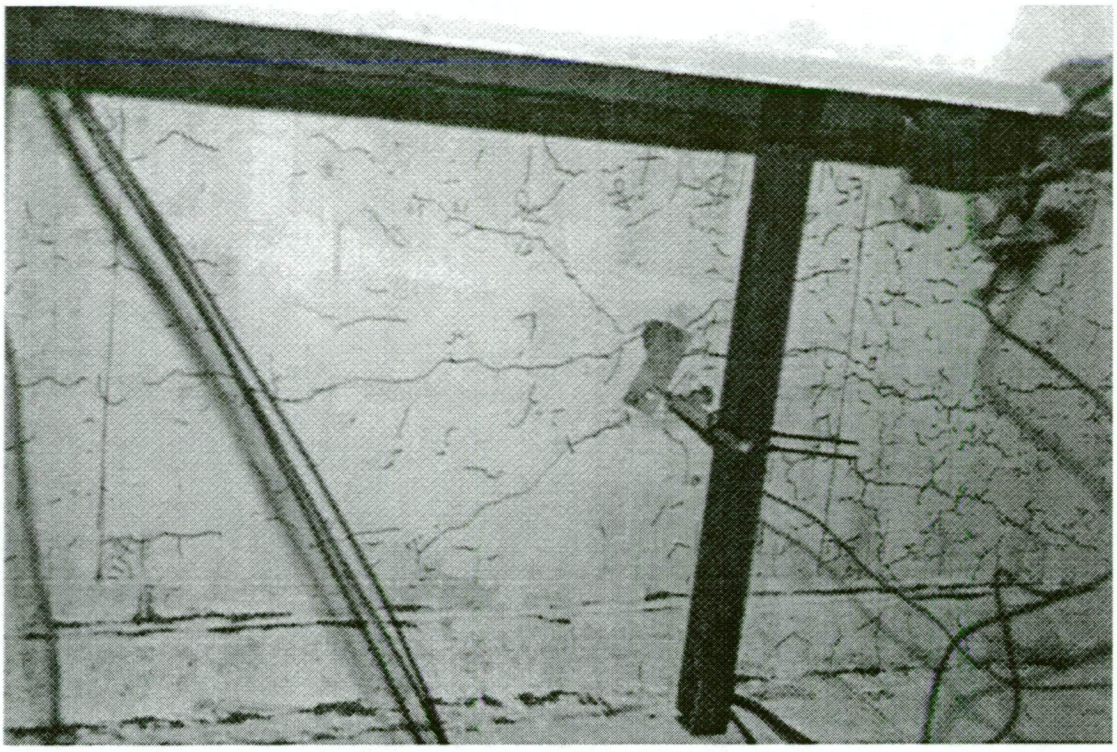

Figure 17.7 - Cracking at 1250 kN Load

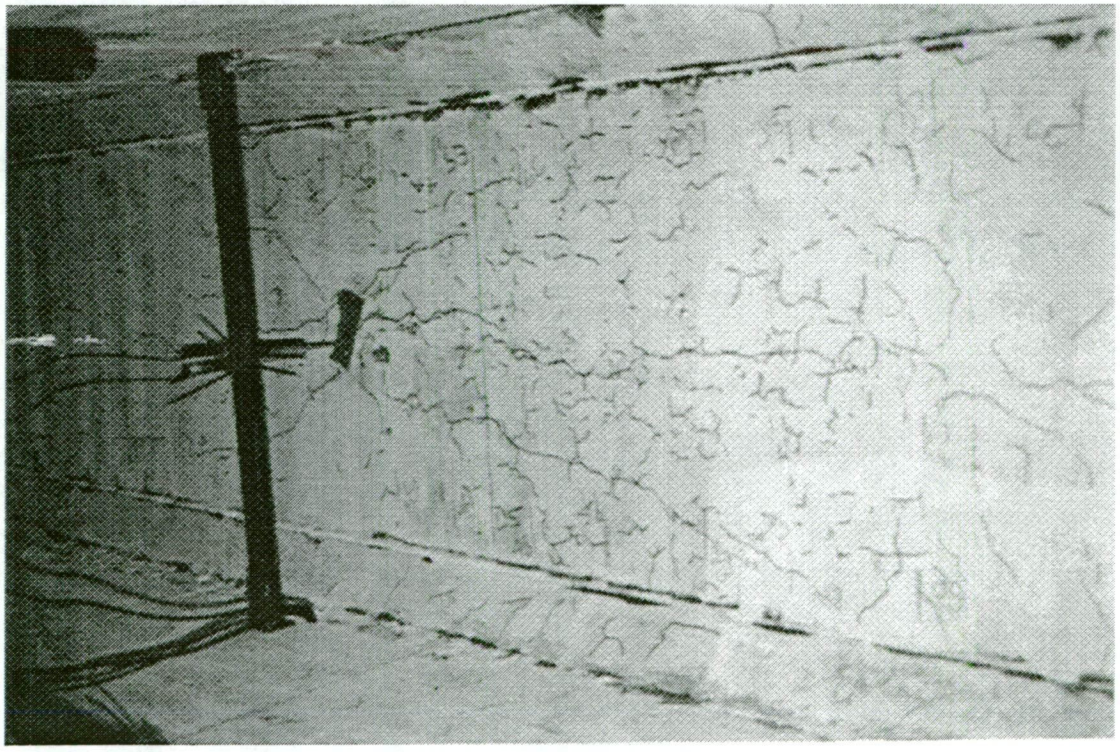

Figure 17.8 - Cracking at 1250 kN Load

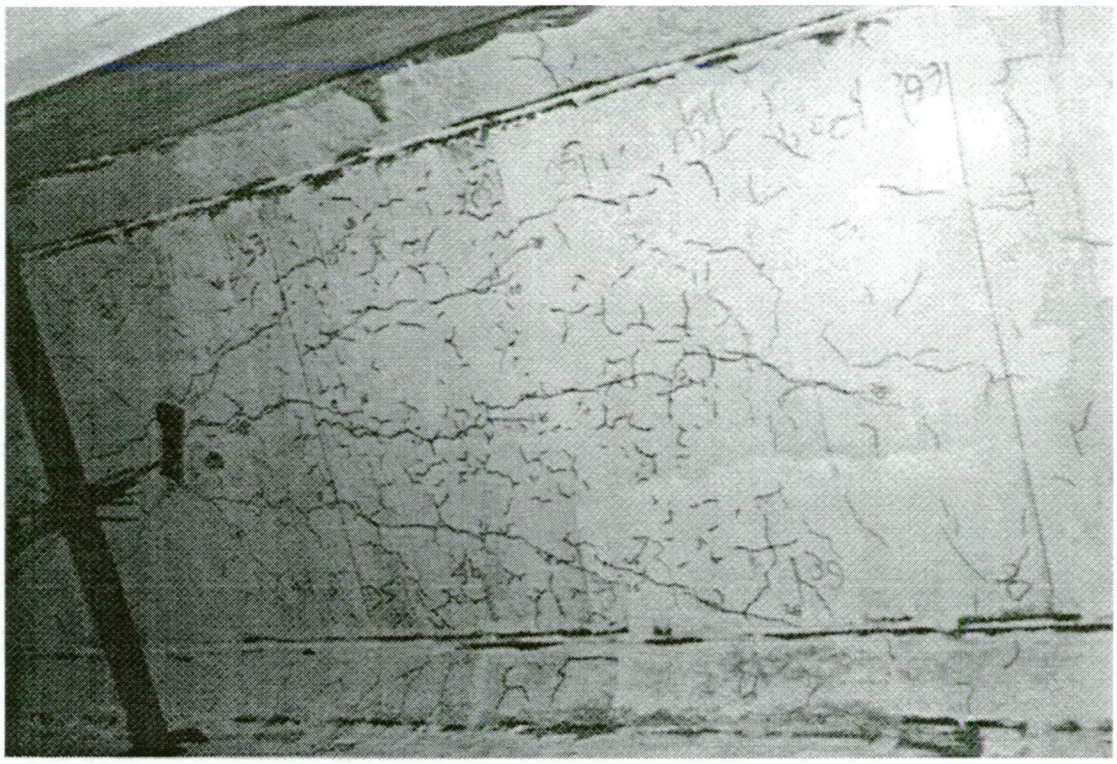

Figure 17.9 - Cracking at 1400 kN Load

17.5 Analysis in Accordance with 1976 NAASRA Bridge Design Specification

Main reinforcement is perpendicular to traffic, continuous over three or more supports and not cast monolithically.

S = 1219 - 381 + 381/2
= 1029 mm

Design bending moment per metre width,

M = 0.8(1.029 + 0.6) * P/10
= 0.130 P kNm/m

P = 70*1.3 (30% impact)
= 91 kN

M = 0.130 * 91
= 11.8 kNm/m

For the deck as designed with bottom transverse reinforcement of 5/8" at 6" centres, 7" deck, 1 1/4" cover,

A_{st} = $\pi(0.625*25.4)^2/4/(6*.0254)$
= 1299 mm^2/m

p = 1299/1000/((7-1.25-0.3125)*25.4)
= 0.0094
n = 6
k = 0.284
j = 0.905

For the design wheel load,

f_s = $11.8*1_{10}6/1299/.905/138$
= 72.8 MPa

f_c = $(72.8/6)*(0.284/0.716)$
= 4.8 MPa

Calculated crack width in accordance with the Bridge Design Specification is given by:

w_c = $Zc'f_w(D-kd)/E_s/(d_1-kd)$
Z = 3.8 for plain reinforcement
c′ = lesser of 85.9 and 138.5
= 85.9
f_w = 72.8 MPa
D = 177.8 mm
kd = 39.5 mm
E_s = 200 000 MPa
d_1 = d
= 138.1 mm
w_c = 0.16 mm

Calculated crack widths for the loads applied during the test are detailed in Table 17.3.

Load (kN)	M (kNm)	f_s (MPa)	f_c (MPa)	w_c (mm)
0	0	0	0	0
400	52	320	21.2	0.73
630	81.9	504	33.4	1.15
750	97.5	600	39.7	1.37
950	123.5	760	50.3	1.74
1050	136.5	840	55.6	1.92
1150	149.5	920	60.9	2.11
1250	162.5	1001	66.2	2.29
1400	182	1121	74.2	2.56

Table 17.3 - Calculated Crack Widths (Bridge Design Specification)

The calculated results compare with the observed crack development of first cracking at a load of 750 kN and crack widths of 0.2mm at a load of 1250 kN.

Estimated deflections are calculated using both gross and effective moments of inertia. For a 1m width of slab,

I_g = $1000*178^3/12$
= $468_{10}6$ mm^4/m

f_r = $0.60\sqrt{F'_c}$
= 3.55 MPa, for F'_c = 35 MPa

Cracked section properties, using transformed steel areas, are calculated below.

Part	A	y	Ay	$A(y-y_c)^2$	I_{self}
Concrete	39200	118.4	$4.64_{10}6$	$15.1_{10}6$	$5.0_{10}6$
Steel	7794	0	0	$76.0_{10}6$	-
Σ	**46986**		**$4.64_{10}6$**		**$5.0_{10}6$**

y_c = 98.8 mm

I_{xx} = $96.2_{10}6$ mm^4/m
= I_{cr}

y_t = 178/2
= 89 mm

M_{cr} = $(f_r I_g / y_t)*10^{-6}$
= 18.9 kNm/m

I_{eff} = $(M_{cr}/M_{max})^3 I_g + [1-(M_{cr}/M_{max})^3] I_{cr}$

For a simply supported beam with a point load,

M = PL/4
δ = $PL^3/48EI$
= $ML^2/12EI$

L = 1.029m

E = 33 GPa

Design moment = 0.130 P kNm/m

Calculated deflections based on gross and cracked sections and measured deflections are detailed in Table 17.4.

Load (kN)	I_{eff} (10^6mm^4)	Calculated deflections (mm)		Measured deflections (mm)
		Gross section	Cracked section	
0	-	0	0	0
400	114	0.30	1.22	0.17
630	101	0.47	2.17	0.32
750	99	0.56	2.64	0.43
950	98	0.71	3.39	0.64
1050	97	0.78	3.76	0.79
1150	97	0.85	4.12	0.81
1250	97	0.93	4.49	0.97
1400	97	1.04	5.03	1.47

Table 17.4 - Calculated and Measured Slab Deflections

Deflections are overestimated using both the gross and cracked section properties until the occurrence of cracking, when the gross section properties correspond reasonably closely. The slab deflections are significantly overestimated for all load conditions when cracked section properties are used.

The Bridge Design Specification provides for the calculation of shear capacities of slabs and footings in the vicinity of concentrated loads or reactions. While the provisions do not relate specifically to the punching shear capacity of the deck, assessments are made for comparative purposes.

d = 138 mm
b_0 = 2((400+138)+(200+138))
= 1752 mm
v = $V*10^3/b_0 d$

$= 0.004136V$ MPa

Allowable shear stress,

$v_{all} = 0.15\sqrt{F'_c}$

$= 0.89$ MPa, for $F'_c = 35$ MPa

V (kN)	v (MPa)
0	0.00
400	1.65
630	2.61
750	3.10
950	3.93
1050	4.34
1150	4.76
1250	5.17
1400	5.79

Table 17.5 - Calculated Punching Shear Stresses

Allowable punching shear stresses are exceeded at a load of 215 kN.

17.6 Other methods of analysis

Bakht and Jaeger (1985) provide charts for the ultimate strengths of concrete deck slabs. Slab properties are as follows:

f'_c = 35 MPa

q = percentage of tensile reinforcement at midspan

= 1299/178,000

= 0.73%

S = slab span (taken as beam spacing)

= 1219 mm

The charts in the book show an unfactored load resistance, R_n, of approximately 1500 kN for the deck slab which corresponds reasonably to the 1400 kN maximum applied load.

For the concrete deck slabs of slab-on-girder bridges, the Ontario code specifies a dynamic load allowance of 0.40, a performance factor ϕ of 0.5 and a load factor of 1.4. For a 70 kN wheel load, the required deck capacity is thus 274 kN; for an unfactored load resistance of 1500 kN, the permissible load would be 380 kN which is below the load at which cracking was first observed.

Long (1975) proposes the 'two-phase approach' to punching shear in slabs where, if the concrete fails in shear before the steel yields, the punching strength is given by:

$P_p = 4(c+d)d \times 0.42\sqrt{f'_c}\,(100\rho)^{0.25}$

c = length of loaded side

= 300 mm average

d = average effective depth to tensile reinforcement

= 138 mm

f'_c = 35 MPa

ρ = actual reinforcement ratio

= 0.0094

P_p = 592 kN

Kirkpatrick et al (1984) however note that the influence of the level of reinforcement on ultimate capacity in rigidly restrained slabs is small due to compressive membrane action. Brotchie and Holley (1971) have suggested that, for a slab with a span-to-depth ratio of 20, the effect of arching was equivalent in load capacity to approximately 2% of conventional reinforcement. The effect increased to an equivalent of 3% of conventional reinforcement with a span-to-depth ratio of 5. The span to depth ratio for the Princess River Bridge deck slab was 1029/178 = 5.8.

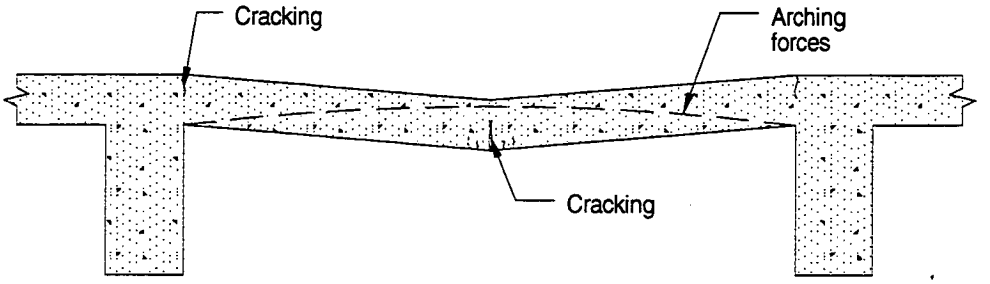

Figure 17.10 - Compressive Membrane Action in Laterally Restrained Slab

The arching effects are considered by using an effective reinforcement ratio which is calculated as follows:

ρ_e	=	effective reinforcement ratio
	=	$k f'_c h^2/(320 \times 0.75d^2)$
k	=	arching moment coefficient (obtained graphically)
	=	0.194
h	=	overall depth of section
	=	178 mm
L	=	slab span
	=	1029 mm
d	=	average effective depth to tensile reinforcement
	=	138 mm
ρ_e	=	0.0471

Substituting 0.0471 for 0.0094 in the earlier equation, predicted ultimate load capacity of slab is:

P_p = 885 kN

Even allowing for arching effects, the calculations still underestimate the capacity of the slab. The importance of compressive membrane action in slab behaviour was confirmed in subsequent work by Kirkpatrick et al (1986) involving tests on new bridge, where test panels were uncracked at service loads of 112.5 kN

17.7 Discussion

The initial and principal crack was longitudinal, with subsequent cracks being radial, indicating predominantly flexural behaviour. Even at the 1400 kN load, which is some 15 times the design loading, there was no evidence of a punching shear type failure.

Slab deflections are overestimated using both gross and cracked section properties until the load when the first cracks were observed. At higher loads, there is reasonable correlation between calculated and observed deflections using gross section properties, but deflections continue to be significantly overestimated using cracked section properties.

Allen (1991) makes the following points in his paper on cracking, serviceability and strength of concrete bridge decks:

1. 'Shrinkage cracking in bridge decks significantly affects the flexural behaviour of the deck.
2. The cracking strength of typical bridge decks is an important parameter in the performance of the deck.
3. Compression membrane action is a post-yield phenomenon.
4. Strength enhancement due to compression membrane action does not improve service behaviour.
5. Test results indicate that service loads may cause flexural cracking in the positive moment region of lightly reinforced isotropic decks.
6. The current AASHTO service-live-load design positive moment roughly corresponds to the cracking moment of typical bridge decks.
7. The maximum negative moment over the interior girders under service loads is much less than the cracking strength of the deck.
8. The measured reinforcing bar stresses in experimental isotropic decks do not correspond to observed cracking.
9. The field performance of isotropic bridge decks shows that reliance on the strength enhancement due to compression membrane action adversely affects the serviceability of these decks.
10. Field observations of isotropic decks show that they exhibit extensive longitudinal cracking in the positive moment region.
11. Cracking in the positive moment region of some isotropic decks has propagated through the deck.
12. Longitudinal cracking in the negative moment region above the girders was not observed in isotropic decks in the field.
13. Cracked behaviour of isotropically reinforced bridge decks validates the current AASHTO service-live-load design positive moment.
14. The orthotropic arrangement of reinforcing is more efficient than the isotropic pattern of reinforcing.
15. The most efficient reinforcing arrangement is a single-layer-bottom-only-orthotropic pattern designed for the positive moment specified by AASHTO.'

A number of observations are outside the scope of the Princess River Bridge testing, but the following observations are made with respect to Allen's points:

- shrinkage cracking in the bridge was of a random nature and unlikely to have affected structural behaviour
- strain measurements of slab reinforcing were not taken to permit an assessment of when compression membrane action began to occur
- flexural cracking from service loads was not observed in the deck
- reflective cracking in the deck surfacing, resulting from cracking in the negative moment regions of the slab, was not observed indicating that negative moments were less than the cracking strength of the deck.

Rankin et al (1991) and Kuang (1991) report on the testing of rectangular restrained reinforced concrete slabs, and use yield line methods for the theoretical assessment of capacities. Both found increased slab capacity due to compressive membrane action, with Rankin et al obtaining better correlation with theoretical capacities; both parties found theoretical assessments to be conservative.

17.8 Summary

Testing of the bridge deck to simulate a wheel load midway between the beams was undertaken to provide further confirmation of the high capacities observed by other researchers.

The deck was loaded to 1400 kN, compared with the design wheel load of 91 kN including dynamic allowances. While significant cracking developed, the maximum observed crack width was 0.2mm. Load and deflection measurements show that the steel in the beams in

fact yielded without failure of the deck slab. Using an allowable steel tensile stress of 125 MPa or an allowable crack width of 0.25mm, the permissible load by the Bridge Design Specification is 156 kN or 142 kN.

The testing confirmed the substantial capacities in bridge decks likely to result from compressive membrane action for short term loadings. Creep effects would be expected to reduce the effect for sustained loadings.

18. ULTIMATE LOAD CAPACITY

18.1 General

Ultimate load testing was undertaken to assess the behaviour of the structure at high loads and to examine whether ultimate behaviour was brittle or ductile.

With vehicle loadings increasing historically at about 10% per annum, overloaded vehicles weighing considerably in excess of legal load limits travelling on Australian roads, and an ageing asset, ductile behaviour is required to avoid catastrophic collapse.

18.2 Loading

The bridge was loaded over the exterior pairs of beams at midspan of the Hobart span using hydraulic jacks, loading beams and ground anchors, as described in the chapter on loading. Hydraulic jacks were connected in pairs, resulting in the same loads in both of the upstream jacks and in both of the downstream jacks.

18.3 Bridge Responses

The measured load-deflection response is detailed in Table 18.1 and shown in Figure 18.1. The residual load at zero jack gauge reading results from the crane at the site being used to lift the loading apparatus against the ground anchors with a slight residual load.

Jack Gauge (MPa)	Total Load (kN)	Deflection (mm)					
		D/s beam	5th beam	4th beam	3rd beam	2nd beam	U/s beam
Prior	0	0	0	0	0	0	0
Nose	230	-0.26	0.14	0.04	0.03	-0.28	0.13
0	60	0.37	0.92	0.77	0.38	0.50	0.93
10	2010	3.86	4.19	3.49	2.76	3.47	4.24
15	3010	8.10	8.85	7.26	7.50	8.63	9.62
Nose	230	1.34	1.32	1.05	1.38	1.38	2.10
15	3010	9.63	9.63	7.47	7.50	9.02	10.03
20	4010	9.46	10.39	15.50	13.76	15.65	16.78
23/24	4710	35.67	11.30	34.75	35.32	36.41	36.72

Table 18.1 - Load-Deflection Response

Total Load (kN)	Remarks
1200	No flexural cracking
2010	Crack widths up to 0.1mm
4010	Crack widths u/s beam to d/s beam - 6mm, 1mm, 0.25mm, 0.2mm, 0.9mm, 0.9mm
4710	Crack with u/s beam 12mm; spalling starting at abutment
4800	Maximum load - deflections increasing

Table 18.2 - Features of Bridge Behaviour

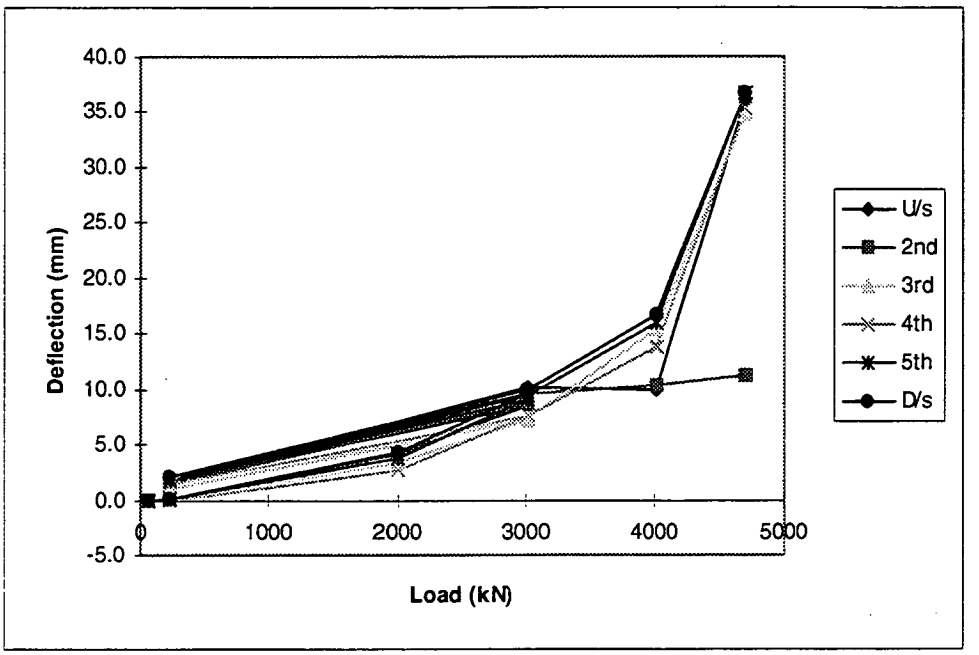

Figure 18.1 - Load-Deflection Response for Individual Beams

The responses parallel each other and it is thus reasonable to plot the average response. It is shown in Figure 18.3.

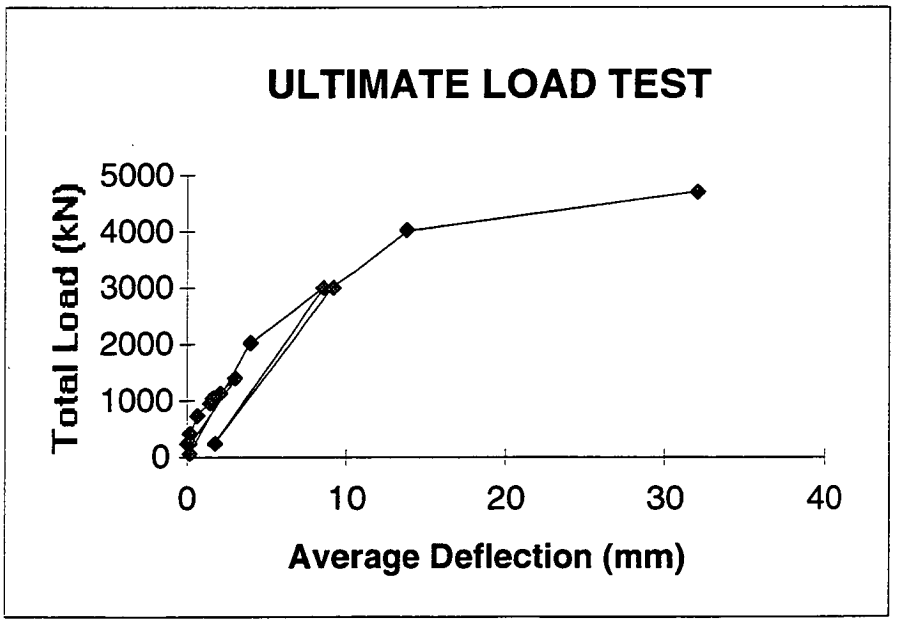

Figure 18.3 - Average Load-Deflection Response

The load-deflection response indicates that yield occurred at a load of approximately 2000 kN, although the actual load is uncertain and may have been affected by the testing for punching shear. In retrospect, it would have been useful to have used smaller increments in the loading. The ability to take those additional measurements was however influenced by the weather at the time of the testing and the ability to maintain loadings and reliably assess gauge readings for smaller increments.

Load (kN)	Midspan strain (uε)					
	U/s	2nd	3rd	4th	5th	D/s
230	256	149	234	239	245	237
60	0	0	0	0	0	0
230	172	161	151	153	159	162
2000	429	328	129	143	479	340
3010	1443	682	369	489	908	838
230	655	11	-30	59	77	139
3010	1931	685	357	479	911	836
4010	8981	1309	752	867	8784	4925
4710	-	12366	2107	16842	14725	-
Ultimate	-	11559	1826	17798	16553	-

Table 18.3 - Load-Strain Responses

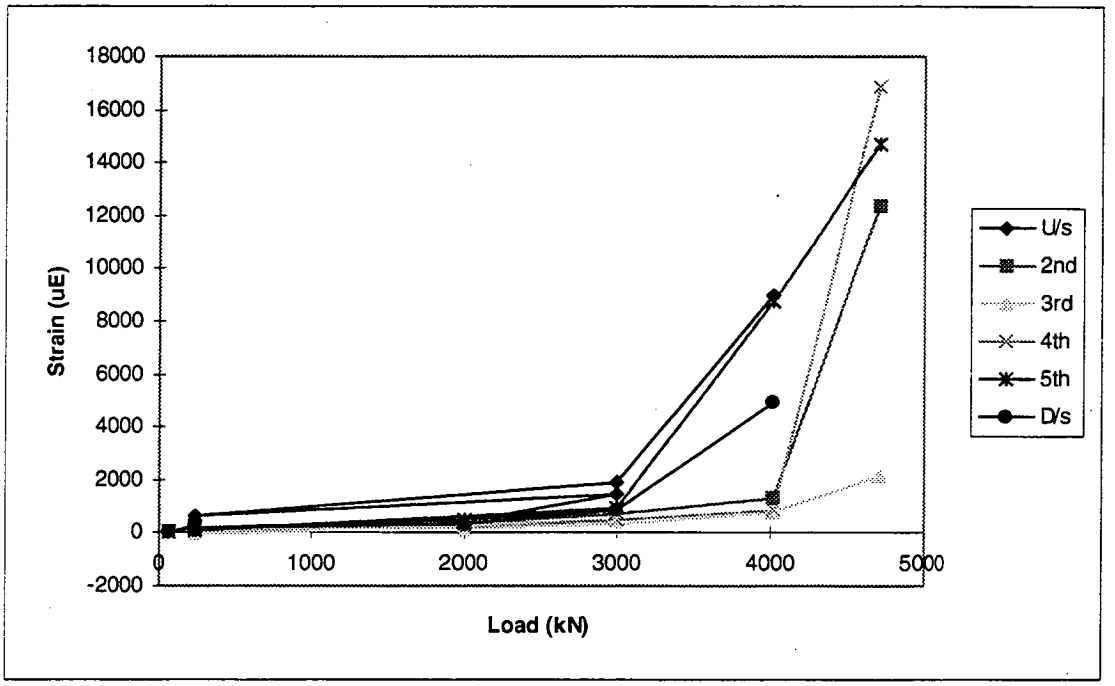

Figure 18.4 - Load-Strain Response

The strain response indicates yield at a load of approximately 3000 kN.

18.4 Bridge Behaviour

Photographs on various aspects of the bridge at ultimate load are shown in the following photographs.

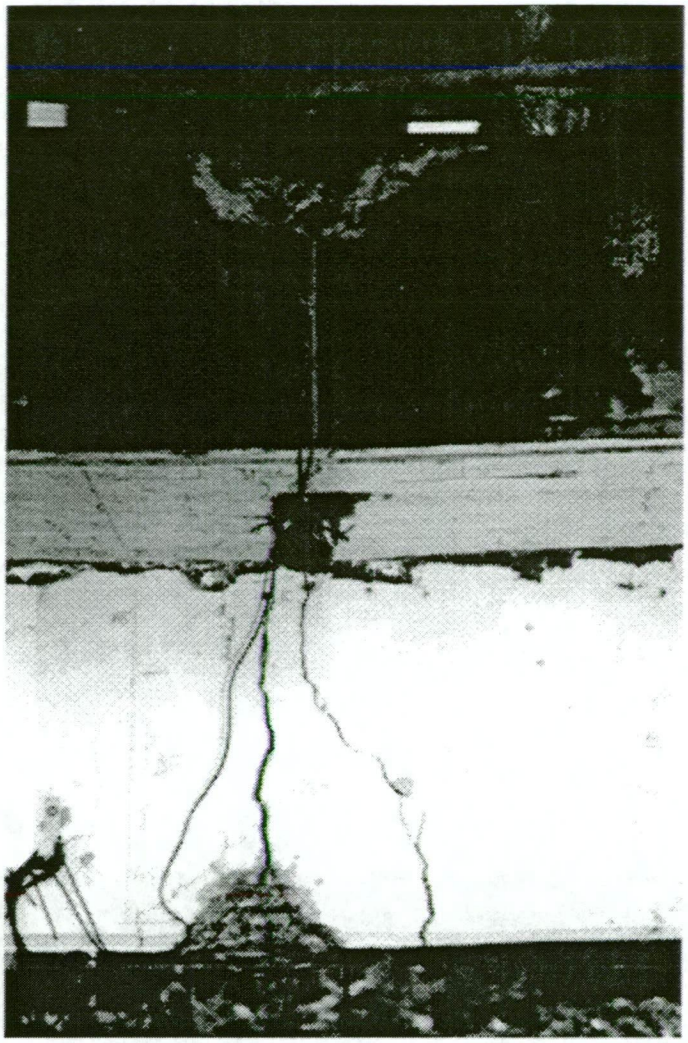

Figure 18.5 - Cracking of Upstream Beam at Ultimate Load

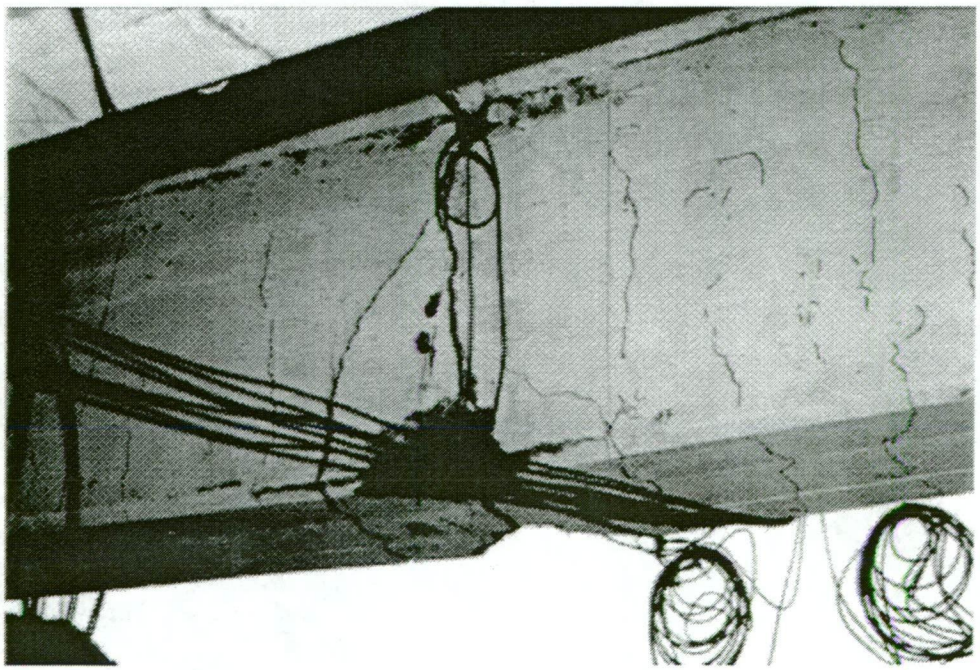

Figure 18.6 - Cracking of Upstream Beam at Ultimate Load

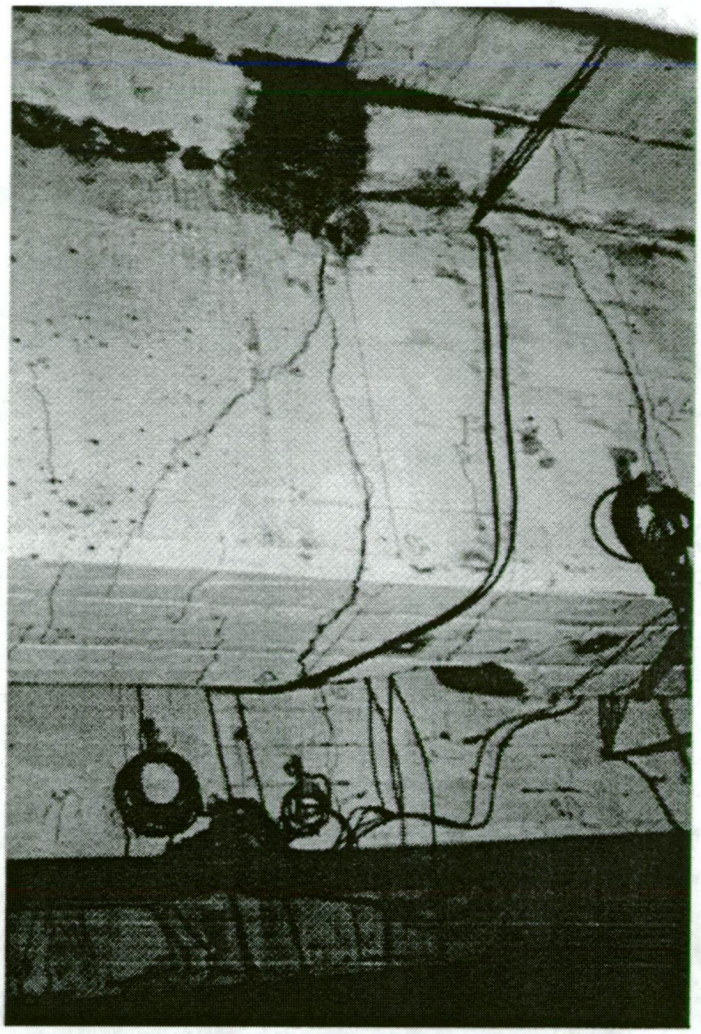

Figure 18.7 - Cracking of Second Beam at Ultimate Load

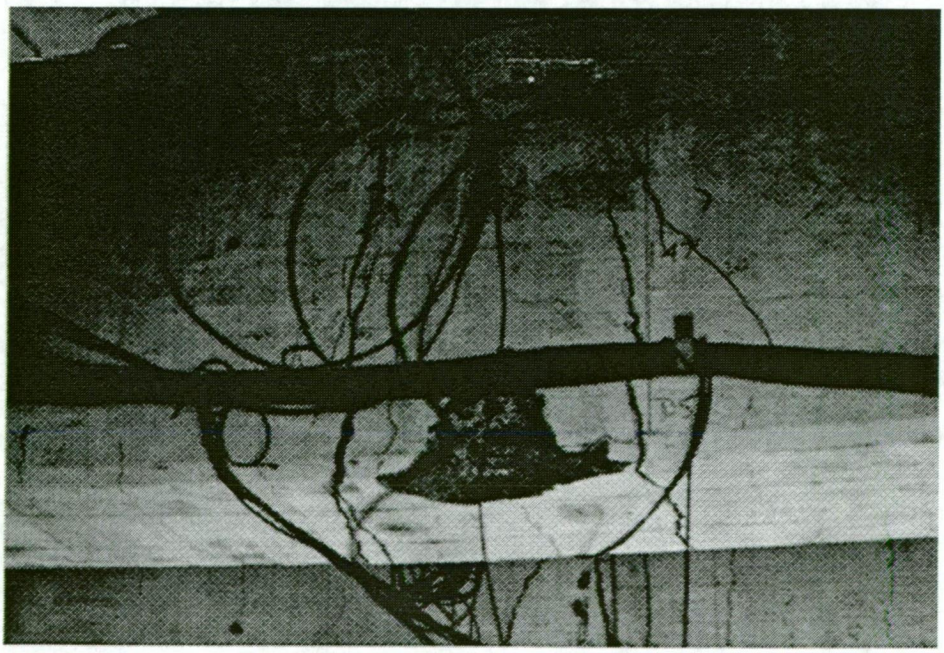

Figure 18.8 - Cracking of Second Beam at Ultimate Load

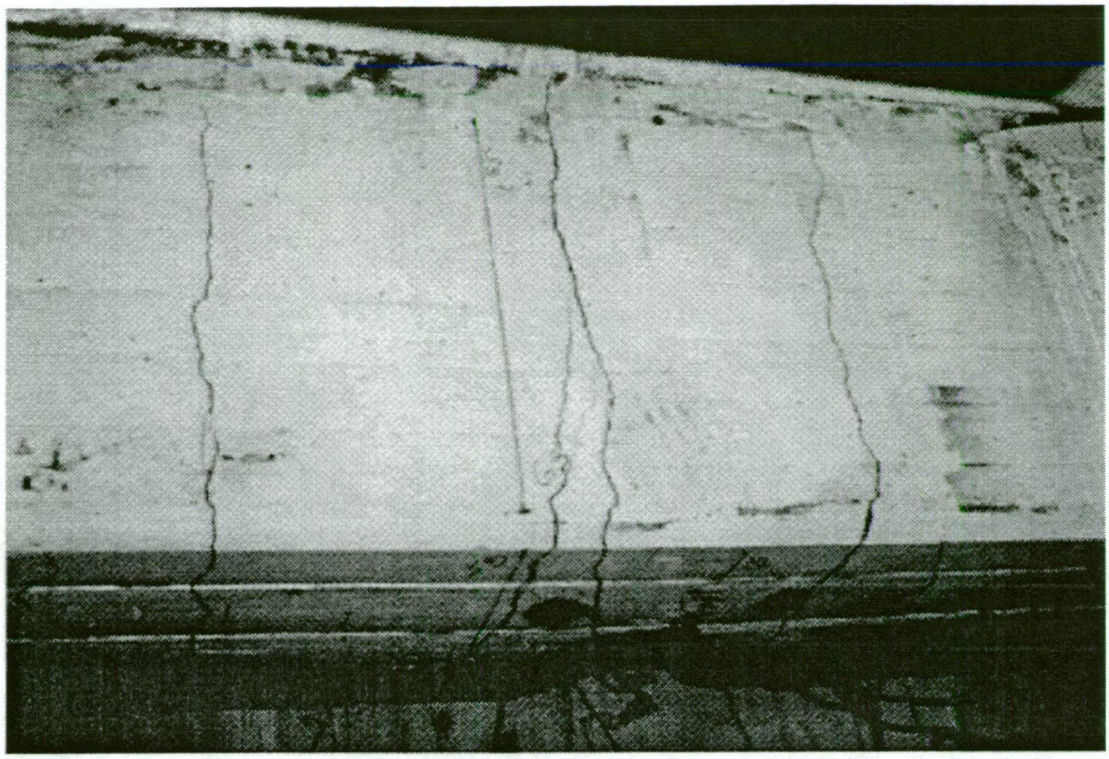

Figure 18.9 - Cracking of Third Beam at Ultimate Load

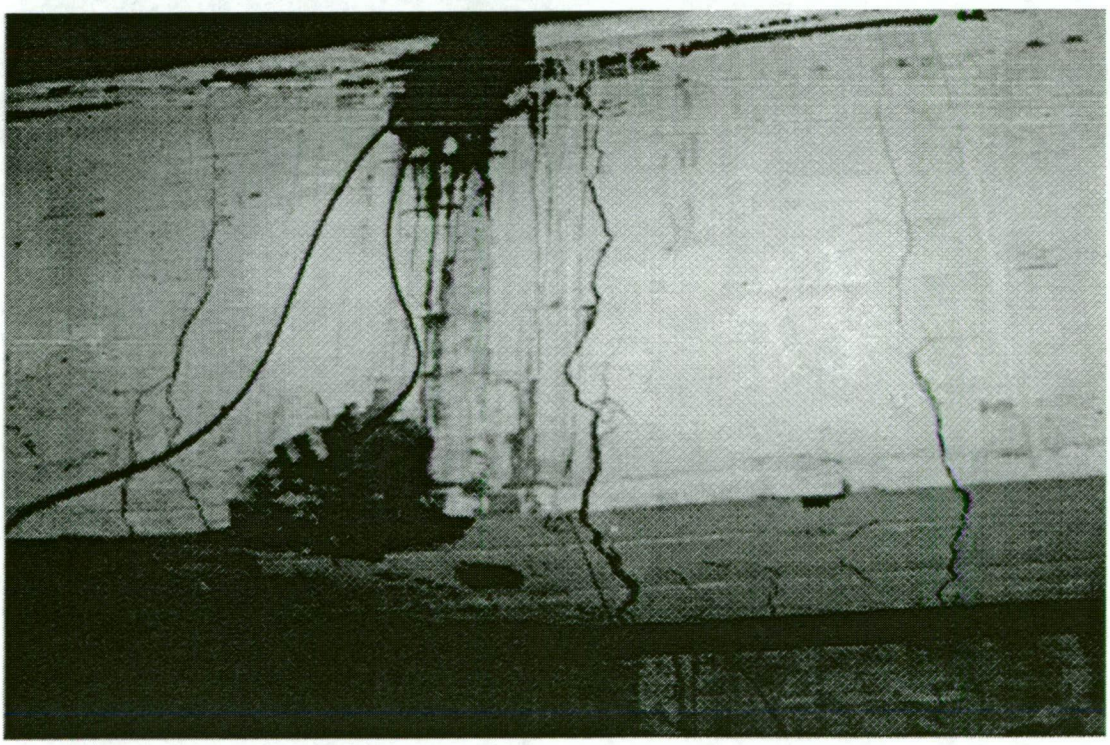

Figure 18.10 - Cracking of Third Beam at Ultimate Load

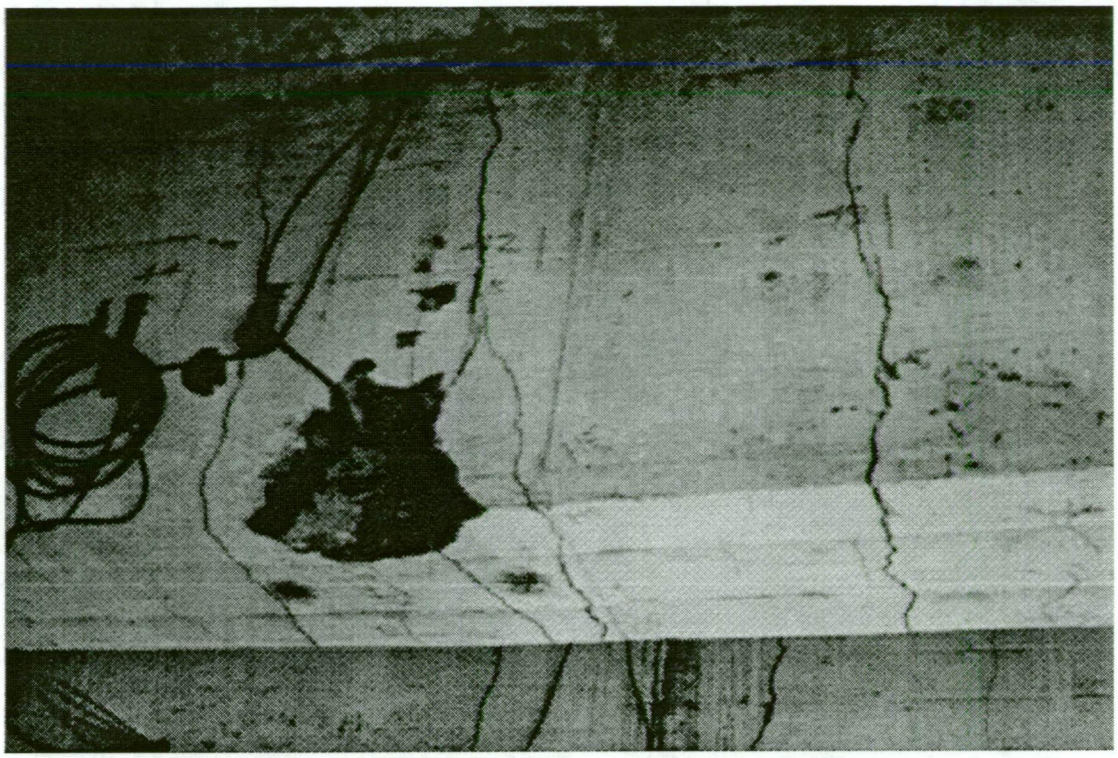

Figure 18.11 - Cracking of Fourth Beam at Ultimate Load

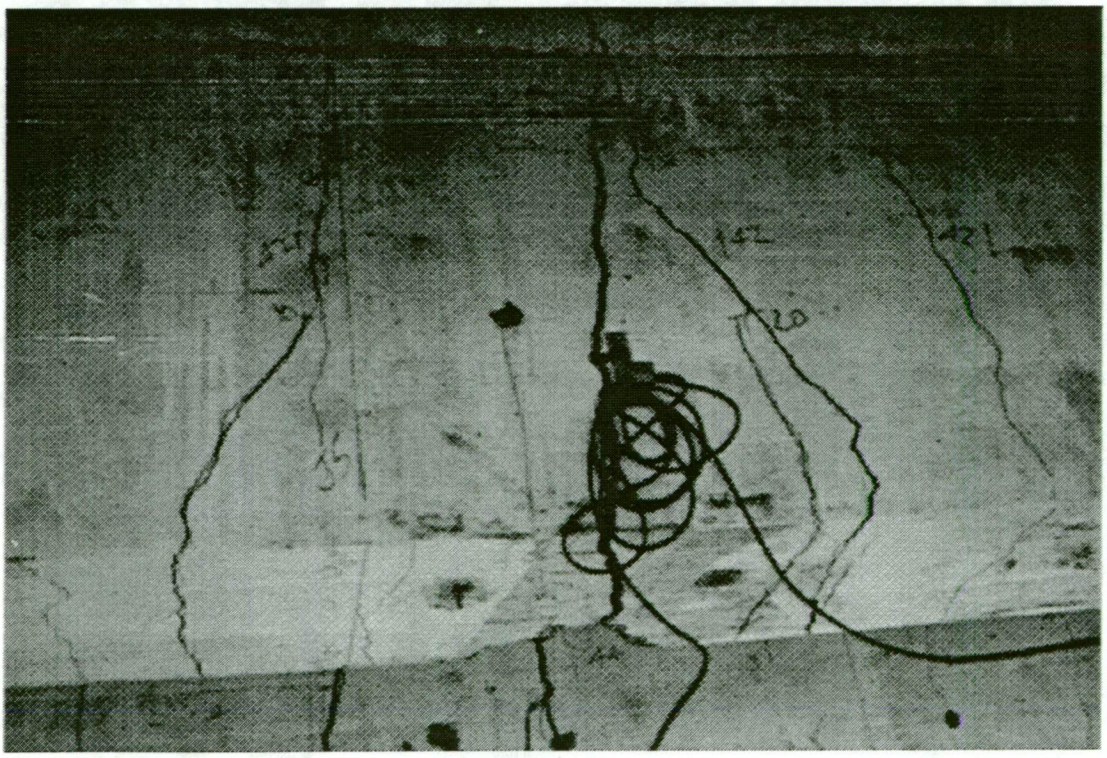

Figure 18.12 - Cracking of Fifth Beam at Ultimate Load

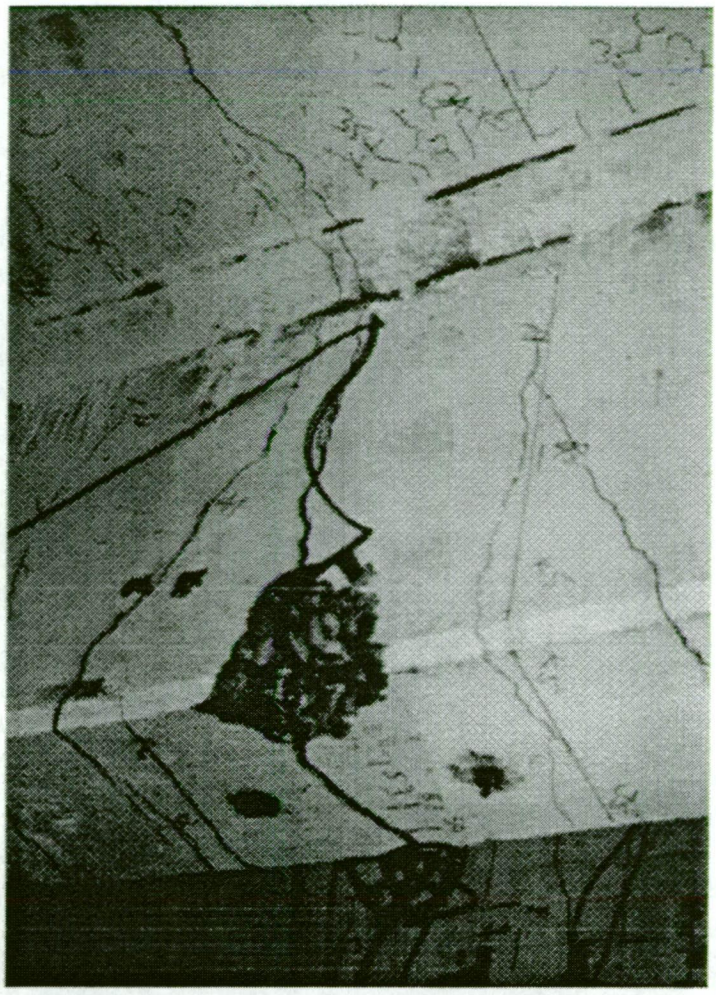

Figure 18.13 - Cracking of Fifth Beam at Ultimate Load

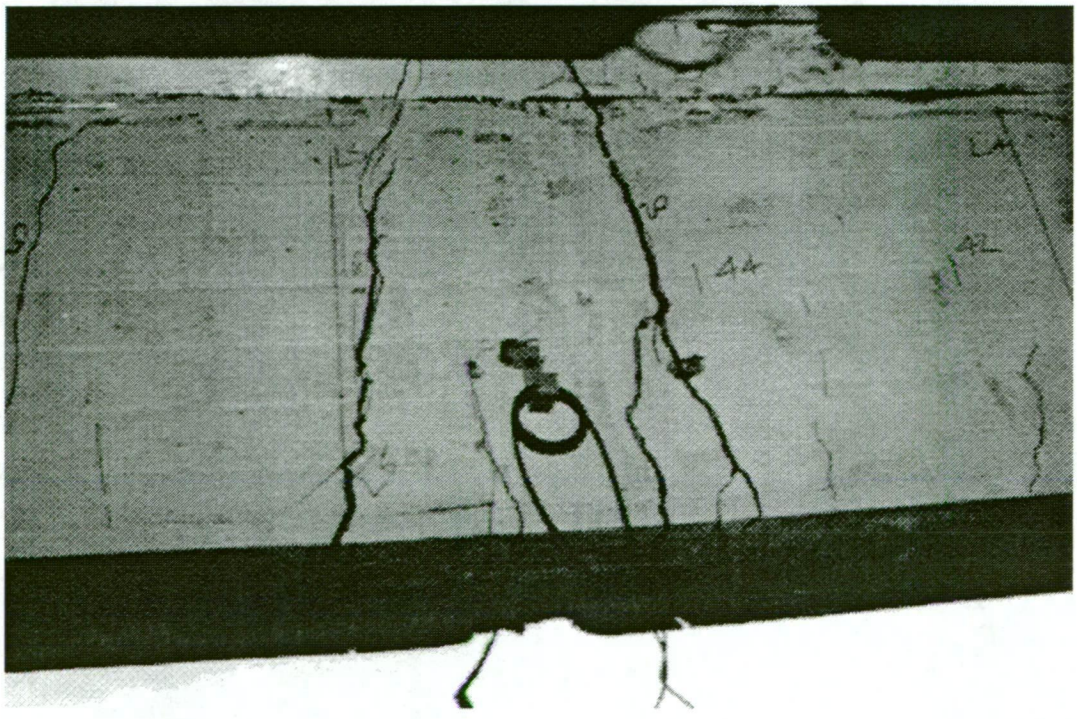

Figure 18.14 - Cracking of Downstream Beam at Ultimate Load

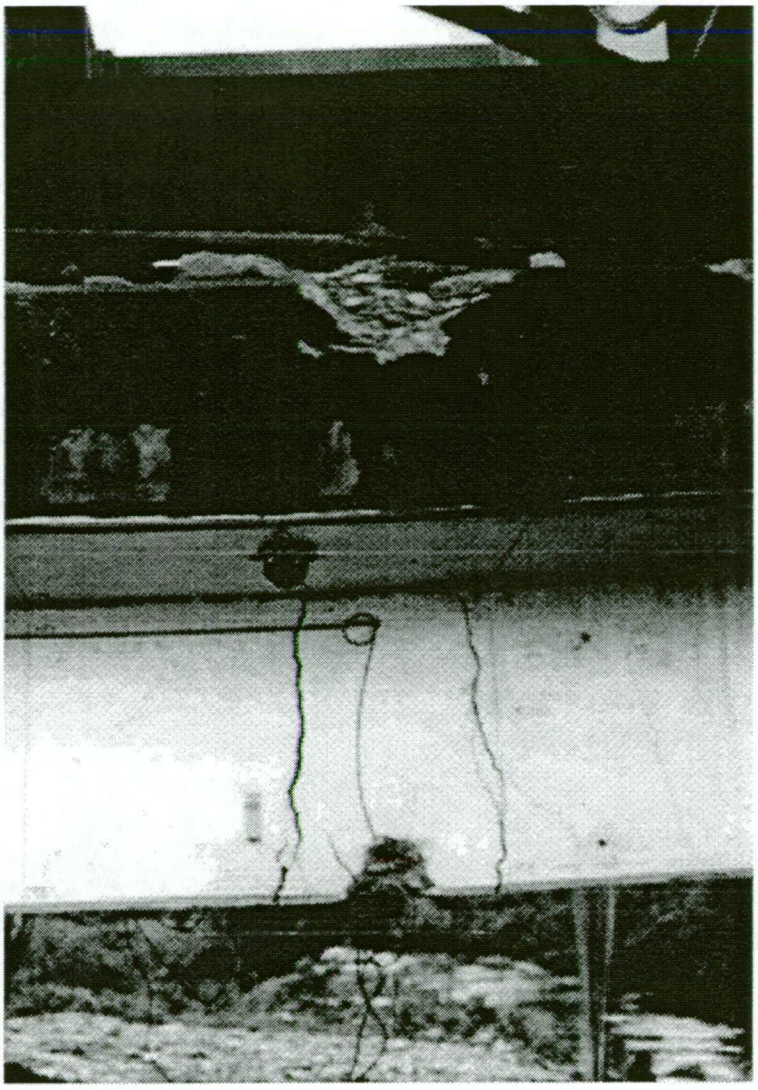

Figure 18.15 - Cracking of Downstream Beam and Crushing of Deck at Ultimate Load

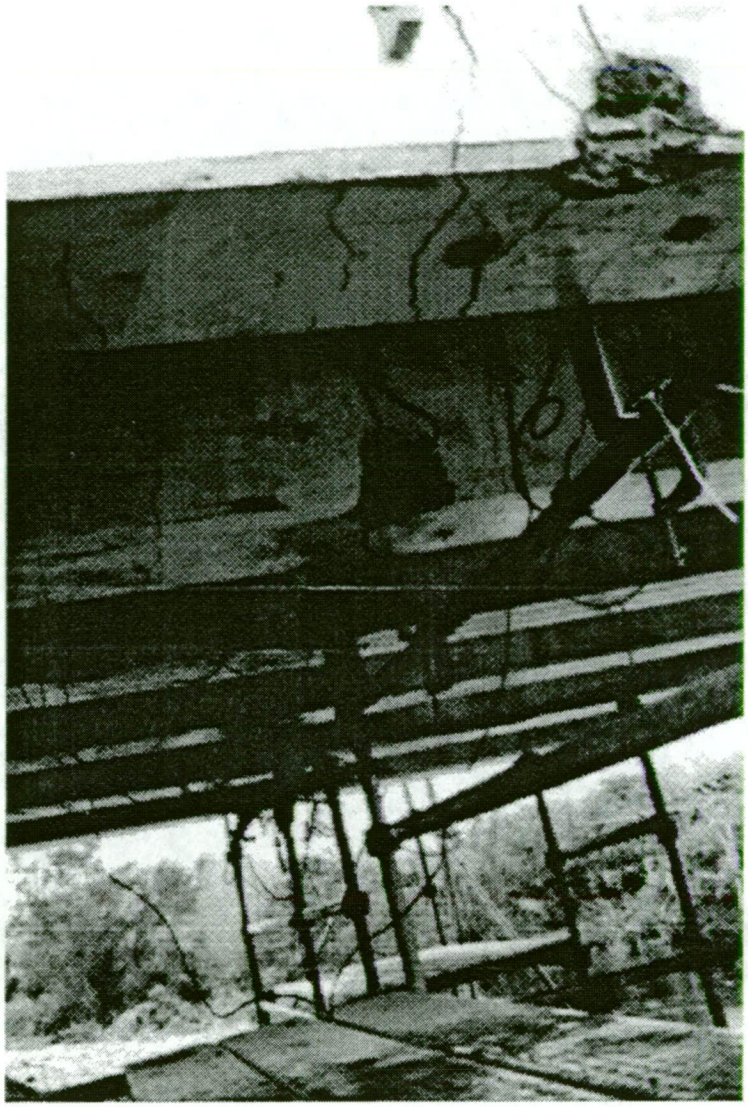

Figure 18.16 - Underside of Superstructure at Ultimate Load

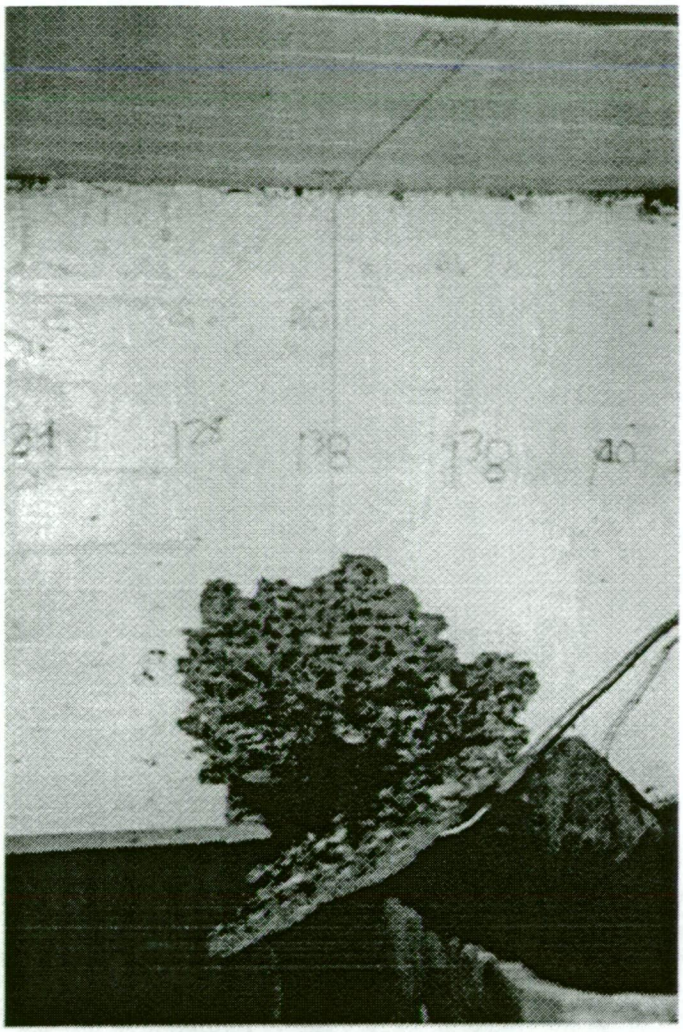

Figure 18.17 - Spalling of Beam at Abutment at Ultimate Load

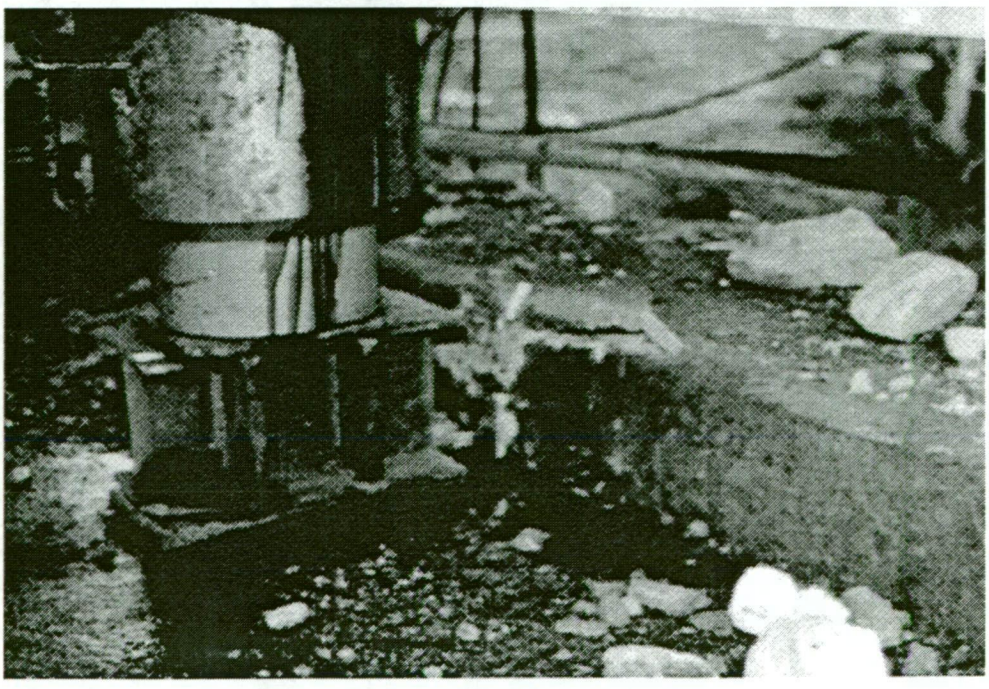

Figure 18.18 - Kerb Crushing at Ultimate Load

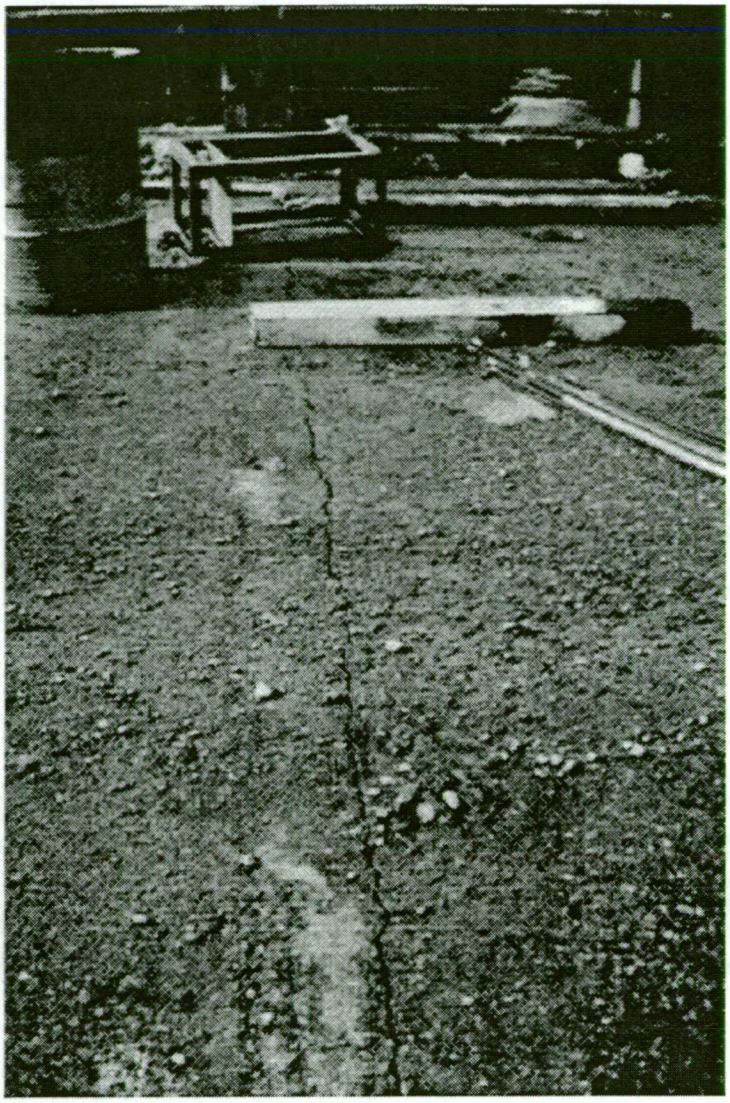

Figure 18.19 - Cracking of Deck Surfacing over Pier at Ultimate Load

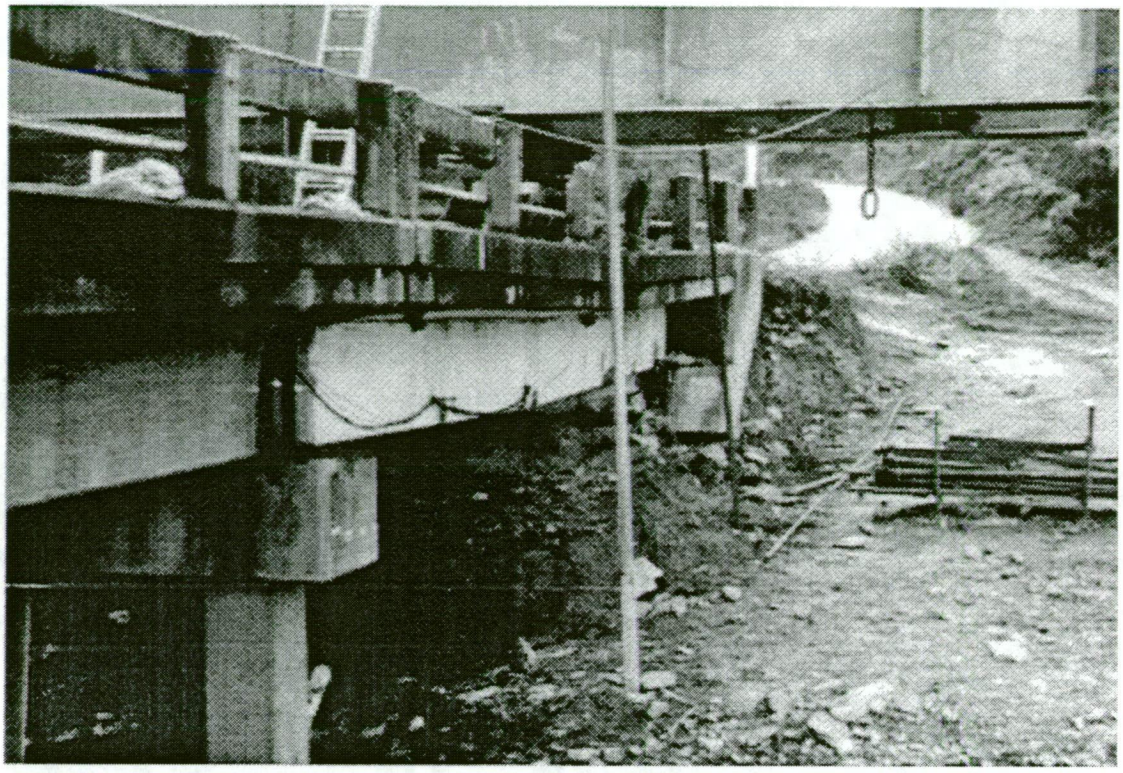

Figure 18.20 - Upstream Side of Bridge at Ultimate Load

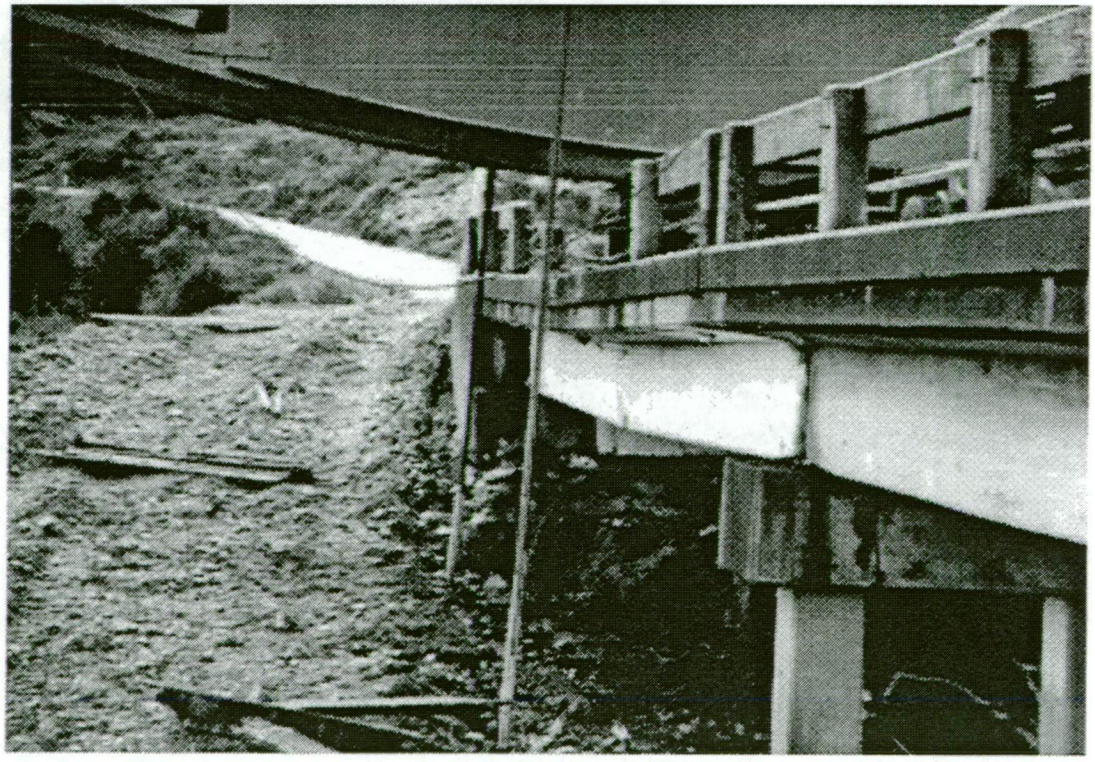

Figure 18.21 - Downstream Side of Bridge at Ultimate Load

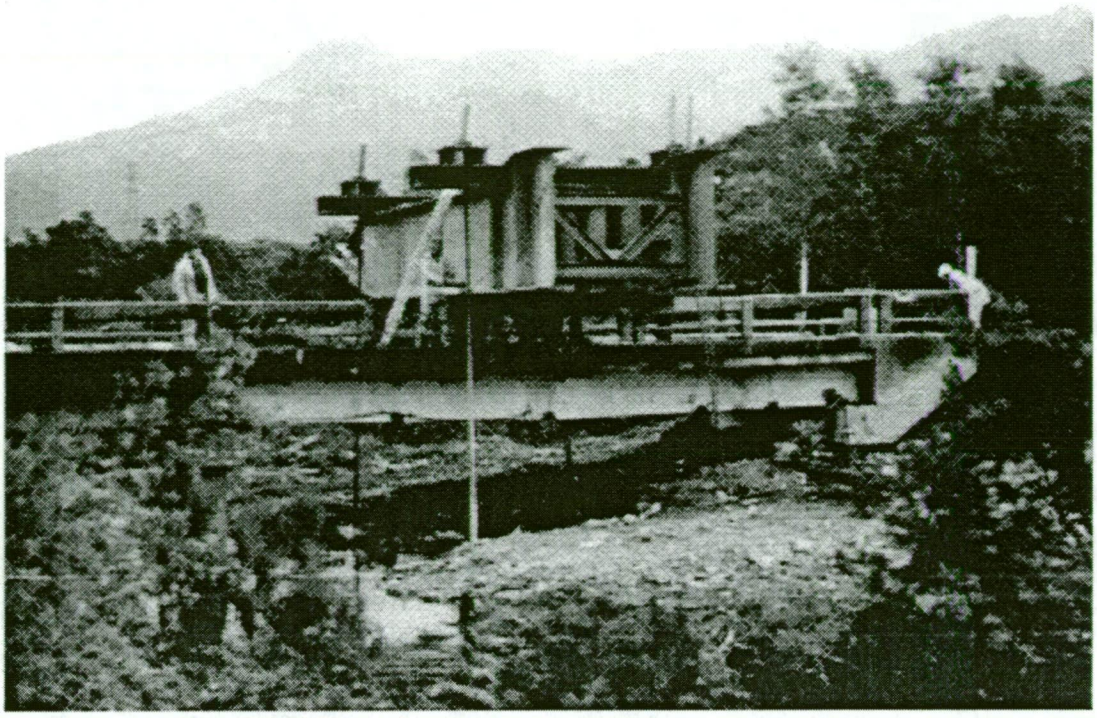

Figure 18.22 - General View of Bridge at Ultimate Load

18.5 Theoretical Capacity at Yield

For the precast beams, using properties from the section on concrete performance

ω_{sw} = 2.58*9.81*0.38*0.685
= 6.6 kN/m

M_{sw} = 6.6*10.364^2/8
= 88.5 kN.m

It is assumed that the beams were used to support the insitu deck with no use of falsework. This is indicated by the reference on the drawings to the casting of 1" cored holes into the beams for shutterings.

For the insitu deck,

ω_d = 2.58*9.81*0.178*1.219
= 5.5 kN/m

M_d = 5.5*10.364^2/8
= 73.7 kN/m

The kerb is assumed to have been cast after the deck and the load carried equally by all beams.

ω_{kerb} = 2*0.229*0.514*2.58*9.81/6
= 0.99 kN/m

M_{kerb} = 0.99*10.364^2/8
= 13.3 kN.m

Total non-composite moment = 88.5+73.7+13.3
= 176 kN.m

Dead load from the bituminous surfacing

$\omega_{asphalt}$ = 0.02*22*1.219
= 0.54 kN/m

$M_{asphalt}$ = 0.54*10.364^2/8
= 7.2 kN.m

For the precast beam

A_{st}	=	6334
d	=	587
b	=	380
p	=	0.0284
n	=	6.0
k	=	0.438
j	=	0.854
M	=	176 kN.m
f_s	=	55.4 MPa
f_c	=	7.2 MPa

Composite section properties are taken from the chapter on load distribution

For the interior beams

A_{st}	=	6334
d	=	842
k	=	0.238
j	=	0.921

For the asphalt

f_s = $7.2_{10}3$/(6334*0.921*0.842)
= 1.5 MPa

f_c = 0.1 MPa

For a yield stress of 280 MPa, available stress until yield
= 280-55.4-1.5
= 223 MPa

available moment = 6334*223*0.921*0.842_{10}-3
= 1096 kN.m

total concrete stress will be 7.2 + 0.1 + 223*0.238/6/(1-0.238)
= 18.9 MPa < ultimate

For the exterior beams,

f_s	=	0.166 M
f_c	=	0.0694 fs

For the asphalt

f_s = 0.166 * 7.2
= 1.2 MPa

f_c = 0.1 MPa

Available steel stress until yield
= 280 - 55.4 - 1.2
= 223 MPa

Available moment = 223/0.166
= 1346 kN.m

Total concrete stress will be 7.2 + 0.1 + 223*0.0694
= 22.8 MPa < ultimate

The grillage analysis is considered to reasonably model the elastic behaviour of the bridge. From the calculations for the loading of the bridge:

	Beam bending moment (kN.m)					
	Beam 1	**Beam 2**	**Beam 3**	**Beam 4**	**Beam 5**	**Beam 6**
4/1000 kN loads	2567	1564	1008	1008	1564	2567
Available moment	1346	1096	1096	1096	1096	1346

Table 18.4 - Beam Bending Moments

For the exterior beams yielding, total applied load P_{yield} is given by

P_{yield} = 4000 * 1346/2567
= 2100 kN

For the interior beams yielding, total applied load P_{yield} is given by

P_{yield} = 4000 * 1096/1564
= 2800 kN

The two estimates are between the yield loads indicated by deflection and strain measurements.

18.6 Theoretical Capacity at Ultimate

For a singly reinforced rectangular concrete section, effective moment capacity M′ is given by:

$$M' = \phi \{ A_{st} f_{sy} d [1 - 0.6 A_{st} f_{sy} / (b d F'_c] \}$$

For the interior beam, neglecting compression reinforcement and using the measured material properties,

A_{st} = 6334 mm^2
f_{sy} = 290 MPa
d = 841 mm
b = 1219 mm
F'_c = 65 MPa for superstructure
ϕ = 0.9 for bending

M′ = 1367 kN.m

Check depth of rectangular stress block

k'd = $A_{st} f_{sy} d / (b d 0.85^2 F'_c)$
= 46.5mm < deck thickness

proportion of steel for balanced failure

p_b = $0.85 \gamma F'_c * 600 / (f_{sy} (600 + f_{sy}))$
= 0.1092
> p (0.0062)

∴ section is under-reinforced.

Available moment = 1367 - 183
= 1184 kN.m

For the exterior beam, neglecting compression reinforcement and using the measured material properties,

A_{st} = 6334 mm^2
f_{sy} = 290 MPa
d = 1071 mm
b = 514 mm
F'_c = 65 MPa for superstructure
ϕ = 0.9 for bending

M' = 1716 kN.m

Check depth of rectangular stress block

k'd = $A_{st}f_{sy}d/(bd0.85^2F'_c)$
= 76mm < kerb thickness

p = 6334/(514*1071)
= 0.0115
< p_b (0.1092)

$\therefore$ section is under-reinforced.

Available moment = 1716 - 183
= 1533 kN.m

For the six beams,
total available moment = (4 * 1184 + 2 * 1533)
= 7802 kN.m

total applied load = 7802 * 4/10.364
= 3011 kN

The calculated total applied load is significantly less than the maximum applied load of 4710 kN, although it is similar to the load of 3010 kN at which it was necessary to unload to bridge because the extension of the ground anchors and deflection of the bridge matched the travel of the hydraulic jacks. The additional capacity may be attributable to a number of factors, including:

- load redistribution and alternative load paths not accounted for in simplified analytical techniques
- arching effects due to the relatively low span to depth ratio
- bearing restraint, with the lead bearing sheets providing little rotational capacity
- strain hardening from the unloading and reloading required to achieve the higher bridge loadings.

Refinement of the estimated capacity may be achievable with non-linear finite element analysis, although this was outside the scope of the test program

18.7 Discussion

The bridge behaved in the desired ductile manner, with a maximum deflection of about 50mm (span/200). Deflections were increasing with no increase in applied load, and the maximum deflection achieved in the testing was in fact constrained by the travel on the hydraulic jacks used to load the structure and the extensions of the ground anchors. The yield point of the bridge is reasonably estimated by the analytical methods, with the ultimate load approximately twice yield load. Simplified techniques underestimate the ultimate load.

Many researchers have found significant reserves of strength in bridges. Gosbell and Stevens (1968) applied a load of over three times that required to initiate cracking to a prestressed concrete bridge. Mufti and Bakht (1991) recommended upgrading of a 5 t load limit to 10 t single posting or 19,26 and 35 tonnes triple posting after full-scale testing of a T-beam bridge. Miller et al (1994) failed a severely deteriorated slab bridge in punching shear at a load of 3,200 kN, equivalent to 22 design HS-20-44 trucks. The general applicability of the results has been confirmed by the Princess River Bridge testing.

If an opportunity occurs for similar testing of another bridge, smaller load increments should be used and there would be an advantage in monitoring applied loads with the same logger as used for bridge responses to facilitate the interpretation of results.

19. SUMMARY AND CONCLUSIONS

19.1 General

Princess River Bridge was a reinforced concrete T-beam bridge located on the Lyell Highway on Tasmania's west coast. The section of highway containing the bridge was flooded by the King River power development in 1991. The bypassing of the highway prior to inundation provided an opportunity to undertake an extensive range of testing between 29 July and 22 August 1991. The testing and results from it are described below. The test program was integrated with work being undertaken for Vicroads on the use of dynamic measurement to assess load capacity and identify defects in bridges.

The geology of the site comprised a low seismic velocity surface layer 1m to 2.5m thick, underlain by a layer 6m to 12m thick of seismic velocity 1130 to 1420 m/s, and thence a layer with velocities of 4000 to 8000 m/s. Rainfall at the site is of the order of 2500 mm per annum with high relative humidities.

The bridge comprised two 10.4m spans of six reinforced concrete T-beams with precast beam elements and insitu reinforced concrete deck. Abutments and the pier were piled with reinforced concrete crossheads.

Because of the diversity of testing, an extensive range of literature was identified and reviewed.

Instrumentation for the test program included strain gauges, accelerometers and displacement transducers.

Testing was undertaken at both working and ultimate live loads. Working loads comprised trucks recovering gravel from the bed of the King River and included one which had been weighed for calibration purposes. For the deck punching shear and ultimate load capacity testing the bridge was loaded with hydraulic jacks acting against the launching nose from the new King River Bridge, with the reaction provided by four prestressed ground anchors. The pattern of loading was determined by grillage analysis and was selected to minimise the applied load required.

Dimensions of the bridge were measured to provide an assessment of compliance with contemporary specifications. The bridge itself was generally within currently permitted dimensional tolerances, although a number of measurements of the precast beams were outside tolerance. It is likely that dimensional deviations follow an approximately normal distribution.

Almost 700 measurements of cover to reinforcement were taken to complement the dimensional survey. The distribution of measurements is again approximately normal, with some skew. Only 52% of the measurements comply with the current Australian Standard requirement of -5+10mm on specified cover. The results are however consistent with those reported by Marrosszeky and Chew and with measurements on a number of other Tasmanian bridges. A more comprehensive and systematic investigation of cover to reinforcement in Tasmanian bridges has been instituted as a result of the test program.

An extensive survey of cracking which existed prior to the test program was undertaken. While little cracking was evident in the precast beams, there was extensive random cracking of widths less than 0.1mm in the deck soffit. It is likely that this was attributable to the use of tongue and groove timber, which would have been relatively permeable and thus affected curing. Because of the environment at the bridge site however, the durability of the bridge had not been adversely affected.

A number of cores were taken for the assessment of concrete performance. Compressive test results from the bridge's construction were not available for comparison. The strength gains are however likely to be consistent with those reported by Washa et al in the United States. The quality of concrete, in terms of cement content and water cement ratio, is likely to have been better than for typical structures of the period, and with the high relative humidities at the site contributed to the lack of carbonation of the concrete.

Tensile testing of the plain steel reinforcement showed a yield stress of 300 MPa, which is higher than the 230 or 250 MPa which would have been expected.

Dimensional tolerances on the two precast beams recovered from the site were within contemporary tolerances, with the exception of some depth measurements because of the requirement for a roughened deck for the casting of the insitu deck. The calculated load for yield of the beam tested in flexure was in agreement with the measured value, although strains at working loads were underestimated. Failure was ductile. The beam had adequate shear capacity, and brittle failure did not occur.

Dynamic measurements were able to readily discern the removal of sections of the concrete bridge fence through changes to vibration modes at higher frequencies. It was however necessary to cut a substantial proportion of reinforcement in one of the beams to generate a comparable change in dynamic response. Further work is thus required before dynamic measurement techniques can be used as a means of condition monitoring.

The assessment of impact effects was constrained by the relatively low sampling frequency and limited duration of measurements. Impact for the cases assessed was estimated to be of the order of 15%, which is lower than code values and those reported by other researchers. It is likely that the high natural frequency of 17.6 Hz, being greater than body bounce and axle hop frequencies for heavy vehicles, resulted in the relatively low dynamic load effects.

There was reasonable correlation between calculated and measured load distributions at working loads, although strains were again underestimated. Simplified distribution factors and grillage analysis were used for the theoretical modelling. There was little variation in calculated results for increasing fineness of meshes for the grillage analysis.

Extensive laboratory and field testing of bridge deck slabs has shown that they possess far more strength than could be possible if transverse moments as predicted by conventional analyses did really exist. A load of 1400 kN was applied to the deck, compared to the design wheel load of 91 kN including impact. A maximum crack width of 0.2 mm was observed. The testing confirmed the substantial reserves of capacity in bridge decks due to compressive membrane action.

The bridge was loaded to failure, with loads applied to the exterior pairs of beams. A total load of 4800 kN was applied, with cracks up to 12 mm in width and a maximum deflection of the order of 50 mm. Bridge behaviour was ductile, with the ultimate load being approximately twice that for yield. The load for yield was reasonably predicted by grillage and elastic methods of analysis.

19.2 Relationship to Program Objectives

A number of broad conclusions can be drawn in respect of achievement of the program objectives:

- contemporary design methods can, using techniques such as distribution factors, grillage analysis and other available computer programs, reasonably predict bridge behaviour, although high degrees of correlation between calculated and measured behaviours may not be achievable
- simplified methods of analysis for load distribution are likely to provide acceptable results

- analytical rating methods are likely to be conservative and, with the observed ductile behaviour at high loads, provide acceptable levels of risk associated with the management of the State's bridge stock
- the test program demonstrated that good durability performance of concretes can be achieved with high cement contents, relatively low water cement ratios and acceptable covers in high rainfall environments. The variability of cover to reinforcement was however highlighted as an issue. The durability results cannot however be transferred to bridges in other environments where lower humidities results in higher carbonation rates or where chlorides or sulphates are present.
- the Department's understanding of bridge behaviour was significantly enhanced by the test program, providing greater confidence in the ability to use existing analytical techniques to model bridge behaviour and in the ductility of bridge behaviour at high loads.

20. ACKNOWLEDGMENTS

The Department of Transport's support and funding for the test program is gratefully acknowledged.

Geoff Mulcahy assisted with the analysis for the ultimate loading rig as the project component of a Degree of Master of Engineering Science at the University of Sydney.

The Cement and Concrete Association provided financial assistance for the concrete durability aspects of the work.

VSL Prestressing assisted with the design of the anchors for the loading rig and undertook their installation and the subsequent loading of the bridge.

Vicroads, ETRS Consultants, University of Melbourne and University of Wollongong undertook testing of the bridge as part of research programs using dynamic responses to assess load capacity and structural deterioration.

Rob Heywood of Queensland University of Technology undertook the Fourier transforms for the Department's dynamic response measurements.

The support and tolerance of my wife Margie and children Heather and Andrew during the testing program and subsequent analysis and writing of this report is also acknowledged.

REFERENCES

ACI Committee 224, 'Causes, Evaluation, and Repair of Cracks in Concrete Structures', ACI Journal Proceedings Vol.81 No.3, American Concrete Institute, Detroit, Michigan, May-June 1984

Aktan A E, Lee K L, Naghavi R and Hebbar, 'Destructive Testing of Two 80-Year-Old Truss Bridges', Transportation Research Record No.1460, Transportation Research Board, Washington D.C.

Allen J H, 'Cracking, Serviceability, and Strength of Concrete Bridge Decks', (1991), Transportation Research Record No.1290, Transportation Research Board, Washington D.C.

Azad A K, Baluch M H, Abbasi M S A and Kareem K, (1994), 'Punching Capacity of Deck Slabs in Girder-Slab Bridges', ACI Structural Journal November-December 1994, American Concrete Institute

Azizinamini A, Boothby T E and Shekar Y, 'Old Concrete Slab Bridges. I: Experimental Investigation' and 'Old Concrete Slab Bridges. II: Analysis', American Society of Civil Engineers, Journal of Structural Engineering, Vol. 120, No.11, November 1994

Bakht B and Jaeger L G, (1985), 'Bridge Analysis Simplified', McGraw-Hill Inc., New York

Bakht B and Jaeger L G, 'Bearing Restraint in Slab-on-Girder Bridges', American Society of Civil Engineers, Journal of Structural Engineering, Vol. 114, No.12, December 1988

Bakht B and Jaeger L G, 'Ultimate Load Test of Slab-on-Girder Bridge', American Society of Civil Engineers, Journal of Structural Engineering, Vol. 118, No.6, December 1992

Bakht B and Moses F, 'Lateral Distribution Factors for Highway Bridges', American Society of Civil Engineers, Journal of Structural Engineering, Vol.114, No.8, August 1988

Bartlett F M and M^{ac}Gregor J G, 'Effect of Core Diameter on Concrete Core Strengths', American Concrete Institute Materials Journal, American Concrete Institute, Detroit, Michigan, September-October 1994

Base G D and Murray M H, 'A New Look at Shrinkage Cracking', Civil Engineering Transactions Vol. CE24 No.2, Institution of Engineers Australia, Canberra, May 1982

Beal D B, 'Strength of Concrete T-Beam Bridges' in 'Strength Evaluation of Existing Concrete Bridges', (1985), American Concrete Institute, Detroit, Michigan

Bishara A G, Liu M C and El-Ali N D, 'Wheel Load Distribution on Simply Supported Skew I-Beam Composite Bridges', American Society of Civil Engineers, Journal of Structural Engineering, Vol.119, No.2, February 1993

Behrens M P and Tongue D J, 'Dynamic Assessment of Bridges - Princess River Bridge, Queenstown, Tasmania', (1992), ETRS Pty Ltd, Melbourne

Brotchie J F and Holley M J, (1971), 'Membrane action in slabs', American Concrete Institute, Publication SP-30, pp 345-377

Cantieni R, (1983), 'Dynamic Load Tests on Highway Bridges in Switzerland - 60 Years Experience of EMPA', Report No.211, EMPA (Swiss Federal Laboratories for Materials Testing and Research), Dübendorf, Switzerland

Chana P S and Desai S B, 'Membrane action, and design against punching shear', The Structural Engineer, Volume 70, No.19, 6 October 1992

Daly, A E and Cullington D W, 'Assessment Implications from Tests on a Model Concrete Beam and Slab Bridge', (1991), Transport and Road Research Laboratory Report 309, Department of Transport, Crowthorn, Berkshire
Vol.116 No.3, March 1990

Darvall P L and Brown H P, (1976), Fundamentals of Reinforced Concrete Analysis and Design', The Macmillan Company of Australia Pty Ltd, South Melbourne

Department of Transport, (1995), Standard Specifications, Hobart

Fang I K, Worley J, Burns N H and Klingner R E, 'Behaviour of Isotropic R/C Bridge Decks on Steel Girders', American Society of Civil Engineers, Journal of Structural Engineering,

Fu G and T J, 'Risk-Based Proof-Load Requirements for Bridge Evaluation', Journal of Structural Engineering Vo.121, No.3., American Society of Civil Engineers, March 1995

Fuller D A, (January 1986), 'The King River Handover Report, Hydrology and Climatology', Hydro-Electric Commission, Hobart

Gardner N J and Shao X-y, (1996), 'Punching Shear of Continuous Flat Reinforced Concrete Slabs', ACI Structural Journal March-April 1996, American Concrete Institute

Gosbell K B and Stevens L K, (1968), 'Test Loading of a Full Scale Bridge', Australian Road Research Board Proceedings Vol.4 Part 2, Melbourne

Hambly E C, (1991), 'Bridge Deck Behaviour', Chapman and Hall, London, United Kingdom

Hearn G and Testa R B, 'Modal Analysis for Damage Detection in Structures', American Society of Civil Engineers, Journal of Structural Engineering, Vol.117, No.10, October 1991

Heywood R J, (1991), 'Bridge Applications of Weigh-In-Motion Data' in 'Bridges - Part of the Transport System', Proceedings of the AUSTROADS Bridge Conference, Brisbane

Heywood R J, (1995), 'Vehicle-Pavement Interaction - Dynamic Loading Issues', Load-Pavement Interaction Workshop, Newcastle

Highway Research Board, 'Special Report 61D - The AASHO Road Test, Report 4, Bridge Research', (1962), National Academy of Sciences - National Research Council, Washington D.C

Hwang E-S and Nowak A S, 'Simulation of Dynamic Load for Bridges', ASCE Journal of Structural Engineering, Vol. 177, No. 5, May 1991

Institution of Engineers Australia, (1987), 'Australian Rainfall and Runoff', Canberra

Jackson P A, (1990), 'The global and local behaviour of bridge deck slabs', The Structural Engineer Vol. 8, No.6, The Institution of Structural Engineers, London, United Kingdom

Kirkpatrick J, Rankin G I B and Long A E, (1986), 'Strength evaluation of M-beam bridge deck slabs', The Structural Engineer Vol. 62B, No.3, The Institution of Structural Engineers, London, United Kingdom

Kirkpatrick J, Rankin G I B and Long A E, (1986), 'The influence of compressive membrane action on the serviceability of beam and slab bridge decks', The Structural Engineer Vol. 64B, No.1, The Institution of Structural Engineers, London, United Kingdom

Kuang J S, (1991), 'Punching Shear Behaviour of Restrained Reinforced Concrete Slabs - Test Report', Department of Engineering, University of Cambridge

Law S S, Ward H S, Shi G B, Chen R Z, Waldron P and Taylor C, 'Dynamic Assessment of Bridge Load-Carrying Capacities, I and II', Journal of Structural Engineering Vol.121 No.3, American Society of Civil Engineers, March 1995

Long A E, (1975), 'A two-phase approach to the prediction of punching strength of slabs', Journal of the American Concrete Institute, Proceedings 72 No.2

Marrosszeky, M and Chew, M, (1989), 'Site Investigation of the Quality of Reinforcement Placement on Buildings and Bridges', Concrete Institute of Australia News Volume 15, Number 4

Miller R A, Aktan A E and Shahrooz B M, (1994), 'Destructive Testing of Decommissioned Concrete Slab Bridge', Journal of Structural Engineering Vol.120 No.7, American Society of Civil Engineers

Miller R and Parekh K, 'Destructive Testing of Deteriorated Prestressed Box Bridge Beam', Transportation Research Record 1460, Transportation Research Board, Washington D.C.

Moses F, Lebet J P and Bez R, 'Application of Field Testing to Bridge Evaluation', ASCE Journal of Structural Engineering, Vol. 120, No. 6, June 1994

Mufti A and Bakht B, (1991), 'Strength Evaluation by Testing of an Old T-Beam Bridge', Research and Development Branch, Ontario Ministry of Transportation, Canada

National Association of State Road Authorities, (1965), 'Highway Bridge Design Specification', Sydney

National Co-operative Highway Research Program, 'Distribution of Wheel Loads on Highway Bridges', (May 1992), Transportation Research Board, Washington, D.C.

Nowak A S, 'Calibration of LRFD Bridge Code', Journal of Structural Engineering Vol.121 No.8, American Society of Civil Engineers, August 1995

Rankin G I B, Niblock R A, Skates A S and Long A E, (1991), 'Compressive membrane action strength enhancement in uniformly loaded, laterally restrained slabs', The Structural Engineer Vol. 69 No.16, The Institution of Structural Engineers, London, United Kingdom

Salawu O S and Williams C, 'Bridge Assessment Using Forced-Vibration Testing', Journal of Structural Engineering Vol.121 No.2, American Society of Civil Engineers, February 1995

Shahrooz B M, Ho I K, Aktan A E, de Borst R, Blaauwendraad J, van der Veen C, Iding R H and Miller R A, 'Nonlinear Finite Element Analysis of Deteriorated RC Slab Bridge', American Society of Civil Engineers, Journal of Structural Engineering, Vol. 120, No.2, February 1994

Sobrino J A and Casas J R, 'Probabilistic Assessment of Prestressed Concrete Bridge', Fourth International Bridge Engineering Conference Proceedings, Transportation Research Board, Washington D.C., August 1995

Standards Association of Australia, (1976), ' Methods of Testing Concrete - Methods for the Determination of the Static Chord Modulus of Elasticity and Poisson's Ratio of Concrete Specimens', Sydney

Tabsh S W and Nowak A S, 'Reliability of Highway Girder Bridges', American Society of Civil Engineers, Journal of Structural Engineering, Vol. 117, No.8, August 1991

Taylor W H, (1977), 'Concrete Technology and Practice', McGraw-Hill Book Company, Sydney

Udoeyo F F and Ugbem P I, 'Dimensional Variations in Reinforced-Concrete Members', Journal of Structural Engineering Vol. 121 No. 12, American Society of Civil Engineers, December 1995

Verma D and Moses F, 'Calibration of Bridge-Strength Evaluation Code', Journal of Structural Engineering, Vol. 155, No. 6, June 1989

VSL Prestressing, 'Ground Anchors', Jan Publications

Washa G W and Wendt K F, (1975), 'Fifty Year Properties of Concrete', ACI Journal January 1975, American Concrete Institute

Washa G W, Saemann J C and Cramer S M, (1989), 'Fifty-Year Properties of Concrete Made in 1937', ACI Materials Journal Vol.86 No.4, American Concrete Institute

Withey K H, 'Tests on a Half-Scale Prestressed Beam and Slab Bridge Deck', (1989), Research Report 198, Transport and Road Research Laboratory, Crowthorne, Berkshire, United Kingdom

Zokaie T, Imbsen R A and Osterkamp T A, 'Distribution of Wheel Loads on Highway Bridges', Transportation Research Record 1290, Transportation Research Board, Washington D.C., 1991

APPENDIX A - DESIGN OF LOADING EQUIPMENT

A.1 Introduction

This appendix describes the design of the loading arrangements for the bridge testing and for the subsequent testing of the individual beams.

The design was undertaken prior to the testing, and a number of assumptions and simplifications were thus required.

A.2 Bridge Ultimate Loading

A.2.1 Design of Loading Rig

For the design of the loading rig, it was first necessary to establish an estimated ultimate capacity for the bridge. Full-scale bridge testing of bridges by others has generally shown significant reserves of strength, and a simplified and conservative approach to estimating capacity was thus taken.

In accordance with the NAASRA Bridge Design Specification, the effective width of the deck as a T-beam flange shall not exceed:

1. one-fourth of the span length of the beam
2. the distance centre to centre of beams
3. twelve times the least thickness of the slab plus the width of the girder stem.

For a span length of 10.364m, the respective values are:

1. 10.364/4 = 2.591m
2. 4'0" = 1.219m
3. 12 * 7" + 15" = 2.514m

Thus

b_{eff} = 1219mm

Materials properties were assumed to be design values derived from the bridge drawings. These are likely to provide lower bound values, particularly with the expected long term gain in concrete strength.

A.2.1.1 Elastic Analysis

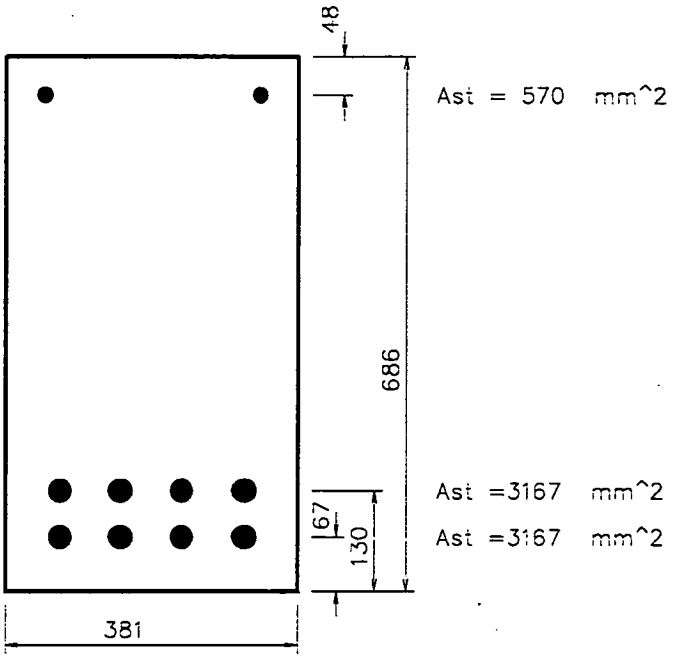

Figure A.1 - Precast Beam

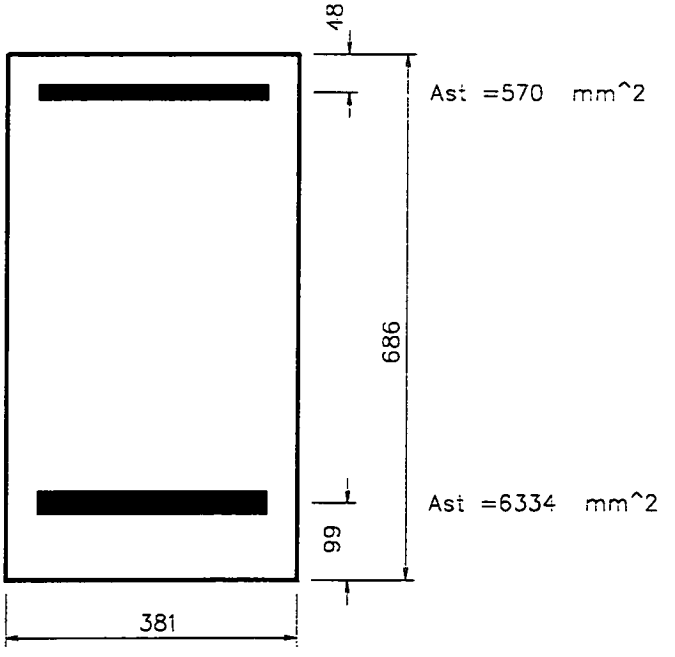

Figure A.2 - Simplified Cross-section for Precast Beam

Assume concrete strength of 3000psi (20.7 MPa)
modular ratio n = 10

For the precast beam, neglecting compression reinforcement

A_s = 6334 mm^2
b = 381 mm
d = 686 - 99
= 587 mm

p	=	0.0283
np	=	0.283
k	=	$-np + \sqrt{((np)^2 + 2np)}$
	=	0.521
j	=	1 - k/3
	=	0.826

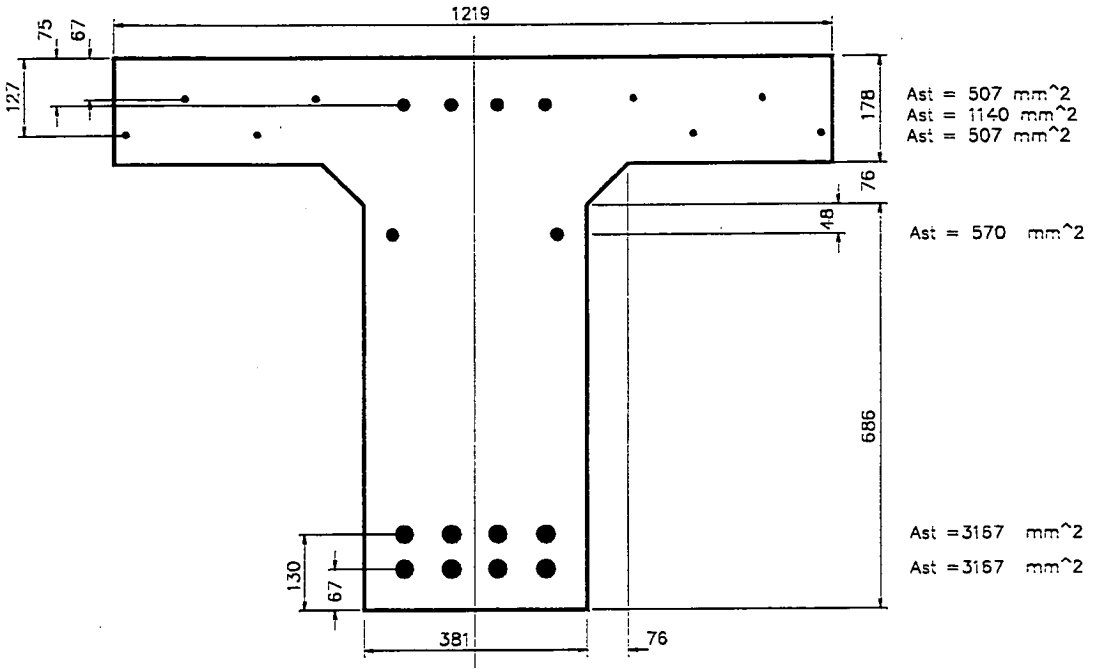

Figure A.3 - Composite T-beam Dimensions

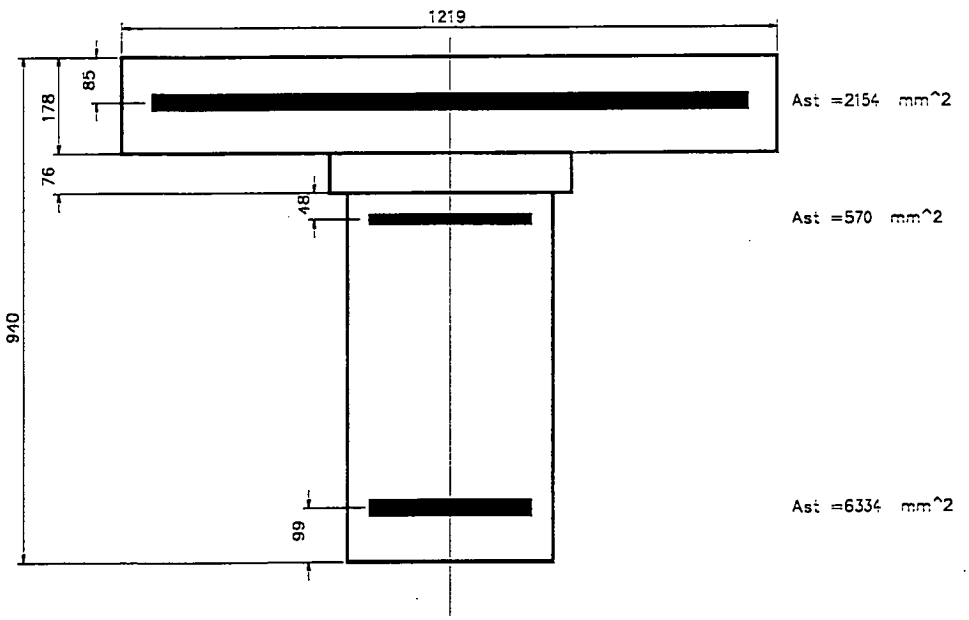

Figure A.4 - Simplified T-beam

For the composite section,

Assume neutral axis in flange, and equating the first moment of area about the neutral axis to zero,

$$1219 * d_n/2 = 63340 ((940-99) - d_n)$$

Solving,

$$d_n = 248 \text{ mm; neutral axis in web}$$

$$178 * 1219 (d_n - 89) + 381 (d_n - 178)^2/2 = 63340 (841 - d_n)$$

Solving,

$$d_n = 255 \text{ mm}$$

Calculate section properties,

Element	A	y	Ay	$A(y-y_c)^2$	I_{self}
Flange	$2.17_{10}5$	752	$1.63_{10}8$	$5.84_{10}9$	$5.73_{10}8$
Web	$4.54_{10}4$	642.5	$2.83_{10}7$	$6.05_{10}7$	$1.45_{10}7$
Steel	63340	0	0	$2.18_{10}10$	0
Total	**$3.26_{10}5$**		**$1.92_{10}8$**	**$2.78_{10}10$**	**$5.87_{10}10$**

$y_c = 588$ mm
$I_{xx} = 28.4_{10}9$ mm^4
$Z_{t\text{-slab}} = 112_{10}6$ mm^4
$X_{t\text{-beam}} = 28_{10}9$mm^4
$Z_{steel} = 48.3_{10}6$ mm^4

It is assumed that the beams were used to support formwork for the casting of the deck slab because of the reference on the drawings to one inch diameter cored holes being cast into the beams with the 'spacing to be determined by approved design of shuttering.' The deck dead load is thus carried by the precast beam alone. It is further assumed that the kerbs were cast after the principal deck pour and that their dead load is thus distributed amongst all beams.

For a concrete density of 25 kN/m^3, and allowing for 25mm of surfacing with a density of 22 kN/m^3,

$$\omega_{deck} = ((0.686 * 0.381 + 0.457 * 0.076 + 1.219 * 0.178) + 0.229 * 0.514/3) * 25 + 6.7 * 0.025 * 22/6$$
$$= 14.4 \text{ kN/m}$$

$$M_{dead} = 14.4 * 10.364^2/8$$
$$= 194 \text{ kN.m}$$

For the precast beam under dead load,

$$f_{s\text{-dead}} = M_{dead}/A_sjd$$
$$= 194_{10}3/(6334 * 0.826 * 0.587)$$
$$= 63.2 \text{ MPa}$$

$$f_{c\text{-dead}} = f_sk/n/(1-k)$$
$$= 6.87 \text{ MPa}$$

For a steel yield stress of 250 MPa, available steel stress

$$f_{s\text{-avail}} = 250 - 63.2$$
$$= 187 \text{ MPa}$$

Available moment,

$$M_{avail} = f_{s\text{-avail}} * Z_{steel}/n$$
$$= 187 * 48.3_{10}6/10 \text{ N.mm}$$

$= \quad 903$ kN.m

Available load for a simply supported beam with a midspan point load,

$P_{avail} = 4 * 903/10.364$

$= \quad 350$ kN

Check concrete stresses,

$f_{c\text{-top slab}} = M_{avail} / Z_{t\text{-slab}}$

$= 903/112$

$= \quad 8.1$ MPa

$f_{c\text{-top beam}} = f_{c\text{-dead}} + M_{avail} / Z_{t\text{-beam}}$

$= 6.87 + 903/28_{10}3$

$= \quad 6.9$ MPa

The capacity of the exterior beams will be greater than that of the interior beams because of the effects of the kerbs.

As a first estimate, assume that the capacity of the exterior beams is 10% greater than that of the interior beams and that the bridge capacity is the sum of the individual beam capacities.

$\therefore$bridge load at yield $= (4 + 2 * 1.1)\ 350$

$= \quad 2200$ kN

A.2.1.2 Ultimate analysis

For a singly reinforced rectangular concrete section, effective moment capacity M′ is given by:

$M' = \phi \{ A_{st} f_{sy} d [1 - 0.6 A_{st} f_{sy} / (b d F'_c] \}$

Neglecting compression reinforcement,

$A_{st} = 6334$ mm^2

$f_{sy} = 230$ MPa

$d = 841$ mm

$b = 1219$ mm

$F'_c = 20$ MPa

$\phi = 0.9$ for bending

$M' = 1056$ kN.m

Available moment

$M'_{avail} = 1056\text{-}194$

$= \quad 860$ kN.m

For a simply supported beam loaded at midspan

ultimate load $= 4 * 860/10.364$

$= \quad 330$ kN

bridge ultimate load $= 6.2 * 330$

$= \quad 2100$ kN

Check for under-reinforced section

steel proportion,

$p = 6334/(1219 * 841)$

$= \quad 0.0062$

proportion of steel for balanced failure

$$p_b = 0.85 \gamma F'_c * 600/(f_{sy}(600 + f_{sy}))$$
$$= 0.85 * 0.85 * 20 * 600/(230(600 + 230))$$
$$= 0.045$$
$$> p$$

$\therefore$ section is under-reinforced.

A.2.1.3 Grillage Analysis

A grillage analysis was used to review the estimates of ultimate load capacity and determine the loading configuration to be used for the ultimate test.

The 'GROPER' program, developed by Technical Systems Australia Pty Ltd, was used for the analysis.

The documentation recommends a maximum grid aspect ratio of three, requiring a minimum of three divisions along the bridge. Four divisions were used to provide output at midspan.

Finer meshes were used to assess convergence, and found to give comparable results.

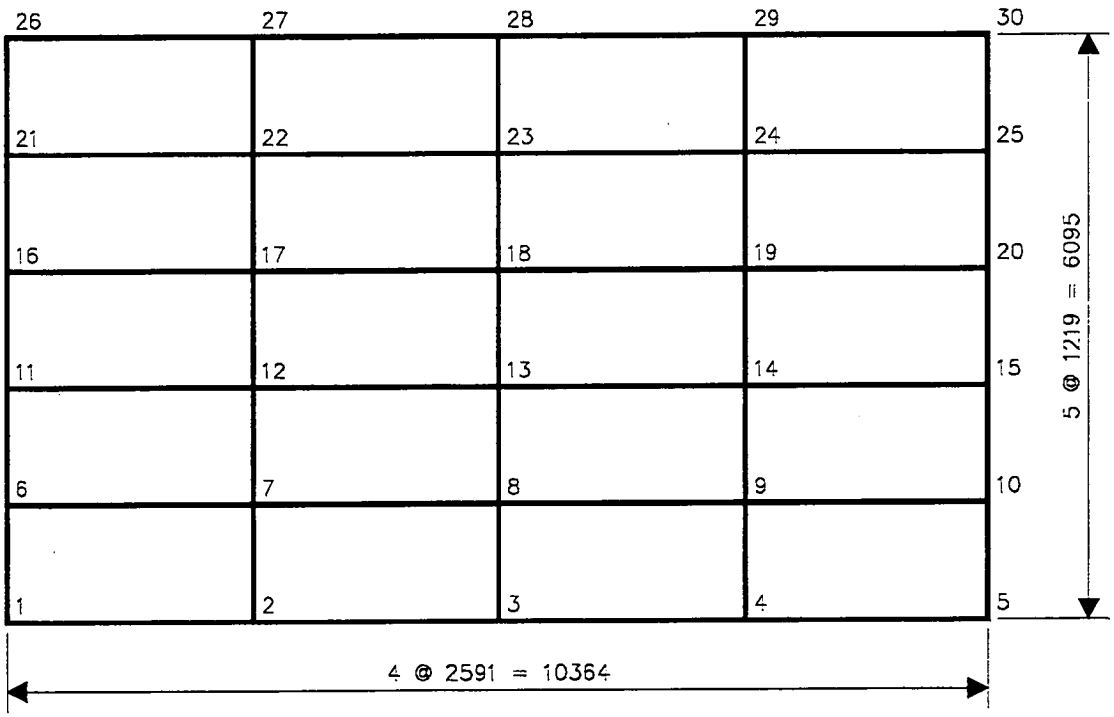

Figure A.5 - Grillage Model

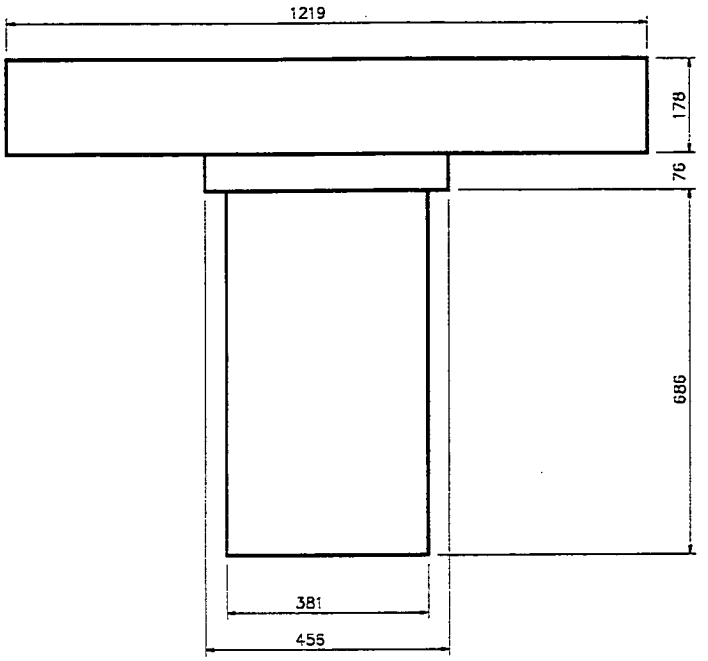

Figure A.6 - Interior Beam Cross-Section for Grillage Analysis

Element	A	y	Ay	$A(y-y_c)^2$	I_{self}
Deck	$2.17_{10}5$	851	$1.85_{10}8$	$1.53_{10}10$	$5.73_{10}8$
Fillet	34700	754	$2.61_{10}7$	$9.82_{10}8$	$1.67_{10}7$
Beam	261000	343	$8.96_{10}7$	$1.53_{10}10$	$1.02_{10}10$
Total	**513000**		**$3.00_{10}8$**	**$3.16_{10}10$**	**$1.08_{10}10$**

y_c = 586 mm

I_{xx} = $42.5_{10}9$ mm^4

Part	b/c	β	J
Deck	6.85	0.301	$1.03_{10}9$
Haunch	6.00	0.299	$5.99_{10}7$
Beam	1.80	0.215	$8.16_{10}9$
Total			**$9.25_{10}9$**

where b = longer side of a rectangular element

c = shorter side of a rectangular element

J = βbc^3

Note that deck torsional inertia is halved because of use of both beam and plate elements in grillage analysis.

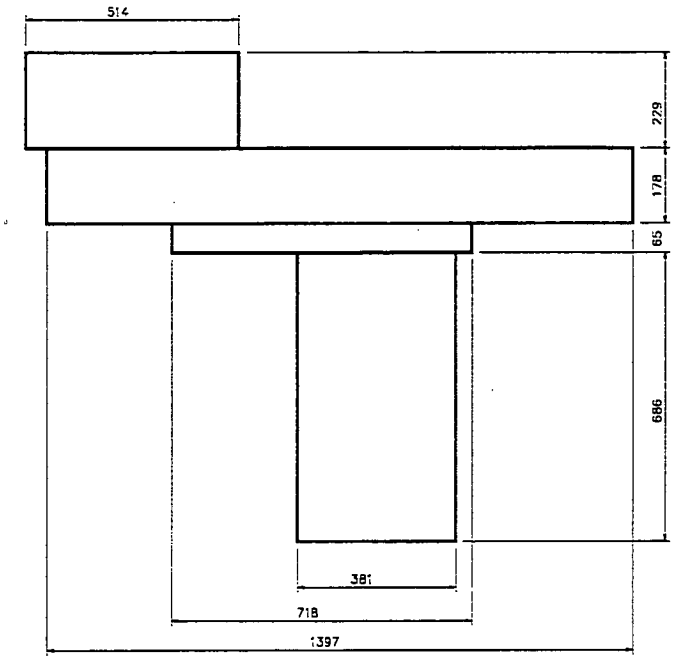

Figure A.7 - Exterior Beam Cross-Section for Grillage Analysis

Element	A	y	Ay	$A(y-y_c)^2$	I_{self}
Kerb	11800	1043	$1.23_{10}8$	$1.60_{10}10$	$5.14_{10}8$
Deck	249000	840	$2.09_{10}8$	$6.81_{10}9$	$6.57_{10}8$
Fillet	46700	718	$3.35_{10}7$	$9.04_{10}7$	$1.64_{10}7$
Beam	261000	343	$8.96_{10}7$	$2.87_{10}10$	$1.02_{10}10$
Total	**674000**		**$4.55_{10}8$**	**$5.17_{10}10$**	**$1.14_{10}10$**

y_c = 675 mm
I_{xx} = $63.1_{10}9$ mm^4

Part	b/c	β	J
Kerb	2.24	0.238	$1.47_{10}9$
Deck	7.85	0.305	$1.20_{10}9$
Haunch	11.1	0.315	$6.21_{10}7$
Beam	1.80	0.215	$8.16_{10}9$
Total			**$10.9_{10}9$**

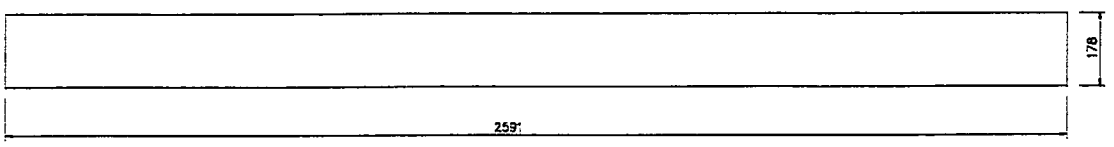

Figure A.8 - Internal Transverse Member

Area = 462000 mm^2
Ixx = $1.22_{10}9$ mm^4
J = $\beta bc^3/2$
= $0.312 * 2591 * 178^3/2$
= $2.28_{10}9$ mm^4

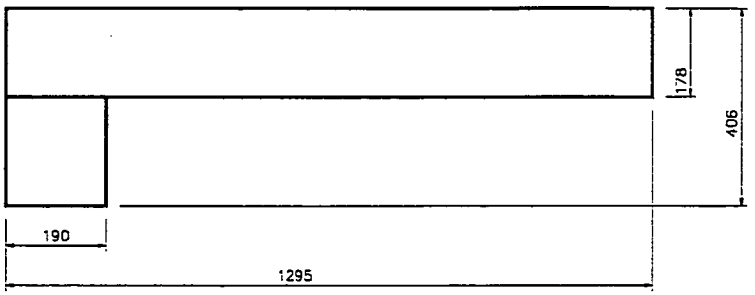

Figure A.9 - External Transverse Member

Element	A	y	Ay	$A(y-y_c)^2$	I_{self}
Deck	231000	317	$7.31_{10}7$	$2.38_{10}8$	$6.09_{10}8$
Diaphragm	43300	114	$4.94_{10}6$	$1.27_{10}9$	$1.88_{10}8$
Total	**274000**		**$7.80_{10}7$**	**$1.50_{10}9$**	**$7.96_{10}8$**

y_c = 285 mm
I_{xx} = $2.30_{10}9$ mm^4

Part	b/c	β	J
Deck	7.28	0.304	$1.11_{10}9$
Diaphragm	1.20	0.165	$2.58_{10}8$
Total			**$1.37_{10}9$**

Assumed concrete properties

F'_c = 20 MPa
γ = 25 kN/m^3
= 2550 kg/m^3
E_c = $0.043 \sqrt{(2550^3 * 20)}$
= 24.8 GPa
μ = 0.2
G_c = $Ec/2(1 + \mu)$
= 10.3 GPa

Results for varying configurations of point loads of 1000 kN are shown in Tables A.1 and A.2 and Figure A.10, with the approximate beam capacity of 900 kN.m included for reference.

	Beam 1	Beam 2	Beam 3	Beam 4	Beam 5	Beam 6
2 Interior Beams	0	0	1000	1000	0	0
4 Interior Beams	0	1000	1000	1000	1000	0
4 Exterior Beams	1000	1000	0	0	1000	1000

Table A.1 - Loading Configurations

	Beam 1	Beam 2	Beam 3	Beam 4	Beam 5	Beam 6
2 Interior Beams	418	725	1408	1408	725	418
4 Interior Beams	1239	1733	2137	2137	1733	1239
4 Exterior Beams	2567	1564	1008	1008	1564	2567

Table A.2 - Beam Bending Moments (kN.m) for 1000 kN loads

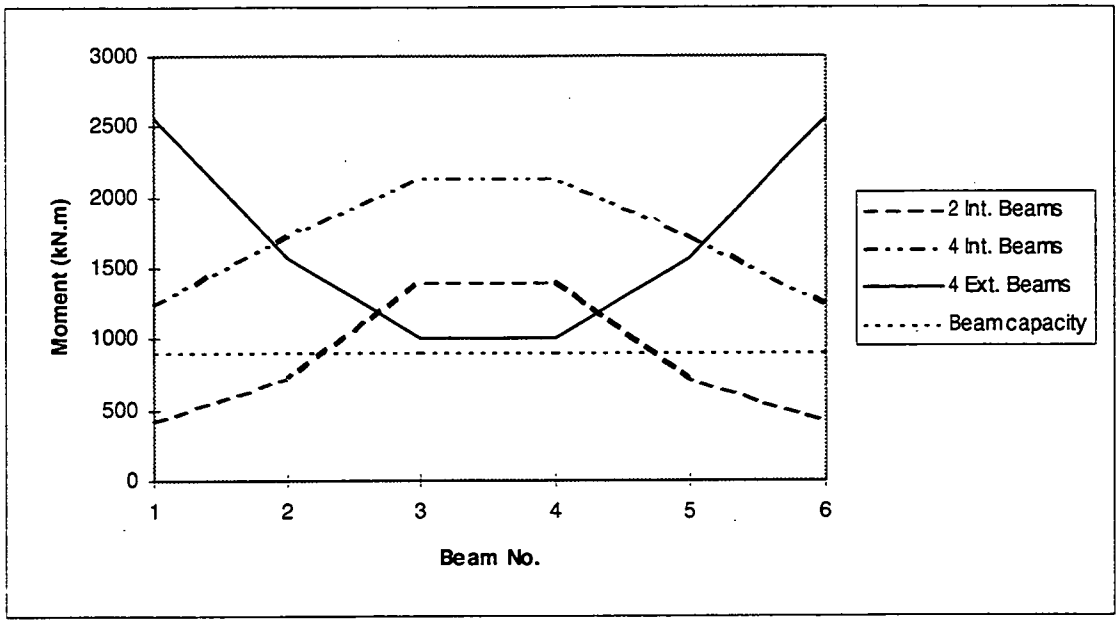

Figure A.10 - Beam Moments for Varying Load Configurations

The analysis indicated that the highest beam moments for a particular load, and thus the lowest ultimate load, would result from loading of the four exterior beams, with the two interior beams unloaded, and that loading configuration was thus adopted for the ultimate load test. The loading configuration is shown in Figure A.11.

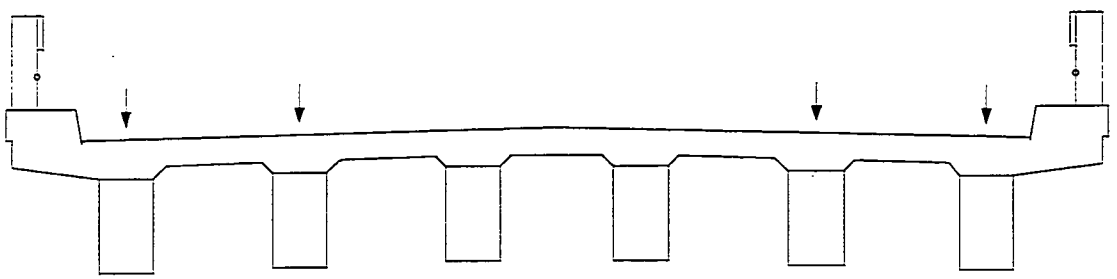

Figure A.11 - Loading Configuration

The initial estimate of the total load for yield of the beams was thus:

$$P_{yield} = 4 * 900 * 1000/2567$$
$$= 1400 \text{ kN}$$

If it is assumed that the ultimate failure load is 3 to 4 times that for initial yield to allow for post-yield steel behaviour, moment redistribution and reserve capacity, then the design load for the loading equipment is between 4200 kN and 5600 kN. A total design load of 5000 kN, or 1250 kN per jack, was thus adopted for the sizing of the loading components.

During preparations for the testing, the launching nose from the incrementally launched steel girder bridge carrying the Lyell Highway deviation across the future lake became available, and the test rig was thus based on the use of the nose. A basic geotechnical investigation indicated that prestressed ground anchors could be used to provide the necessary reaction.

The loading rig was generally designed to satisfy normal allowable stress levels for structures. The 40% overstress permitted in bridge design codes would provide a reserve to allow for any additional capacity of the bridge, the short term nature of the applied loadings and the difference between yield and ultimate capacities.

Basic allowable stresses are dependent upon the yield stress of the members. For the minor members, the yield stress was 250 MPa; for the launching nose a yield stress of 350 MPa applies. For most elements, slenderness effects were minimal.

The allowable bending stress is given by:

$$F_b = 0.55\, F_y$$

The allowable shear stress on the web is given by:

$$F_v = 0.33\, F_y$$

Allowable stresses are summarised in Table A.3.

	Bending		Shear	
	Basic	**40% overstress**	**Basic**	**40% overstress**
250 Grade	137.5 MPa	192.5 MPa	82.5 MPa	115.5 MPa
350 Grade	192.5 MPa	269.5 MPa	115.5 MPa	161.7 MPa

Table A.3 - Allowable Stresses

A.2.2 Loading Rig

The loading rig configuration is shown in Figure A.12.

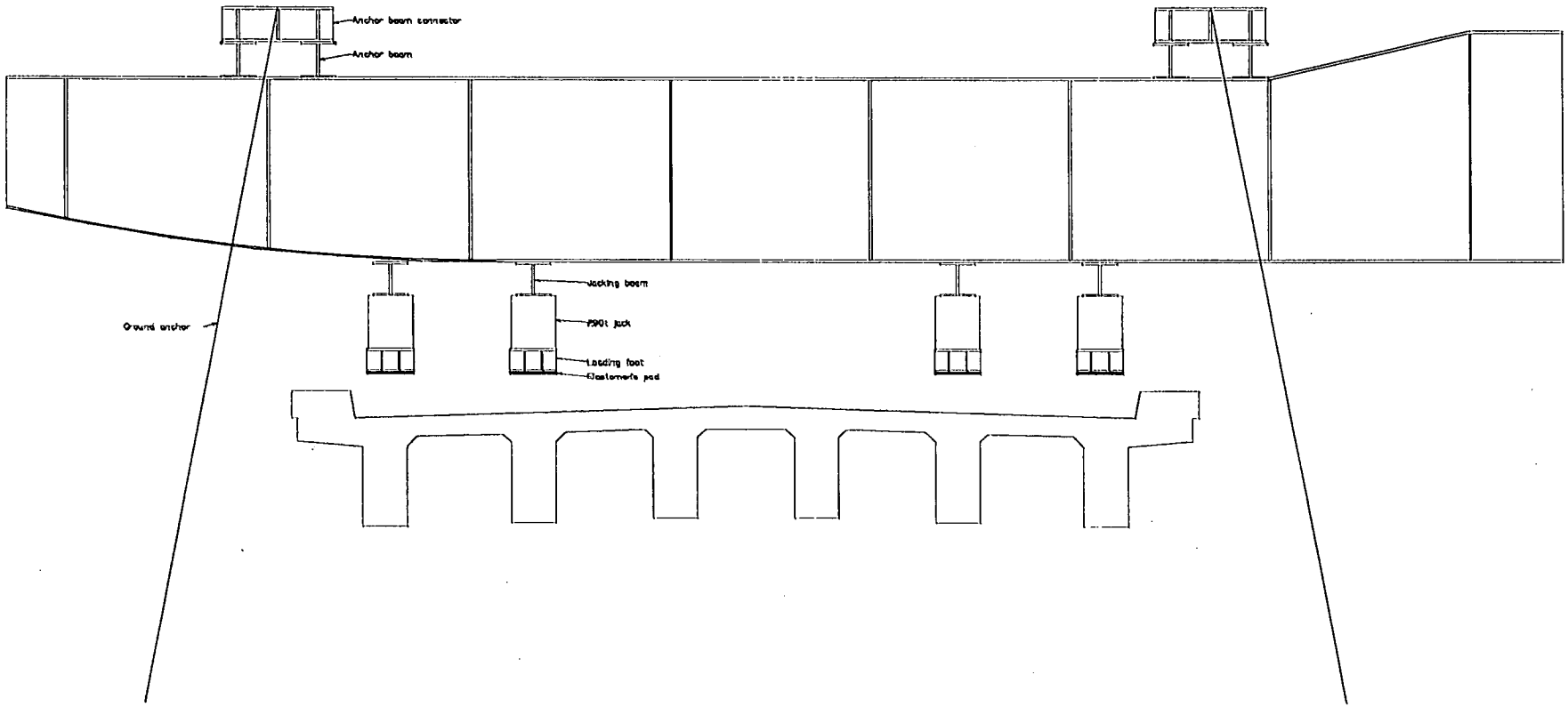

Figure A.12 - Loading Rig Configuration

A.2.3 Hydraulic Jacks

Hydraulic jacks used for loading the bridge were 270t capacity VSL prestressing jacks. Calibration test results (Test number 1089 of 12 July 1991 by VSL) are detailed in Table A.4 and Figure A.13.

Working Gauge (MPa)	Manometer (MPa)	Load (kN)	Repeatability (%)
10	9.38	466.3	0.9
20	19.42	974.0	0.7
30	29.38	1472.0	0.3
40	39.56	1976.7	0.5
50	49.75	2474.3	0.6
55	54.71	2723.3	0.3

Table A.4 - Jack Calibration

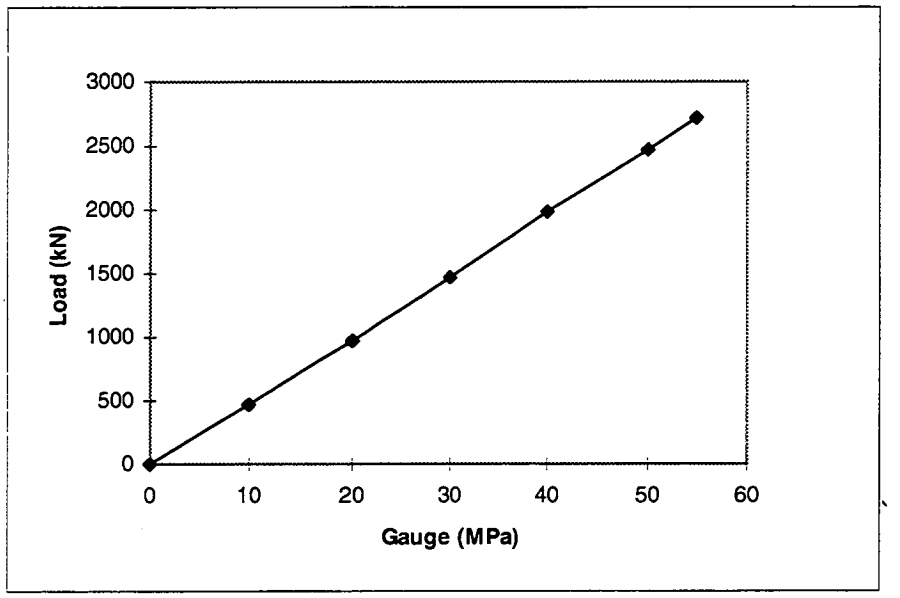

Figure A.13 - Jack Calibration

A.2.4 Jacking Beam

Loads were applied to the bridge by 4 hydraulic jacks acting through 400mm lengths of 200UC sections, with a 400 x 200 x 20 elastomeric pad between the column section and the deck surface to simulate a tyre footprint. No detailed design was undertaken, although stiffeners were welded into the columns.

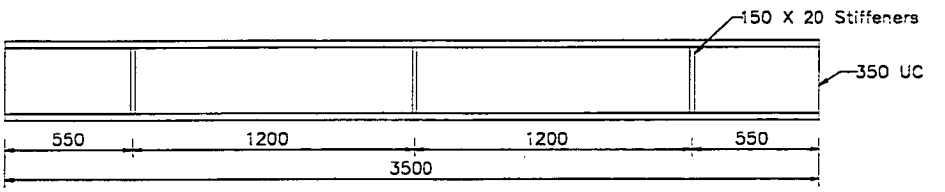

Figure A.14 - Jacking Beam

For a load of 1250 kN at midspan with the spacing of the launching nose beams 2.4m,

M = 1250 * 1.2/4

= 375 kN.m

For a 310UC283

$Z = 4310_{10}3\ mm^3$

Bending stress,

$\sigma = 375_{10}3/4310$

$= 87\ MPa$

Shear stress on web,

$v = 1250_{10}3/(247*26.9)/2$

$= 94\ MPa$

Beam stresses are considered acceptable.

A.2.5 Reaction Beam

The reaction beam comprised two plate girders of the cross-section shown in Figure A.15, spaced 2400 mm apart.

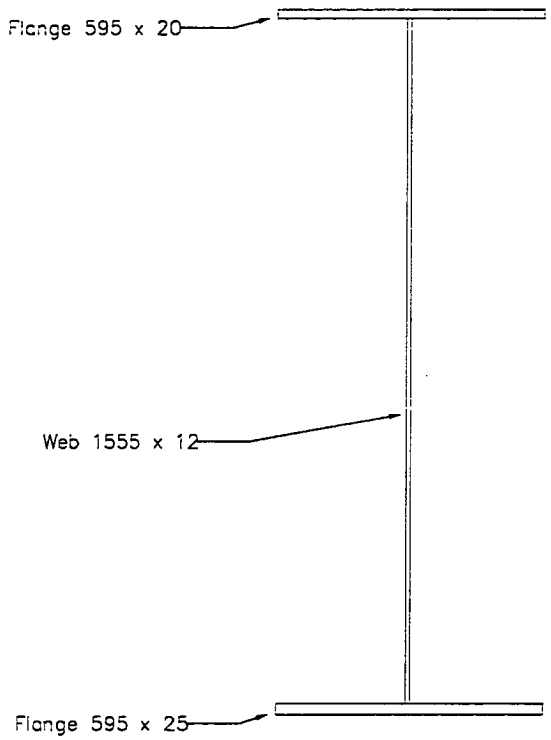

Figure A.15 - Reaction Beam Cross-Section

Section properties are calculated below.

Element	A	y	Ay	$A(y-y_c)^2$	I_{self}
Top flange	11900	1590	$18.9_{10}6$	$8.39_{10}9$	-
Web	18660	802.5	$15.0_{10}6$	$0.05_{10}9$	$3.76_{10}9$
Bottom flange	14875	12.5	$0.2_{10}6$	$8.09_{10}9$	-
Total	**45435**		$34.1_{10}6$	**$16.5_{10}9$**	**$3.76_{10}9$**

$y_c = 750\ mm$

$I_{xx} = 20.3_{10}9\ mm^4$

$Z_{top} = 23.9_{10}6\ mm^3$

$Z_{bot} = 27.1_{10}6 mm^4$

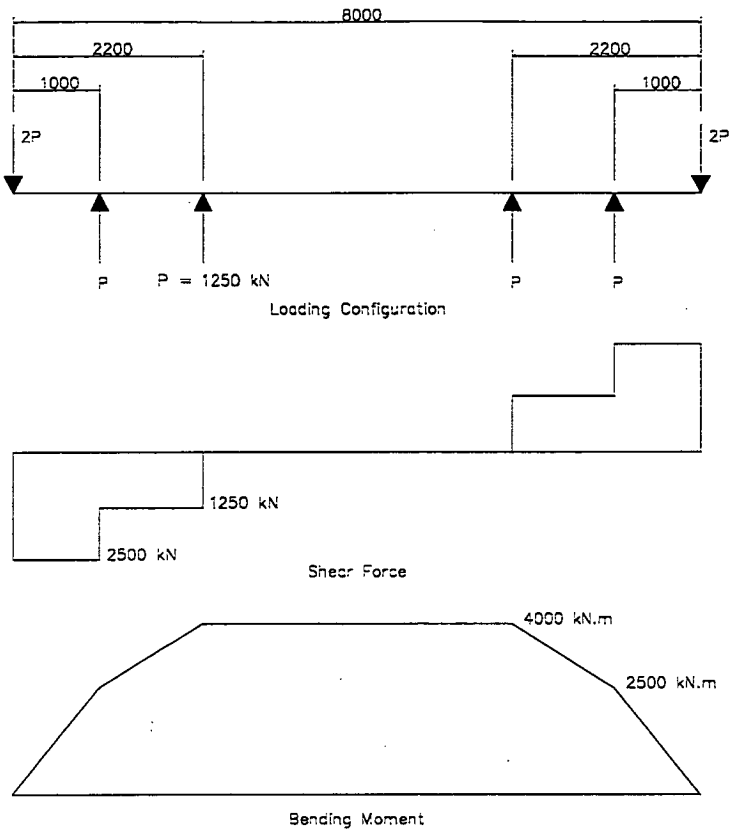

Figure A.16 - Reaction Beam Loading and Forces

The bending moments and shear forces are applied to the two beams in the launching nose; design forces for each beam are thus a bending moment of 2000 kN.m and a shear force of 1250 kN.

The calculated bending stress is:

$f_{tension}$ = 2000/23.9
= 84 MPa

$f_{compression}$ = 2000/27.1
= 74 MPa

The calculated shear stress on the web is:

f_v = $1250_{10}3/1555*12$
= 67 MPa

Considering slenderness effects to determine the allowable compressive bending stress

F_y = 350 MPa
E_s = 200 GPa
L_b = 1716 mm (cross-bracing spacing)
r' = radius of gyration of compression flange
= $595/\sqrt{12}$
= 172 mm

F_{bc} = $0.55\ F_y\ [1 - F_y\ (L_b)^2/(4\ \pi^2\ E_s\ (r')^2)]$
= 184 MPa

For a slender stiffened web:

web thickness, t = 12 mm

stiffener spacing, d = 1716 mm

allowable shear stress, F_v = $(900t/d)^2$
= 40 MPa

with 40% overstress, F_v = 55 MPa

Bending stresses are acceptable. While calculated shear stresses were higher than those allowable for a slender stiffened web, they were considered acceptable because of the nature of the loading and the significant stiffening and cross-bracing in the launching nose.

A.2.6 Anchor Beam Assemblies

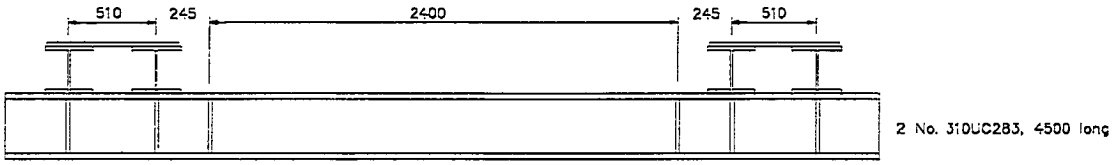

Figure A.17 Anchor Beam Assemblies

The innermost stiffeners correspond with the beams of the launching nose, and the maximum moment and shear from the reaction of the ground anchors.

Design shear = 1250 kN
= 625 kN/beam

Design moment = 1250 (0.245 + 0.510/2)
= 625 kN.m
= 315 kN.m/beam

For a 310UC283, bending stress
f_b = $315_{10}3/4310$
= 73 MPa

Shear stress
f_v = $1250_{10}3/(26.9*277)$
= 84 MPa

The stresses are considered acceptable.

The anchor beams were spaced at 680 mm and connected with pairs of 250UC89.5 sections.
Design shear force = 1250/2/2
= 315 kN

Design bending moment = 625 * 0.68/4
= 106 kN.m

Bending stress
f_b = $106_{10}3/1100$
= 96 MPa

Shear stress
f_v = $315_{10}3/(10.5*226)$
= 133 MPa

While the shear stress is high, it was considered acceptable because of the nature of the element and the loading, and the distributed nature of the loading with the relatively large contact areas.

A.2.7 Ground Anchors

The ground anchors were selected to use readily available prestressing elements commensurate with the estimated ultimate load. VSL Type 12 provides for up to 12 number 12.5 mm diameter prestressing strands with an ultimate capacity of 2210 kN. At the design load of 1250 kN, strands would be stressed to approximately 60% of the minimum breaking load.

The geotechnical investigation had shown that the geology of the site comprised a soil layer of depth 1m to 2m with low seismic velocity (about 300m/s), underlain by a second soil layer, possibly of gravels, cobbles and/or boulders, with depth 5m to 15m, and thence rock with a seismic velocity in excess of 4000m/s.

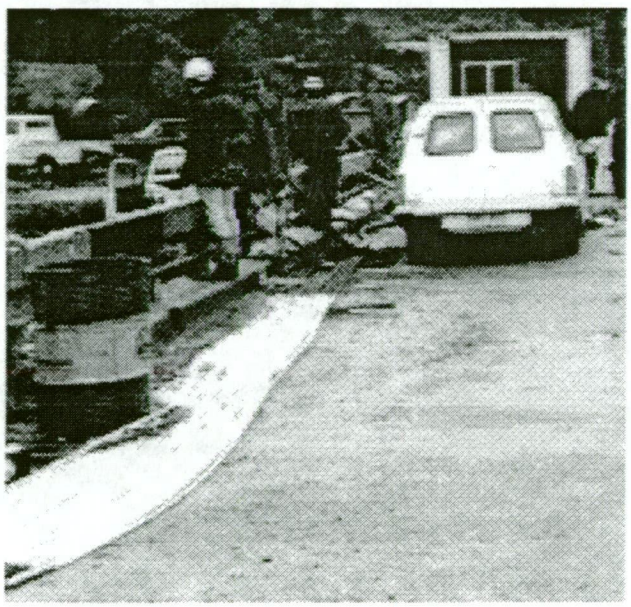

Figure A.18 - Ground Anchor Cables (Note sheathing for debonded sections)

It was proposed that the rock anchors be inclined at an angle of 15° to the vertical to assist with the stability of the loading frame.

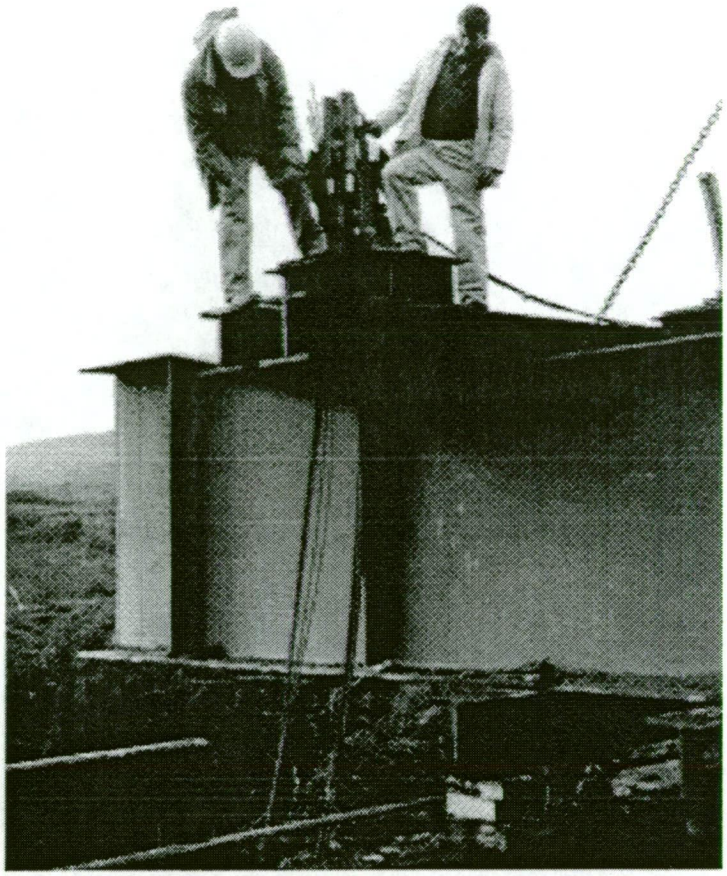

Figure A.19 - Stressing of Anchors

For cohesive soils or rock, the NAASRA Bridge Design Specification requires the depth of the anchorage to be calculated as the height of an inverted cone having a semi-vertical angle of 45° measured to the top of the anchor grout, or a semi-vertical angle of 30° measured to the bottom of the anchor grout, whichever provides the greater volume.

For a semi-vertical angle of 45°, a capacity of 2210kN, soil density 17.2kN/m^3 and length of anchorage l,

$$\begin{aligned} \text{mass of cone} &= \pi(l \tan 45°)2l * 17.2/3 \\ l &= (2210*3/17.2\pi)^{1/3} \\ &= 5.0\text{m} \end{aligned}$$

For a semi-vertical angle of 30°, a capacity of 2210kN, soil density 17.2kN/m^3 and length of anchorage l,

$$\begin{aligned} \text{mass of cone} &= \pi(l \tan 30°)2l * 17.2/3 \\ l &= (2210*3/17.2\pi\tan^2 30°)^{1/3} \\ &= 7.2\text{m} \end{aligned}$$

The soil layers were considered unsuitable for anchoring, and the design was thus based on fixing the anchors within the rock layer. The VSL handbook on ground anchors provides guidance on the determination of the embedment length. Measured values of bond strength are given in Table A.5.

Type of material	Bond strength, MPa
Soft sandstone and mudstone	0.4
Hard sandstone	2.0
Limestone	2.7
Granite	3.0
Basalt	3.9

Table A.5 - Rock Anchor Bond Strengths

The seismic velocity of >4000m/s indicates a very good, moderately weathered, unrippable rock. For an assumed bond strength of 3 MPa, a 100 mm diameter hole and a 2m bond length, the capacity of the anchorage is:

$$T_b = \pi 100 * 2000 * 3 / 10^3$$
$$= 1885 \text{ kN}$$

The factor of safety for the design load of 1250 kN is:

$$S_b = 1885/1250$$
$$= 1.51$$

At the ultimate capacity of the strands of 2210 kN, the factor of safety is:

$$S_b = 1885/2210$$
$$= 0.85$$

Based on the above calculations and discussions with VSL Prestressing, the anchors were drilled a minimum of 3m into the rock layer, with at least the first 1m debonded. The arrangement is shown in Figure 8.21.

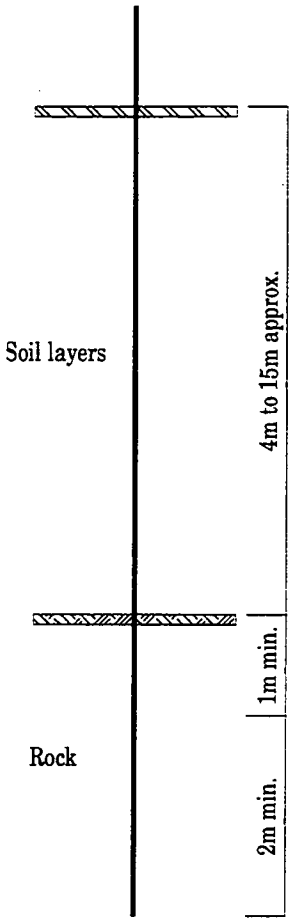

Figure A.20 - Ground Anchors

A.2.8 Substructures

A basic assessment of the capacities of the substructures to carry the ultimate loads was made assuming an equivalent depth of fixity for piles of 4m below the effective ground level, giving equivalent pile lengths of 5m for abutments and 7m for piers.

Gross concrete cross-sections were used for the structural analysis.

For the abutment crosshead of cross-section 32" wide by 24" deep,

$A_{xx} = 813 * 610$

$= 496000\ mm^2$

$I_{xx} = 813*610^3/12$

$= 15.4_{10}9\ mm^4$

For the abutment piles of cross-section 14" square,

$A_{xx} = 356 * 356$

$= 127000\ mm^2$

$I_{xx} = 356*356^3/12$

$= 1.34_{10}9\ mm^4$

For the pier crosshead of cross-section 32" wide by 24" deep,

$A_{xx} = 813 * 610$

$= 496000\ mm^2$

$I_{xx} = 813*610^3/12$

$= \quad 15.4_{10}9 \text{ mm}^4$

For the pier piles of cross-section 16" square,

$A_{xx} = 406 * 406$

$= 165000 \text{ mm}^2$

$I_{xx} = 406*406^3/12$

$= 2.26_{10}9 \text{ mm}^4$

For the superstructure,

beam and deck dead load = 14.4 kN/m

beam overall length = 34'11"

support reaction = 14.4 *10.64/2

= 153 kN/beam

From the grillage analysis, support reactions for an applied load of 1250 kN per jack are:

exterior beam = 1.25 * 202

= 255 kN

second beam = 1.25 * 738

= 920 kN

interior beam = 1.25 * 60

= 75 kN

Total reactions from superstructure and applied load are thus

exterior beam = 410 kN

second beam = 1075 kN

third beam = 230 kN

For the crossheads,

dead load = 0.813 * 0.61 *25

= 12.4 kN/m

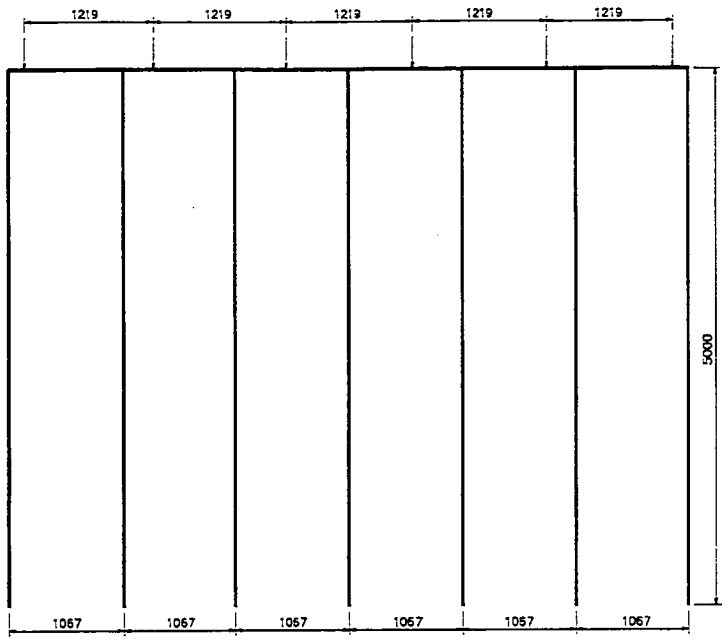

Figure A.21 - Abutment

Bending moments due to the superstructure dead and live loads were determined using a moment distribution for the crosshead, neglecting effects of the piles because of their relatively low stiffnesses. The maximum bending moment is 175 kN.m and the maximum pile load is 864 kN, say 880 kN with the dead load of the crosshead.

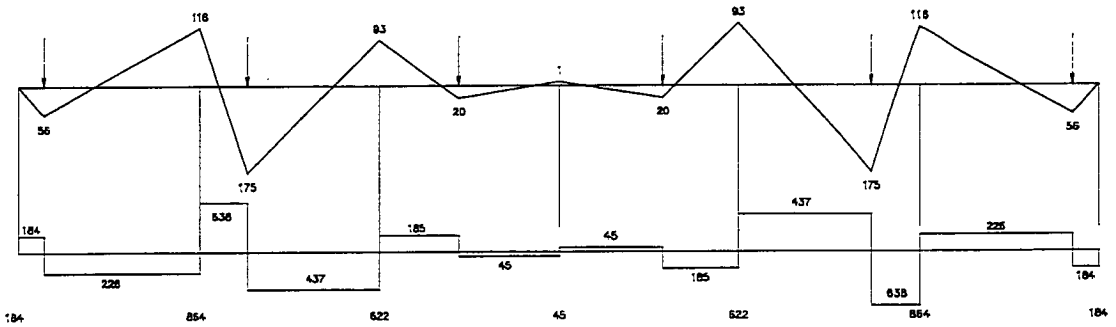

Figure A.22 - Abutment Bending Moments, Shear Forces and Reactions

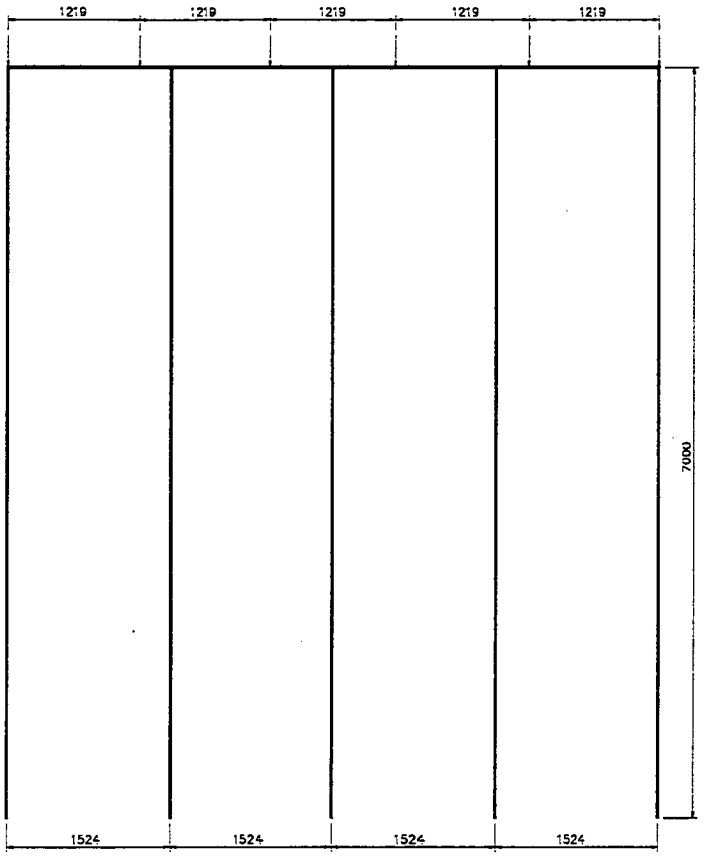

Figure A.23 - Pier

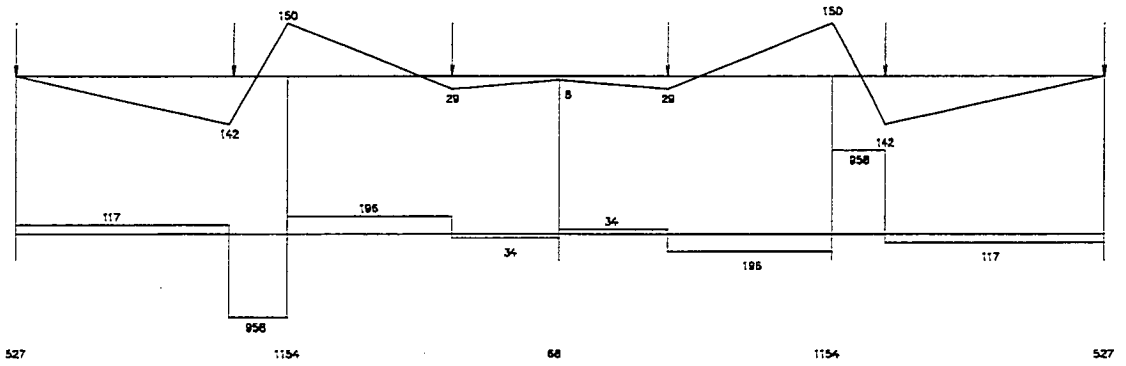

Figure A.24 - Pier Bending Moments, Shear Forces and Reactions

For the abutment, reinforcement is the same at the top and bottom of the section. Neglecting compression reinforcement,

Ast	=	$4\pi 19^2/4$	4 no. 3/4" bars
	=	1140 mm^2	
d	=	610 mm	
b	=	813 mm	
p	=	0.0023	
n	=	10	
k	=	0.152	
j	=	0.949	
M	=	175 kN.m	
f_s	=	265 MPa	
f_c	=	4.8 MPa	

While the steel stress is high, it was considered acceptable as an ultimate load condition with the calculation having ignored compression reinforcement and some load redistribution likely.

Maximum shear force is 638 kN for the superstructure load, say 650 kN with abutment dead load

Shear stress, υ = $650_{10}3/610/813$
= 1.31 MPa

For a steel proportion of 0.0023 and F'_c = 20 MPa, the basic allowable shear stress is 0.19 MPa.

V'_s = $(1.31-0.19)*610*813/10^3$
= 555 kN

A_υ = $V'_s*103/f_s/d$
= $555_{10}3/125/610$
= 7.28

For 4 legs of 1/2" diameter reinforcing at 6" spacing,
A_υ = $4*\pi*12.7^2/4/152.4$
= 3.32

The maximum shear force used for the previous calculations occurs within the distance, d, from the face of the support or bearing. Using the next greatest shear force of 437 kN, say 450 kN,

Shear stress, υ = $450_{10}3/610/813$
= 0.91 MPa

V'_s = $(0.91-0.19)*610*813/10^3$
= 357 kN

A_υ = $V'_s*103/f_s/d$
= $357_{10}3/125/610$
= 4.68

The calculations indicate that the abutment is overstressed under ultimate load conditions. The overstress is considered acceptable given the nature of the loading, the likely higher strength of the concrete and the short spacings between faces of supports

For the abutment piles, maximum load is 864 kN, say 880 kN

For the pier, reinforcement is the same at the top and bottom of the section. Neglecting compression reinforcement,

Ast	=	$6\pi19^2/4$	6 no. 3/4" bars
	=	1701 mm^2	
d	=	610 mm	
b	=	813 mm	
p	=	0.0034	
n	=	10	
k	=	0.230	
j	=	0.923	
M	=	150 kN.m	
f_s	=	157 MPa	
f_c	=	4.7 MPa	

Stresses are considered acceptable for ultimate load condition.

Shear stress, υ = $960_{10}3/610/813$
= 1.94 MPa

Basic allowable shear stress is 0.21 MPa; the situation is thus similar to the abutment. Away from the supports the maximum shear force is about 200 kN.

Shear stress, υ = $200_{10}3/610/813$
= 0.40 MPa

Stresses are considered acceptable for the ultimate load condition.

Structural capacities of piles are assessed for them acting as columns. Pile restraint is assumed to be fixed against translation and rotation at the equivalent depth to fixity of the pile and restrained against rotation but not translation at the crosshead.

	Abutment	**Pier**
Pile size	14" x 14" 356 mm x 356 mm	16" x 16" 406 mm x 406 mm
Maximum pile load	864 kN, say 880 kN	1154 kN, say 1170 kN
l_c	5m	7m
l_e (= $1.2l_c$)	6m	8.4m
d_c	356 mm	406 mm
l_e/d_c	16.9	20.7, say 20
For a short tied column	$Pt = 0.8\ (0.225\ F'_c A_g + A_{ls} f_{sc})\ 10^{-3}$	
F'_c	20 MPa	20 MPa
A_g	127000 mm^2	165000 mm^2
A_{ls}	2027 mm2 (4 no. 1" bars assumed)	
f_{sc}	90 MPa	
P_t	602 kN	739 kN
P_{tl}	$P_t\ (1.3 - 0.03\ l_e/d_c)$	
	478 kN	518 kN
P_{tl} (for F'c = 40 MPa)	839 kN	933 kN

Table A.6 - Pile Structural Capacities

The standard pile drawings and the geotechnical investigation indicate that the piles will be end- bearing on the rock with seismic velocity exceeding 4000 m/s. The calculated bearing stresses are as follows:

	Abutment	Pier
Pile size	14" x 14" 356 mm x 356 mm	16" x 16" 406 mm x 406 mm
Maximum pile load	880 kN	1170 kN
Bearing stress	6.9 MPa	7.1 MPa

Table A.7 - Pile Bearing Stresses

The typical ultimate base resistances for rocks given in the NAASRA Bridge Design Specification are shown in Table A.8.

Rock Type	Ultimate Base Resistance (kPa)
Igneous and gneissic rocks in sound condition	30 000
Hard sandstones and massively bedded limestones	20 000
Schists and shales	15 000
Hard shales, mudstones, siltstones and soft sandstones	10 000
Clay shales	5 000
Hard solid chalk without caves	3 500 - 5 000

Table A.8 - Typical Ultimate Base Resistance Values for Rocks

The bearing stresses are considered acceptable for the ultimate load condition.

A.3 Individual Beam Loading

From analysis for design of loading rig, the moment at steel yield is

M_{yield} = 6334 * 250 * 0.826 * 587 *10^{-6}

= 770 kN.m

Check concrete stress

f_c = 250 * 0.521/10/(1-0.521)

= 27 MPa

The concrete stress is higher than normally allowable, but is considered reasonable for ultimate load testing. Allowing for plastic behaviour of the beam, the design moment for the loading equipment was taken as 900 kN.m.

For loading at third points to create a pure moment region, design load

P = 900 *3/10.364

= 260 kN

Figure A.25 - Precast Beams and Loading Equipment

Hand operated 50t hydraulic jacks were available for testing and used to apply beam loads, with the reaction provided by the transverse beams used for the bridge testing and prestressing strands grouted into the floor of the Lutana Quarry.

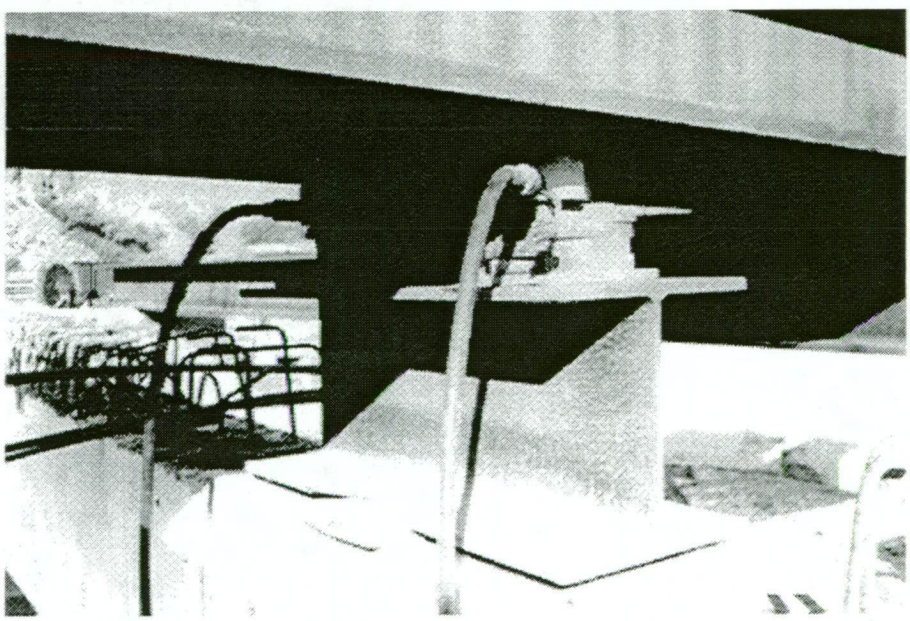

Figure A.26 - Beam Loading Arrangement

3 no. 12.5mm diameter prestressing strands have a capacity of 552 kN at 100% of minimum breaking load and 359 kN at 65% of minimum breaking load, and were used for the testing.

The quarry floor comprised sound igneous rock, and the depth of embedment to develop 550 kN capacity for a hole diameter of 75mm and bond stress of 2MPa is:

$$l = 550_{10}3/(2\pi 75)$$
$$= 1170 \text{ mm}$$

A nominal anchorage length of 5m was used.

Checking weight of cone of material, assuming rock density of 25 kN/m^3

ω = $\pi 5^3 * 25/3$

3200 kN

The capacity of loading system is thus adequate for bending without detailed analysis. It was also considered to provide adequate capacity for testing in shear.